GENETIC AND CHEMICAL BIOLOGY STUDIES OF *MYCOBACTERIUM TUBERCULOSIS* PH-DRIVEN ADAPTATION

By

Shelby J. Dechow

A DISSERTATION

Submitted to
Michigan State University
in partial fulfillment of the requirements
for the degree of

Microbiology and Molecular Genetics – Doctor of Philosophy

2021

ABSTRACT

GENETIC AND CHEMICAL BIOLOGY STUDIES OF *MYCOBACTERIUM TUBERCULOSIS* PH-DRIVEN ADAPTATION

By

Shelby J. Dechow

Mycobacterium tuberculosis (Mtb) endures robust immune responses by sensing and adapting to its host environment. One of the first cues the bacterium encounters during infection is acidic pH, a characteristic of its host niche – the macrophage. Targeting the ability of Mtb to sense and adapt to acidic pH has the potential to reduce survival of Mtb in macrophages. A high throughput screen of a >220,000 compound small molecule library was conducted to discover chemical probes that inhibit Mtb growth at acidic pH. From this screen, AC2P20 was identified as a chemical probes that kills Mtb at pH 5.7 but is inactive at pH 7.0. Through a combination of transcriptional profiling, mass spectrometry, and free thiol abundance and redox assays, I show that AC2P20 likely functions by depleting intracellular thiol pools and dysregulating redox homeostasis. Findings from this study have helped define new pathways involved in Mtb's response to acidic pH using a chemical genetic approach.

Upon sensing acid stress, Mtb can adapt accordingly by entering a nonreplicating persistent state, resulting in increased tolerance to host immune pressures and antibiotics. During growth *in vitro*, when given glycerol as a sole carbon source, Mtb responds to acidic pH by arresting its growth and entering a metabolically active state of nonreplicating persistence, a physiology known as acid growth arrest. To answer how Mtb regulates and responds to acidic pH, I performed genetic selections to identify Mtb mutants defective in acid growth arrest. These selections identified enhanced acidic growth (*eag*) mutants which all mapped to the proline-proline-glutamate *ppe51* gene and resulted in distinct amino acid substitutions: S211R, E215K, and A228D. I demonstrated that expression of the PPE51 variants in Mtb promotes significantly enhanced growth at acidic pH showing that the mutant alleles are sufficient to cause the dominant gain-of-function, *eag* phenotype. Furthermore, I performed single carbon source experiments and radiolabeling experiments showing that PPE51 variants preferentially uptake glycerol at an enhanced rate,

suggesting a role in glycerol acquisition. Notably, the *eag* phenotype is deleterious for growth in macrophages, where the mutants have selectively faster replication but reduced virulence in activated macrophages as compared to resting macrophages. This supports that acid growth arrest is a genetically controlled, adaptive process that could act as a potential targetable physiology in future TB therapeutics.

My work with the carbonic anhydrase inhibitor, ethoxzolamide, sought to combine genetic and chemical biology to better understand pH-adaptation in Mtb. Ethoxzolamide is a potent inhibitor of Mtb carbonic anhydrase activity and the PhoPR regulon, suggesting a previously unknown link between carbon dioxide and pH-sensing. We hypothesized that the production of protons from carbonic anhydrase activity could be modulating PhoPR signaling. Mtb has three carbonic anhydrases (CanA, CanB, and CanC), and by using CRISPRi and gene knockout, I show that CanB is required for pathogenesis in macrophages, but I did not observe a function in controlling PhoPR signaling. However, transcriptional profiling at different pH and CO_2 concentrations show that PhoPR is induced by high CO_2 and also revealed a core subset of CO_2 responsive genes independent of PhoPR or acidic pH regulation. Overall, these studies defined new functions for thiol- and redox-homeostasis, glycerol uptake, and CO_2-concentration in regulating Mtb adaptation to acidic environments and provide new targets for the development of acidic pH-dependent therapeutics.

This dissertation is dedicated to
My parents, Phil and Lori Dechow. Thank you for your unwavering support.
My partner, Adam Seroka, my love and my rock.
My cat, Kitten, for the endless cuddles and snuggles during grad school.

ACKNOWLEDGEMENTS

I would like to sincerely thank Dr. Robert Abramovitch for his mentorship and support these last five years. You are always so encouraging and show the greatest excitement for data at every lab meeting that we hold. Rob, you are the epitome of what it means to be a great mentor, and it is not lost on me that you work so hard to be your students' number one advocate every single day. It has been an absolute pleasure to work under your guidance, and I will truly miss the lab when I leave.

I would also like to thank Dr. Richard Neubig, Dr. Shannon Manning, Dr. Christopher Waters, and Dr. Andrew Olive for their guidance as my committee members. You all believed in my capabilities as a scientist, challenged me when I needed challenging, and helped guide my projects to completion. I am grateful for your mentorship, and I am beyond excited to have you read this dissertation.

Additionally, I would like to thank my fellow lab mates, past and present. Dr. John Williams, we started this Ph.D. journey together, and it has been so exciting to see you move on to bigger and better things. Thanks for being a true friend, supportive colleague, and a great scientist to look up to. I wish you nothing but the greatest success in your academic career. Dr. Elizabeth Haiderer, thank you for also being a great lab colleague. You are always willing to help out at a moment's notice and ensure lab life is the best it can be. I wish you all the best in your career as a scientist and veterinarian. Ife Eke and Veronica Albrecht, thank you for choosing Rob's lab and taking up John's and my mantle. I look forward to seeing your future accomplishments in the lab and wish you nothing but the best success.

To all of you, thank you again for helping me to become a better scientist. You have made my time here at Michigan State University very special, and it is bittersweet to watch this chapter in life close.

TABLE OF CONTENTS

LIST OF TABLES

LIST OF FIGURES

KEY TO ABBREVIATIONS

3-NP……...…….3-Nitropropionate

ABPP……Activity-based protein profiling

ANOVA……...……Analysis of variance

ATc……..…….Anhydrotetracycline

ATP……Adenosine triphosphate

BDQ……..Bedaquiline

BMDM……Bone marrow-derived macrophages

BMMO media……Bone marrow-derived macrophage media

bp…….....Base pairs

CA……Carbonic anhydrase

CBB…….Cumulative bacterial burden

CCCP……Carbonyl cyanide m-chlorophenyl hydrazone

CFU……...……Colony forming units

CMFDA…….5′-chloromethylfuoroscein diacetate

CO_2……..Carbon dioxide

CoA…….Coenzyme A

CPM…….……...Counts per minute

CQ……Chloroquine

DAT……...…Diacyltrehalose

DMSO……...……Dimethyl sulfoxide

EC_{50}…….….Half-maximal effective concentration

ERG……..….Ergothioneine

EtBr…….……Ethidium bromide

ETZ……..Ethoxzolamide

EV……..…..Empty vector

FoR…….Frequency of resistance

GAPDH……..glyceraldehyde 3-phosphate dehydrogenase

GFP……..Green fluorescent protein

GGC……...….Gamma-glutamylcysteine

GSH…….…..Glutathione

H^+…….……..Proton

H_2O_2……...…Hydrogen peroxide

HCO_3^-……...…… Bicarbonate

HTS…….....High-throughput screen

ICL……...……Isocitrate lyase

INH……Isoniazid

LC/MS…….Liquid chromatography/mass spectrometry

MDR…….Multi-drug resistant

MES……..2-(N-morpholino)ethanesulfonic acid

MOPS…….…3-(N-morpholino)propanesulfonic acid

Mtb……..*Mycobacterium tuberculosis*

NAC……..…… N-acetylcysteine

NRP……..Non-replicating persistence

OA……...Oxaloacetate

OADC……..Oleic acid, albumin, dextrose, catalase

OD…….....Optical density

PAT……..Polyacyltrehalose

PBS……...……..Phosphate buffered saline

PE/PPE…….……Proline-glutamate/proline-proline-glutamate

PEP……....Phosphoenolpyruvate

PMF……..…Proton motive force

POA…….Pyrazinoic acid

PZA……....Pyrazinamide

RFU……...Relative fluorescence units

RIF…….Rifampicin

RMSD……. Root mean square deviation

RNA-seq……..…….RNA sequencing

ROS……...……Reactive oxygen species

SD…….……..Standard deviation

SDS…….……Sodium dodecyl sulfate

SL……..…Sulfolipid

TAG…….....Triacylglycerol

TB…….…...Tuberculosis

TCS……...Two-component regulatory system

TLC…….….Thin layer chromatography

Tn……...…Transposon

TN-seq……...…Transposon sequencing

WGS……..……Whole genome sequencing

WT……...……Wild type

XDR……...…Extensively drug resistant

ΔΨ…….....Membrane potential

CHAPTER 1 – Defining new pH-dependent physiologies in *Mycobacterium tuberculosis*

Introduction

Over one quarter of the global human population is thought to be latently infected with *Mycobacterium tuberculosis* (Mtb), which contributed to an estimated 1.4 million deaths in 2019 alone[1]. Mtb owes its success as a pathogen to the ease with which it spreads (i.e. aerosolized droplets containing as few as 1-3 bacilli[2]) and its ability to avoid killing by macrophages and other host immune responses[3]. Although Mtb can remain quiescent in the human host for decades, approximately 5-10% of infected individuals risk developing active TB disease during their lifetime[1]. Even more alarming is the increasing incidences of multi- and extensively-drug-resistant (MDR and XDR)-TB. The standard treatment for active TB is a multidrug regimen taken for six months; however, infection with MDR-TB can extend therapy for two or more years[1]. Under various environmental and antibiotic stresses, Mtb will also enter a state of non-replicating persistence (NRP) and develop phenotypic drug tolerance, effectively evading antibiotic bactericidal activity[4-7]. Finding novel drug targets and shortening TB treatment is imperative in combatting drug-resistant and drug-tolerant infections.

Mtb senses and adapts to host immune cues as part of its pathogenesis. One important environmental cue sensed by Mtb is the acidic pH of its host niche – the macrophage. Mtb's ability to sense and adapt to acidic pH makes it an attractive pharmacological target. Mutants that are susceptible to acid stress (i.e. PhoPR, MarP, Rv2136c) exhibit virulence defects in macrophages and are highly attenuated in mycobacterial *in vivo* infection models[8-11], suggesting that chemically targeting these physiologies may have therapeutic potential. However, Mtb can shift to an NRP state in response to acid stress, promoting antibiotic tolerance, prolonged infection, and potential reactivation of disease[12,13]. Therefore, it is not only imperative to identify new pH-dependent physiologies as potentially susceptible drug targets, but also find compounds that disrupt Mtb's transition into NRP, thereby promoting total Mtb eradication during infection. In this chapter, I will discuss host relevant acid stresses and key Mtb physiologies and pathways that enable it to slow its growth, remodel its metabolism, and regulate global gene expression in response to acidic pH. I will also give an overview on mutants that promote acid resistance or growth at acidic pH and the screening strategies used to find them. Lastly, I will discuss the therapeutic potential of disrupting

pH-driven adaptation in Mtb and the growing class of compounds that exhibit pH-dependent activity and/or target physiologies important for acid adaptation.

M. tuberculosis colonization of acidic environments

Bacterial pathogens must adapt to changing environmental conditions in order to survive inside their host niche. Pathogens with an intracellular lifestyle are faced with hostile immune responses and must sense and adapt accordingly. The ability to sense and adapt to bactericidal host defenses is essential for Mtb as its host niche is the macrophage, whose purpose is to kill pathogenic invaders[14]. Thus, Mtb has developed strategies to make the macrophage amenable for survival and replication. To achieve this, Mtb initially inhibits fusion of the phagosome and lysosome in inactivated macrophages, residing in a mildly acidic environment (pH ~6.2)[15]. Mtb disrupts phagosomal acidification by secreting a phosphatase (PtpA) into the host cytosol that binds V-ATPase (a proton-pumping complex that drives acidification[16]) and dephosphorylates the vacuolar protein sorting (VPS) machinery required for membrane fusion and trafficking of V-ATPase to the phagosome[17,18]. Inhibition of phagosome maturation is not limited to Mtb; it has also been observed in other mycobacterial species including *M. leprae*[19], *M. bovis* BCG[20], and *M. avium*[21]. The survival strategies of *Mycobacterium* spp. differ in comparison to other facultative intracellular pathogens that colonize phagosomes. *Listeria monocytogenes* requires low pH in order to activate the hemolysin it needs to escape the phagosome[22], while *Salmonella typhimurium* needs an acidic environment to synthesize factors that allow for persistence[23]. Additionally, *Coxiella burnetii* cannot initiate replication without first sensing low pH[24]. The diverse repertoire of responses and adaptations to phagosomal acidification appear to be important for pathogen infection and may serve as targets for controlling these pathogens.

Arrest of phagosome maturation during Mtb infection can eventually be overcome. Immunological activation of the macrophage results in phagosomal-lysosomal fusion and acidification to ~pH 4.5-5.0[15,25], whereupon Mtb may restrict its growth in order to survive[15]. Decrease in pH following phagosomal-lysosomal fusion is rapid and occurs within 15 to 60 minutes[26]. However, Mtb can perforate the phagosome,

granting cytosolic access[27,28]. ESX-1, a type VII secretion system, mediates phagosomal perforation and exports ESAT-6/CFP-10 which dissociate under acidic conditions found in the phagosome, allowing ESAT-6 to access and perturb the phagosomal membrane[27-29]. Additionally, the Mtb lipid, pthiocerol dimycocerosates (PDIM), is required for optimal ESAT-6 activity, both acting in concert to induce phagosomal damage and rupture[30]. Ultimately, phagosomal rupture could result in neutralization and allow Mtb to access cytosolic carbon sources that are otherwise absent in the phagosome[31]. Together, these results show that Mtb experiences different immunological states of the phagosome and responds appropriately to ensure its growth and survival. This ability to respond distinctly to different acidic environments shows that Mtb is capable of sensing and adapting to acidic pH.

Slowed growth and metabolic remodeling at acidic pH

Mtb is characterized as a slow-growing pathogen and exhibits a wide range of doubling times, from ~20 hours in vitro to 70 days in mice[32,33]. Our understanding of how Mtb arrests its growth *in vivo* is limited. However, *in vitro* studies of host- relevant stresses (i.e. hypoxia and nutrient starvation) show that Mtb enters a non-replicating persistent (NRP) state, whereupon it completely arrests its growth, remodels its metabolism, and becomes more tolerant to antibiotics[5,13,34-36]. Aspects of these observations have also been replicated in acid stress models *in vitro*[8,9,37-39]. Mtb will incrementally slow its growth in rich medium starting at pH 6.4, with complete growth arrest observed at pH 5.0[39]. Mtb will also completely arrest its growth in minimal media buffered to pH 5.7 in the presence of glycerol as a sole carbon source[37]. Additionally, slowed Mtb growth occurs in mildly acidic (pH 6.0-6.5) defined Sauton medium under elevated Mg^{+2} levels (100 μM), with complete growth arrest observed at low Mg^{+2} levels (10 μM)[38]. Amid extreme acidic culture conditions (pH 4.5), Mtb is able to maintain a relatively neutral intrabacterial pH (~pH 7.2) and maintain viability[9]. This demonstrates that slowed growth is not attributed to intrabacterial acidification and suggests mechanisms are in place which Mtb regulates growth arrest in response to changes in pH.

Metabolic remodeling is a hallmark of NRP and is observable under *in vitro* environmental stress conditions including acidic pH[37]. During infection Mtb is thought to primarily metabolize cholesterol and other host lipids as carbon sources[40-43], producing acetyl-CoA, propionyl-CoA, pyruvate, and glycerol [43,44]. An overrepresentation of genes involved in fatty acid synthesis and degradation[45] suggests environmental stresses and available carbon sources may function together to regulate Mtb physiology. This is supported by studies of acidic pH and host-associated carbon sources which show that acid growth arrest is dependent on the presence of available glycolytic carbon sources (i.e. glucose and glycerol)[37]. Further mechanistic studies of pH-dependent Mtb growth regulation link acidic pH and carbon source availability to a reduced cytoplasm, sulfolipid synthesis, and central carbon metabolism remodeling[37]. Interestingly, Mtb can resuscitate its growth at acidic pH in the presence of host-derived carbon sources (i.e. phosphoenolpyruvate [PEP], pyruvate, acetate, oxaloacetate [OA] and cholesterol) which function at the intersection of glycolysis and the TCA cycle (a.k.a. the anaplerotic node)[37]. This discovery suggests that the anaplerotic node is the location of a pH-dependent metabolic switch that may promote Mtb growth on permissive carbon sources during pathogenesis at acidic pH. This is further supported by the observation that anaplerosis-associated genes, phosphoenolpyruvate carboxykinase (*pckA*) and isocitrate lyase (*icl*), are induced in an acidic pH-dependent manner[37]. Deletion of the *pckA* and *icl* results in reduced growth at acidic pH[12,37]. Furthermore, carbon source-specific growth arrest at acidic pH appears to be an Mtb-specific adaptation associated with pathogenesis; the non-pathogenic mycobacterium strain, *M. smegmatis*, grows well at acidic pH regardless of carbon source[37]. Together, these data suggest Mtb remodels its metabolism around the anaplerotic node. Altogether, metabolic remodeling is required for pH adaptation, and carbon source-specific growth arrest at acidic pH is associated with Mtb pathogenicity.

Mtb sensing and gene regulation at acidic pH

While Mtb remodels its carbon metabolism to promote growth at acidic pH[12], it also contains regulatory mechanisms to slow its growth and enter acid growth arrest. *In vitro* and *in vivo* transcriptional profiling studies of Mtb in response to acidic pH show a robust transcriptional response[37,46,47], supporting

that Mtb can sense a low pH environment and modulate its physiology accordingly. Transcriptional studies of the phagosomal acidic pH regulon show significant overlap with the PhoPR two-component regulatory system regulon, which is comprised of the sensor histidine kinase PhoR and the response regulator PhoP[48]. Specifically, the induction of 25 genes is shared between both regulons[46,48], suggesting some pH-dependent physiologies are controlled by PhoPR. Mutants in *phoP* are attenuated for virulence in infected macrophages, mice, and guinea pigs[10,39], further supporting that Mtb regulatory responses to low pH are important for virulence and acid adaptation.

Experimental findings show that the PhoPR regulon is strongly induced *in vitro* at pH 5.7, and induction of the regulon begins at the same pH (~6.4) that Mtb begins to exhibit slowed growth[39]. The association of slowed growth with *phoPR* induction and decreasing pH suggests that the PhoPR regulon plays a role in regulating pH adaptation (Figure 1.1)[39]. Additionally *phoPR* regulates genes associated with carbon metabolism and redox homeostasis[37,48,49], suggesting that *phoPR* plays a critical role in altering metabolic processes in response to acidic environments. Together, these findings link carbon source-dependent growth arrest with the induction of the PhoPR regulon and add another layer of regulation utilized by Mtb when exposed to an acidic environment.

Transcriptional profiling is a valuable tool that can be utilized to identify whole system pathways and specific genes modulated by acidic pH. Several studies have used transcriptional profiling, Microarray or RNA sequencing (RNAseq), to identify genes specifically regulated by acidic pH and/or conditional environments in concert with a pH-stress response[37,39,46,47,50]. Fisher *et al.* was one of the first to analyze Mtb's global transcriptional response to acidic pH using microarrays and real-time reverse transcription-PCR, and discovered 81 genes that were differentially expressed, including many involved in lipid metabolism[47]. Using microarrays as well, Walters *et al.* and Gonzalo-Asensio *et al.* both showed that PhoP positively regulated genes involved in lipid and carbon metabolism while Rohde *et al.* and Abramovitch *et al.* further revealed that the PhoPR regulon is induced during the initial stages of pathogenesis in macrophages, an inherently acidic environment[15,46,48,49]. Newer RNA-seq methods have helped elucidate pH-induced or repressed genes in a carbon-source dependent or independent manner, as well as *phoPR*-

dependent transcriptional changes in response to acidic pH[37,50]. Using RNA-seq, Baker *et al.* showed that acid regulated genes are associated with carbon metabolism, lipid anabolism, and replenishment of oxidized cofactors, supporting the previous connections made between acid-inducible and PhoPR-regulated genes[37]. Together, transcriptional profiling can be used to identify key genetic regulators of pH-driven adaptation. In turn, these genetic elements can also be used to develop fluorescent transcriptional reporters for assessing gene expression in response to changes in the pH environment, like the CDC1551(*aprA'*::GFP) reporter strain developed by Abramovitch *et. al*[39]. The *aprABC* locus is induced when exposed to low pH *in vitro* and in macrophages and is also dependent on PhoPR regulation, making it an ideal reporter candidate for examining pH and phagosomal-inducible transcriptional changes[39,46]. Overall, transcriptional profiling is a useful tool for elucidating the metabolic requirements of Mtb undergoing acid stress, as well as understanding how pH-regulated genes integrate into a multi-stress or *in vivo* pathogenesis transcriptional profile of Mtb.

Genetic studies identifying mutants with altered pH-dependent adaptations

Establishing non-replicating persistence is important for Mtb to survive acid stress. However, a growing body of literature reveals mutants that are capable of resisting acid stress or overcoming acid growth arrest altogether *in vitro*. These mutants can be leveraged to reveal mechanisms of physiological and genetic adaptation to acidic pH, and furthermore, could act as potential targetable physiologies in future TB therapeutics.

In early phases of macrophage infection, Mtb undergoes rapid replication which is ultimately deleterious to its survival, and coincides with a decrease in overall bacterial viability[33]. It is not until Mtb enters a phase of slower cell division roughly two days following macrophage infection that the rate of killing begins to decrease. During this time of slowed growth, Mtb appears to adapt to the macrophage environment and establish a productive infection[33]. These observations are supported by computational modeling of the host immune response to Mtb infection where persistent infection and bacterial survival is contingent on establishing slow mycobacterial growth[51]. As previously mentioned, the mild acidity of the

host macrophage is an important trigger for differential gene expression and Mtb intracellular survival. In *in vitro* stress models of Mtb growth at low pH in both rich and minimal media, Mtb will slow its growth or completely arrest growth altogether[6,9,12,37-39]. Unlike other *in vitro* single stress models (i.e. starvation[52] and hypoxia[13]) where Mtb experiences physiological limitations that result in its cessation of growth, *in vitro* acid stress media and acid stress growth models contain all necessary nutrients and supplementation required to establish mycobacterial growth[43]. This suggested that pH-dependent cessation of growth may be genetically controlled. We have pursued this hypothesis in our lab and shown that pH-dependent growth arrest is a reversible phenotype through mutant forward genetic selection using the acid growth arrest model: minimal media buffered to pH 5.7, with glycerol as the sole carbon source[12,53].

Forward genetic screening methods conducted in our lab have identified three independent amino acid substitutions (S211R, E215K, and A228D) in *ppe51* that allow for substantial growth to occur at acidic pH. These mutations were identified as dominant, gain-of-function mutations and regarded as enhanced acid growth (*eag*) mutants[12,53]. PPE51 is a mycobacteria-specific protein that is implicated in glycerol and nutrient uptake, an observation that has been studied by our lab as well as others[12,53-56]. In fact, studies described later in Chapter 3 show that PPE51 *eag* variants grow specifically on glycerol, a carbon source that is normally non-permissive for growth at acidic pH (Figure 3.3)[37]. Transcription of *ppe51* is induced at acidic pH independent of growth arrest in a *phoP*-dependent manner as well as 2 hours post-infection in macrophages[37,46,50]. Gouzy and colleagues observed that unlike host-relevant lipids, glycolytic carbon sources like glycerol do not promote Mtb growth at acidic pH likely through a mechanism of reduced glyceraldehyde 3-phosphate dehydrogenase (GAPDH) activity and accompanying reduction in glycolytic flux at acidic pH[57]. It is possible that increased expression of wild type (WT) *ppe51* at low pH may try to compensate for reduced glycolytic flux, and that *ppe51 eag* variants can overcome reduced glycolytic flux entirely in *in vitro* models of acid stress with glycerol.

Other mutants that also allow for growth to occur *in vitro* in acidic media could also be described as *eag* variants. When *phoPR* is deleted, mutants exhibit significantly enhanced growth on pyruvate as the sole carbon source at acidic pH when compared to WT Mtb[37]. Although pyruvate is permissive for WT Mtb

growth at pH 5.7, the enhanced growth of *ΔphoPR* in the same culture conditions suggests that functional PhoPR is required to slow Mtb growth at acidic pH. Similarly, a *tgs1* mutant, a triacylglycerol synthase, also exhibits enhanced growth in low pH 7H9 culture adjusted to pH 5.5[6]. While WT Mtb and the *tgs1* complement are able to replicate in the same culture conditions, the *Δtgs1* strain continued to grow more rapidly overall, providing another example of an *eag* phenotype. Baek and colleagues also showed that a *ΔdosR* mutant, the response regulator of the DosRST TCS and regulator of *tgs1*[58], shows a similar growth phenotype to *Δtgs1* under acid stress[6], and could also be described as having an *eag* phenotype as well.

Mutants have also been discovered that resist killing at acidic pH but cannot replicate. Tischler and colleagues showed that *ΔpstA2* and *ΔpstS1* exhibit enhanced resistance and cell viability in acidified 7H9 medium (pH 4.5) compared to the WT control[59]. While both *pstA2* and *pstS1* knockout mutants and the WT exhibited an overall decrease in bacterial viability at acidic pH, sensitivity to acidic pH was significantly more reduced in *ΔpstA2* and *ΔpstS1* compared to the WT. Both PstA2 and PstS1 are part of the Pst (phosphate-specific transport) uptake system in Mtb that transports inorganic phosphate (P_i)[60]. More specifically, PstA2 is a membrane-spanning protein and PstS is a substrate-binding protein with high affinity for P_i[60]. It was proposed that WT Mtb may transport the monobasic form of phosphate and an additional proton, leading to acidification of the cytoplasm. In contrast, *ΔpstA2* and *ΔpstS1* Mtb might exhibit impaired protonated phosphate transport, resulting in fewer protons in the cytoplasm and increased acid resistance. Some other considerations for the growth of these mutants include the acidified medium which was buffered to pH 4.5. While Mtb is able to survive and maintain viability at pH 4.5 in phosphate-citrate buffered medium[9,61], the 7H9 medium used in this study contained albumin-dextrose-saline enrichment and Tween-80, which could potentially release free fatty acids that are toxic to Mtb at low pH[62-66]. However, Mtb is able to cease growth and maintain viability in 7H9 media containing oleic acid-albumin-dextrose-catalase enrichment and buffered slightly higher at pH 5.0[39,57]. It is plausible that *ΔpstA2* and *ΔpstS1* Mtb may exhibit greater acid resistance and bacterial viability and growth in a different media type or a slightly less acidic media altogether.

Transposon mutagenesis is a powerful approach that can be used to identify genes essential for survival during Mtb pH-dependent growth arrest and pH-driven adaptation. Transposon mutagenesis requires the construction of a transposon insertion library, which involves the relatively random integration of a transposon into a genetic element, thereby disrupting its function[67]. Vandal *et al.* used transposon mutagenesis to identify genes responsible for conferring acid resistance[9], by screening 10,100 Mtb transposon mutants in 96-well plates for their impaired ability to recover from exposure to 7H9 medium with Tween-80 buffered to pH 4.5. They identified 21 genes with independent transposon insertions that showed sensitivity to acidified 7H9 medium[9]. Two mutants (Rv2136c and MarP) maintained their sensitivity in 7H9 amended with Tyloxapol and phosphate-citrate buffer, both buffered to pH 4.5, and were also highly attenuated for virulence *in vivo*[8,9].

Chemical biology is a useful approach that can tackle the basic research aims of finding new pH-dependent physiologies, while also exploring the applied research potential of finding new therapeutics and novel mechanisms of action. Our lab's discovery that ETZ inhibits the PhoPR regulon showed that chemical genetics can be used to identify physiologies important for Mtb survival at acidic pH. ETZ functions as a carbonic anhydrase (CA) inhibitor and revealed a potential link between carbon dioxide sensing, CA activity, PhoPR signaling, and pH-dependent pathogenesis (Figure 1.1.)[50]. In another example of chemical biology approaches, compounds that are pH-selective Mtb growth inhibitors can be harnessed as chemical genetic tools for exploring pathways required for Mtb growth and survival at acidic pH. AC2P36 and AC2P20 are pH-selective compounds that demonstrate Mtb's sensitivity to thiol-oxidative stress at acidic pH (Figure 1.1)[68,69]. Additionally, chemical probes can be powerful tools when coupled with previously mentioned genetic approaches, like transcriptional profiling, to elucidate novel pH-responsive pathways. For example, the use of AC2P36 and AC2P20 in combination with transcriptional profiling at acidic pH is how we determined that both compounds were modulating redox and thiol homeostasis, sensitizing Mtb to chemical treatment (Table 1.1)[68,69]. Taken together, the independent approaches of transposon mutagenesis, transcriptional profiling, and chemical biology can reinforce and complement each other to find new pH-driven adaptation pathways and physiologies.

Methods for screening compound activity against Mtb pH-driven adaptation

The primary goals of TB drug development are to find compounds that shorten the duration of treatment, improve safety and tolerability, provide greater efficacy, combat multidrug (MDR) and extensively drug-resistant (XDR) TB, and improve treatment options for latent TB infections. pH-driven adaptation is an attractive target for drug development efforts, and many TB researchers have developed methodologies or streamlined efforts for evaluating compounds that disrupt pathways allowing Mtb to survive in acidic environments.

Two main screening methods are often used to identify antimycobacterial compounds: phenotypic screens against whole cells or isolated molecular target-based screens. Phenotypic whole-cell high-throughput screening (HTS) is an invaluable tool to rapidly identify hit compounds from extensive chemical libraries. This approach has been adopted to identify compounds that specifically interfere with intrabacterial pH (pH_{IB}) homeostasis[70,71]. Specifically, Darby and colleagues developed a whole-cell HTS method using Mtb expressing a pH-sensitive, ratiometric GFP (pHGFP) that allowed for measurements of pH_{IB} on live cells[70-72]. This study used whole-cell screening of a natural product library to identify disruptors of Mtb pH_{IB}, and in doing so identified top four hit compounds: 1048, 20E11, 1G9, and 23A6 (agrimophol) (Figure 1.1 and Table 1.1)[70]. Early *et al.* also capitalized on the use of pH-sensitive GFP and adapted it for a HTS of a diverse compound library against Mtb pH_{IB} which helped identify five top hit compounds: IDR-0020850, IDR0054790, IDR0099118, IDR-0040669, and IDR-0081053 (Figure 1.1. and Table 1.1) [71,73]. While both studies successfully identified new disruptors of pH_{IB}, pH-driven adaptation is not solely reliant on maintaining a hospitable pH_{IB}. PhoPR plays a role in pH-driven adaptation, and directly induces ~50 pH-regulated genes, including the Acid and Phagosome Regulated locus, *aprABC*[36,39,48,49]. *aprABC*'s promoter is directly bound by PhoP and is induced in a pH-dependent manner and in macrophages[36,39,74]. To identify chemical probes that inhibit the PhoPR regulon, our lab generated an acid-inducible biosensor strain by cloning the *aprA* promoter upstream of GFP, and used it to identify ETZ as an inhibitor of *phoPR* signaling (Figure 1.1 and Table 1.1)[39,50]. RNA-seq of ETZ-treated Mtb caused the downregulation (>2-fold, $P < 0.05$) of 45 genes, all of which were also downregulated in the *phoP::*Tn mutant and confirmed that

ETZ inhibits PhoPR regulon induction[50]. While ETZ is not growth inhibitory *in vitro*, it does reduce Mtb survival *in vivo*, showing that inhibition of pH-adaptation pathways required for virulence can be sensitized in multi-stress environments, further supporting that disrupting pH-adaptation pathways can be used for new drug development.

When a pH-dependent physiology is known, target-based screening can be a powerful tool for identifying active molecules. Maintaining intrabacterial pH homeostasis (pH_{IB}) is critical for Mtb survival during acid stress. MarP is a membrane serine protease that is required for conferring acid resistance, and catalytically inactive MarP fails to maintain pH homeostasis both *in vitro* and *in vivo*, sensitizing Mtb to acid stress[9,11]. Therefore, MarP is an attractive therapeutic target. To address the therapeutic potential of targeting a gene essential for acid resistance, Zhao and colleagues performed a HTS of 324,751 synthetic organic compounds against MarP to chemically inhibit MarP activity and potentially sensitize Mtb to acidic host conditions[75]. In doing so, Zhao used target-based screening methods to establish benzoxazinones as specific inhibitors of MarP, and further identified BO43 as a potent MarP inhibitor that disrupted Mtb's pH_{IB} (Figure 1.1 and Table 1.1)[75]. In their approach, Zhao screened the 300,000+ organic chemical library against the purified, recombinant extracellular domain of MarP by competition with an activity-based probe[75]. This allowed them to screen for compounds that interfered with the binding of the probe to MarP's serine hydroxyl and subsequently read decreases in probe fluorescence polarization. Other pathogenic mycobacterial species like *M. avium* subsp. *paratuberculosis* also rely on a serine protease with over 92% similar to Mtb's MarP to maintain its pH_{IB}, strongly suggesting that pH_{IB}-disrupting chemicals like BO43 could eventually be co-opted to counteract acid resistance in multiple mycobacterial pathogenic species[76].

A technique that Zhao used, and one that is part of a growing number of chemical proteomic approaches, is activity-based protein profiling (ABPP). ABPP utilizes small molecule probes to identify potential protein binding partners[77]. This allows for enzyme function to be characterized in its native biological systems. For target-based HTS, an enzyme-specific probe tagged with a fluorophore emits a strong signal when it reacts with its target protein; however, in the presence of a competitor, the signal is decreased[78]. Additionally, this technology can also be used to identify unknown targets of compounds

identified from phenotypic HTS. In support of this, Zhao and colleagues used click chemistry-ABPP (CC-ABPP) in a second study to identify the binding partner of the pH_{IB} inhibitor agrimophol, Rv3852 (Figure 1.1)[70,79]. Altogether, ABPP allows for screening and rapid observation of target-specific inhibitors and has shown already to be a valuable approach for finding new inhibitors of pH-regulated genes required for Mtb's survival.

Classifying chemical probes that target pH-dependent pathways

A growing body of literature supports the classification of compounds that exhibit activity against Mtb and that are pH-dependent and/or target pH-dependent physiologies. These compounds can be further defined by their ability to disrupt intrabacterial pH homeostasis (pH_{IB}), activity as ionophores, disruption of membrane potential, or exhibiting unique properties altogether. Furthermore, not all of the compounds described herein exhibit pH-dependent activity (i.e. they have activity at both neutral and acidic pH) and can still inhibit Mtb's survival at acidic pH or target pH-dependent physiologies. This demonstrates that the classification of compounds that disrupt Mtb's survival at acidic pH remains broad and includes a diverse grouping of compounds.

After important genes that function to maintain Mtb's intrabacterial pH homeostasis were discovered, several studies have sought to specifically find inhibitors of pH_{IB}[70,71,75]. Since the pH of the phagosome that Mtb resides in can range from mildly acidic (pH 6.2) to very acidic (pH 4.5)[15,25,80,81], Mtb's survival is dependent on its ability to sense external pH and maintain a relatively neutral internal pH to preserve its viability[9]. Thus, pH homeostasis is an attractive target because disrupting it at acidic pH can potentially sensitize Mtb to acid stress. MarP mutants provide compelling genetic evidence for this, as MarP mutants fail to maintain pH_{IB} in acid and are severely attenuated for virulence in *in vivo*[8,9]. In recent years, numerous compounds have been identified that disrupt Mtb pH_{IB}: bedaquiline[82], IDR-0020850, IDR-0054790, IDR-0099118, IDR-0040669, IDR-0081053[71], nitazoxanide[83], monensin[70], 1048, 20E11, 1G9, 23A6 [70], BO43[75], and imidazopyradines[84,85]. Despite all of these compounds disrupting pH_{IB}, they share almost no structure similarity (Table 1.1). Furthermore, known mechanisms or targets of pH_{IB}-disrupting

compounds are also diverse, even if they target similar pathways. For example, bedaquiline and the imidazopyridine series both target major components of Mtb's electron transport chain (Figure 1.1); however, they target different components: the ATPase and QcrB, respectively. Additionally, not all pH_{IB} inhibitors are reliant on acidic pH conditions for activity. This is highlighted by bedaquline, which does not exhibit pH-dependent activity; however, the IDR compounds rely on acidic pH conditions to exhibit either selective or enhanced activity (Table 1.1). Taken together, pH_{IB} inhibitor structure and diversity of activity suggests that there are many different pathways and genes regulating pH_{IB}, and that distinct targets exist that can potentially sensitize Mtb to acid stress. Furthermore, these compounds can be useful tools to uncover new physiologies important for maintaining pH_{IB}.

The membrane potential ($\Delta\Psi$) and the transmembrane proton concentration gradient (ΔpH) are the two components that drive the proton motive force (PMF) (Figure 1.1). It is important to make the distinction between compounds that disrupt membrane potential through a targeted, enzymatic approach or exhibit non-specific, depolarization of the membrane (i.e. ionophores). Compounds that affect the PMF via membrane potential disruption are attractive targets not only because it is essential for mycobacterial survival[9], but also because acidic pH has been shown to decrease Mtb's membrane potential compared to neutral pH[86]. In addition to disrupting pH_{IB}, nitazoxanide also reduces Mtb's membrane potential, which is further augmented by acidic pH[83], and acts as a strong stimulator of autophagy and inhibitor of mTORC1 signaling, a major negative regulator of autophagy[87]. Furthermore, its activity against replicating and nonreplicating Mtb suggests that nitazoxanide has a potentially novel mechanism of action and multiple targets[83,88]. Compound 16 disrupts Mtb membrane potential in a pH-dependent manner, and has been proposed as a new tool to evaluate Mtb membrane potential disruption at acidic pH because it exhibits a greater degree of separation compared to DMSO than CCCP[89]. Monensin is another membrane potential disruptor that also acts as an ionophore (Table 1.1)[70]. While used as a general ionophore assay control, monensin does have therapeutic potential and has been used to treat *M. avium* subsp. *paratuberculosis* infections in cattle[90,91].

A third grouping of compounds are those that do not necessarily inhibit pH_{IB}, disrupt membrane potential, or act as ionophores as their proposed mechanism of action. Rather, they have unique or novel mechanisms of action, and appear to disrupt functional pathways important for Mtb's survival under acidic conditions. These compounds include AC2P20[68], AC2P36[69], C10[92], auranofin[93,94], ethoxzolamide[50], 4-OH-OPB[95], trifluoroperazine[96], D157070[97], DPLG-2[98], 8-hydroxyquinoline[99], CLBQ14[100], Compound 4[101], itaconic acid[102], 3-nitropropionate[103], and chloroquine[104]. Specifically, there appears to be a group amongst this set of compounds that are actively targeting genes and/or pathways important for maintaining thiol and redox homeostasis in Mtb. AC2P20, AC2P36, and 4-OH-OPB (an oxyphenbutazone) all appear to have pH-dependent activity and covalently modify thiol-containing morphology in Mtb, disrupting redox homeostasis and resulting in the formation of reactive oxygen species and depletion of free thiols (Figure 1.1 and Table 1.1) [68,69,95]. This approach is likely resulting in greater thiol-oxidative stress and further sensitizes Mtb to acidic pH. Auranofin, although it exhibits non-specific activity at both neutral and acidic pH, causes a decrease in free thiol concentrations by inhibiting TrxB2, a thioredoxin reductase (Figure 1.1 and Table 1.1)[94]. Chloroquine (CQ) is an antimalarial agent that inhibits phagosomal acidification (Figure 1.1 and Table 1.1)[105]. Its activity against Mtb has been attributed to multiple mechanisms: inhibiting macrophage efflux pumps, limiting iron availability, and inhibiting phagosome–lysosome fusion[104-108]. Mishra and colleagues observed that pH acidification was required for redox-dependent multidrug tolerance, and that addition of CQ increased the killing efficacy of INH and RIF by five-fold[109]. These studies show compelling evidence that thiol-redox homeostasis has implications as a targetable pH-dependent physiology.

Other compounds in this grouping target unique physiologies completely. C10 inhibits respiration and metabolism through an undefined mechanism and decreases Mtb viability at acidic pH[92]. Ethoxzolamide (ETZ), a carbonic anhydrase (CA) inhibitor, inhibits PhoPR signaling, an important TCS for regulating pH-driven adaptations (Figure 1.1)[50]. ETZ inhibits Mtb CA activity in whole cells and Mtb survival in macrophages, but its exact mechanism of action in modulating Mtb physiology has yet to be fully elucidated (Figure 1.1). Johnson *et al.* showed that ETZ does not reduce Mtb growth *in vitro* but does

reduce Mtb growth in macrophages and mice. This is consistent with previous observations of *phoPR* knockout mutants, which again are highly attenuated *in vivo*[10,110]. Likewise, itaconic acid is a covalent inhibitor of isocitrate lyase (ICL) activity in Mtb[102], and has been shown to disrupt Mtb pH homeostasis and membrane potential when grown on propionate or acetate (Figure 1.1 and Table 1.1)[111]. 3-Nitropropionate (3-NP) is also a potent inhibitor of ICL activity[103]; however, data by Eoh and Rhee suggests that it may act preferentially on succinate dehydrogenase activity, rather than ICL activity[112]. 3-NP does inhibit recombinant Mtb ICL[113], and Baker *et al.* showed that 3-NP inhibits Mtb growth at acidic pH, but no change in growth at neutral pH, suggesting a pH-dependent requirement for ICL activity[37]. It is possible that 3-NP activity may be conditional and dependent on whether Mtb is undergoing hypoxia[112] or exposed to acidic pH[37]. ICL promotion of anaplerotic metabolism and strong induction by acidic pH makes itaconic acid and 3-NP useful tools to probe metabolic and pH-dependent pathways in Mtb. D157070 also has non-specific pH-dependent activity, and blocks resistance to nitric oxide-induced stress in concert with acidic pH[97]. Resistance to reactive nitrogen intermediates is mediated by a NADH-dependent peroxidase and peroxynitrite reductase system that is encoded by an alkyl hydroperoxide reductase subunit C (AhpC), an alkyl hydroperoxide reductase subunit D (AhpD), dihydrolipamide acyltransferase (DlaT), and lipoamide dehydrogenase (Lpd)[114,115]. D157070 directly targets DlaT, reducing Mtb viability under nonreplicating conditions (Figure 1.1)[97]. It should be noted, that nonreplicating conditions in this study utilized rich medium buffered to pH 5.5[97], and that AhpCD, which complexes with DlaT, is induced at acidic pH[37], supporting that D157070 may act on pH-dependent metabolic pathways. DPLG-2, a proteasome inhibitor, is similar to D15070 in that it too exhibits activity at acidic pH in concert with nitrosative stress (Table 1.1)[98]. CLBQ14 and Compound 4 both target Mtb methionine aminopeptidases (Figure 1.1) and are equally effective at inhibiting non-replicating Mtb in low pH, hypoxic medium compared to replicating Mtb[100,101]. Taken together, these compounds show that targets which are important for maintaining Mtb viability during acid stress are varied and distinct and that more consideration is needed for finding similar or novel physiologies altogether. Furthermore, there are still compounds which exhibit activity at acidic pH that have yet to be fully defined (i.e. trifluoperazine, 8-hydroxyquinoline) (Table 1.1).

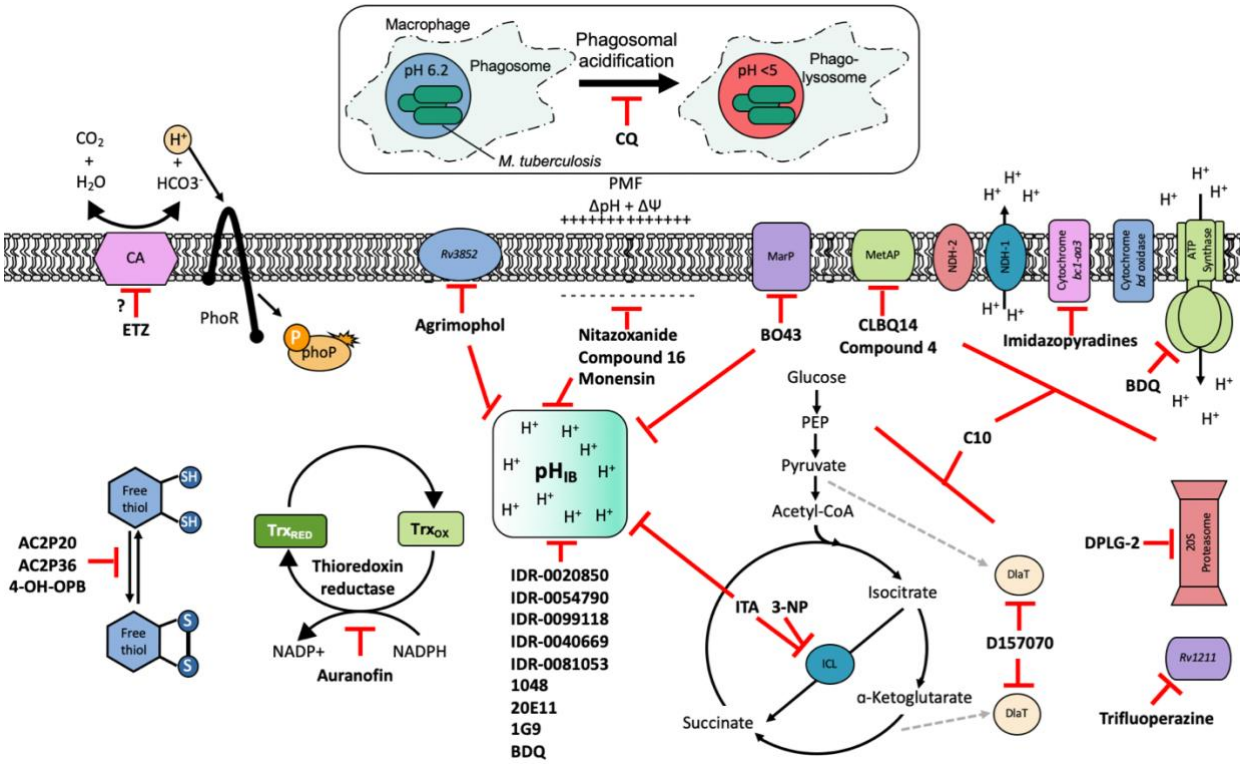

Figure 1.1. Small molecules targeting *M. tuberculosis* pH-adaptation pathways. Acidic pH modulates key pathways and physiologies involved in redox homeostasis, carbon metabolism, and pH homeostasis. This model summarizes known pH-responsive physiological adaptations and small molecules (described in Table 1.1) that disrupt intrabacterial pH (pH_{IB}), membrane potential (ΔΨ), carbon metabolism, redox homeostasis, and the electron transport chain (ETC). PhoPR is induced by acidic pH, possibly via the interconversion of carbon dioxide and water into bicarbonate and protons by carbonic anhydrase (CA). Ethoxzolamide (ETZ) inhibits CA and PhoPR regulon signaling[50]. Mtb undergoes reductive stress at acidic pH and relies on pathways that generate oxidized cofactors to mitigate this stress. Compounds that target thiol metabolism and redox homeostasis (AC2P20, AC2P36, 4-OH-OPB, and auranofin) enhance reactive oxygen species (ROS) accumulation and exacerbate Mtb's sensitivity to thiol-oxidative stress. Chloroquine (CQ) inhibits phagosomal acidification and disrupts pH-and redox-mediated drug tolerance[109]. Numerous compounds exhibit pH-dependent or enhanced activity at acidic pH and disrupt Mtb's ability to maintain a neutral pH_{IB}. These compounds (IDR-0020850, -0054790, -0099118, -0040669, -0081053, 1048, 20E11, 1G9, agrimophol) do not act as ionophores, suggesting that they target a protein important for maintaining pH_{IB}. Only agrimophol has had its target (Rv3852) elucidated, but its function remains to be defined. Several compounds (nitazoxanide, compound 16, and monensin) lower pH_{IB} by interrupting Mtb's ΔΨ and proton motive force (PMF). MarP is a serine protease that functions to maintain Mtb's acid tolerance. BO43 directly targets MarP, also disrupting Mtb's pH_{IB}. Mtb undergoes metabolic remodeling at acidic pH. Isocitrate lyase, (ICL) is induced in a pH-dependent manner and is inhibited by itaconic acid (ITA) and 3-nitropropionate (3-NP). ITA also disrupts pH_{IB}, when given propionate as a carbon source. Dihydrolipoamide acyltransferase (DlaT) is inhibited by D157070 and is required for Mtb survival during infection[115], linking it to metabolic adaptation during environmental stress. C10 selectively reduces Mtb growth at acidic pH by inhibiting respirations and/or metabolism through a yet unknown mechanism. Respiration and the ETC are likely modulated by acidic pH, and several compounds target ETC proteins including imidazopyradines (Cytochrome *bc1-aa3*) and bedaquiline (BDQ) (ATP Synthase). Some compounds (CLBQ14, compound 4, DPLG-2, and trifluoperazine) have their targets resolved and exhibit activity at acidic pH, but how they impact pH-adaptation has yet to be defined. Together these compounds disrupt important pH-adaptation physiologies and serve to sensitize Mtb to acid stress.

Table 1.1. Compounds that target pH-adaptation Mtb physiology

Compounds	Compound Structure	pH-dependent activity[a]	Disrupts intrabacterial pH (pH_{IB})	Disrupts Membrane potential	Mechanism of Action	References
AC2P20	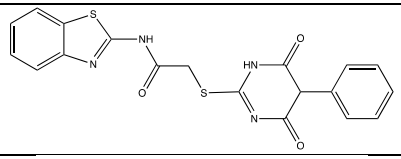	Selective	No	Undetermined	Covalent modification, formation of reactive oxygen species, and depletion of free thiols	Dechow *et al.* (2021)
AC2P36	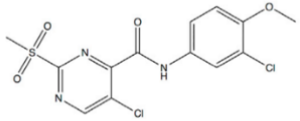	Enhanced	No	Undetermined	Covalent modification, formation of reactive oxygen species, and depletion of free thiols	Coulson and Johnson, *et al.* (2017)
C10	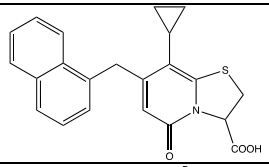	Selective	Undetermined	Undetermined	Inhibits respiration and/or metabolism	Flentie *et al.* (2019)
Bedaquiline	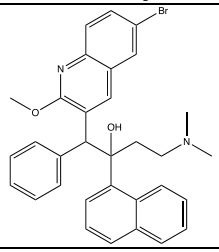	Non-specific	Yes	No	Inhibits the Mtb proton pump, ATP synthase	Andries *et al.* (2005)
Auranofin	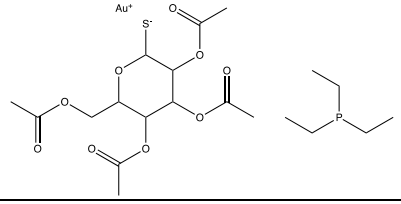	Non-specific	Undetermined	Undetermined	Inhibits the thioredoxin reductase enzyme (TrxB2), decreases free thiol concentrations	Harbut *et al.* (2015)

Table 1.1. (cont'd)

IDR-0054790	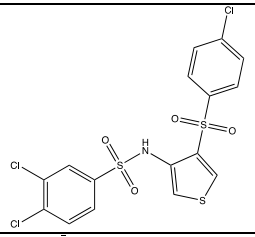	Selective	Yes	No	Undetermined	Early *et al.* (2019)
IDR-0099118	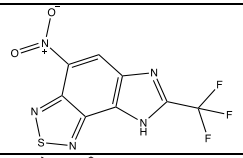	Selective	Yes	No	Undetermined	Early *et al.* (2019)
IDR-0040669	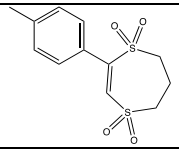	Enhanced	Yes	No	Undetermined	Early *et al.* (2019)
IDR-0081053	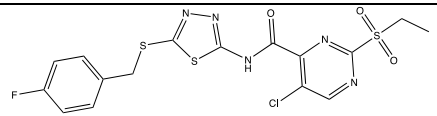	Enhanced	Yes	No	Undetermined	Early *et al.* (2019)
Ethoxzolamide	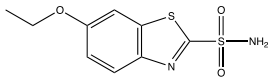	Non-specific	No	Undetermined	Inhibits PhoPR signaling, important TCS for pH-driven adaptations	Johnson *et al.* (2015)
Nitazoxanide	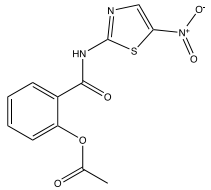	Enhanced	Yes	Yes	Stimulates autophagy and inhibits signaling by mTORC1, a major negative regulator of autophagy	de Carvalho *et al.* (2011); Lam *et al.* (2012)
Monensin	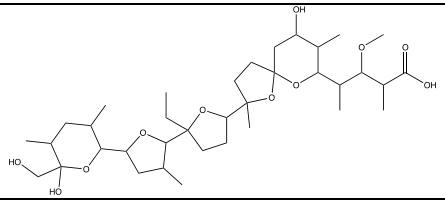	Undetermined, but is active at acidic pH	Yes	Yes	Sodium/hydrogen ionophore that disrupts pH_{IB} below limit of detection	Darby *et al.* (2013),

Table 1.1. (cont'd)

1048	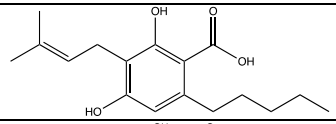	Selective	Yes	No	Undetermined	Darby *et al* (2013)
20E11	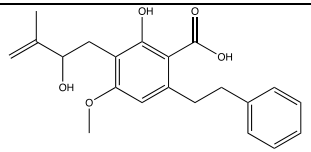	Selective	Yes	No	Undetermined	Darby *et al.* (2013)
1G9	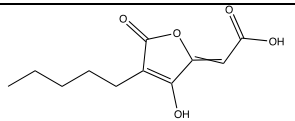	Selective	Yes	No	Undetermined	Darby *et al.* (2013)
23A6 (Agrimophol)	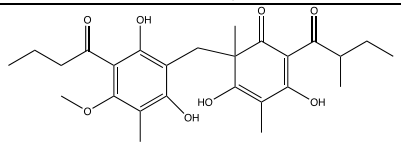	Enhanced	Yes	No	Targets Rv3852, protein of unknown function	Darby *et al.* (2013); Zhao *et al.* (2015)
4-OH-OPB	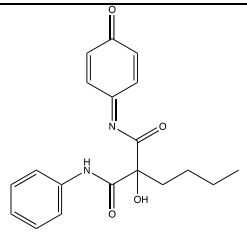	Selective	Undetermined	Undetermined	Covalent modification, formation of reactive oxygen species, and depletion of thiols and flavins	Gold *et al.* (2012)
Trifluoperazine	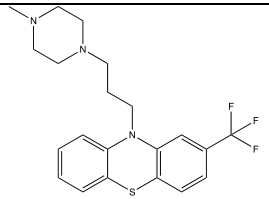	Enhanced	Undetermined	Undetermined	Inhibits protein and lipid synthesis, targets Rv1211, a Calmodulin-like-protein that complexes with calcium	Advani *et al.* (2012)
D157070	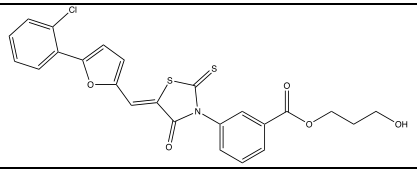	Non-specific, but requires non-replication at neutral and acidic pH	Undetermined	Undetermined	DlaT inhibitor, an enzyme that Mtb requires for resisting nitric oxide-derived reactive nitrogen intermediate stress	Bryk *et al.* (2008)

Table 1.1. (cont'd)

DPLG-2	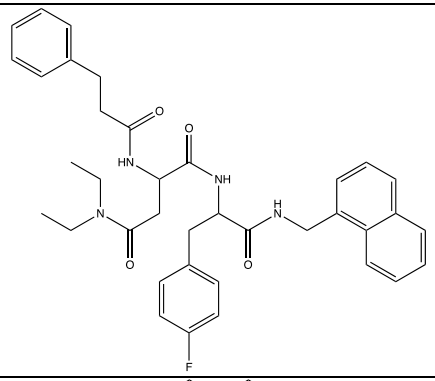	Undetermined, but is active at acidic pH with nitrosative stress	Undetermined	Undetermined	Mtb 20S proteasome inhibitor	Lin *et al.* (2013)
8-hydroxyquinoline	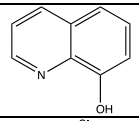	Non-specific	Undetermined	Undetermined	Undetermined	Darby *et al.* (2010)
CLBQ14	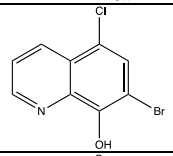	Undetermined, but is active at acidic pH	Undetermined	Undetermined	Targets Mtb's methionine aminopeptidase	Olaleye *et al.* (2011)
Compound 4	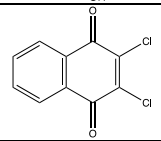	Undetermined, but is active at acidic pH	Undetermined	Undetermined	Targets Mtb's methionine aminopeptidase	Olaleye *et al.* (2010)
BO43	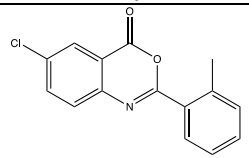	Selective	Yes	Undetermined	Inhibitor of MarP, acylates MarP and lowers Mtb's pH_{IB} and survival at low pH	Zhao *et al.* (2015)
Imidazopyradine series	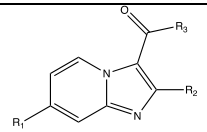	Undetermined, but is active at acidic pH	Yes	Undetermined	Targets QcrB, a component of the terminal cytochrome oxidase, and disrupts the electron transport chain	Moraski *et al.* (2013); O'Malley *et al.* (2018)
Itaconic acid	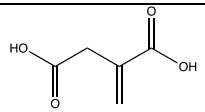	Selective	Yes, but only on propionate	Yes, but only on acetate or propionate	Itaconic acid covalently binds to isocitrate lyase, inhibiting its activity	Eoh and Rhee (2014); Kwai *et al.* (2021)

Table 1.1. (cont'd)

3-Nitropropionate	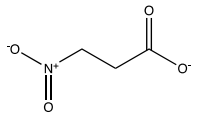	Selective	Undetermined	Undetermined	Inhibits succinate dehydrogenase activity (hypoxia) and isocitrate lyase activity (acidic pH)	Baker *et al.* (2014); Eoh and Rhee (2013); Muñoz-Elías *et al.* (2005)
Compound 16	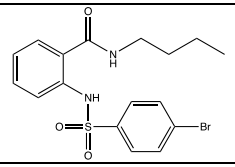	Selective	Undetermined	Yes	Undetermined	Smith *et al.* (2019)
Chloroquine	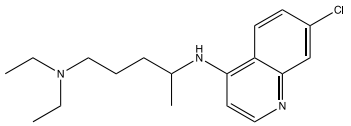	Undetermined	Undetermined	Undetermined	Inhibits phagosomal acidification, disrupts Mtb pH-and redox-dependent drug tolerance	Crowle *et al.* (1990); Matt *et al.* (2017); Mishra *et al.* (2019)

[a] pH-dependent activity determined based on whether the compound exhibits selective activity (only exhibits activity at acidic pH), enhanced activity (exhibits greater activity at acidic pH over neutral pH), or non-specific activity on Mtb growth under acidic conditions *in vitro.* Compound was listed as 'active at acidic pH' if acidic conditions were tested, but pH-dependent activity of compound remains undetermined.

The pyrazinamide conundrum: decoding its pH-dependent activity

Pyrazinamide (PZA) is an FDA-approved prodrug whose activation is achieved through Mtb PncA, a nicotinamdiase[116]. Moreover, PZA revolutionized TB therapy, decreasing treatment times from 9-12 months down to 6 months[117,118]. PZA exhibits high *in vivo* activity and has long been regarded for decades as having activity at acidic pH but not neutral pH *in vitro* [119,120]. Previous reports suggested that PZA's pH-dependent activity was due to the increased accumulation of the active form of pyrazinamide, pyrazinoic acid (POA), acting as a ionophore and uncoupler of the proton motive force, conferring cytoplasmic acidification (Table 1.2)[121,122]. In contrast, newer data suggests that PZA can sensitize Mtb at neutral pH when exposed to lower temperature, overexpression of PncA, nutrient-limited neutral pH medium, or *in vivo* (Table 1.2)[123-127]. Peterson *et al.* also show that PZA/POA does not exhibit robust ionophore activity as previously thought, and that its antitubercular activity is independent of intrabacterial acidification[124].

PZA resistance is associated with coenzyme A (CoA) and fatty acid metabolism[127,128]. Given that PhoPR is an important regulator of cell wall lipids (i.e. SL and acyltrehalose)[49,129] that utilize CoA-containing precursors[42], it is possible that PhoPR-regulated, acid-responsive genes could have an impact on PZA activity and requires further investigation. Additionally, a new study by Fontes and colleagues tries to dispel previous reports of increased PZA activity at neutral pH, instead claiming that the acid-base equilibrium of POA drives the pH-dependence of PZA activity[122]. The authors provide evidence showing that when the pH of the medium is lowered, equilibrium shifts from deprotonated, negatively charged POA towards protonated, neutral POA, which may act as an ionophore, uncoupling the proton motive force (Table 1.2)[122]. Fontes suggests that results by den Hertog *et al.* and Peterson *et al.* detailing PZA activity at neutral pH can be explained by the POA acid-base equilibrium, and proposes that the results of both studies are actually due to accumulation of protonated, neutral POA in solution and not anionic POA[122]. For this reason, the data surrounding PZA activity and its disputed impact on pH homeostasis is a developing and hotly-debated area of study[122,130]. Numerous mechanisms of action for PZA have been proposed, with an equally great number of studies opposing said models[130]. Determining whether PZA has pH-dependent activity or whether it acts as an ionophore, shows that classifying PZA and likely other compounds in terms

of how they target or modulate pH-dependent pathways is complex and open for interpretation. PZA remains part of the current therapy regimen to treat drug sensitive, multidrug (MDR) and extensively drug-resistant (XDR) TB[1]. This is in part due to PZA's great lung tissue penetration among patients with a variety of different pulmonary TB lesion types, and highlights its versatility in treating both drug-susceptible and drug-resistant TB in clinical settings[131].

Table 1.2. Summary of studies supporting and refuting the PZA ionophore hypothesis[a]

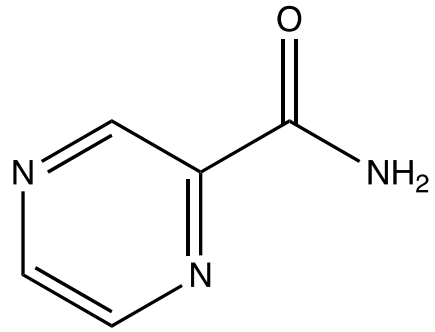

In support: Ionophore hypothesis	Against: Ionophore hypothesis
• Increased accumulation of the active form of pyrazinamide at low pH, pyrazinoic acid (POA), acts as an ionophore and uncoupler of the proton motive force, acidifying the cytoplasm. [Zhang *et al.* (1999); Zhang *et al.* (1999); Fontes *et al.* (2020)] • PZA exhibits enhanced activity at acidic pH [McDermott and Tompsett (1954)] • PZA activity is driven by acid-base equilibrium and the accumulation of protonated, neutral POA [Fontes *et al.* (2020)]	• POA does not induce cytoplasmic acidification or disrupt the proton motive force [Peterson *et al.* (2015)] • POA sensitizes Mtb at neutral pH [Peterson *et al.* (2015); den Hertog *et al.* (2016); Gopal *et al.* 2016; Via *et al.* (2015); Lanoix *et al.* (2016)] • POA does not act as an ionophore [Peterson *et al.* 2015]

[a] Table derived from Gopal *et al.* (2019).

Combatting phenotypically drug tolerant Mtb at acidic pH

Bacteria whose growth is halted by acidification of growth media, Mtb included, can become tolerant to antibiotics in a phenomenon known as phenotypic drug tolerance[132-135]. However, previous work from our lab has shown that the *eag* variants in *ppe51* render Mtb susceptible to INH and RIF treatment specifically at acidic pH while WT is able to persist under these treatment conditions[12]. Faster replication in macrophages is associated with enhanced killing[33]. In contrast, slower growth rates imposed by macrophage-derived pressures correlate with greater Mtb survival[51], supporting that *eag* variants have enhanced sensitivity to antibiotic treatment because they are unable to establish NRP. Likewise, PhoPR functions to slow Mtb growth at acidic pH, and knockout *phoPR* mutants are highly attenuated *in vivo*[10,110]. A recent study by Bellerose and colleagues showed that transposon mutants of *phoP* and *ppe51* were hypersensitive to multidrug treatment in mice[55]. The authors generated a *Δppe51* mutant and found that it was significantly more sensitive to pyrazinamide (PZA) treatment during mouse infection compared to WT Mtb[55]. Together, these studies indicate a role for WT PPE51 and PhoPR in modulating Mtb adaptation to acidic pH and establishing phenotypic drug tolerance in Mtb.

Recent work by Mishra and colleagues show that acidic pH can also generate replicating, drug tolerant Mtb[109]. They found that phagosomal acidification is required for establishing phenotypically drug tolerant Mtb by altering its redox physiology, possibly mediated by PhoPR[37,109]. Interestingly, Mishra found that phagosomal acidification drives heterogeneity in the redox physiology of actively replicating Mtb, which exhibit a more reduced mycothiol redox potential and antioxidant capacity. Additionally, pharmacological disruption of phagosomal acidification with chloroquine (Figure 1.1) was able to counteract drug tolerance *in vivo*, supporting a link between phagosomal pH, redox metabolism, and phenotypic drug tolerance[109]. These data are consistent with findings by Liu *et al.*, who observed enhanced drug tolerance in activated macrophages was driven in part by acidic pH[135].

Chemically disrupting pH-adaptation pathways to prevent Mtb from entering a state of non-replicating persistence or generating a reduced redox potential, and thus establishing drug tolerance, is a desirable achievement for future TB therapeutics[7]. Proof-of-concept for this approach was demonstrated

for the drug chloroquine, which disrupts pH- and redox-homeostasis to kill Mtb [109]. Phenotypic whole-cell HTS and target-based screening methods can be readily adapted in future studies to find compounds that inhibit Mtb phenotypic drug tolerance at acidic pH. Similarly, these approaches can also be harnessed to find new compounds that probe acid adaptive pathways and proteins which may render Mtb hypersensitive, specifically in combination with existing anti-TB drugs like PZA. Given that ETZ inhibits *phoPR* regulon induction, it would be interesting to see whether combinatorial therapy of ETZ and PZA could yield similar hypersensitivity that was observed in Mtb mutants lacking functional *phoP*[55]. Shortening TB therapy is a key challenge in combatting the TB epidemic, and it is possible targeting pH-dependent physiologies will play an important role in defining new, shorter treatment regimens.

Concluding Remarks

Targeting pH-driven adaptation has been shown to have promising pre-clinical implications for treating TB infections. Furthermore, basic research studies investigating Mtb's metabolic and growth adaptation to acidic pH show that *in vitro* acid growth arrest is a carbon source-and-pH-dependent type of growth arrest. My work has sought to investigate both of these concepts. Chapter 2 explores the mechanism of action of a pH-dependent compound, AC2P20, and seeks to identify physiologies important for acidic pH-dependent adaptation. In Chapter 3, I conduct studies on the function PPE51 and investigate its role in acid growth arrest, specificity for growth on individual carbon sources, metabolic regulation, and role in pathogenesis by genetically, phenotypically, mechanistically, and biochemically characterizing PPE51 mutants incapable of arresting their growth at acidic pH. In Chapter 4, I investigate why ETZ inhibits the PhoPR pathway and examine potentials links between carbonic anhydrase activity, CO_2-sensing, and PhoPR signaling and their impact on Mtb pathogenesis. Together, these studies show that we can use chemical biology and genetics to define mechanisms of Mtb pH-driven adaptation and their role on pathogenesis.

CHAPTER 2 – AC2P20 selectively kills *M. tuberculosis* at acidic pH by depleting free thiols

The discovery and characterization of AC2P20 presented in this chapter has been previously published:

Dechow, S. J., Coulson, G. B., Wilson, M. W., Larsen, S. D. & Abramovitch, R. B. AC2P20 selectively kills *Mycobacterium tuberculosis* at acidic pH by depleting free thiols. ***RSC Advances*** 11, 20089-20100, doi:10.1039/D1RA03181C (2021).

Author Contributions

S.J.D., G.B.C., and R.B.A. conceived the project. S.J.D performed the time-dependent and concentration-dependent killing assays, RNAseq analysis, mass spectrometry, free thiol assay, and ROS assay. G.B.C. conducted the initial characterization studies including Mtb and *M. smegmatis* EC_{50} assays and the RNAseq experiment. M.W.W. and S.D.L. contributed to mass spectrometry analysis. S.J.D. and R.B.A. wrote the manuscript.

Abstract

Mycobacterium tuberculosis (Mtb) senses and adapts to host immune cues as part of its pathogenesis. One environmental cue sensed by Mtb is the acidic pH of its host niche in the macrophage phagosome. Disrupting the ability of Mtb to sense and adapt to acidic pH has the potential to reduce survival of Mtb in macrophages. Previously, a high throughput screen of a ~220,000 compound small molecule library was conducted to discover chemical probes that inhibit Mtb growth at acidic pH. The screen discovered chemical probes that kill Mtb at pH 5.7 but are inactive at pH 7.0. In this study, AC2P20 was prioritized for continued study to test the hypothesis that it was targeting Mtb pathways associated with pH-driven adaptation. RNAseq transcriptional profiling studies showed AC2P20 modulates expression of genes associated with redox-homeostasis. Gene enrichment analysis revealed that the AC2P20 transcriptional profile had significant overlap with a previously characterized pH-selective inhibitor, AC2P36. Like AC2P36, we show that AC2P20 kills Mtb by selectively depleting free thiols at acidic pH. Mass spectrometry studies show the formation of a disulfide bond between AC2P20 and reduced glutathione, supporting a mechanism where AC2P20 is able to deplete intracellular thiols and dysregulate redox homeostasis. The observation of two independent molecules targeting free thiols to kill Mtb at acidic pH further supports that Mtb has restricted redox homeostasis and sensitivity to thiol-oxidative stress at acidic pH.

Introduction

Mtb pathogenesis is driven by its ability to exploit and adapt to the intracellular host environment. During pathogenesis, Mtb encounters a variety of stressors including nitrosative, oxidative, acidic pH, and hypoxic stress [136]. In response to these stresses, Mtb alters its physiology in order to survive the hostile macrophage environment and modulate expression of virulence genes critical for its pathogenicity. Acidic pH is an initial environmental cue that Mtb senses upon infection of the host macrophage[31,46]. For survival within the resting macrophage, Mtb inhibits fusion of the phagosome and lysosome and resides in a mildly acidic phagosome (pH 6.4)[15]. Activation of the macrophage leads to phagosome acidification and Mtb resists this acid stress, maintaining a relatively neutral cytoplasmic pH, even at pH <5.0[8,9,81,137]. In addition to expressing mechanisms to survive acid stress, Mtb also exhibits pH-and-carbon source dependent growth adaptations. Mtb will completely arrest its growth in minimal media buffered to pH 5.7 with glycerol as the sole carbon source[37]. During this growth arrest, Mtb exhibits carbon source specificity, and will only arrest growth on glycolytic carbon sources (i.e. glucose and glycerol)[37]. However, when given specific carbon sources (i.e. phosphoenolpyruvate, pyruvate, acetate, oxaloacetate, and cholesterol), Mtb resuscitates its growth at pH 5.7 in minimal media, and thus, exhibits direct metabolic remodeling during pH stress[37]. Collectively, these studies show that in response to acidic pH, Mtb has multiple mechanisms in place whereby it alters its physiology for survival and virulence.

When Mtb is cultured at acidic pH or in macrophages, the bacterium has an imbalanced redox state with a more reduced cytoplasm[37,138], a phenomenon referred to as reductive stress[31,139]. It is hypothesized that acidic pH may cause redox imbalances due to adaptations of the electron transport chain that promote oxidative phosphorylation while maintaining cytoplasmic pH homeostasis[31]. These adaptations could lead to an accumulation of reduced co-factors such as NADH/NADPH. Implications for this type of reductive stress include altered Mtb metabolism, slowed growth, and non-replicating persistence. Fatty acid synthesis is thought to help mitigate reductive stress via the oxidation of NADPH and is supported by the induction of genes associated with lipid metabolism and anaplerosis at low pH[31,37,39,46]. One of these induced genes is WhiB3, a regulatory protein that senses Mtb's intracellular redox state through its [4Fe-4S] cluster and acts

to mitigate reductive stress[139-141]. WhiB3 is thought to counter this reductive stress via its role as a metabolic regulator, whereby it controls the anabolism of virulence lipids: poly- and diacyltrehalose (PAT/DAT), pthiocerol dimycocerosate (PDIM), and sulfolipids (SL-1)[141]. Production of these methyl-branched polar lipids requires NADPH; therefore, WhiB3 helps alleviate reductive stress by channeling excess reductants into fatty acid synthesis[141]. This results in the re-oxidation of reducing equivalents needed to maintain intracellular redox homeostasis. Changes in central metabolism, including the induction of anaplerotic pathways driven by isocitrate lyases (*icl*) and phosphoenolpyruvate carboxykinase (*pckA*) at acidic pH[12], and the dependence on carbon sources that feed the anaplerotic node[37], may also provide metabolic flexibility required to balance redox homeostasis at acidic pH.

Mechanisms important for pH adaptation (i.e. metabolism, cytoplasmic pH-homeostasis, and redox homeostasis) present an attractive source of novel targetable physiologies for drug discovery. pH homeostasis can be targeted by compounds like the benzoxazinone, BO43, which inhibits the serine protease MarP, resulting in the disruption of intrabacterial pH homeostasis[75]. Additionally, ionophores have also been discovered to kill Mtb at acidic pH[70,71]. Respiration has been shown to be important for maintaining pH-homeostasis[142,143]. Compounds targeting respiration include bedaquiline (BDQ), a F_1F_o-ATP-synthase inhibitor, and the small molecule, C10. BDQ has been shown to act as an ionophore and disrupt the Mtb transmembrane pH gradient[144], while C10 exhibits enhanced Mtb killing at acid stress[92]. Thiol-redox homeostasis also has implications as a targetable pH-dependent physiology. Auranofin depletes free thiols by targeting an essential thioredoxin reductase (TrxB2)[94,145]. Together, these results demonstrate the druggability of physiologies important for acidic pH-dependent adaptation.

PhoPR, a two-component regulatory system (TCS), is important for regulating Mtb virulence and intracellular survival[10,39,49]. Additionally, signaling from PhoPR has been shown to play an important role in pH adaptation[37,46,48]. Our lab previously conducted a reporter based, whole cell high-throughput screen (HTS) of > 220,000 small molecules for inhibitors of PhoPR signaling at acidic pH[50,69]. Compound activity was assessed in rich media buffered to pH 5.7 using a pH-inducible Mtb fluorescent reporter strain to identify either direct inhibitors of the PhoPR regulon or pH-selective inhibitors of Mtb growth. This screen

successfully identified inhibitors of PhoPR-dependent signaling, including the carbonic anhydrase (CA) inhibitor, ethoxzolamide (ETZ)[50]. This screen also identified compounds that selectively kill Mtb at pH 5.7 but not pH 7.0 and do so independently of PhoPR. One of these compounds, called AC2P36 (5-chloro-N-(3-chloro-4-methoxyphenyl)-2-methylsulfonylpyrimidine-4-carboxamide),[69] functions by directly depleting intracellular Mtb thiol pools, by forming covalent adducts with free thiols. Depletion of free thiols interferes with redox buffering pathways and induces formation of cytoplasmic reactive oxygen species (ROS) at acidic pH, thus sensitizing Mtb to thiol-oxidative stress[69]. AC2P36 also selectively kills Mtb and potentiates the activity of TB drugs: isoniazid, clofazimine, and diamide. We hypothesize that reductive stress at acidic pH selectively sensitizes Mtb to thiol targeting activity of AC2P36. These results indicate that free thiols are a pH-selective target, and that Mtb sensitivity to killing is enhanced under thiol oxidative stress.

In this study, we report on a new chemical probe isolated from a prior screen, AC2P20 (N-1,3-benzothiazol-2-yl-2-[(4,6-dioxo-5-phenyl-1,4,5,6-tetrahydropyrimidin-2-yl)thio]acetamide) (Figure 2.1A), that selectively kills Mtb at acidic pH. AC2P20 was identified as a PhoPR-independent, pH-selective inhibitor of Mtb growth. Through transcriptional profiling we observed that genes modulated by AC2P20 treatment significantly overlap with genes modulated by AC2P36 treatment. Although both compounds are structurally distinct, like AC2P36, AC2P20 also exhibits killing of Mtb at pH 5.7, disrupts thiol homeostasis by depleting intracellular free thiol pools, and increases reactive oxygen species (ROS) production. Thus, AC2P20 is a second structurally unique pH-selective chemical probe that exhibits thiol-depletion as a mechanism-of-action for killing at acidic pH. This finding further reinforces the vulnerability of Mtb to perturbations of redox homeostasis at acidic pH.

Experimental

Bacterial strains and growth conditions

M. tuberculosis strains Erdman and CDC1551 and *M. smegmatis* strain mc^{2}155 (expressing GFP from a replicating plasmid) were used in all experiments unless specified. Mtb was cultured in Middlebrook 7H9

media enriched with 10% oleic acid-albumin-dextrose-catalase (OADC), 0.05% Tween-80, and glycerol. Cultures were maintained in vented T-25 culture flasks and grown at 37 °C and 5% CO_2. To maintain a specific pH, 7H9 media was strongly buffered to pH 7.0 with 100 mM 3-(N-morpholino)propanesulfonic acid (MOPS) or pH 5.7 with 100 mM 2-(N-morpholino)ethanesulfonic acid (MES). Mtb was grown to mid-late log phase (OD_{600} 0.5-1.0) before exposure to buffered 7H9 for use in experiments detailed below. *M. smegmatis* cultures were grown in identical 7H9 media conditions at a starting OD_{600} of 0.05 at 37°C in a shaking incubator (200 rpm).

Selection for AC2P20 resistant mutants

Mtb CDC1551 and Mtb Erdman strains were grown to an OD_{600} of 0.6-1.0, spun down, and resuspended in 7H9 media buffered to pH 5.7. Mtb cells were plated at 10^9 cells per mL on 7H10 agar media buffered to pH 5.7 and supplemented with 10 µM, 20µM or 40 µM AC2P20. Plates were incubated at 37°C for over 12 weeks without any significant isolated colonies appearing. This experiment was performed three times with similar results.

Transcriptional profiling and data analysis

Mtb cultures were grown at 37°C and 5% CO_2 in standing T-25 culture flasks to an OD_{600} of 0.5 in 8 mL of 7H9 buffered media. Treatment conditions examined include (i) 20µM AC2P20 at pH 5.7 and (ii) an equivalent volume of DMSO at pH 5.7 as the baseline control. Each culture was incubated for 24 hours and treatment conditions were conducted in two biological replicates. Following incubation, total bacterial RNA was extracted as previously described[37,46] and sequencing data was analyzed using SPARTA (ver. 1.0)[146]. Genes identified were filtered based on $\log_2$ CPM < 5 and $\log_2$ FC < 1. A Chi-square analysis with Yates correction was conducted to test the statistical relationship between gene overlap with the AC2P36 transcriptional profile as described by Coulson *et al.*[69]. The RNAseq data has been deposited at the GEO database (accession # GSE151884).

Half-maximal effective concentration (EC_{50}) determination and spectrum of activity in other mycobacteria

Mtb cultures were incubated in buffered 7H9 media (pH 5.7 or pH 7.0) at a starting OD_{600} of 0.2, with 200 µL aliquoted into 96-well microtiter assay plates (CoStar #3603). Cultures were treated with a 2.5-fold dose-response of AC2P20 (80 µM-0.13 µM) and incubated standing for 6 days at 37 °C and 5% CO_2, with bacterial growth assessed by optical density (OD_{600}). Cultures treated with an equivalent volume of DMSO or 0.3 µM rifampin were used as negative and positive controls, respectively. Each condition was performed in duplicate and representative of three individual experiments. EC_{50} values were determined using GraphPad Prism software (ver. 7.0). AC2P20 activity against *M. smegmatis* was also performed in 96-well assay plates in 7H9 buffered media (pH 7.0 or 5.7). *M. smegmatis* cultures were seeded at a starting OD_{600} of 0.05 with 200 µL aliquoted into each well. An 8-point 2.5-fold dilution series starting at 80 µM was conducted and cultures were incubated for 3 days with shaking (100 rpm). Plates were read for GFP fluorescence.

Mycobactericidal activity of AC2P20

Mtb was initially cultured in 7H9 media (pH 5.7 or 7.0) at a starting OD_{600} of 0.2 in 96-well assay plates. Cultures were treated with a 2.5-fold dose-response of AC2P20 (80 µM to 0.33 µM). An equivalent volume of DMSO was included as a control. Each treatment condition was conducted in triplicate and incubated for 7 days. Following incubation, treated wells were serially diluted in 1× Phosphate-Buffered Saline (PBS) and plated for colony forming units (CFUs) on 7H10 agar plates supplemented with 10% OADC and glycerol. Bactericidal activity was determined by comparing CFUs from the initial inoculum to CFUs following treatment.

Cytoplasmic pH-homeostasis

Mtb washed with PBS (pH 7.0) was labelled with Cell Tracker 5′-chloromethylfuoroscein diacetate (CMFDA) and analyzed using methods previously described[147]. Mtb treated with AC2P20 in PBS (pH 5.7)

was assayed for cytoplasmic pH changes over the course of 24-hours. Excitation ratio results were converted to pH via a standard curve generated using nigericin-treated Mtb in buffers of known pH. Treated Mtb results were then compared to the DMSO and nigericin negative and positive controls, respectively.

Measurement of endogenous reactive oxygen species

CellROX Green fluorescent dye (Invitrogen) was used to detect accumulation of endogenous reactive oxygen species (ROS) in Mtb as previously reported[69,148]. Mtb grown to mid-late log phase was pelleted and re-suspended at a starting OD_{600} of 0.5 in 5 mL of buffered 7H9 media (pH 5.7 or 7.0) lacking catalase. Cultures prepared in duplicate were treated with two separate concentrations of AC2P20 (2 μM and 20 μM) and incubated for 24 hours at 37 ℃. Following treatment, cultures were incubated with 5 mM CellROX Green (Thermo Fisher) for 1 hour at 37 ℃ and then washed twice with 1× PBS + 0.05% Tween80. Washed cells were resuspended in 0.6 mL 1× PBS and aliquoted into triplicate wells in 96-well microtiter plates. Wells were measured for fluorescence and optical density, with florescence being subsequently normalized to cell growth for ROS analysis. AC2P36 (2 μM and 20 μM) and equivalent volumes of DMSO served as positive and baseline controls, respectively.

Detecting intracellular free thiol pools

Mtb grown in 7H9 OAD media lacking catalase was inoculated at a starting OD_{600} of 0.25 in 8 mL of buffered 7H9 OAD media (pH 5.7 or 7.0) also lacking catalase. Cultures were prepared in duplicate and treated with either DMSO, 2 μM AC2P20, 20 μM AC2P20, 20 μM AC2P36, or 20 μM auranofin. Treated cultures were incubated for 24 hours at 37 ℃, normalized by OD_{600}, and washed twice in 1× PBS supplemented with 0.05% tyloxapol. Cells were resuspended in 0.75 mL of thiol and redox assays buffer (100 mM potassium phosphate pH 7.4, and 1 mM EDTA) and lysed by bead beating for 2 minutes at room temperature. Supernatants were removed and saved for analysis using the Cayman thiol detection assay kit (Caymen Chemical) as previously described[69]. Thiol concentrations were measured in (nM) against a glutathione standard.

Mass spectrometry

Mass spectrometry was used to detect the formation of AC2P20 adducts. Aqueous solutions of 80 µM AC2P20 were prepared separately and incubated with either reduced glutathione (100 µM), N-acetylcysteine (100 µM), or hydrogen peroxide (100 µM) for 1 hour at room temperature in Tris-HCl buffer (pH 5.7, 7.0, or 8.5). Samples were analyzed using the Waters Xevo G2-XS QTof mass spectrometer (Milford, MA, USA) in both positive and negative electrospray ionization (ESI) modes. Samples were run with the following ion source parameters: capillary voltage, 2 kV; sampling cone, 35 V; source temperature, 100°C; desolvation temperature, 350°C; cone gas flow, 25 L/h; desolvation gas flow, 600 L/h. Ultra-performance liquid chromatography (UPLC), using water and acetonitrile as solvents, was carried out for the chromatographic separation of compounds. The LC parameters were as follows: flow rate, 0.2 mL/min; water/acetonitrile solvent gradient, 50/50 for 2 min. Mass analysis was performed at <1500 Da. This experiment was repeated twice in duplicate with similar results seen at both positive and negative ESI.

Results

AC2P20 exhibits pH-dependent growth inhibition of M. tuberculosis

Two high throughput screens (HTS) using Mtb fluorescent reporters were conducted in order to detect inhibitors of two separate Mtb two-component regulatory systems (TCS): DosRST and PhoPR[4,50,69,149]. A chemical library of >220,000 small molecules was previously screened, with compound hits being defined as those that inhibited reporter fluorescence or Mtb growth. These compounds were further classified as TCS target inhibitors or growth inhibitors. The screens only differed in the reporter strain used and the pH of the medium, which was neutral or acidic in the DosRST and PhoPR inhibitor screens, respectively. Comparing growth inhibiting hits from these two screens identified a subset of compounds that selectively inhibited Mtb growth at acidic pH independent of PhoPR signaling. These compounds were classified as pH-selective growth inhibitors if they exhibited >50% growth inhibition at acidic pH and < 10% inhibition at neutral pH. AC2P20 (N-1,3-benzothiazol-2-yl-2-[(4,6-dioxo-5-phenyl-1,4,5,6-tetrahydropyrimidin-2-yl)thio]acetamide) (Figure 2.1A) exhibited >5-fold selectivity at acidic pH

and was characterized as one of these pH-selective inhibitors of Mtb growth. The pH-dependent activity of AC2P20 was confirmed by determining its half-maximal effective concentration (EC_{50}). Mtb treated with an 8-point dose-response of AC2P20 for six days at pH 5.7 results in dose-dependent growth inhibition with an EC_{50} of 4.3 μM, however, has a >10-fold higher EC_{50} of ~60 μM at pH 7.0 (Figure 2.1B). AC2P20 also exhibits mycobacterial selectivity for Mtb compared to *M. smegmatis*, which has an EC_{50} > 80 μM at acidic pH and does not exhibit growth inhibitory activity at neutral pH (Figure A.2.1A). Time-dependent and concentration-dependent killing assays were conducted to define whether AC2P20 is bactericidal or bacteriostatic. Mtb treated with 20 μM AC2P20 exhibits pH-selective inhibition of Mtb growth in acidic conditions and results in approximately 2-log fold reduction in CFUs over 5 days (Figure 2.1C). In contrast, DMSO controls and AC2P20 treatment in neutral conditions have no impact on growth. The concentration-dependent killing assay shows that AC2P20 is bactericidal at ~32 μM and bacteriostatic at 12 μM (Figure 2.1D). Cytoplasmic pH was measured to determine whether AC2P20 functions as an ionophore. Treatment with AC2P20 does not modulate the cytoplasmic pH of Mtb compared to the nigericin positive control (Figure A.2.1B). Together, these data show that AC2P20 activity is pH-dependent, bactericidal, and does not alter Mtb cytoplasmic pH homeostasis.

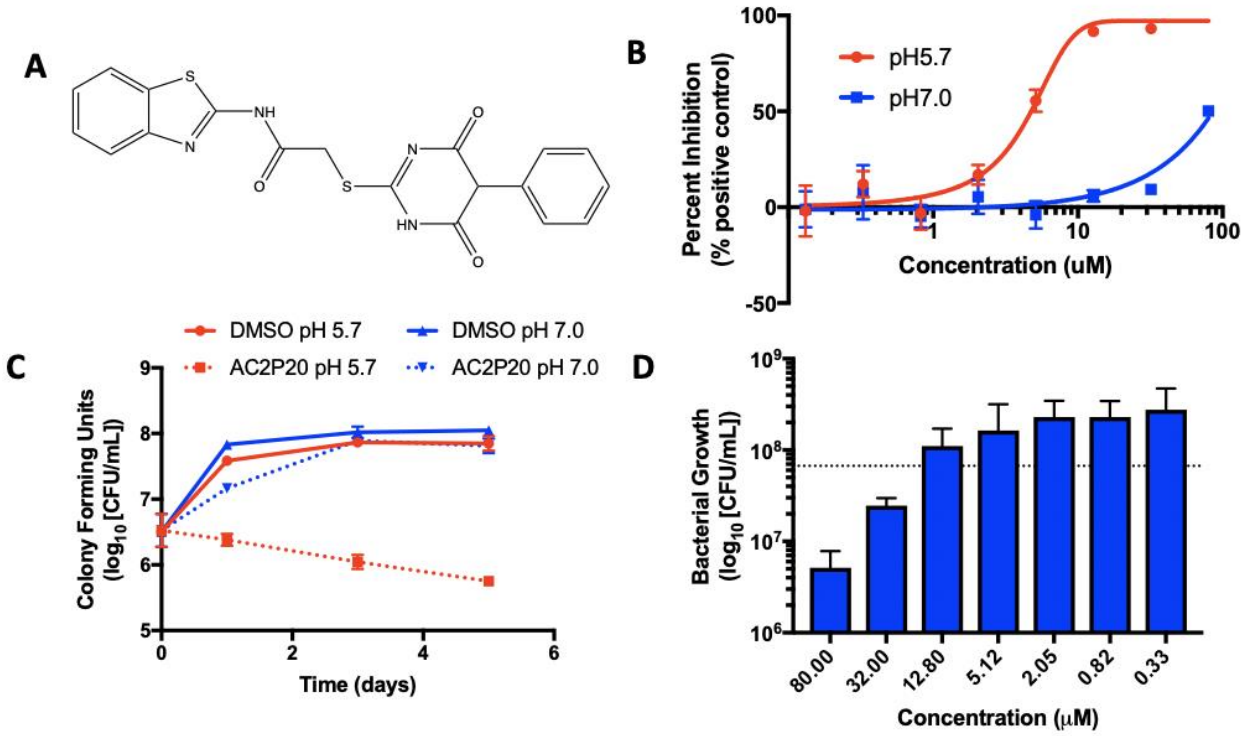

Figure 2.1. AC2P20 inhibits Mtb growth in a pH-dependent manner. A) The chemical structure of AC2P20 ((N-1,3-benzothiazol-2-yl-2-[(4,6-dioxo-5-phenyl-1,4,5,6-tetrahydropyrimidin-2-yl)thio]acetamide). **B)** Mtb growth is inhibited in a dose-dependent manner when treated with AC2P20 at pH 5.7 and exhibits an EC_{50} of 4.3 μM following six days of treatment. Treatment with AC2P20 at pH 7.0 Mtb requires concentrations >60 μM to see growth inhibitory effects. **C)** Mtb treated with 20 μM of AC2P20 and grown in buffered 7H9 media (pH 5.7) for 5 days shows time-dependent killing as indicated by ~100-fold reduction in viability compared to the DMSO control. Time-dependent killing is not observed in neutral conditions. **D)** Mtb was treated with a dose-response of AC2P20 at pH 5.7 for 7 days, then assessed for dose-dependent killing by plating for colony-forming units (CFUs). The dotted line indicates the CFUs plated on Day 0.

AC2P20 induces a thiol oxidative stress response similar to AC2P36

To isolate resistant mutants and thereby find potential targets for AC2P20, 10^9 Mtb cells were plated on 7H10 agar media buffered to pH 5.7 containing 10 µM, 20 µM or 40 µM AC2P20. Despite several weeks of incubation each time at 37°C, no spontaneous mutants were isolated from multiple rounds of screening for resistant mutants to AC2P20. Following our resistance screening attempts, transcriptional profiling was conducted to define Mtb physiologies targeted following AC2P20 treatment. Mtb CDC1551 cultures were prepared in rich media (pH 5.7) and treated with 20 µM AC2P20 or DMSO control for 24 hours. Mtb treated with AC2P20 caused induction of 156 genes (>2-fold, $q < 0.05$) and repression of 81 genes (>2-fold, $q < 0.05$) (Figure 2.2A). Using MycoBrowser[150] to classify gene function, we found that the functional pathway most induced by AC2P20 (excluding conserved hypotheticals) was intermediary metabolism and respiration (Figure 2.2B). Differentially induced genes included genes involved in sulfur metabolism (*cysT, sirA, mec*), transcriptional regulation of the stress response (*sigH, sigB, rshA*), and redox homeostasis (*katG, trxB1, trxC*) (Figure 2.2C). Notably, differentially regulated genes from AC2P20 treated cells overlapped with differential gene expression profiles previously characterized for the pH-selective Mtb growth inhibitor, AC2P36[69]. Gene enrichment analysis showed a statistically significant overlap between groups AC2P20 and AC2P36 differentially expressed genes ($p<0.0001$) (Figure 2.2D). Based on RNAseq data and the gene enrichment analysis, both AC2P36 and AC2P20 exhibit a transcriptional profile indicative of redox and thiol-oxidative stress. For example, both transcriptomes show induction of the alternative sigma factor SigH regulon which plays a central role in regulating thiol-oxidative stress during Mtb pathogenesis[151-153]. SigH is responsible for regulating genes involved in thiol metabolism including thioredoxin (*trxC*), thioredoxin reductases (*trxB1, trxB2*), and cysteine biosynthesis and sulfate transport (*cysO, cysM, cysA, cysW, cysT*). Additionally, SigH-regulated *moeZ* is induced in both transcriptomes, which is involved in sulfation of enzymes and plays a dual role in molybdopterin biosynthesis and CysO activation[154]. While the SigH regulon exhibits a direct response to thiol-oxidative stress, it is also highly induced under oxidative stress conditions[151]. In addition, non-SigH regulated oxidative stress responsive genes include *katG* (catalase-peroxidase), *thiX* (a thioredoxin), and *furA* (transcriptional regulator), which

are upregulated in both AC2P20 and AC2P36. Interestingly, Rv0560c, a methyltransferase, is the most upregulated gene in Mtb treated with AC2P20, AC2P36, or C10[69,92]. Rv0560c is induced in mutants resistant to a cyano-substituted fused pyrido-benzimidazole, known as compound 14, and provides resistance by methylating and inactivating compound 14[155]. Rv0560c is not directly upregulated by the SigH regulon or oxidative stress, but rather by salicylate[156], and may be involved in the synthesis of redox cycling agents[45,157,158]. Therefore, induction of thiol-homeostasis metabolism genes and *katG* in response to AC2P20 treatment suggests an increased need for the generation of low molecular weight thiols, which are important for detoxification of toxic reactive oxygen species (ROS) and maintaining redox homeostasis in Mtb.

Despite significant overlap between the AC2P20 and AC2P36-treated regulons, there are pathways that are distinctly different in the transcriptional profiling comparisons. Classification of gene function for the 180 AC2P36-induced genes (>2-fold, $q < 0.05$) showed that the functional category most induced (excluding conserved hypotheticals) was intermediary metabolism and respiration, the same as AC2P20. However, major differences were noted between categories of both induced gene sets for AC2P20 and AC2P36. For example, induction of lipid metabolism genes comprised roughly 3.33% of the total genes induced by AC2P36 compared to 12.82% for AC2P20 (Figure 2.2B and A.2.2A). Noticeably, AC2P20 appeared to upregulate several mycolic acid biosynthesis pathway and operon genes (*fas*, *acpM*, *kasA*, *accD6*) (Figure A.2.2B). In contrast, these genes were repressed following AC2P36 treatment. Other lipid metabolism genes not observed in AC2P20 transcriptional data, but actively repressed by AC2P36 include *scoA/B*, *accD1*, *Rv3087*, and *fadE35*[69]. Additionally, transcriptional profiling showed that methylcitrate synthase and methylcitrate dehydratase genes (*prpC* and *prpD*, respectively) were oppositely modulated in both regulons; AC2P20 repressed *prpC/D* expression while their expression was induced by AC2P36 (Figure A.2.2B). Other functional categories that saw large quantitative changes between both transcriptional profiles include cell wall and cell wall processes and virulence, detoxification and adaptation. Fewer cell wall and cell wall processes genes were induced by AC2P36 compared to AC2P20, while the number of virulence, detoxification and adaptation functional genes were increased following

AC2P36 treatment (Figure A.2.2A). The transcriptional differences observed between both regulons demonstrates that despite the shared similarities in regulation of thiol-redox homeostasis and regulatory genes, distinct differences exist between how pathways are modulated following AC2P20 and AC2P36, with lipid metabolism being most notable.

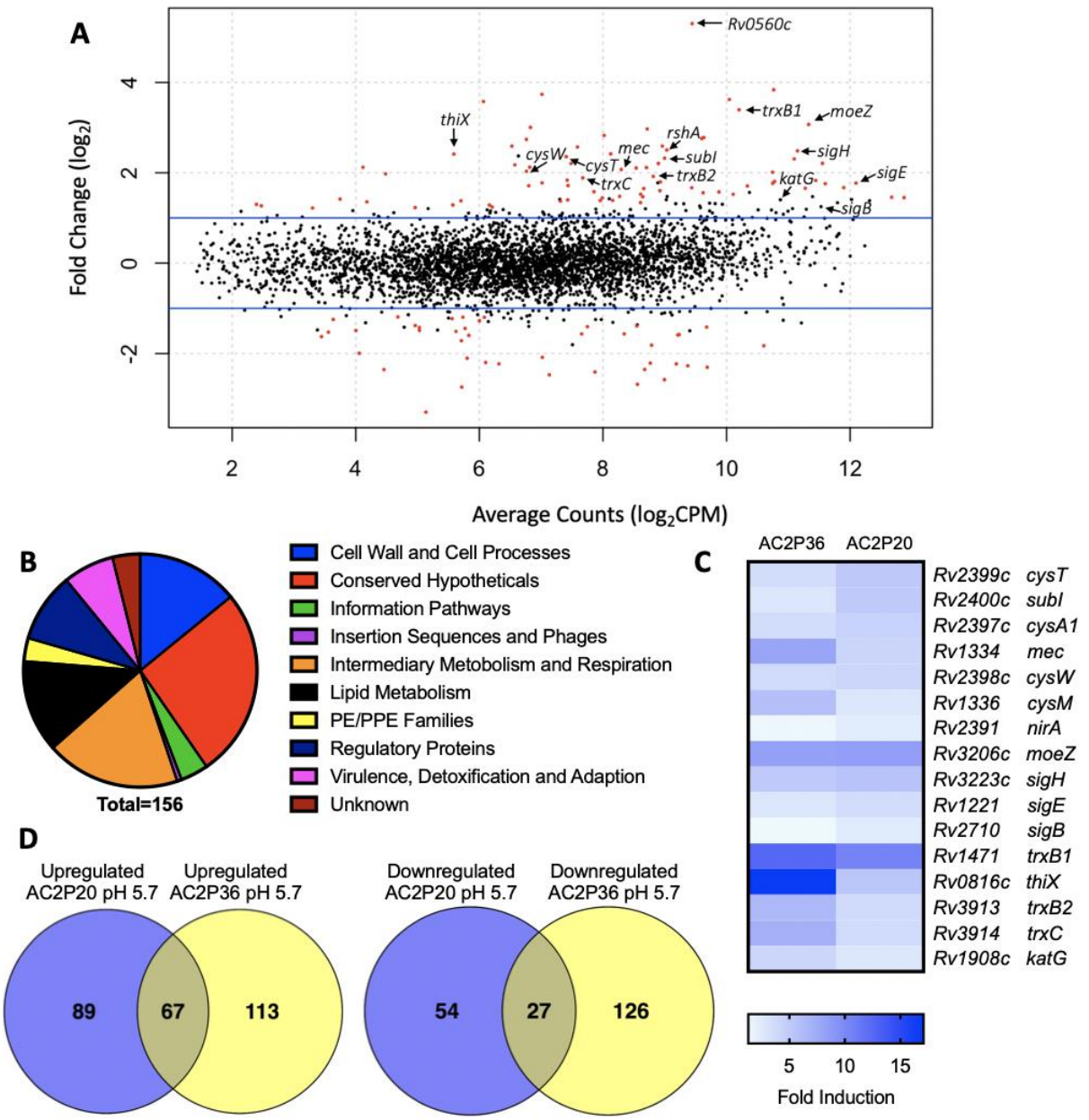

Figure 2.2. AC2P20 treatment promotes a thiol-and-redox-stress response. A) Mtb differential gene expression data after being treated for 24 hours with 20 µM AC2P20 at pH 5.7. Genes indicated include those involved in sulfur metabolism, transcriptional regulation, and redox homeostasis. Statistically significant genes ($q < 0.05$) are highlighted in red. **B)** A pie chart depicting the functional classification breakdown of significantly induced genes (>2-fold, $q < 0.05$) following the analysis of AC2P20-treated Mtb RNA-seq profile. **C)** Heatmap comparing 16 upregulated genes (between AC2P20 and AC2P36 at pH 5.7 that are involved in sulfur metabolism, transcriptional regulation, and redox homeostasis . Genes were annotated with the H37Rv genome. **D)** Venn diagrams comparing upregulated and downregulated gene overlap (>2-fold, $q < 0.05$) between AC2P20-treated and AC2P36-treated Mtb [29].

AC2P20 forms an adduct with the low molecular weight thiol, GSH

Although AC2P36 and AC2P20 have distinct structures, both compounds contain a similar thiol-containing pyrimidine group. In AC2P36, it is thought that the methylsulfone moiety acts as an electron-withdrawing group which allows a thiolate anion to undergo nucleophilic attack on the C-2 carbon of the pyrimidine ring in order to release methanesulfinic acid or methanesulfinate (Figure A.2.2C)[69]. This interaction is thought to result in the formation of a sulfide bond and depletion of available free thiols. Indeed, heteroaromatic sulfones have been recently described as tunable agents for cysteine-reactive profiling[159,160]. Based on these observations with AC2P36, and the noted similarity with the thiol-containing pyrimidine group, we hypothesized that AC2P20 may have a similar mechanism of action and undergo covalent modification of free thiols. To test this hypothesis, 80µM AC2P20 was incubated with 100µM reduced glutathione (GSH) for one hour in basic, neutral, and acidic conditions and analyzed via mass spectrometry. Incubation of AC2P20 with GSH resulted in the formation of an adduct at pH 5.7 with an exact molecular weight of ~529 Da (Figure 2.3A, C, Table A.2.1). There is also adduct formation in neutral and basic conditions (Figure A.2.3A and B) although with lower peak intensity. AC2P20 incubated with DMSO does not appear to fragment in the absence of GSH in any of these conditions. (Figure 2.3B, Figure A.2.3C and D). In the positive ESI mode (Figure 2.3C), a neutral fragment of 129 Da is lost from the adduct with a peak seen at ~401 Da, consistent with a loss of the glutamate fragment from GSH [161]. Fragmentation of AC2P20 is also observed when incubated with GSH at pH 5.7, with peaks at ~222 Da, ~206 Da, ~194 Da, and ~178 Da aligning with possible fragments of the pyrimidine group of AC2P20 (Table A.2.1). The peak observed at ~391 Da is a mass spectrometry plasticizer and common contaminant that can be used for mass calibration[162]. We also looked at N-acetylcysteine (NAC), a derivative of GSH, and its ability to form an adduct with AC2P20. A peak was observed at ~384 Da, aligning with the formation of an AC2P20-NAC adduct (Figures A.2.4A, Table A.2.1). Interestingly, higher peak intensities of these adducts were observed at neutral and basic conditions (Figures A.2.4B and C). This is possibly due to NAC having a pKa ~9.5, and therefore favoring the adduct reaction with AC2P20 under these conditions. Together, these findings support that AC2P20 reacts with low molecular weight thiols and thiol groups. Additionally, we looked at

whether AC2P20 still forms an adduct with GSH in the presence of the oxidant, H_2O_2. It was thought that H_2O_2 may cause the formation of intermediate sulfenic acid and oxidize GSH, resulting in the formation of glutathione (GSSG)[163]. After incubating AC2P20 with both GSH and H_2O_2, we still observed disulfide bond formation between AC2P20 and GSH, indicating that GSSG is probably not being produced (Figure A.2.4D). These results suggest that AC2P20 is capable of forming a disulfide bond with low molecular weight thiols.

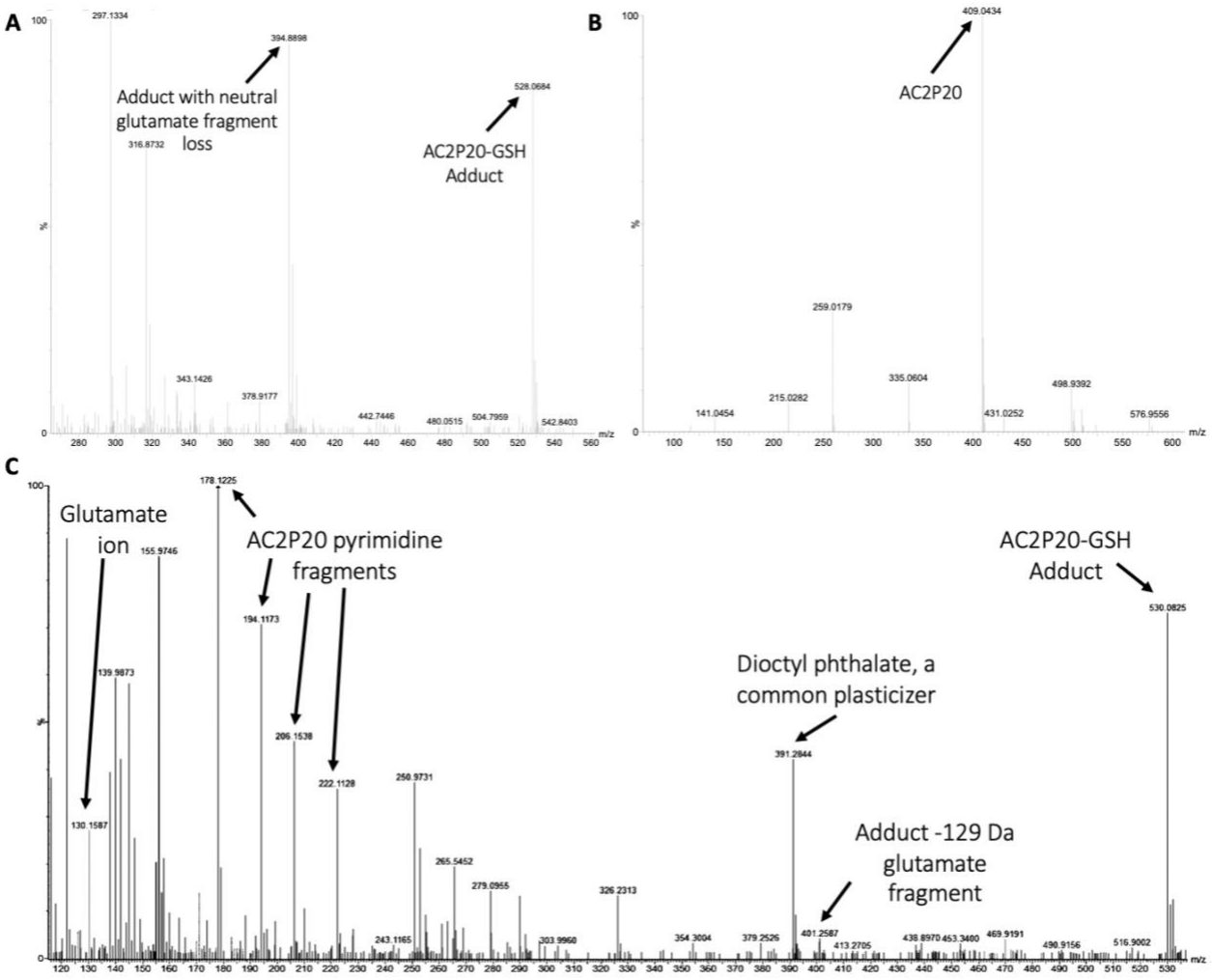

Figure 2.3. AC2P20 forms adducts with free thiols at acidic pH. A) AC2P20 was incubated in Tris-HCl buffer, pH 5.7 with reduced glutathione (GSH) for one hour. An AC2P20-GSH adduct (~528 Da) was confirmed via mass spectrometry. Samples were run in duplicate and observed in negative ESI mode. **B)** In the absence of GSH, AC2P20 incubated with DMSO does not fragment at pH 5.7. Only the parent molecule is observable at a molecular weight of ~409 Da. Samples were run in duplicate and observed in negative ESI mode. **C)** AC2P20-GSH adduct formation at pH 5.7 (~530 Da) was also observed in positive ESI mode, as well as adduct loss of the glutamate fragment (~401 Da) and subsequent fragmentation of the AC2P20 molecule and its pyrimidine fragments. Samples were run in duplicate.

AC2P20 depletes free thiols and causes an accumulation in ROS in Mtb at acidic pH

Given that an adduct is able to form between AC2P20 and GSH, we sought to test the ability of AC2P20 to deplete free thiols in Mtb. For this assay, Mtb was treated with AC2P20 (2 μM and 20 μM) in both acidic and neutral conditions for 24 hours. Auranofin (20 μM) was used as a positive control because it inhibits Mtb's thioredoxin reductase, TrxB2, thereby disrupting thiol- and redox-homeostasis[94]. AC2P36 (20 μM) was also included in the assay to compare thiol depleting activities of both compounds. Following AC2P20 treatment, a statistically significant reduction in free thiol concentrations was observed intracellularly in Mtb at pH 5.7 where free thiols are reduced by ~2.8-fold to ~133nM compared to the DMSO vehicle control at ~380 nM (Figure 2.4A). As expected, we also see free thiol depletion in Mtb following treatment with both positive controls, supporting the observation seen with AC2P20. In contrast to auranofin, AC2P20 treatment at neutral pH does not exhibit any statistically significant reduction in free thiols, supporting the pH-selective activity of this compound. Interestingly, AC2P36 does exhibit some activity in neutral conditions. This is possibly due to AC2P36 still exhibiting some growth inhibitory activity at neutral pH at ~30 μM, whereas AC2P20 requires much higher concentrations (~60 μM) to see a similar inhibitory effect.

Depletion of total free thiols will result in disrupted redox homeostasis and therefore may result in enhanced ROS accumulation. To test this hypothesis, we conducted an assay measuring intracellular ROS production in Mtb. Mtb was incubated with 2 μM and 20 μM AC2P20 for 24 hours, treated with CellROX fluorescent dye for 1 hour, and then assayed for relative fluorescence and optical density. AC2P36 (2 μM and 20 μM) was included as the positive control, because it has previously been shown to accumulate intracellular ROS following treatment. At acidic pH, 20 μM AC2P20 exhibits ~3-fold increase in intracellular ROS production compared to DMSO (Figure 2.4B). AC2P20 (20 μM) also increases ROS accumulation ~3-fold greater in acidic conditions compared to neutral pH, where there is little ROS accumulation compared to DMSO. AC2P36 (20 μM) also increases ROS production ~2-fold at pH 5.7, which is consistent with previous observations. These data support a mechanism whereby enhanced ROS accumulation can be driven by pH stress and is further exacerbated by AC2P20 treatment.

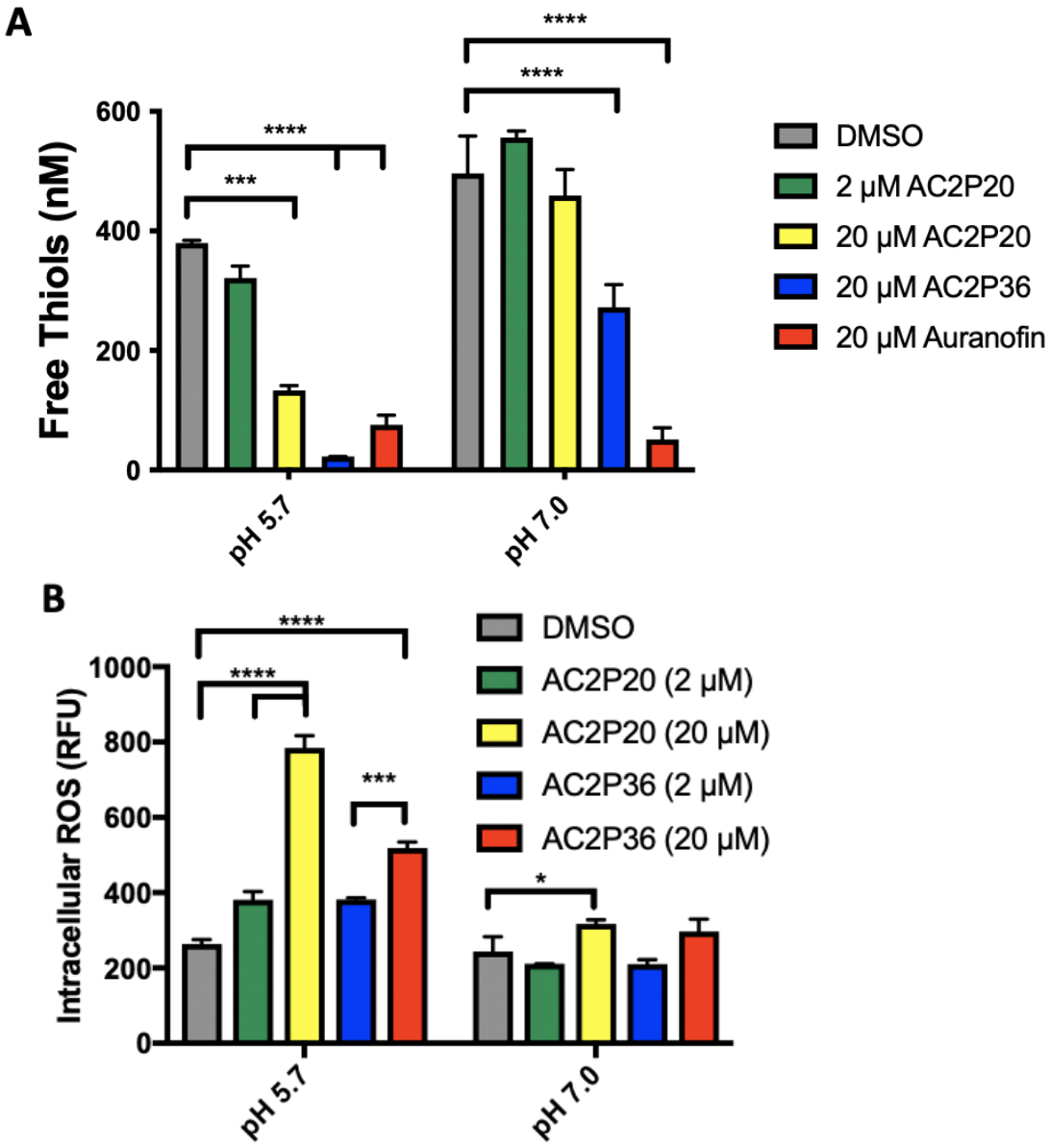

Figure 2.4. AC2P20 depletes free thiols and induces intracellular ROS accumulation. A) Treatment of Mtb with AC2P20 leads to a pH-dependent decrease in free thiols. Free thiol depletion is observed at pH 5.7 with AC2P20 treatment. AC2P36 is a pH-dependent chemical probe known to deplete free thiol pools and serves as a positive control. Statistical significance was calculated using a two-way ANOVA (*$p<0.05$). **B)** ROS accumulate under AC2P20 treatment at acidic conditions. Mtb treatment with AC2P20 leads to a pH-dependent increase in intracellular reactive oxygen species (ROS). ROS was detected using a final concentration of 5 μm fluorescent dye, CellROX Green, and normalized to an OD_{595}. DMSO was used as a control. Statistical significance was calculated using a one-way ANOVA (*$p<0.05$).

Discussion

Based on the chemical structure of AC2P20 and the adduct it forms with GSH at pH 5.7, we propose a reaction model where the benzothiazole-mercaptoacetamide group covalently modifies free thiols, forming stable adducts. Shown here is a potential mechanism for the generation of adducts observed by mass spectrometry (Figure 2.3A and C). Disulfide bond formation between GSH (307.32 Da) and the free benzothiazole-mercaptoacetamide group (223.29 Da) results in a molecule mass of 529 Da, which can be observed in both positive and negative ESI modes (Figure 2.5A, Table A.2.1). Loss of the neutral glutamate fragment from the AC2P20-GSH adduct results in a peak at 401 Da (ESI+). We suspect AC2P20 may be undergoing hydrolysis, however, we do not observe the phenyl-dioxopyrimidine fragment (204 Da). We do observe a fragmented phenyl-dioxopyrimidine group at 178 Da which may be due to the sample's molecules breaking into charged fragments during mass spectrometry. The absence of a 204 Da fragment may also suggest that adduct formation could be occurring via a different chemical process. However, the observation of an adduct supports that the formation of disulfide bonds between AC2P20 and other thiol-containing molecules could be occurring in Mtb (Figure 2.5B).

Redox homeostasis represents a potentially important Mtb vulnerability at acidic pH. Mtb experiences reductive stress during hypoxia and at acidic pH [138]. Genes important for mitigating redox stress are shown to be directly regulated by acid stress; therefore, disruption of redox homeostasis results in the loss of Mtb protection against acid stress[138]. Furthermore, direct perturbations to either redox-homeostasis or pH-homeostasis results in decreased drug tolerance and enhanced Mtb killing[109]. Indeed, chloroquine has recently been shown to kill Mtb *in vivo* by targeting redox homeostasis[109] and auranofin also shows promising antimycobacterial activity[93,94]. Furthermore, agents targeting respiration may similarly have activity by promoting redox imbalance. Thus, targeting redox-homeostasis represents an important new approach to treating TB. Like AC2P36, we have discovered a second, albeit novel, pH-selective compound (AC2P20) that directly targets free thiols to perturb redox homeostasis. Both AC2P36 and AC2P20 deplete free thiol pools and increase intracellular ROS as part of their killing mechanisms. Interestingly, AC2P20 depletes less free thiols than AC2P36, but has a greater increase in intracellular ROS. This suggests that

although both appear to target Mtb free thiols, there are differences in their mechanisms. One hypothesis is that release of the phenyl-dioxopyrimidine group could also be targeting a secondary unknown Mtb physiology, possibly explaining the higher ROS increase that is observed compared to AC2P36 (Figure 2.4B). Both compounds also form adducts with the low molecular weight thiol, GSH; however, there are major chemical scaffold differences. AC2P36 captures thiols with the release of methylsulfinate while AC2P20 is cleaved to generate benzothiazole-mercaptoacetamide, which then goes on to form disulfide bonds. Although AC2P20 and AC2P36 compounds are structurally unique and have distinct mechanisms-of-action, they do exhibit similar physiological effects on Mtb, supporting the conclusion that thiol redox homeostasis is specifically vulnerable to inhibition at acidic pH.

Several studies in Mtb show a link between low pH- and oxidative stress responses[8,37,69,109,164]. At acidic pH *in vitro*, Mtb exhibits a more reduced cytoplasm and a shift from glycolysis to fatty acid synthesis [37]. This metabolic remodeling is thought to occur in order to generate more oxidized cofactors to mitigate reductive stress. However, a more reduced cytoplasm in Mtb may also play a role in protecting Mtb against oxidative stress. A recent study comparing the RNAseq profiles of reduced MSH redox potential (E_{MSH}-reduced), intraphagosmal Mtb, and pH stress supports this claim and shows that E_{MSH}-reduced transcriptome has significant overlap with the pH-regulon[109]. When we compare the E_{MSH}-reduced, intraphagosomal Mtb, and pH stress regulons with AC2P20 and AC2P36 transcriptional profiles, we again see overlap in redox sensitive genes (i.e. *katG*, *trxB2*, and *whiB3*) which are important for protection against oxidative stress.

While both AC2P20 and AC2P36 share these similar gene induction characteristics, there are differences in specific thiol-related genes. For example, methionine synthesis (i.e. *metK*, *metA*, *metC*) appears modulated by AC2P36 treatment, but induction of these genes is absent in AC2P20 transcriptional data. Likewise, AC2P20 strongly induces sulfate reduction via adenosine 5′-phosphosulfate (*cysH*, *nirA*), however, these genes are not modulated by AC2P36. These differences may reflect differences in how these compounds sequester free thiols and which free thiols in particular are being modified. While mycothiol is the most abundant free thiol in Mtb (present in millimolar amounts)[165], it is plausible AC2P20

targets other low molecular weight thiols such as ergothioneine (ERG)[148] or gamma-glutamylcysteine (GGC)[166]. Our mass spectrometry data also supports AC2P20 may be generally targeting free thiols, forming adducts with both GSH and NAC, which would indicate that (1) AC2P20 can target a thiol group in general, and (2) it can directly target a cysteine derivative. Further profiling experiments would need to be undertaken to determine in which molecular contexts AC2P20 targets free thiols and indeed, other related molecules are being developed as tools for cysteine-reactive profiling[159,160].

Conclusions

The discovery of two independent molecules selectively killing Mtb at acidic pH by depleting free thiols provides further support for our hypothesis that Mtb is highly sensitive to thiol homeostasis stress at acidic pH and this pathway is a valuable new target for TB drug discovery. AC2P20 or AC2P36 in their present state, will not likely make useful drugs, as they could react with host thiols and thus be neutralized prior to reaching Mtb or could be cytotoxic. However, they independently point the way to further efforts to target this pathway. Indeed, the thioredoxin reductase inhibitor auranofin is in early clinical trials to treat TB and similarly functions by depleting free thiols by a distinct, indirect mechanism. Several groups are pursuing compounds that have enhanced killing at acidic pH but have mostly focused on bacterial pH-homeostasis[70,71,75]. This new work further validates targeting thiol homeostasis as an alternative target to kill Mtb at acidic pH. Other chemotypes, such as auranofin, that do so indirectly are likely the most promising route. However, it could be possible to develop the compounds related to AC2P20 or AC2P36 into prodrugs that are activated by a Mtb specific enzyme, thus releasing the thiol-reactive warhead selectively inside the bacterial cell. Notably, for both AC2P20 and AC2P36 we could not isolate resistant mutants. This is consistent with the compounds having a broad target (free thiols) and not a specific protein, where resistant mutants could be selected. Therefore, it is possible that should a compound targeting free thiols be developed, the evolution of resistance may be slower as compared to a traditional antibiotic.

In conclusion, our findings have uncovered a novel thiol-targeting chemical probe, AC2P20. AC2P20, in combination with AC2P36, can be classified as a new class of compounds that render Mtb

especially sensitive to changes in thiol homeostasis at acidic pH. Further experiments to examine the mechanism of this sensitivity can be undertaken using AC2P20 or AC2P36 as chemical probes. For example, using TN-seq, identification of mutants that become sensitive to AC2P20 and AC2P36 at a neutral pH or have enhanced sensitivity at acidic pH, may reveal key functional pathways required for maintaining thiol-homeostasis. AC2P20 or AC2P36 in their present state, will not likely make useful drugs, as they could react with host thiols and thus be neutralized prior to reaching Mtb or could be cytotoxic. However, it could be possible to develop the compounds into prodrugs that are activated by a Mtb specific enzyme, thus releasing the thiol-reactive warhead selectively inside the bacterial cell.

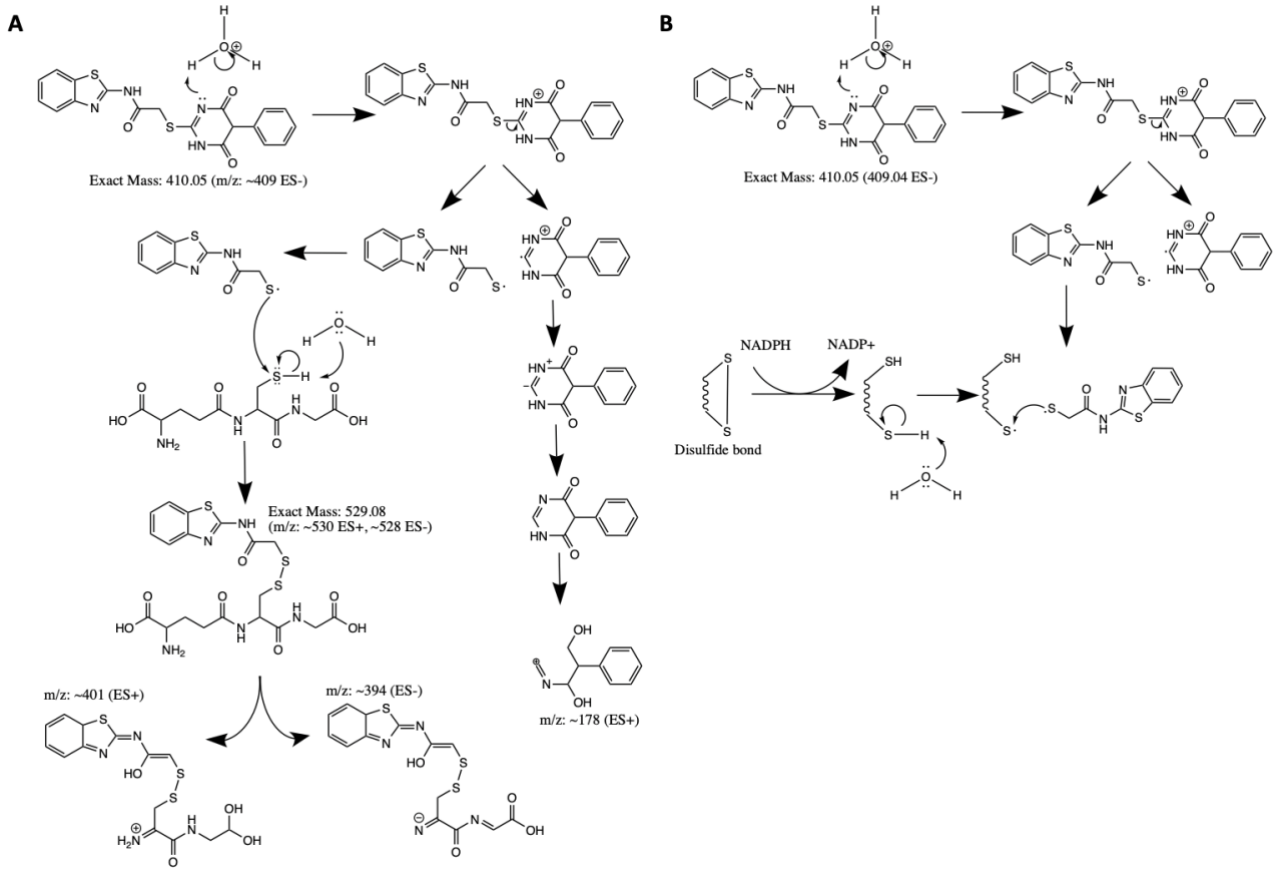

Figure 2.5. Proposed mechanism for AC2P20 adduct formation. A) Proposed reaction mechanism for the formation of a disulfide bond between AC2P20 and GSH at pH 5.7. **B)** Proposed stable covalent bond formation between AC2P20 and free thiols in Mtb during redox cycling.

Acknowledgements

We thank Christopher Colvin and Javiera Ortiz for technical assistance on the high throughput screening and cytoplasmic pH assays, respectively. Research on this project was supported grants from the NIH-NIAID to RBA (U54AI057153, R01AI116605, R21AI105867) and AgBioResearch.

CHAPTER 3 – *ppe51* variants enable growth of *Mycobacterium tuberculosis* at acidic pH by selectively promoting glycerol uptake

*This work is available as a preprint at bioRxiv (**doi:** https://doi.org/10.1101/2021.05.19.444820)*

.

Shelby J. Dechow, Jacob J. Baker, Megan Murto, and Robert B. Abramovitch

Author Contributions

S.J.D., J.J.B., and R.B.A. conceived the project. S.J.D performed all of the experimental studies. M.M. conducted thermal stability assay studies. S.J.D. and R.B.A. wrote the manuscript. All authors reviewed the manuscript.

Abstract

In defined media supplemented with single carbon sources, Mtb exhibits carbon source specific growth restriction. When supplied with glycerol as the sole carbon source at pH 5.7, Mtb establishes a metabolically active state of nonreplicating persistence known as acid growth arrest. We hypothesized that acid growth arrest on glycerol is not a metabolic restriction, but rather an adaptive response. To test this hypothesis, we selected for and identified several Mtb mutants that could grow under these restrictive conditions. All of the mutants were mapped to the *ppe51* gene and resulted in variants with three different amino acid substitutions– S211R, E215K, and A228D. Expression of the PPE51 variants in Mtb promoted growth at acidic pH showing that the mutant alleles are sufficient to cause the dominant gain-of-function, *eag* phenotype. Testing growth on other single carbon sources showed the PPE51 variants specifically enhanced growth on glycerol, suggesting *ppe51* plays a role in glycerol uptake. Using radiolabeled glycerol, enhanced glycerol uptake was observed in Mtb expressing the PPE51 (S211R) variant, with glycerol overaccumulation in triacylglycerol. Notably, the *eag* phenotype is deleterious for growth in macrophages, where the mutants have selectively faster replication and reduced virulence in activated macrophages as compared to resting macrophages. Recombinant PPE51 protein exhibited differential thermostability in the WT or S211R variants in the presence of glycerol, supporting the model that *eag* substitutions alter PPE51-glycerol interactions. Together, these findings support that *ppe51* variants selectively promote glycerol uptake and that slowed growth at acidic pH is an important adaptive mechanism required for macrophage pathogenesis.

Introduction

During infection, *Mycobacterium tuberculosis* (Mtb) senses and adapts to a variety of immune cues including hypoxia[167,168], nutrient limitation[35,169], pH changes[81], and nitrosative and oxidative stress[151]. Exposure to these stresses can promote Mtb to establish slowed growth or a non-replicating persistent (NRP) state. NRP bacteria are tolerant to immune and antibiotic-mediated killing[13,134,170], therefore understanding mechanisms underlying NRP may promote new methods to shorten the course of TB therapy.

Following macrophage infection, Mtb senses the mildly acidic pH of the phagosome and broadly remodels its gene expression[46]. Adaptation to acidic pH includes the induction of the PhoPR regulon, induction of ESX-1 secretion, and remodeling of central metabolism and cell envelope lipids[171]. Defects in adaptation to acidic pH reduce Mtb virulence in macrophages and animals[39,50,172,173], therefore, pH dependent adaptation is required for Mtb virulence.

Previous studies conducted by our lab sought to understand the interplay of acidic pH and Mtb central metabolism. We observed that Mtb exhibits selectivity of the carbon sources on which it can growth at pH 5.7 relative to pH 7.0. For example, Mtb incubated at acidic pH with glycerol as a sole carbon source is restricted for growth and establishes a viable, metabolically active state of NRP called acid growth arrest[12,31,37]. Acid growth arrest is observed on a variety of other carbon sources associated with glycolysis and TCA cycle. Interestingly, Mtb can resuscitate its growth at acidic pH by addition of specific carbon sources, such as pyruvate, acetate, oxaloacetate [OA] and cholesterol, which function at the intersection of glycolysis and the TCA cycle (a.k.a. the anaplerotic node)[37]. This discovery suggests that the anaplerotic node is the location of a pH-dependent metabolic switch that may promote Mtb growth on permissive carbon sources during pathogenesis at acidic pH, and that metabolic remodeling is required for pH adaptation[171].

It is puzzling that Mtb cannot grow at acidic pH on specific carbon sources, as Mtb is provided with oxygen as a terminal electron acceptor and a carbon source that is well utilized at pH 7.0. Thus, acid growth arrest is different from other NRP models, where the bacterium is missing a key factor required for growth (*e.g.* oxygen or nutrients in the hypoxia or starvation models of NRP). Therefore, we hypothesized

that acid growth arrest is not an actual restriction on growth, but an adaptation by the bacterium to slow and arrest its growth. In a previous study, our lab sought to identify genes regulating acid growth arrest by selecting for mutants incapable of arresting their growth on minimal medium agar plates, buffered to pH 5.7 with glycerol as the carbon source. From this screen, novel missense mutations were identified in *ppe51* (H37Rv annotated Mtb gene, *Rv3136*) and were named enhanced acid growth (*eag*) mutants [12]. PPE51 is part of the PE and PPE mycobacterial protein family. Named for their unique N-terminus motifs Pro-Glu (PE) and Pro-Pro-Glu (PPE), most of these proteins have remained largely enigmatic in their functional roles[45,158]. However, a growing body of literature in recent years has assigned diverse putative functional roles for PE and PPE proteins including immune evasion[45,174-177], calcium binding[178], iron utilization[179,180], Mg^{2+} and PO_3^{2-} transport[54], fibronectin binding[181], and lipase activity[182,183].

Mounting evidence suggests that some PE and PPE proteins may play important roles in Mtb nutrient acquisition. Examination of *pe* and *ppe* evolution reveals an expansion of this protein family corresponding with Type VII or ESX secretion systems, where it is thought that ancestral *pe* and *ppe* genes inserted into an *esx* gene cluster and expanded alongside this secretion system during subsequent gene duplication events [175,184,185]. Secretion via ESX provides a route for PE and PPE proteins to access the cell surface and nutrients in the host cell milieu, which is supported by high-throughput proteomic evidence showing direct surface localization of PE and PPE proteins[54,179,186-188]. Mtb contains five ESX secretion systems[189], with ESX-5 contributing to the majority of PE and PPE secretion[184,186,190]. Furthermore, ESX-5 and its cognate PE and PPE proteins have been implicated in the uptake of fatty acids and possibly the utilization of other nutrient substrates[186]. ESX-3-mediated PE and PPE proteins are thought to play a role in iron acquisition, whereby they have been shown to be directly involved in mycobactin-mediated iron uptake and heme uptake[179,191,192]. Taken together, these results provide direct examples of Mtb acquiring and utilizing host resources through secretion of PE and PPE proteins.

Based on these findings showing a role for PPE proteins in transport and that PPE51 *eag* variants could grow on glycerol, we hypothesized in our 2018 study[12], "that these amino acid substitutions may increase Mtb growth by modulating mycomembrane permeability, possibly by modulating the channel size

or specificity of PPE51, which may function as a porin to enhance access to glycerol or other nutrients at acidic pH." The goal of this study was to test this hypothesis and further define the role of PPE51 in glycerol acquisition and pathogenesis. Notably, concurrent with this study, recently published studies confirmed the hypothesis that PPE51 is an exported cell surface-associated protein and linked to the nutrient acquisition of glycolytic carbon sources [54,56,193]. Here, we show that in a saturating forward genetic selection only three PPE51 variants, S211R, E215K and A228D were isolated as *eag* mutants. The PPE51 variants specifically promoted growth at pH 5.7 on glycerol and no other tested carbon sources, supporting the notion that these substitutions selectively promote glycerol utilization. Radiolabeling studies show that the S211R variant has enhanced uptake of glycerol and accumulation of triacylglycerol (TAG), showing that the variants promote glycerol uptake. Differential thermal stability of WT versus S211R variant PPE51 proteins in the presences of glycerol, support the variant has direct and differential interactions with glycerol, but similar interactions with the non-permissive substrate glucose. Structural modeling supports that PPE51 forms a structure homologous with bacterial nutrient transporters, with the variants altering the predicted ligand specificity. These data are consistent with a model where PPE51 promotes uptake of glycerol across the mycomembrane by acting like a porin and that variants alter the conformation to enhance glycerol uptake. *eag* variants exhibit enhanced replication and reduced virulence in activated macrophages, supporting a role for pH-dependent slowed growth during macrophage pathogenesis.

Materials and Methods

Bacterial strains and growth conditions

All experiments were performed with *M. tuberculosis* strains Erdman and CDC1551. Mtb was grown at 37 °C and 5% CO_2 in vented T-25 culture flasks containing Middlebrook 7H9 media with 10% oleic acid-albumin-dextrose-catalase (OADC), 0.05% Tween-80, and 0.2% glycerol. For acid stress and single carbon source experiments, MMAT defined minimal media was used as described by Lee *et al.* [43]: 1 g/L KH_2PO_4, 2.5 g/L Na_2PO_4, 0.5 g/L $(NH_4)_2SO_4$, 0.17 g/L L-Asparagine monohydrate, 10 mg/L $MgSO_4$, 50 mg/L ferric ammonium citrate, 0.1 mg/L $ZnSO_4$, 0.5 mg/L $CaCl_2$, and 0.05% Tyloxapol. MMAT media was buffered

with 100 mM 3-(N-morpholino)propanesulfonic acid (MOPS) for experiments requiring pH 6.6-7.0 and 100 mM 2-(N-morpholino)ethanesulfonic acid (MES) for experiments requiring pH 5.5-6.5 [38]. For growth curve experiments, Mtb was grown to mid-late log phase (OD_{600} 0.6-1.0) and seeded in MMAT at a starting OD_{600} of 0.05. Optical density measurements were conducted by removing 500 µL of samples at each time point. Viability assays were performed in a similar manner with samples being diluted 10-fold in PBS + 0.05% Tween-80 and plated for viable colony forming units (CFUs) on 7H10 + 10% OADC agar plates.

Genetic selection and sequencing

A wild type Erdman Mtb population of $4x10^9$ bacteria was plated on MMAT agar plates (1 g/L KH_2PO_4, 2.5 g/L Na_2PO_4, 0.5 g/L $(NH_4)_2SO_4$, 0.17 g/L L-Asparagine monohydrate, 10 mg/L $MgSO_4$, 50 mg/L ferric ammonium citrate, 0.1 mg/L $ZnSO_4$, 0.5 mg/L $CaCl_2$, and 0.05% Tyloxapol) supplemented with 10 mM glycerol as the sole carbon source and buffered to pH 5.7 with 100 mM MES [38]. Plates were incubated at 37 °C with spontaneous mutants appearing around week eight and isolated for growth. Single-colony isolates were confirmed as enhanced acid growth (*eag*) mutants under acidic conditions in liquid MMAT (pH 5.7) media amended with 10 mM glycerol. Whole genome sequencing (WGS) was performed on genomic DNA isolated from mutants representing various levels of enhanced growth as well as a wild type Erdman control. Samples were sequenced using the Illumina MiSeq in a 2x250-bp paired end format. Base calling was done by Illumina Real Time Analysis v1.18.54, demultiplexed, and converted to FastQ using Illumina Bcl2fastq v2.19.1. Low-quality bases were trimmed and adapter sequences were removed using Trimmomatic (v0.36)[194] and aligned sequence reads to the Erdman reference genome using BWA-MEM[195]. SNPs and indels were identified using Genome Analysis ToolKit (GATK)[196].

Generation and analysis of ppe51 knockout

The *ppe51* gene was replaced with a hygromycin resistance (Hyg^R) cassette in both Erdman and CDC1551 Mtb strain backgrounds using a new chromosomal engineering system called ORBIT (for "oligonucleotide-

mediated recombineering followed by Bxb1 integrase targeting") that combines site-specific recombination with homologous recombination[197]. An ORBIT recombineering plasmid (pKM444) expressing RecT annealase and Bxb1 integrase from the anhydrotetracycline (ATc)-inducible Ptet promoter and containing a kanamycin resistance (Kan^R) cassette was first transformed into Mtb, selected for KanR, induced with ATc, and generated into electrocompetent cells. Electrocompetent cells were then transformed with a knockout integration plasmid (pKM464) harboring Hyg^R and targeting oligonucleotide. Hygromycin-resistant colonies were isolated and cured of the kanamycin-containing recombineering plasmid. Genomic DNA was extracted from transformants and the 5' and 3' junction sites of the knockout were confirmed by PCR and sequencing using ORBIT target-specific and *ppe51*-specific primers (Figure A.3.7B-D, Table A.3.1). Gene replacement was further verified via quantitative real time PCR (qRT-PCR) (Figure A.3.7E). *Δppe51* was complemented with WT and variant *ppe51* from their native promoter and confirmed by qRT-PCR (Figure A.3.7F).

pH-and-glycerol dose response combination growth assays

Mtb cultures were incubated in a range of pH buffered MMAT media (pH 5.0-pH 7.0) at a starting OD_{600} of 0.2 in 96-well plates. Cultures were treated with 2.5-fold dose-response (0.13-80 mM) of glycerol and incubated over the course of 21 days, with growth assessed by optical density. Bacterial viability was assessed by diluting wells 10-fold and plating for viable CFUs on 7H10 + 10% OADC agar plates. Optical density data was converted to percent of maximum well-growth and normalized based on no carbon control at pH 5.5 (0%) and maximum Mtb growth on glycerol at pH 6.5 (100%). Each condition and time-point experiment was conducted in triplicate and representative of multiple individual experiments.

Radiolabeled glycerol uptake assay

Mtb Erdman cultures were pre-adapted for 3 days in MMAT media (pH 5.7 or pH 7.0) containing 10 mM glycerol. Following adaptation, Mtb was washed twice with PBS+0.05% Tween-80 and resuspended in the same buffered MMAT media amended with 10 mM glycerol and 6 μCi of [U-^{14}C] Glycerol. Samples were

removed over the course of 24 hours, fixed with 4% paraformaldehyde, and assessed for total radioactivity using scintillation counting. All strains used for radiolabel uptake experiments were repeated in two biological replicates.

Analysis of metabolism of radiolabeled lipids into Mtb lipids

Mtb Erdman cultures were pre-adapted as described above for the uptake experiments. Following pre-adaptation, cultures were seeded at a starting OD_{600} of 0.2 in MMAT media (pH 5.7 or pH 7.0) + 10 mM glycerol and set up in two biological replicates. Lipids were labeled with 6 µCi of [U-^{14}C] Glycerol for 6 days, and samples were pelleted and washed with PBS before lipid extraction. Total lipids were extracted and Folch washed as previously described[37] and ^{14}C-incorporation was measured using scintillation counting. For thin layer chromatography (TLC), 5,000 counts per minute (CPM) of each pH 5.7 sample and 10,000 CPM of each pH 7.0 sample was loaded on a 100-cm^2 high-performance TLC silica gel 60 aluminum sheet (EMD Millipore) and analyzed with a chloroform:methanol:water (90:10:1 v/v/v) solvent system[129]. Sulfolipids, TAG, and PDIM were separated as previously described[37,39,129] and quantified using a phosphor screen and Typhon imager and ImageJ software[198].

Replication during acid growth arrest

For measurement of replication during acid growth arrest, WT Mtb, *Δppe51*, and *ppe51* native variants in both CDC1551 and Erdman backgrounds carrying the pBP10 plasmid[199] were inoculated into MMAT media (pH 5.7 and pH 7.0) + 10 mM glycerol and in the absence of kanamycin. Plasmid loss and percentage of bacteria still containing the pBP10 was determined by plating for CFUs on 7H10 + 10% OADC agar plates ±25 µg/uL kanamycin. Rates of growth, death, and cumulative bacterial burden were quantified using equations as previously described[32]. Specifically, equations 10, 11, and 13, as detailed in the supplemental materials of Gill *et al.* were used to calculate rate of replication, rate of death, and numbers of dead bacteria, respectively. The Mtb segregation constant (s = 0.18± 0.023) – the frequency of Mtb daughter cells losing plasmid per generation as previously determined by Gill *et al.* – was used for calculations in this study.

Macrophage pathogenesis studies

Bone Marrow-derived macrophages (BMDMs) were extracted and infected with the panel of complemented strains built into the CDC1551 *Δppe51* knockout background at a multiplicity of infection (MOI) of 1:1 using previously described methods[200]. BMDMs were activated by treating with 100 units/mL IFN-γ overnight, followed by treatment with 10 ng/mL lipopolysaccharide overnight. Infected BMDMs were lysed at days 0, 3, 6, and 9 and intracellular bacterial lysates were serially diluted and enumerated on 7H10 + 10% OADC agar plates. Each strain for each timepoint was performed in triplicate. BMDMs were also infected with CDC1551 strains containing the pBP10 replication clock plasmid as described in the pBP10 *in vitro* experiments using the same macrophage infection methods described above with minor modifications. BMDMs infected with pBP10-containing strains were lysed at days 0, 2, 4, 6, and 8 and enumerated on 7H10 + 10% OADC agar plates ±25 µg/uL kanamycin selection. Calculations for pBP10 plasmid loss and replication dynamics were performed as described in the *in vitro* pBP10 experiments.

Recombinant PPE51 protein expression and purification

The ORF of PPE51 was amplified using pET23::*ppe51*_FWD and pET23::*ppe51*_REV primers (Table A.3.1) and cloned into the pET23a+ vector containing a C-terminal polyhistidine (His)-tag. The cloned protein has a deletion of the final four C-terminal amino acids. Transformants propagated in *E. coli* BL21(DE3) were selected on LB agar plates containing ampicillin. The S211R mutation was introduced into the pET::*ppe51*-WT construct using the site-directed mutagenesis primers PPE51-S211R_FWD and PPE51-S211R_REV (Table A.3.1) and the QuikChange™ Site-Directed Mutagenesis Kit. Overnight cultures were expanded into 250 mL of fresh LB media with ampicillin at an initial inoculum OD_{600} of 0.05 and grown to an OD_{600} of 0.6 at 37 °C with shaking at 200 rpm. Proteins were then induced with 1 mM of isopropyl-ß-D-thiogalactopyranoside (IPTG) at 18°C for 20 hours. Culture was then harvested via centrifugation at 4000 rpm for 25 minutes at 4°C. Pellets were then lysed for 30 minutes on ice with occasional vortexing in ice-cold lysis buffer (50 mM phosphate buffer [pH 7.6], 200 mM NaCl, 0.1% Triton X-100, 0.1 mg/mL PMSF, 0.5 mg/mL lysozyme). Because PPE51 possibly interacts with glycerol, glycerol

was completely removed from all buffers used during the purification process. Cells were further lysed by sonication and cell lysate was clarified via centrifugation at 14,000 rpm for 30 minutes at 4°C. Supernatant was loaded onto a nickel ion-containing affinity resin column and bound overnight with shaking at 4°C. Protein was washed first with wash buffer containing no imidazole and a second time with wash buffer containing 50 mM imidazole. PPE51 protein was then eluted into (4) 1 mL fractions with elution buffer containing 200 mM imidazole. Recombinant PPE51 was quantified using the Qubit assay.

PPE51 protein thermostability assay

The thermostability assay was performed as previously described[201] with 13.5 µL of 0.635 mg/mL of batch-purified PPE51 samples aliquoted into PCR tube containing 1.5 µL of 100 mM glycerol, yielding a final glycerol concentration of 10 mM. Samples were incubated for 20 minutes at room temperature and transferred to PCR thermocyclers where they were incubated for an additional 5 minutes at the following temperatures: 35, 40, 45, 50, 55, 60, and 65°C. Samples were then centrifuged at 4000 rpm for 10 minutes to pellet precipitated protein. After centrifugation, soluble protein was removed from the tubes and detected in Western blots using mouse anti-His tag monoclonal antibody followed by HRP-conjugated anti-mouse IgG secondary antibody. Enhanced chemiluminescence (ECL) Western blotting substrate (Pierce) was used for Western blot detection. The AI600 Chemiluminescent Imager was used to visualize and analyze Western blot results.

Results

All isolated eag mutants have spontaneous mutations in ppe51

During acid growth arrest in minimal media, Mtb is provided all required nutrients including a metabolically utilized carbon source and a terminal electron acceptor. This suggests that acid growth arrest is not due to a physiological limitation presented by the growth environment but rather is a regulated process whereby Mtb adapts to its acidic environment. A previously published forward genetic selection tested this hypothesis using a CDC1551 transposon mutant library containing >100,000 was plated on MMAT defined

minimal media agar with glycerol at pH 5.7 and resulted in 98 transposon (Tn) mutants and two spontaneous WT mutants[12]. These mutants were isolated and confirmed as *enhanced acid growth* (*eag*) mutants based on their ability to grow well compared to native WT Mtb at pH 5.7 in liquid MMAT supplemented with glycerol [12]. Interestingly, complementation attempts with the Tn mutants did not restore growth arrest, and whole genome sequencing identified spontaneous mutations in *ppe51* in both Tn and WT mutant backgrounds [12]. To repeat a saturating selection, in the absence of transposon mutagenesis, a second forward genetic selection was performed on MMAT agar buffered to pH 5.7 with glycerol, using a larger bacterial population ($4x10^9$ bacteria) in the Erdman Mtb strain (Figure 3.1A). From the WT Erdman selection, 98 spontaneous *eag* mutants were isolated of which 52 were colony-purified and confirmed for enhanced growth under acidic conditions in liquid MMAT containing glycerol (Figure 3.1B, Figure A.3.1A-D). The *eag* isolates exhibited an up to ~4-fold increase in growth compared to WT Erdman which exhibited complete growth arrest (Figure 3.1B). Of these *eag* mutants, 22 were selected for whole genome sequencing. Remarkably, all 22 isolates had single nucleotide polymorphisms (SNPs) mapping to the *ppe51* gene (Table 3.1). All mutations were non-synonymous (S211R, A228D, and E215K) and were centrally located within a 50 bp region on the *ppe51* gene (Figure A.3.2). The S211R and A228D variants were also identified in the prior Tn mutant CDC1551 selection, with E215K being a novel mutation found in the new Erdman selection.

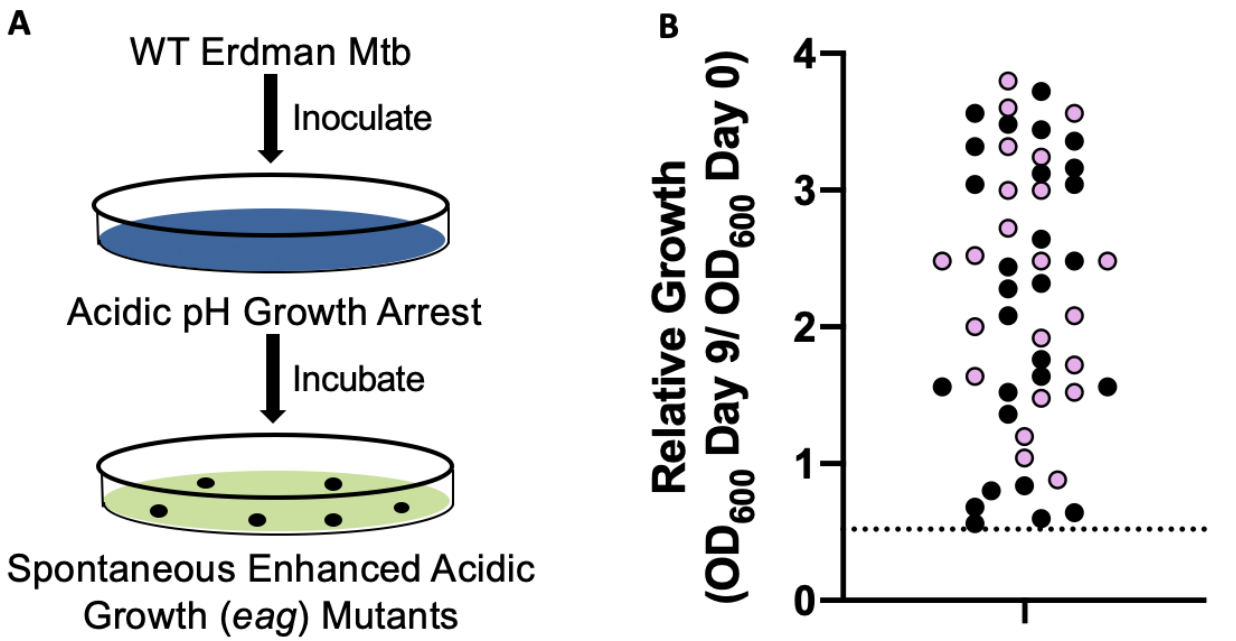

Figure 3.1. Selection and characterization of mutant strains able to grow at acidic pH. A) Schematic of the forward genetic selection used to acquire *eag* mutants. The appearance of distinct colony growth after 8 weeks was indicative of mutants that were unable to arrest their growth at pH 5.7 **B)** Growth phenotypes of isolated mutants were determined by measuring Day 9 OD_{600} and compared to OD_{600} from the initial inoculum. Each dot represents mutants that were isolated from MMAT agar plates and confirmed for enhanced growth in liquid MMAT (pH 5.7). Pink-colored data points indicate mutants chosen for whole-genome sequencing. The dotted line represents relative WT Erdman growth (< ratio of 1).

Table 3.1. Whole genome sequencing results of isolated colony variants.

Plate No.	Mutant No.	SNP Location	Nucleotide Change	Amino Acid Change	Quality Score
Plate 1	*eag1.7*	3497961	G**C**C→G**A**C	A228D	5478
	eag1.8	3497911	AG**C**→AG**A**	S211R	6929
	eag1.12	3497961	G**C**C→G**A**C	A228D	7373
	eag1.14	3497911	AG**C**→AG**A**	S211R	6328
	eag1.33	3497911	AG**C**→AG**A**	S211R	5270
Plate 2	*eag2.1*	3497961	G**C**C→G**A**C	A228D	4417
	eag2.2	3497961	G**C**C→G**A**C	A228D	6803
	eag2.3	3497911	AG**C**→AG**A**	S211R	5205
	eag2.6	3497911	AG**C**→AG**A**	S211R	5976
	eag2.8	3497961	G**C**C→G**A**C	A228D	4270
	eag2.14	3497921	**G**AG→**A**AG	E215K	3442
	eag2.16	3497911	AG**C**→AG**G**	S211R	4575
Plate 3	*eag3.2*	3497961	G**C**C→G**A**C	A228D	4140
	eag3.4	3497961	G**C**C→G**A**C	A228D	3292
	eag3.9	3497911	AG**C**→AG**G**	S211R	3645
	eag3.15	3497911	AG**C**→AG**A**	S211R	3784
	eag3.23	3497911	AG**C**→AG**G**	S211R	4609
Plate 4	*eag4.5*	3497961	G**C**C→G**A**C	A228D	5153
	eag4.7	3497911	AG**C**→AG**G**	S211R	5107
	eag4.12	3497911	AG**C**→AG**G**	S211R	5179
	eag4.21	3497961	G**C**C→G**A**C	A228D	3958
	eag4.24	3497911	AG**C**→AG**G**	S211R	5517

ppe51 mutations are sufficient to overcome growth arrest

Given that *ppe51* variants exhibit enhanced growth at acidic pH, we investigated the function of the variant alleles in the presence of the WT *ppe51* allele. Expression constructs of WT or mutant *ppe51* were transformed into WT CDC1551 or WT Erdman Mtb strains carrying the native *ppe51* allele. Expression strains were grown in MMAT at pH 5.7 with glycerol as a carbon source. Expression of *ppe5*1-S211R and *ppe51*-A228D variants in WT Mtb resulted in significantly enhanced growth under acidic conditions (Figure 3.2A). In contrast, expression of WT *ppe51* and the empty vector exhibited complete growth arrest at pH 5.7. The E215K allele was also not sufficient at overcoming growth arrest which may explain why it has only been observed once across two independent forward genetic selections. Additionally, all expression strains grew equally well at pH 7.0 (Figure A.3.3), showing that the observed growth phenotype is pH-specific. Interestingly, although the growth phenotype with A228D expression resulted in enhanced growth at acidic pH, it grew at a slower rate compared to S211R expression strains in both CDC1551 and Erdman backgrounds. We examined individual variant alleles from the selection (Figure 3.1B) and observed that S211R variants significantly grouped together at a higher rate of growth compared to A228D and E215K (Figure 3.2B and C). Together, these results demonstrate that the *eag* mutations confer a dominant, gain-of-function growth phenotype, and specific mutations are associated with differential strength of the phenotype.

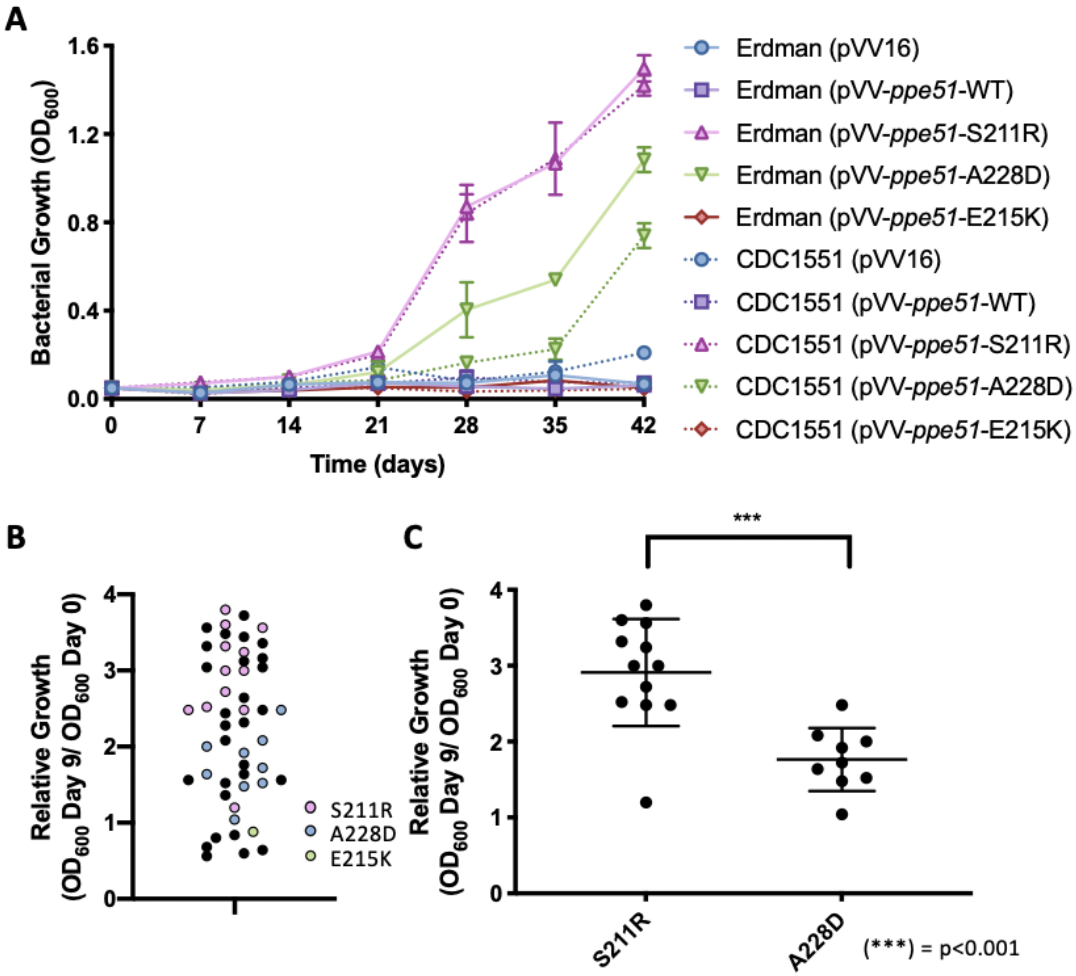

Figure 3.2. PPE51 variants drive the *eag* phenotype and exhibit phenotypic and carbon source-dependent growth differences. A) Growth curve of WT Mtb (Erdman and CDC1551 strains) expressing *ppe51* and *eag* variants. Growth of pVV16 empty vector and pVV-*ppe51*-WT were compared to WT carrying the expression constructs of the mutant alleles (S211R, A228D, and E215K) in minimal media (pH 5.7 + glycerol). Expression of *eag* mutant alleles in WT Mtb results in significantly enhanced growth under acidic conditions. This experiment was repeated three times in duplicate. Error bars indicate standard deviation. **B)** *eag* variants show distinct clustering of variant type based on relative growth. **C)** Statistical analysis of growth differences between native *eag* strains containing S211R or A228D was performed using an unpaired t-test (***P < 0.001) with Welch's correction.

PPE51 variants selectively promote growth on glycerol

Based on the enhanced growth phenotype that the variants exhibit at acidic pH, we hypothesized that this phenotype may be due to *ppe51* variants modulating mycomembrane permeability, resulting in enhanced nutrient uptake. To test this hypothesis, we conducted an Ethidium Bromide (EtBr) assay looking at permeability with WT Mtb expression constructs (empty vector, WT, and S211R) in both CDC1551 and Erdman backgrounds. With the EtBr assay we did not observe differences in the rate of uptake between the WT and *eag* expression strains in either CDC1551 or Erdman (Figure A.3.4), suggesting that the growth phenotype is not due to a general increase in permeability. We then hypothesized that the growth phenotype may be due to nutrient-specific uptake. We explored this possibility by growing CDC1551 and Erdman expression strains (empty vector, *ppe51* and *ppe51*-S211R) in liquid minimal media (pH 5.7) in the presence of various growth-permissive (*e.g.* pyruvate, acetate, cholesterol) and non-permissive (*e.g.* glucose, glycerol, propionate) carbon sources[37]. After 20 days we found that enhanced acid growth was only observed with *ppe51*-S211R in the presence of 10 mM glycerol, a normally non-permissive carbon source at pH 5.7, in both CDC1551 and Erdman (Figure 3.3, Figure A.3.5, Figure A.3.6A-B). All expression strains exhibited enhanced growth on permissive carbon sources in both Mtb backgrounds, which is consistent with what has been previously published[37]. Notably, the *ppe51* S211R variant specifically promotes growth on glycerol, but not glucose, another proposed nutrient associated with PPE51-dependent uptake[54,56], demonstrating the variant is selective for glycerol.

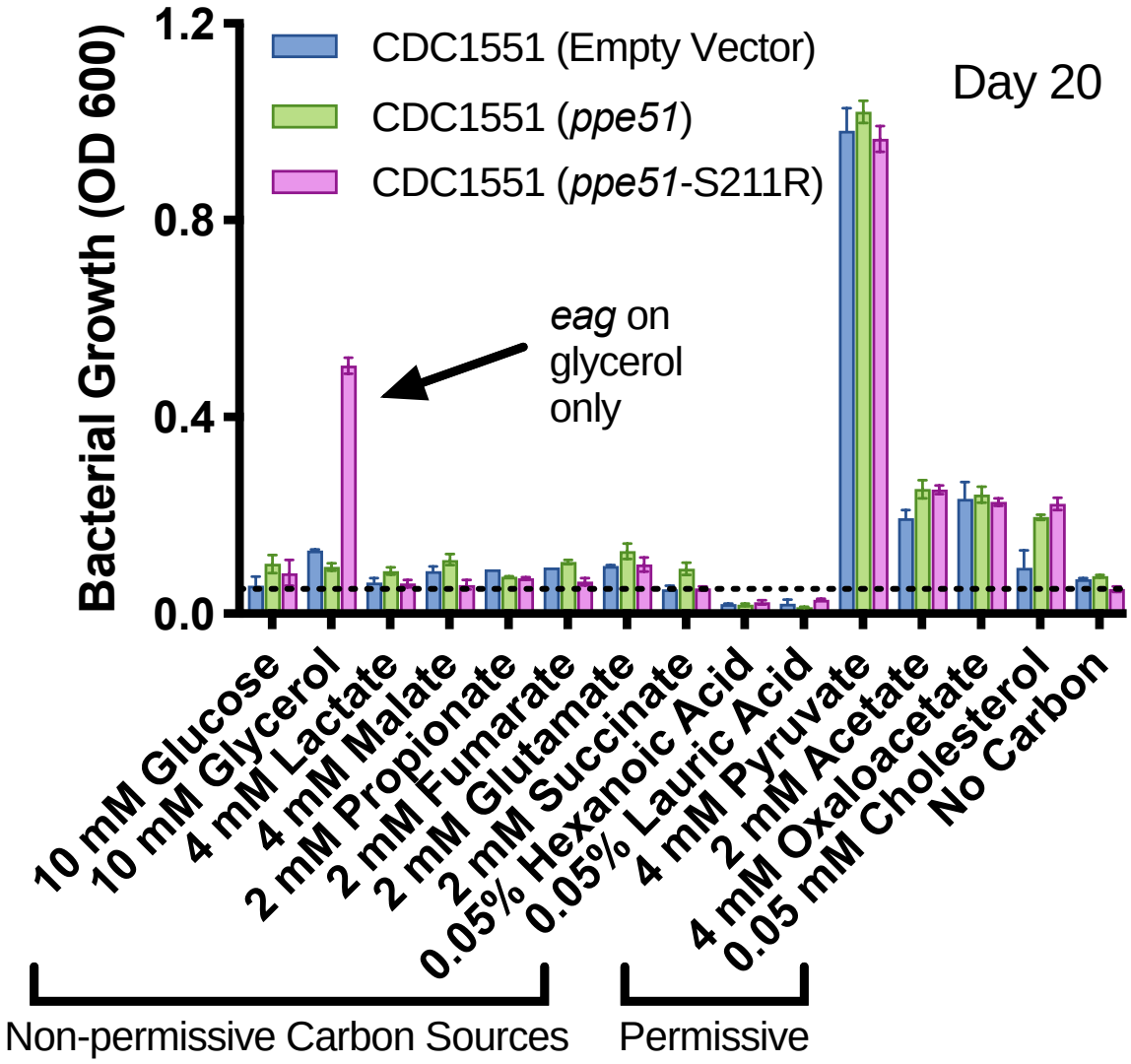

Figure 3.3. Analysis of the CDC1551 S211R variant growth on various carbon sources. CDC1551 expression strains were grown in MMAT medium (pH 5.7) in the presence of various growth-permissive (i.e. pyruvate acetate, OA) and non-permissive (i.e. glucose, propionate, lactate) carbon sources. *ppe51*-S211R (pink bars) growth is carbon source specific and only exhibits enhanced growth on glycerol, a normally non-permissive carbon source at pH 5.7. Growth on permissive carbon sources is not impacted by *ppe51*-S211R. The horizontal dotted line indicates the starting density of 0.05 OD_{600}. Similar results were observed in Erdman (Figure A.3.5). Mean ± SD are shown in the bar graph.

ppe51 is not required for survival during acid growth arrest

Transcriptional profiling studies previously conducted show that *ppe51* is significantly induced during acid growth arrest[37]. We hypothesized that *ppe51* may be required for Mtb to promote survival when exposed to acid growth arresting conditions. To test this hypothesis, a Δ*ppe51* knockout strain was generated in both CDC1551 and Erdman Mtb using the mycobacteria-specific ORBIT system (Figure A.3.7A)[197]. Successful knockout of *ppe51* was confirmed by sequencing the *oriE* and HygC junction sites of Δ*ppe51*, PCR amplification of the entire knockout region, and qRT-PCR (Figure A.3.7B-E). Complementation constructs containing the native *ppe51* promoter were introduced into Δ*ppe51* carrying WT *ppe51*, variant *ppe51* (S211R, A228D, E215K) and a double variant (S211R+A228D). An empty complementation vector was also introduced into Δ*ppe51*. The presence of these constructs was also confirmed via qRT-PCR (Figure A.3.7F). Growth curves of the complementation constructs grown in growth arresting conditions showed that WT and empty vector strains exhibit growth arrest at pH 5.7, whereas the variant complemented strains exhibited enhanced growth in both CDC1551 and Erdman (Figure 3.4A, Figure A.3.8A). Additionally, the S211R, A228D, and S211R+A228D variant complemented strains grow slightly better compared to E215K in both CDC1551 and Erdman Mtb strain knockout backgrounds, which aligns with previous expression growth curve and relative growth data (Figure 3.2A and B). At pH 7.0, all WT and complemented strains showed similar levels of growth (Figure A.3.8B and C). To examine the role of *ppe51* in survival, a viability assay was performed with the previously described panel of strains. The empty vector and WT-complemented Δ*ppe51* maintain viability over the course of 40 days at pH 5.7 (Figure 3.4B, Figure A.3.9A). The complemented *ppe51* variants also maintain viability and replicate at pH 5.7. At pH 7.0, all WT and complemented strains maintain viability and exhibit similar increases in CFUs over the course of 18 days (Figure A.3.9B and C).

The stable viability of WT or Δ*ppe51* mutant may be due to growth arrest or, alternatively, balanced growth and death. To determine if the strains are truly growth arrested we examined replication using the pBP10 clock plasmid, transformed into WT Mtb, Δ*ppe51*, and *eag* variants in both CDC1551 and Erdman backgrounds[32]. The strains were incubated in minimal media (pH 5.7 and 7.0) with glycerol for 40 days.

We observed that the WT and Δ*ppe51* strains do not replicate under acid growth arrest conditions in both strain backgrounds (Figures 3.4C, Figure A.3.10B). In contrast, we are able to observe high rates of replication in the *eag* variants at pH 5.7 (Figure 3.4C, Figure A.3.10B). We then compared *eag* variants calculated cumulative bacterial burden (CBB) to total CFUs counted on nonselective plates and observed that greater rates of replication in the *eag* variants is associated with a high death rate, yielding a large difference between CBB and total CFUs (Figure 3.4D, Figure A.3.10D-F). When *in vitro* pBP10 growth studies were conducted at pH 7.0 with all strains, we observed similarly high rates of replication and plasmid loss across all strains (Figure A.3.10A and C). Interestingly, these results show that enhanced growth at acidic pH is driven by higher replication, but this growth is offset somewhat by a higher death rate, supporting the conclusion that faster replication at acidic pH is deleterious to Mtb survival.

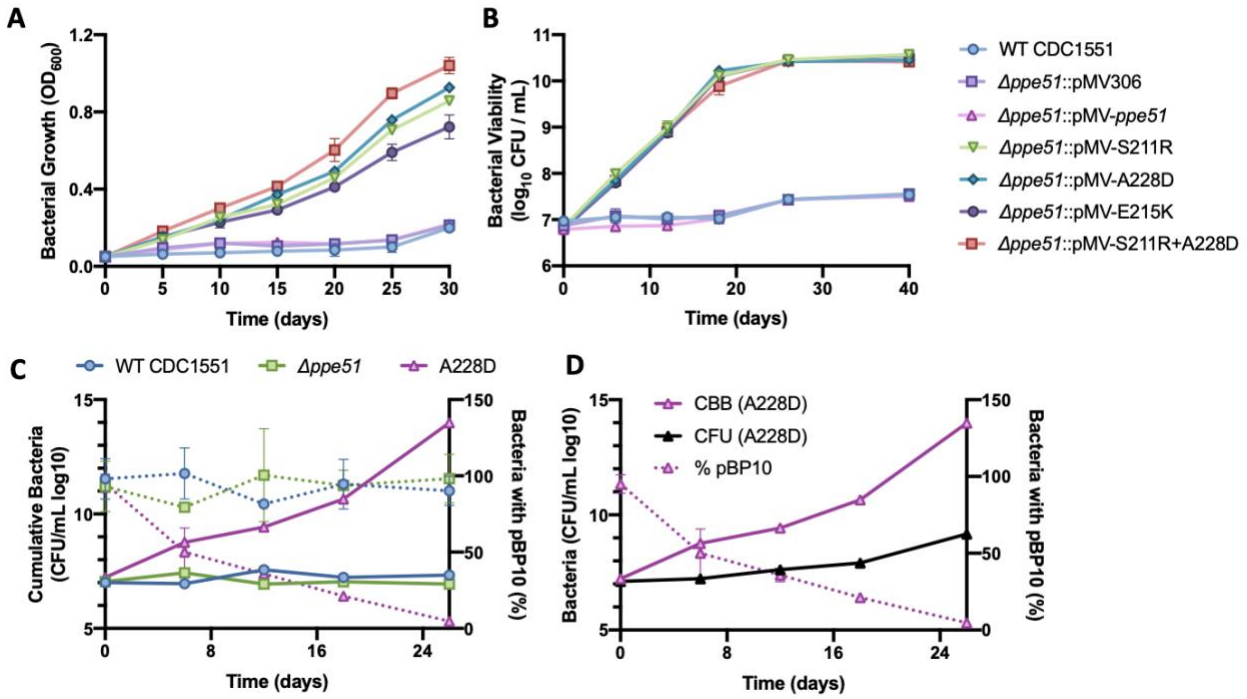

Figure 3.4. Viability and replication dynamics of *eag* mutants. A) Growth curve of *Δppe51* complemented from its native promoter with the WT *ppe51* allele or mutant alleles and performed under acid growth arrest conditions: minimal media buffered to pH 5.7 with glycerol as a carbon source. *eag* variants promote Mtb growth at pH 5.7, while *Δppe51* complemented with WT *ppe51* maintains growth arrest. This experiment was repeated two times. n = 3. Error bars indicate standard deviation. **B)** Viability of Mtb strains as measured by colony-forming units (CFUs). This experiment was repeated two times. n = 3. Error bars indicate standard deviation. **C)** CDC1551 Mtb containing the native variant allele, A228D, continues to replicate during acid growth arrest conditions, but WT Mtb and *Δppe51* cease replication. To estimate replication dynamics of the indicated strains, clock plasmid replication data was obtained from CFU counts (right axis, dotted lines). CFUs of plasmid-free and plasmid-bearing strains were then used to calculate cumulative bacterial burden (CBB) of total live, dead, or degraded Mtb (left axis, solid lines). This experiment was repeated two times. n = 3. Error bars indicate standard deviation. **D)** Replication dynamics of the native A228D (CDC1551) variant, comparing CBB (cumulative bacterial burden), CFU (total CFUs from nonselective plating), and % pBP10 (percentage of bacteria carrying plasmid).

Acidic pH limits glycerol uptake and PPE51 variants overcome this restriction

Pyruvate can rescue growth on glycerol in a concentration-dependent manner at pH 5.7[37]. However, it is unknown whether glycerol concentration affects acid growth arrest. We hypothesized that acid growth arrest may be driven by glycerol starvation and the PPE51 variants promote growth by promoting enhanced uptake of glycerol. If this is the case, we would expect to see a dependence of glycerol concentration and acidic pH on growth. To examine this, we examined checker-board dose responses combining varying pH levels (pH 6.5-5.5) and glycerol concentrations (80 mM-0.13 mM) using the panel of isogenic strains. The standard concentration of glycerol used in our acid growth arrest model is 10 mM. Growth in the wells was analyzed using optical density (OD_{600}) and data was normalized to wells containing the highest (100%) levels of growth and wells with no carbon representing the lowest (0%) levels of growth. Growth assays were performed for 21 days, and the data shown is Day 14 which is representative for the duration of the experiment. Interestingly, we found that growth arrest appears to be both pH and glycerol concentration-dependent, with growth partially rescued at high concentrations of glycerol (~80 mM) for WT, Δ*ppe51*::pMV306 and Δ*ppe51*::pMV-*ppe51* at pH 5.7 (Figure 3.5, Figure A.3.11). Additionally, we observed higher levels of growth at lower glycerol concentrations (~0.82 mM) at pH 5.7 with the complemented *ppe51* variants compared to the empty vector and WT *ppe51* complemented strains. Growth could also be rescued with high glycerol concentration (~32 mM) for variants at pH 5.5. Interestingly, the presence of the double *ppe51* variant (S211R+A228D) overcomes growth arrest at pH 5.5 at even lower glycerol concentrations (~5.12 mM) compared to the single variants, indicating that the presence of two *eag* point mutations confers a slight growth advantage during acid growth arrest. Concentrations of glycerol below 0.33 mM do not rescue growth starting at pH 6.0 in any *eag* strains, which could be due to glycerol being fully consumed. Similarly, these observations were also made in the native *eag* variants in both CDC1551 and Erdman, while WT exhibited a reduced capacity for glycerol uptake (Figure A.3.12). Together, these findings suggest that Mtb has reduced capacity to uptake glycerol in a pH-dependent manner, and that PPE51 variants function by promoting enhanced uptake of glycerol.

Based on these checkerboard results, *ppe51* appears to restrict its growth on glycerol at acidic pH. Additionally, WT Mtb has been shown to completely arrest its growth at pH 5.7 on 10 mM glycerol; however, it is able to maintain viability for up to 40 days, remains metabolically active, and incorporate limited amounts of exogenous ^{14}C-glycerol into lipids[12]. To further test the hypothesis that Mtb restricts glycerol uptake at acidic pH and that *eag* variants promote enhanced glycerol uptake, a radiolabeling experiment using ^{14}C-glycerol was conducted with WT Erdman and the Δ*ppe51* complemented strains previously described. Strains were pre-adapted for three days in MMAT (pH 5.7 or 7.0) with 10 mM glycerol and washed with PBS prior to radiolabeling with 6 μCi of ^{14}C-glycerol. Samples were collected over the course of 24 hours, washed, and analyzed for radiolabel uptake by scintillation counting. All complemented strains containing a *ppe51* variant accumulated ^{14}C-glycerol at a similarly increased rate of approximately 300% compared to the WT Mtb strain (Figure 3.6A). These results are consistent with radiolabeling that was conducted with the pVV16 empty vector, S211R expression strain, and native *eag*-S211R variant where we observed similar enhanced glycerol uptake at ~ 60% with strains containing S211R compared to WT empty vector (Figure A.3.13A). We also looked at glycerol uptake with WT CDC1551, empty vector, and complemented S211R at pH 7.0. We did not observe significant differences in glycerol uptake between strains, and the rate of uptake was similar to the complemented *ppe51* variant strains at pH 5.7 (Figure A.3.13B). Together, these results show that Mtb does restrict glycerol uptake at pH 5.7 regardless of whether *ppe51* is functionally intact. In contrast, strains containing *ppe51* variants have significantly enhanced glycerol uptake.

While the radiolabeling strongly indicated that glycerol was being taken up by the strains, it did not answer whether glycerol was being metabolized by Mtb and incorporated into lipids or binding to the mycomembrane without uptake across the plasma membrane. To address this question, we performed lipid radiolabeling with ^{14}C- glycerol. WT Erdman and Δ*ppe51* complemented strains were pre-adapted for three days in the same culture conditions as the previously described radiolabeled uptake experiment. The operon controlling sulfolipid synthesis is induced in a *phoPR*-dependent and a pH-dependent manner[37,48,129]. We examined sulfolipids by TLC, resolving them in a polar solvent system. Bands consistent with sulfolipid

were observed to specifically accumulate at pH 5.7 (Figure 3.6B) with no accumulation occurring at pH 7.0 (Figure A.3.13C). Triacylglycerol (TAG) has been shown to accumulate during periods of hypoxic and pH-stress[37,202], and pathways involved in TAG synthesis play a role in reducing Mtb growth by redirecting carbon flux away from the TCA cycle[6]. Interestingly, we found that TAG accumulated specifically in the complemented S211R strain at pH 5.7 (Figure 3.6C). A nonpolar solvent system was used to separate lipids, and the bands observed migrated to a position consistent with TAG. In contrast, we did see similar TAG accumulation across all strains at pH 7.0 (Figure A.3.13D). The observation of labeled lipids in both growth arrested and growing Mtb at acidic pH, shows that glycerol is imported and metabolized at acidic pH, with enhanced uptake in the S211R variant.

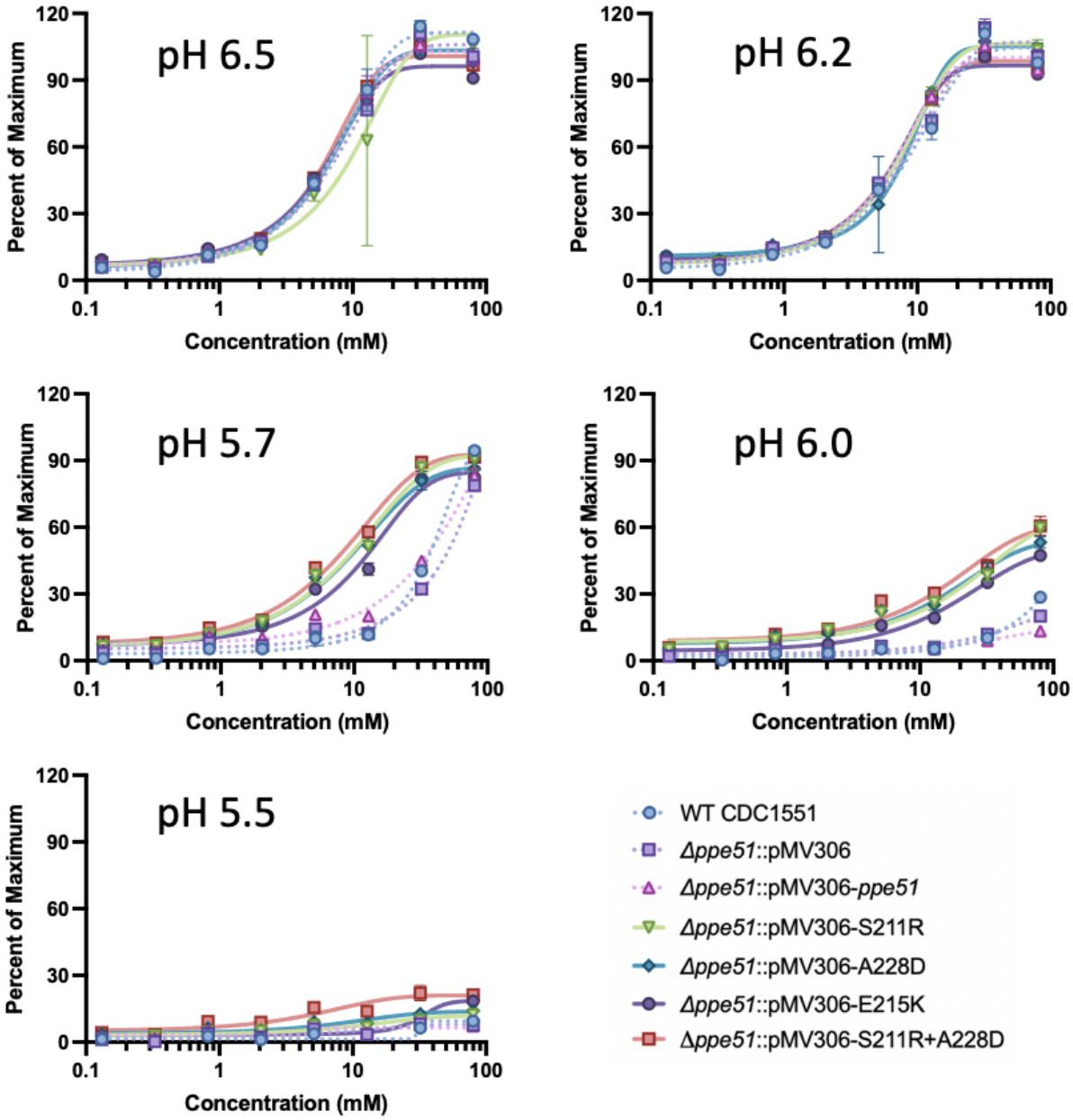

Figure 3.5. Mtb restricts glycerol uptake at low pH. Growth of WT CDC1551, *Δppe51* (empty vector), and *Δppe51* complemented strains in minimal media supplemented in a dose-dependent manner with glycerol and buffered to one of five pH levels (pH 6.5, 6.2, 6.0, 5.7, or 5.5). All strains exhibit a reduced capacity for growth starting ~2 mM glycerol compared to higher glycerol concentrations. At decreasing pH, WT, *Δppe51*(empty vector), and *Δppe51*::pMV-WT restrict their ability to uptake glycerol, whereas any variant complement is able to maintain glycerol uptake. However, restricted growth can be rescued at high concentrations of glycerol (~80 mM) at pH 5.7 for WT, *Δppe51*(empty vector), and *Δppe51*::pMV-*ppe51*, and pH 5.5 for variant complements. Growth analyses were performed at Day 14 following initial inoculation with data being shown as percent of the maximum well-growth. All conditions were conducted in triplicate and representative of multiple independent experiments. Similar data were observed in a native *eag* mutant (Figure S11B). Error bars indicate standard deviation.

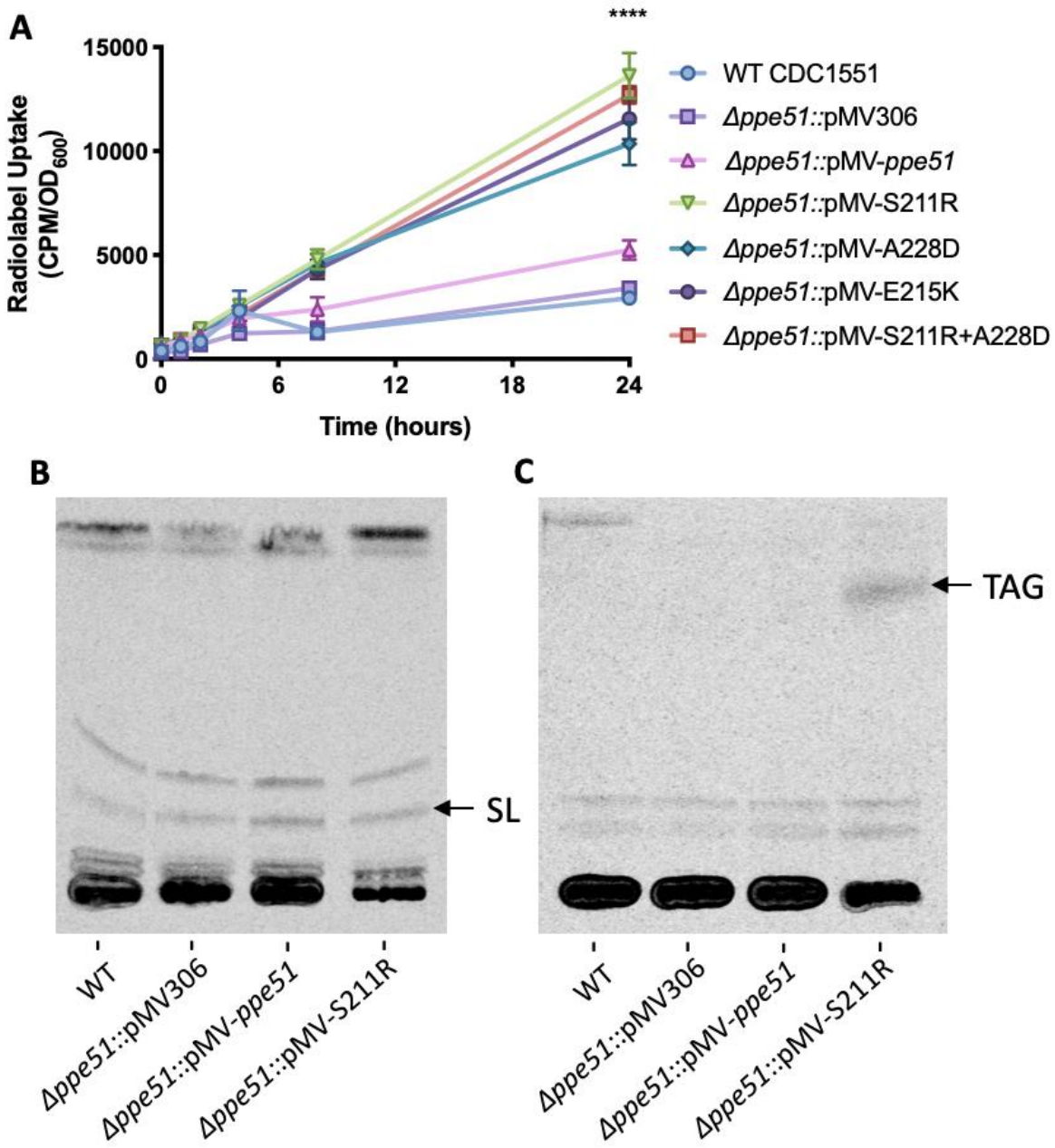

Figure 3.6. *eag* variants exhibit enhanced ^{14}C-glycerol uptake and incorporation into lipids. A) Strains expressing *eag* variants uptake ^{14}C-glycerol at an enhanced rate. Mtb was pre-adapted for 3 days in MMAT (pH 5.7) with 10 mM glycerol and subsequently washed prior to the addition of radiolabeled glycerol. ^{14}C-glycerol uptake was measured using scintillation counting at various time-points over the course of 24 hours. Significance was determined by two-way ANOVA (Tukey's multiple comparisons test; ****P < 0.0001). Error bars indicate standard deviation. **B)** Incorporation of ^{14}C-glycerol into sulfolipids at acidic pH. Sulfolipid is indicated with an arrow and accumulates at a similar rate in each strain. Strains were analyzed in duplicate with representative results being shown. **C)** Incorporation of ^{14}C-glycerol into TAG at acidic pH. TAG are indicated with an arrow and are absent from all strains except for *Δppe51*::pMV-S211R. Strains were analyzed in duplicate with representative results being shown.

Mutations in PPE51 are the main drivers behind enhanced acid growth

All of the isolated *eag* mutants on glycerol had mutations in *ppe51* with a frequency of resistance (FoR) of ~10^{-7}. We hypothesized that additional glycerol *eag* mutants with lower FoR could be isolated by repeating the screen in the Δ*ppe51* mutant. We conducted this second forward genetic screen with the knockout under the same growth arresting conditions as previously described. We plated 10^9 bacterial cells of WT Mtb and native Δ*ppe51* in the CDC1551 and Erdman background on MMAT agar plates buffered to pH 5.7 with glycerol as a carbon source. After 12 weeks of incubation at 37 °C, we observed an average of 556 CFU/mL on the WT CDC1551 plates compared to only 35 CFU/mL on plates containing Δ*ppe51* (Figure 3.7A and B). We also observed an average of 1,055 CFU/mL on the WT Erdman plates compared to 25 CFU/mL on plates containing Δ*ppe51* (Figure 3.7A and B). The control plates, which had only MMAT liquid media (pH 5.7) plated, did not contain any bacterial growth as expected. The few colonies that did appear on the knockout plates were smaller and more punctate compared to those growing on the WT plates. Indeed, we did observe a lower FoR on plates containing Δ*ppe51*-CDC1551 and Δ*ppe51*-Erdman (Figure 3.7B). We picked knockout-containing colonies and confirmed for the *eag* phenotype in liquid MMAT (pH 5.7) with glycerol compared to WT growth (Figure 3.7C), where we observed enhanced acid growth in nine mutants confirmed in Δ*ppe51*-CDC1551 and two mutants confirmed in Δ*ppe51*-Erdman. Δ*ppe51*-CDC1551 mutants exhibited upwards of 12-fold enhanced growth compared to WT CDC1551, while Δ*ppe51*-Erdman had an upwards of 5-fold increased growth compared to its respective WT.

Based on the results of this additional forward genetic screen, mutations occurring in *ppe51* appear to be the main driver behind enhanced acid growth. However, the confirmation of *eag's* in the Δ*ppe51* background strongly suggests that there are likely other genes controlling Mtb growth at acidic pH. Because of the higher FoR seen in the WT forward genetic screens and the high prevalence of mutations in PPE51, it is likely we missed these additional mutants when picking colonies for *eag* confirmation. All nine Δ*ppe51*-CDC1551 and the two Δ*ppe51*-Erdman isolates were sent for WGS. Analysis of the sequencing results show six Δ*ppe51*-CDC1551 harboring distinct SNPs in *ppe60*, all conserved within a 20 bp region (Table 3.2). We also observe a shared SNP occurring in *eccC*$_5$, an essential component of the ESX-5

secretion system, in both CDC1551 and Erdman strains (Table 2). In addition to PPE51, the confirmation of these mutations in a Δ*ppe51* background suggests that there are other genetic components controlling *eag* that may also play a role in Mtb acid adaptation. These mutations are completely novel and require future consideration and study.

A

B

Strain	Seeded bacterial cells (CFU/mL)	Average Mutants (CFU/mL)	Average Frequency of Resistance
WT CDC1551	$1x10^9$	556	$5.56x10^{-7}$
ΔPPE51-CDC	$1x10^9$	35	$3.50x10^{-8}$
WT Erdman	$1x10^9$	1055	$1.06x10^{-6}$
ΔPPE51-Erd	$1x10^9$	25	$2.50x10^{-8}$

C

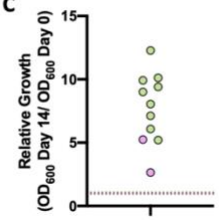

Figure 3.7. Mutations in *ppe51* are the main drivers behind *eag* colony formation. A) WT Mtb (CDC1551 and Erdman) and *Δppe51* were plated at 10^9 CFU on minimal media agar plates buffered to pH 5.7 with 10 mM glycerol. *Δppe51* were plated on triplicate plates and incubated for 12 weeks. Representative images from three independent experiments are shown. **B)** Viable CFUs from each plate were enumerated following 12 weeks of incubation. The frequency of resistance was calculated as a ratio of colony numbers and the number of seeded bacterial cells. **C)** *Δppe51 eag* growth confirmation plot. Growth phenotypes of isolated mutants were determined by measuring Day 14 OD_{600} and compared to OD_{600} from the initial inoculum. Each dot represents mutants that were isolated from MMAT agar plates and confirmed for enhanced growth in liquid MMAT (pH 5.7). Green-colored and pink-colored data points indicate CDC1551 and Erdman mutants, respectively. The dotted lines represent relative WT CDC1551 (green) and Erdman (pink) growth (ratio of ~1).

Table 3.2. Summary results of unique variants isolated from the PPE51 knockout forward genetic screen.

Mutant No.	SNP Location	Nucleotide Change	Gene Name
CDC 2.1	3,889,322	G355V (GGA→GTA)	*ppe60*
	3,889,324	H356Y (CAC→TAC)	*ppe60*
CDC 2.2	3,889,343	P362L (CCG→CTG)	*ppe60*
CDC 2.3	3,889,337	G360V (GGG→GTG)	*ppe60*
CDC 2.4	3,889,334	G359V (GGC→GTC)	*ppe60*
CDC 2.5	3,889,334	G359V (GGC→GTC)	*ppe60*
CDC 3.1	2,017,191	P172L (CCC→CTC)	*eccC5*
CDC 3.4	2,017,191	P172L (CCC→CTC)	*eccC5*
CDC 3.6	3,889,336	G360W (GGG→TGG)	*ppe60*
Erd 3.1	2,017,191	P172L (CCC→CTC)	*eccC5*

PPE51 variants have selectively reduced growth in activated macrophages

ppe51 is induced in a pH-dependent and *phoP*-dependent manner within 2 hours following phagocytosis by macrophages[46], suggesting that *ppe51* is important for pathogenesis. We hypothesized that *ppe51* or its *eag* variants may be required for pathogenesis, specifically in activated macrophages, where the phagosome is acidified. To test this hypothesis, resting and activated primary murine bone marrow-derived macrophages (BMDMs) were infected with WT CDC1551 and Δ*ppe51* mutant and complemented variant strains. In resting macrophages, we did not observe significant differences in Mtb growth between the strains (Figure 3.8A), with all of the strains growing ~1.25-log over nine days. In contrast, in activated macrophages, while the WT, Δ*ppe51* empty vector, and Δ*ppe51* WT complemented strain still exhibit ~1.25-log increase in growth, the *ppe51* complemented variants show significantly lower growth (Figure 3.8B). These results show that *ppe51* variants are selectively attenuated for virulence in activated macrophage environment, which is consistent with a pH-dependent phenotype that is observed *in vitro*.

Rohde *et al*. showed that rapid replication of intracellular Mtb is associated with greater Mtb killing by the macrophage[46]. We observed *in vitro* that variants had enhanced death during replication at acidic pH, and we hypothesized that the *eag* variants may be replicating faster than the WT in macrophages but have lower CFUs due to enhanced death rates. To test this hypothesis, we infected BMDMs with native CDC1551 WT, *Δppe51*, and A228D variant containing the pBP10 plasmid as described previously. Infection was conducted over the course of 8 days with cells lysed and plated for viable CFUs every 2 days. We observed an initial ~0.5 log decrease in viable CFUs in both WT and *Δppe51* around day 2 that is consistent with observations made by Rohde *et al*.[33], and supports their findings that Mtb exhibits delayed adaptation to survive and replicate within macrophages (Figure 3.8C). Both WT and *Δppe51* then replicated over the course of 8 days inside activated BMDMs as evident by their ~1 log increase in CFUs starting at day 2. In contrast, the A228D variant lacks this initial adaptation period and instead show a continual ~1 log decrease in CFUs over the course of 8 days. Calculating the CBB of the A228D variant shows a large difference between the CBB and CFUs, demonstrating that the A228D variant is replicating at a higher rate and dying at an even greater rate. These strains are able to replicate and survive better in resting BMDMs

compared to activated BMDMs (Figure A.3.14). We conclude that slowed growth in response to acidic pH inside activated macrophages is necessary for mycobacterial survival and that the *eag* variants do not sufficiently slow their growth inside macrophages, resulting in enhanced killing. These results also support that the PPE51 variant is promoting uptake of a carbon source during macrophage infection, suggesting that Mtb may metabolize glycerol when growing in macrophages.

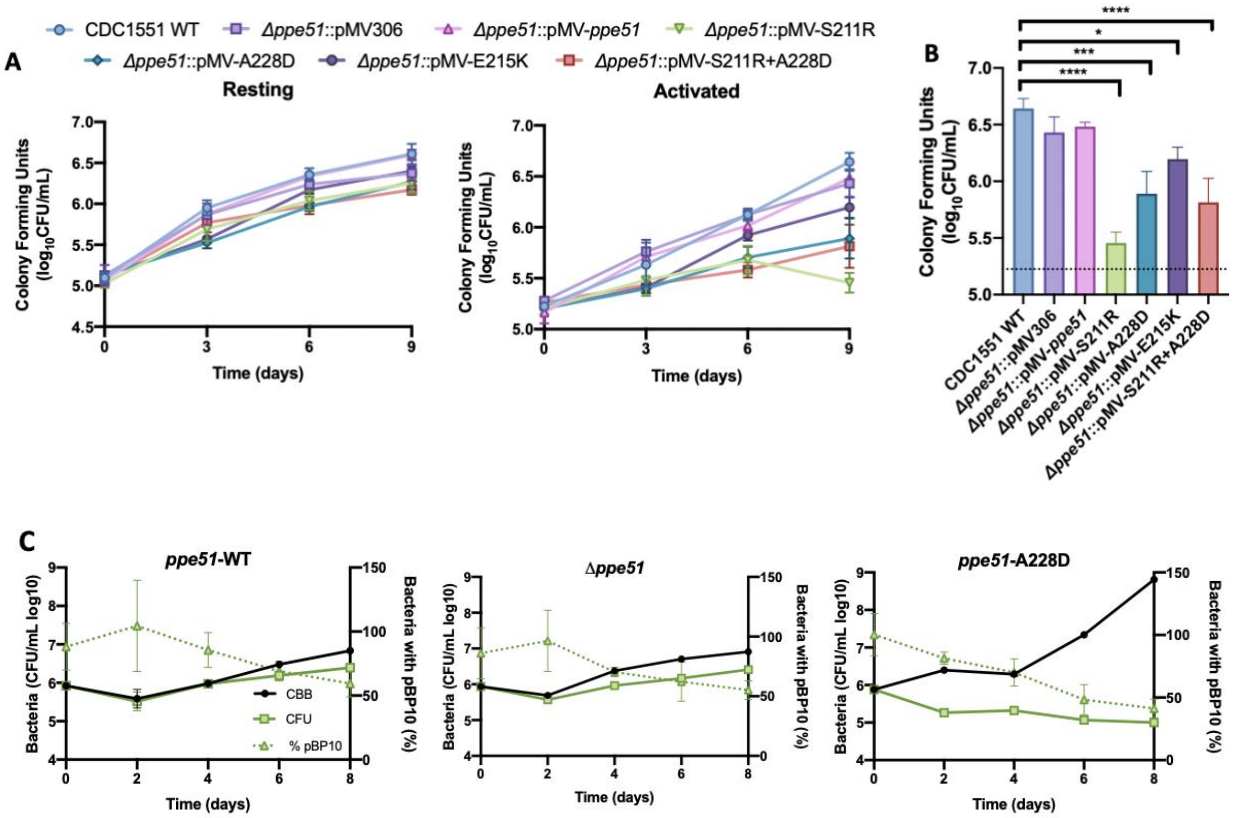

Figure 3.8. *eag* variants exhibit selectively enhanced replication and reduced survival in activated macrophages. A) BMDMs infected with the isogenic panel of CDC1551 *Δppe51* complemented strains and WT CDC1551. Growth is similar for all strains in resting macrophages, but in activated BMDMs, WT, *Δppe51*(empty vector), and *Δppe51*::pMV-*ppe51* exhibit ~1.25 log increase in growth compared to variant complements which show a lower log increase in growth (~0.25-1). Data shown was conducted in triplicate and representative of three independent experiments. Error bars indicate standard deviation. **B)** Statistical analysis of growth differences between *Δppe51* complemented strains at Day 9 in activated BMDMs. Significance was determined by one-way ANOVA (Tukey's multiple comparisons test; *P < 0.05, ***P < .001, ****P < 0.0001). Mean ± SD are shown in the bar graph. **C)** Activated BMDMs infected with native WT CDC1551, *Δppe51*, and A228D variant strains containing the pBP10 replication clock plasmid. CFUs on selective plates were compared to CFUs on nonselective plates and used to calculate frequency of plasmid-bearing bacteria (% pBP10), cumulative bacterial burden (CBB) of total live and dead bacteria, and total enumerated colonies on nonselective plates (CFU). Data shown was conducted in triplicate and representative of two independent experiments. Error bars indicate standard deviation.

Differential thermal stability of PPE51 and the S211R variant proteins support direct interactions between PPE51 and glycerol

We hypothesized that the *eag* variants promote PPE51 uptake of glycerol by altering PPE51 structure and its affinity for glycerol. Changes in the thermal stability of the protein would provide evidence supporting this hypothesis. C-terminal his-tagged recombinant PPE51 and PPE51 (S211R) variant proteins were expressed and purified from *E. coli* (Figure A.15A and B, Table A.3.2). Glycerol was omitted from the reagents used in the purification process and loading dye. All reagents were buffered to pH 7.6. In the absence of glycerol, we observed differential stability between the WT and S211R PPE51 variants, with the WT and S211R proteins completely denaturing at 60 ºC and 50 ºC, respectively, supportive of a significant structural change by the amino acid substitution (Figure 3.9A and B). In glycerol, the WT protein exhibited enhanced stability, completely denaturing at 65 ºC, a shift of 5 ºC, and the S211R protein completely denaturing at 60 ºC, a shift of 10 ºC. These findings support that glycerol/PPE51 interactions, with differential stability shifts dependent on the S211R substitution.

We previously noted that PPE51 S211R did not promote the growth on glucose and therefore, examined the thermal stability in glucose. We observed reduced stability of the WT protein in glucose, completely denaturing at 55 ºC and did not observe any differences in stability with the S211R protein in glucose, supporting the stability shifts are selectively dependent on glycerol (Figure 3.9A and B). Together, these data show that glycerol selectively increases the thermal stability of PPE51, with enhanced impact on the S211R variant, lending further support for a mechanism whereby PPE51 directly binds glycerol for uptake and acquisition into the Mtb cell.

Based on the *eag* phenotype and differences in thermal stability, we hypothesized that these substitutions may have a significant impact on protein structure and thus conducted *in silico* modeling of PPE51 using the Iterative Threading ASSEmbly Refinement (I-TASSER) server for protein structure and function prediction[203]. The best fit model of PPE51-WT had a moderately high confidence score (C-score) of -0.86 on a scale of -5 (low confidence) to 2 (high confidence) (Figure 3.9C). Interestingly, threading of the sequence against known transporter structures produced a porin-like model with a possible channel.

This model was matched to all structures in the Protein Data Bank (PDB) library. The top 10 proteins from the PDB with the closest structural similarity were all predicted to be nutrient transporter proteins (Figure A.3.15C) An overlay of the S211R variant (blue) with PPE51-WT model shows that the introduction of this substitution confers a noticeable conformation shift in the predicted protein structure (Figure 3.9C). For PPE51-WT, the top two predicted ligands were maltose and a monoacylglycerol derivative (78N) with one predicted ligand binding site for maltose being within the 18 amino acid residue range of the *eag* variants, located at residue 225 (Figure A.3.15D). Additionally, the predicted top Gene Ontology terms for the molecular function, biological process, and cellular component are hexose:hydrogen symporter activity (GO:0009679), transmembrane transport (GO:0055085), and integral to membrane (GO:0016021), respectively (Figure A.3.15E). While these *in silico* results are predictions, they provide further support for a role with PPE51 acting as a nutrient transporter for Mtb. Furthermore, all *eag* mutations mapped to a single alpha helix on the predicted I-TASSER model, with S211R and E215K located at the top of the predicted channel and A228D located within the center channel structure (Figure A.3.15F) and the substitutions, altered the modeled substrate interaction, further supporting our model for PPE51 variants acting to promote uptake of glycerol by altering the protein structure and ligand interactions.

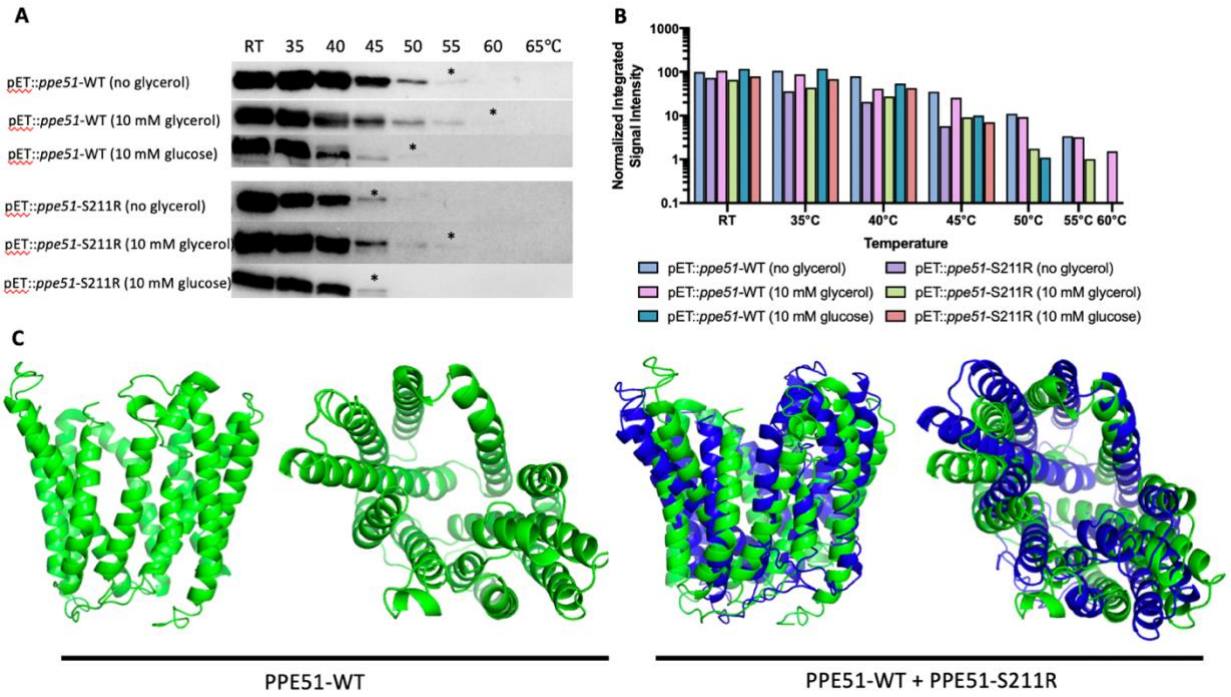

Figure 3.9. Glycerol differentially interacts with recombinant WT PPE51 or S211R variant proteins. **A)** Recombinant WT PPE51 and S211R proteins were assessed for thermostability under no glycerol, 10 mM glycerol, and 10 mM glucose conditions. The protein was preincubated at room temperature (RT) for 20 minutes and subjected to eight different temperature conditions as indicated for five minutes. Following heating, samples were spun down to pellet the protein precipitate. Soluble protein was removed and analyzed by Western Blotting. (*) represents the highest temperature where soluble protein was detected. **B)** Signal intensity of individual bands were measured and normalized to the pET::*ppe51*-WT (no glycerol) band at RT. Samples containing glycerol continue to show detectable signal intensity up to 55°C for pET::*ppe51*-S211R and 60°C for pET::*ppe51*-WT. **C.** *in silico* protein structure modeling and function prediction for PPE51. The peptide sequence of PPE51-WT (green) and PPE51-S211R (blue) were analyzed using the Iterative Threading ASSEmbly Refinement (I-TASSER) approach[203]. Both WT and variant PPE51 were modeled without constraint and appear to form a porin-like structure with an inner channel. PPE51-S211R is modeled against the WT to show the slight conformational changes that occur with the introduction of this mutation. PPE51-WT and PPE51-S211R structures received C-scores of -0.86 and -1.24, respectively, which is a measure of structure confidence on a range of -5 (low) to 2 (high)[203]. A model with C-score >-1.5 usually indicates a correct fold.

PDIM biosynthesis is disrupted in the ppe51 deletion strains

Surprisingly, we found that the *Δppe51* mutant generated in this study does not have the same growth or glycerol uptake compared to previous studies that have generated similar knockouts of knockdowns of *ppe51*[54-56]. We also found that the *Δppe51* grew just as well as other strains at pH 7.0 on glycerol (Figures A.3.8B and C). This observation was previously made by Wang *et al.*, who showed that mutations in phthiocerol dimycocerosates (PDIM) biosynthesis were responsible for permeabilizing the mycomembrane and compensating for the loss of functional *ppe51*[54]. We sequenced the genomes of *Δppe51* mutants in both the CDC1551 and Erdman backgrounds and found that both *Δppe51* mutants had evolved mutations in PDIM biosynthesis pathway genes (*ppsC* in *Δppe51*-CDC1551, and *ppsD* in *Δppe51*-Erdman) (Figure 3.10A). We confirmed for loss of functional PDIM by radiolabeling it with ^{14}C-glycerol and ^{14}C-acetate for six days and extracting total lipids for TLC analysis. As expected, we observed loss of functional PDIM accumulation in the *Δppe51*::pMV-EV compared to WT Mtb radiolabeled at both pH 5.7 and pH 7.0 with ^{14}C-acetate and ^{14}C-glycerol, respectively (Figures 3.10B and A.3.16). However, despite the occurrence of these PDIM mutations in the *Δppe51* mutants, no PDIM mutations were present in the sequenced *eag* variant mutants used in this study or WT Mtb, highlighting that the *eag* variants remain gain-of-function, dominant mutants (Figure 3.2A), that selectively promote uptake of glycerol (Figure 3.3) and promote enhanced uptake of glycerol and enhanced replication *in vitro* and macrophages (Figures 3.6A, 3.4C, 3.8C, A.3.12, A.3.13A, A.3.14). Conclusions for the PPE51 knockout or *eag* variants in the *ppe51* knockout background, must take into account that these strains are also PDIM mutants. Overall, we did not observe any differences in the *eag* mutants if they were in a WT or *ppe51*/PDIM mutant background, supporting that these gain-of-function *eag* phenotypes are independent of PDIM levels.

A

Mutant #	SNP Location	Nucleotide Change	Gene Name
Δppe51-CDC	3,252,696	$(C)_{7\rightarrow8}$	*ppsC*
Δppe51-Erd	3,257,228	S220R (AGC→AGA)	*ppsD*

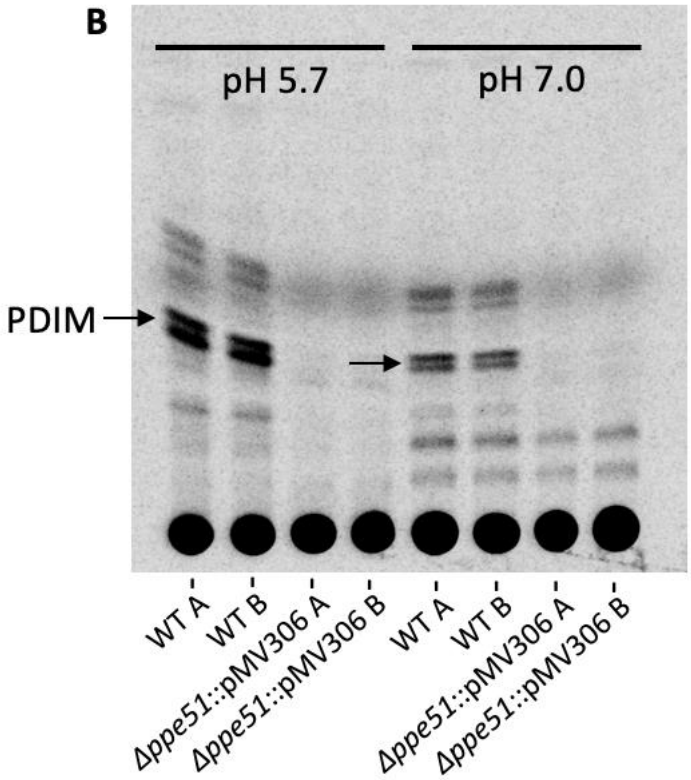

Figure 3.10. *ppe51* knockout strains contain background mutations that disrupt PDIM biosynthesis. **A)** Whole genome sequencing results of *Δppe51* show a nucleotide insertion in *ppsC* and a point mutation in *ppsD* in CDC1551 and Erdman backgrounds, respectively. **B)** Incorporation of ^{14}C-acetate into PDIM at acidic and neutral pH. PDIM is indicated with an arrow and accumulates in the WT strain at both pH 5.7 and pH 7.0 but is absent in the *ppe51* knockout mutant. Strains were analyzed in duplicate with representative results being shown.

Discussion

Mtb exhibits complex regulatory and physiological adaptations when grown in acidic environments, including changes in growth rate. The underlying basis of slowed growth in mildly acidic environments is still not fully resolved, but appears to be associated with metabolic and redox stress, that may be linked to balancing cytoplasmic pH-homeostasis and respiration[171]. Providing specific carbon sources, such as pyruvate or acetyl-CoA, relieve this metabolic stress and enable Mtb to grow similarly well at acidic and neutral pH[12,37]. However, it has been puzzling as to why Mtb cannot grow on glycerol at acidic pH, as it has a carbon source and oxygen, everything it needs to grow. In this study, we found that Mtb limits uptake of glycerol at acidic pH to restrict its growth and that mutations in *ppe51* promote uptake of glycerol at acidic pH and enable growth. That is, Mtb can grow well at acidic pH on glycerol, but has adapted instead to stop growth.

We further show that this pH-dependent metabolic adaptation is required for pathogenesis. Selectively in activated macrophages, where the pH of the phagosome is more acidic, we observed a virulence defect in strains expressing the *eag* variants. Notably, using a replication clock plasmid, we found that *eag* variants have enhanced growth in macrophages, but even greater killing, the balance of which results in reduced fitness. Thus, slowed growth in macrophages, in an activation dependent manner is dependent on the restriction of metabolism at acidic pH, and that PPE51 variants overcome this restriction to the detriment of the pathogen. This finding supports that the nutrient imported by the PPE51 variant is relevant to the macrophage environment. We showed that the variants specifically promote uptake of glycerol, therefore, it is plausible that glycerol is a key regulator of Mtb growth in the macrophage. It has been previously shown that Mtb can uptake TAG in macrophages[204], TAG is abundant in granulomas[205], and Mtb exports the TAG lipase LipY[206], therefore, it is possible glycerol is released from TAG during infection, and restriction of glycerol uptake plays an important role in slowing growth during infection. Studies examining the interactions of PPE51 *eag* variants, LipY and glycerol metabolism genes during pathogenesis will be undertaken to test this hypothetical model.

It is a striking finding that all of the *eag* mutants selected were in *ppe51* and that they all clustered with a highly conserved region of 18 amino acid residues (residues 211-228). Three single amino acid substitutions (S211R, A228D, and E215K) greatly altered WT *ppe51* function and promoted growth under acid stress when given the non-permissible carbon source, glycerol. S211R was able to confer the greatest enhanced growth, whereas A228D conferred moderate enhanced growth and E215K exhibited the least amount of enhanced growth, comparatively (Figure 3.2B). The growth phenotypes of the native mutant alleles were further recapitulated in expression studies in a WT Mtb background as well as a *Δppe51* background, where again we observed overall greater *eag* with the S211R variant compared to A228D and E215K (Figures 3.2A, 3.4A, A.3.8A). Given that the phenotype was conserved in PDIM containing strains (the initially isolated mutants and the expressors in the WT) and PDIM lacking strains (the *ppe51* deletion mutants), this demonstrates that the gain-of-function phenotype is independent of PDIM. This region of PPE51 may play a key role in protein-substrate interactions, and indeed with recombinant proteins, we observed differential stability in the variant protein and its interaction with glycerol. Interestingly, the structural modeling showed substitutions in this region altered the predicted ligand of the modeled transporter, supporting further study of this critical region for modulating PPE51-ligand interactions.

Another key finding of this study is that glycerol uptake is restricted at acidic pH. Data supporting this conclusion include the reduced uptake of radiolabeled glycerol at acidic pH as compared to neutral pH (Figures 3.6A, Figure A.313A and B), the dependence of glycerol concentration and pH in regulating growth (Figures 3.5, A.3.11 and A.312), and the ability of PPE51 variants to enhance growth and glycerol uptake at acidic pH (Figures 3.6A and S13A and B). How Mtb restricts glycerol uptake is still not known, but it is puzzling that PPE51 is strongly induced at acidic pH and counter to a model where PPE51 promotes in glycerol uptake, but Mtb restricts glycerol uptake at acidic pH. This contradiction remains unresolved and points to a new known unknown of Mtb metabolism restriction at acidic pH. Notably, growth on glycerol-containing mixtures can exceed growth compared to growth on glycerol alone[207], suggesting that Mtb may need to restrict glycerol to regulate its growth while consuming other carbon sources it encounters during infection.

We identified that the *eag* variants selectively enabled growth on glycerol alone compared to WT Mtb (Figure 3.3). The identification of this carbon specificity with PPE51 *eag* variants implies a putative role for PPE proteins in nutrient acquisition, a model that is strongly supported by data put forth by Ates *et al.*, Mitra *et al*. and Wang *et al*. These studies showed that PE and PPE proteins located at the cell envelope and cell surface play a vital role in nutrient uptake for Mtb. Ates *et al.* provides strong evidence that the type VII secretion system, ESX-5, is essential for mycobacterial growth and nutrient uptake. In this study, essentiality of ESX-5 could be rescued by altering cell wall lipid composition or introducing the *M. smegmatis* outer membrane porin, *mspA*, which mediates cell wall permeability and influx of hydrophilic nutrients[208-210]. ESX-5 mutations in *M. marinum* result in significantly reduced growth on medium with Tween-40 or Tween-80 as the sole carbon source, and the ESX-5 mutant strain exhibits significantly impaired uptake of fluorescently-labeled fatty acids compared to WT and complemented strains[186]. These data support ESX-5 facilitating the uptake of fatty acids to be used as a carbon source through the secretion of PE and PPE proteins. In support of Ates' ESX-5 substrate nutrient influx hypothesis, Mitra and colleagues[179] showed direct evidence tying PE and PPE proteins to iron acquisition. Mitra identified Mtb transposon mutants that were resistant to a toxic heme analog[179]. The mutants were in three previously uncharacterized genes of which two were PPE proteins, PPE36 and PPE62[179]. Furthermore PPE62 was shown to be surface-accessible and predicted structure indicates that it may form a β-barrel that resembles *Haemophilus influenzae* heme cell surface receptor[179,211] and that heme transport is facilitated into the cell by the periplasmic lipoprotein DppA[212]. Finally, the Wang *et al.* study provided direct evidence that PPE51 is exported to the mycomembrane to promote uptake of glycerol and glucose, possibly by acting like a porin. Notably, loss of function *ppe51* mutants have altered sensitivity to antibiotics, including pyrazinamide[213] and meropenem[214], suggesting that PPE51 mediated impacts on carbon source uptake or mycomembrane permeability play a role in drug susceptibility, supporting further studies of PPE51 as a target for potentiating antibiotics.

Here, we present a model that integrates the current understanding of PE and PPE nutrient acquisition with our findings (Figure 3.11), wherein PPE51 embeds itself into the outermost layer of the

cell envelope and is surface accessible to glycerol[54,193,215]. Gene expression profiling data supports induction of *ppe51* by *phoP* and acidic pH[37,50]. Phylogenetic evidence shows that PPE51 is duplicated alongside ESX-5[184], which has been shown to mediate the secretion of most PE/PPE proteins in *M. marinum*, including PPE51[186,190]. We propose that an unknown periplasmic nutrient transporter helps mediate the import of glycerol across the plasma membrane and into the cell from initial import by PPE51. *pe/ppe* families have high variation rates between *Mycobacterium tuberculosis* complex (MTBC) genomes with *ppe51* being the single exception in showing almost no variation[216]. However, under the specific pressure of our genetic selection (Figure 3.1A), we have shown that we can select for mutations that enhance PPE51's proposed uptake of glycerol (Figure 3.11). Furthermore, our initial *in silico* modeling of PPE51 suggests that it can form a porin-like structure consistent with a role in transport and ligand-binding sites for carbon nutrient sources (Figure 3.9C). Based on these data, we further propose an *eag* mutant model, whereby the *eag* amino acid substitutions introduce conformational changes that allow for a possible PPE51-porin structure to widen or enhance the binding the glycerol, allowing enhanced transport through the mycomembrane.

This study has focused on the role of the *eag* PPE51 variants, and the not the *Δppe51* mutant, due to confounding mutations in PDIM in the deletion strains. It is interesting that both deletion mutants (in Erdman and CDC1551) evolved these mutations during the construction of the mutants and suggests there may have been a selective advantage for the mutations. Indeed, Wang *et al*., showed that *ppe51* knockouts only had a glycerol uptake phenotype when the PDIM was restored in the mutant. This finding is consistent with our observation that the *Δppe51* mutants in this study did not have a growth defect in glycerol, presumably due to the lack of PDIM, whereas the *ppe51* mutants in the Wang *et al.,* study were defective for growth. Given the conservation of the *eag* mutants in strains with or without PDIM, we conclude that PDIM level do not appreciably impact the enhanced uptake of glycerol in *eag* variants. However, it is also possible that differences for the PPE51 mutants between this study and the others may be driven by genomic differences. Both Wang *et al* and Korycka-Machała *et al.* used the H37Rv Mtb strain for their knockout and CRISPRi knockdown studies, respectively. However, sequence analysis of the region directly upstream of *ppe51* in both CDC1551 and Erdman compared to H37Rv shows an almost total deletion of the *ppe50*

gene preceding *ppe51*. The *ppe50* sequence is also not present anywhere else in the CDC1551 or Erdman genome except for a matching 66 bp sequence that precedes *ppe51* in both genomes. The large sequence difference in the *ppe51* promoter region between strains could imply an additional reason why we see strong phenotypic growth differences between our respective growth selections of *ppe51* knockouts.

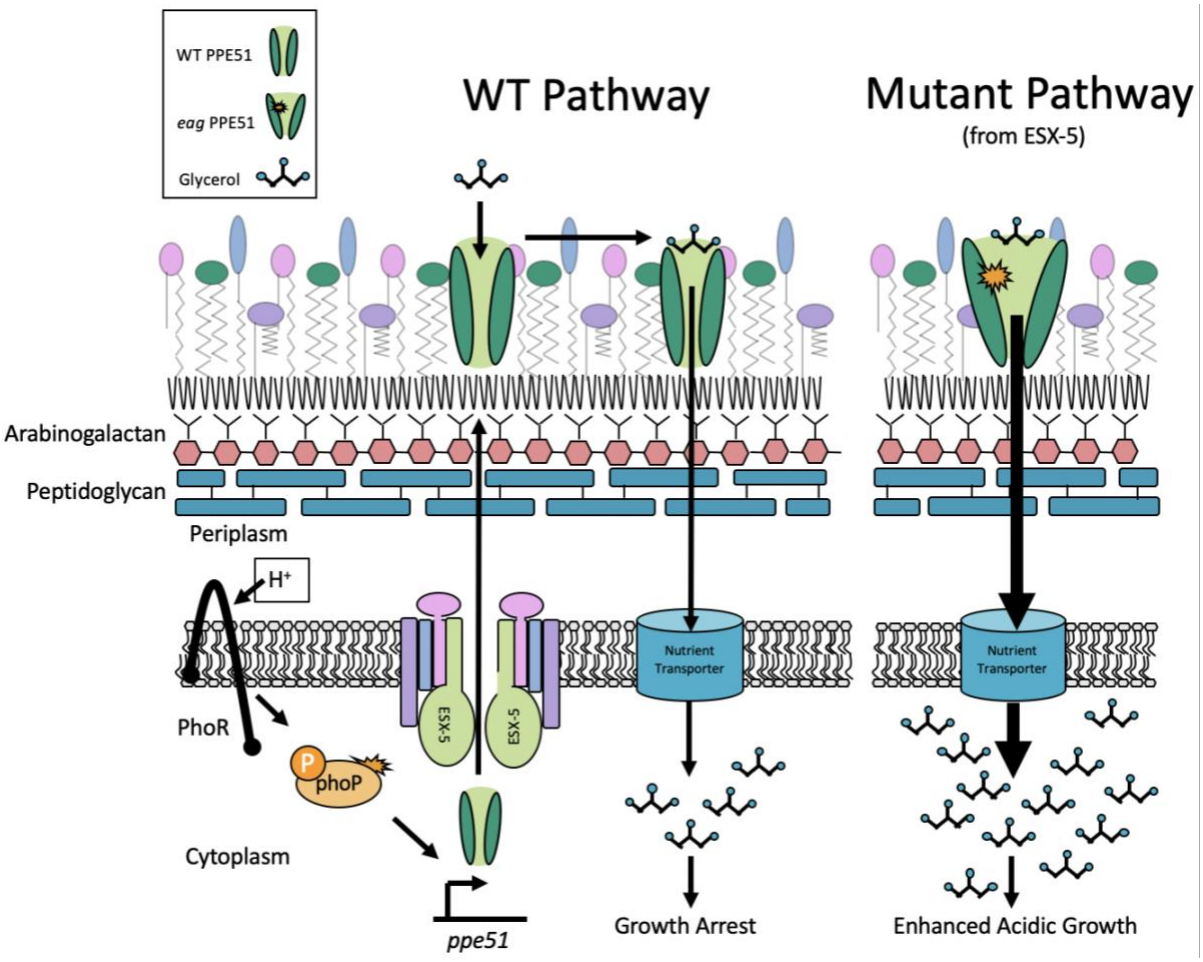

Figure 3.11. A proposed model for the role of *ppe51* and *eag* variants in glycerol acquisition. Presented is a hypothetical model, in which *ppe51* expression is induced by PhoP under acidic conditions. PPE51 is thought to be secreted through ESX-5 and embeds itself into the mycomembrane, making itself surface-accessible. At this interface, it could interact with glycerol and promote transport across the mycomembrane (WT Pathway). PPE51 variants may function by having an altered channel opening or ligand binding surface, allowing for enhanced glycerol transport across the mycomembrane and leading to the enhanced growth phenotype observed during acid growth arrest (Mutant Pathway).

Acknowledgements

We thank members of the Abramovitch lab for critical reading of the manuscript and Prof. David Sherman for sharing the pBP10 clock plasmid. This research was supported by a grant from the NIH-NIAID (R01AI116605) and AgBioResearch.

CHAPTER 4 – Defining the interplay of carbon dioxide and the carbonic anhydrase CanB in regulating *M. tuberculosis* PhoPR signaling and virulence

This work is in preparation for journal submission. The following authors contributed to the development of this project: **Shelby J. Dechow**, Rajni Kumar, Benjamin K. Johnson, and Robert B. Abramovitch.

Author Contributions

S.J.D., B.K.J., R.G., and R.B.A. conceived the project. R.G. and B.K.J. performed the fluorescence reporter experiments. S.J.D. carried out the RNA-seq analysis, qRT-PCR studies, and macrophage infections. R.G. and S.J.D. constructed and confirmed the CRISPRi constructs and ORBIT knockouts. R.G. conducted the RNAseq experiments. S.J.D. and R.B.A. wrote the manuscript.

Abstract

Mycobacterium tuberculosis (Mtb) is the etiological agent of the severe respiratory disease tuberculosis. To be a successful pathogen, Mtb relies on its ability to sense environmental stimuli through transcriptional regulators and induce virulence gene expression. The two-component regulatory system, PhoPR, is implicated in pH-sensing within the macrophage because it is strongly induced by acidic pH both *in vitro* and the macrophage phagosome. However, a direct link between acidic pH and PhoPR signaling has yet to be determined. Following a high throughput screen it was found that the carbonic anhydrase (CA) inhibitor ethoxzolamide (ETZ) inhibits PhoPR signaling. CA promotes the interconversion of CO_2 and water into bicarbonate and a proton. Based on this finding, it was hypothesized that CO_2 plays a role in controlling PhoPR signaling, possibly by modulating the proton accumulation in the mycomembrane in a CA-dependent manner. Mtb has three CA (CanA, CanB, and CanC) and using CRISPR interference knockdowns and gene deletion mutants, we assessed which CAs regulate PhoPR signaling and virulence. We first examined if CA played a role in Mtb pathogenesis and observed that only CanB was required for virulence in macrophages, where the knockdown strain had ~1 log reduction in virulence. Given that ETZ inhibits virulence, PhoPR signaling and CA activity, we hypothesized that CanB may be required to induce the PhoPR regulon at acidic pH. However, in a *canB* knockdown strain, we did not observe differential regulation of a biomarker gene of PhoPR signaling, demonstrating a complex and still undefined link between CO_2, CA activity, PhoPR signaling and virulence. To further define the interplay of CO_2 and Mtb signaling, we conducted transcriptional profiling experiments at varying pH and CO_2 concentrations. As hypothesized, we observed the induction of PhoPR at acidic pH is dependent on CO_2 concentration, with a subset of core PhoPR regulon genes dependent on both 5% CO_2 and acidic pH for their induction. Transcriptional profiling also revealed core CO_2 responsive genes that were differentially expressed independently of the PhoPR regulon or the acidic pH-inducible regulon. Notably, genes regulated by a second two component regulatory system, TrcRS, may be associated with adaptation to changes in CO_2.

Introduction

Mycobacterium tuberculosis (Mtb) virulence is dependent on its ability to sense environmental stimuli and adjust its physiology accordingly. One of the major intracellular stresses that Mtb faces is fluctuation in pH of the acidifying macrophage phagosome[46,217]. The Mtb two-component regulatory system (TCS), PhoPR, is associated with Mtb pH sensing. Over half of the PhoPR regulon is significantly up-regulated within two hours following macrophage infection, and its induction is dependent on phagosome acidification[46]. PhoPR is required for Mtb virulence in macrophages, mice and guinea pigs, where deletion mutants are attenuated for growth in these models. PhoPR also controls sulfolipid expression, which was recently shown to play a role in promoting cough and presumably transmission [218]. Thus, PhoPR could play a role for the duration of infection, from the initial stages of macrophage infection, survival and replication in macrophages and transmission to new hosts. While the PhoPR regulon is regulated by acidic pH, it is possible that it is directly or indirectly regulated by pH or possibly other reported signals like magnesium or chloride[48,219]. Notably, it was recently shown that the PhoPR regulon is inhibited by treatment with ethoxzolamide (ETZ), an FDA-approved carbonic anhydrase (CA) inhibitor[50,220,221], providing a hypothetical link between carbon dioxide (CO_2), pH sensing, and PhoPR regulation.

CO_2 is a gas that plays a vital role in altering physiological and pathophysiological processes across all life, including photosynthesis, oxidative metabolism, and cell signaling[222]. As such, most organisms have evolved CO_2-sensing mechanisms in order to adjust their physiology accordingly, thus, implying that being able to sense CO_2 levels is key for organism survival. For bacteria, sensing changes in CO_2 concentration is important for infecting and colonizing host tissues. Many bacterial species experience the shift from ambient CO_2 levels (0.03%) to higher CO_2 levels (5%) as they enter their host organisms, and it is during this change when many undergo their pathogenic differentiation[222,223]. For example, *Vibrio cholerae* naturally inhabits aquatic ecosystems where it forms commensal or symbiotic relationships with marine organisms[224]. However, removal of pathogenic *V. cholerae* from aquatic environments and introduction into the human host induces virulence. The increase in CO_2 levels found within the human host leads to subsequent increases in enterotoxin production in *V. cholerae* [225]. Specifically, *V. cholerae*

relies on CA activity to initiate enterotoxin production and virulence, which is shown to be significantly reduced following treatment with ETZ[226].

Carbonic anhydrases (CA) are ubiquitous metalloenzymes found in most biological organisms. These enzymes catalyze the essential interconversion of carbon dioxide (CO_2), bicarbonate (HCO_3^-), and a proton (H^+), a process that is characterized by rapid equilibration of all three components by CA[223]. Because CO_2, HCO_3^-, and pH/H^+ are in tight equilibrium with each other, and fluctuation in any one of these molecules can be reflected in the other two, pH can act as an indirect indicator of CO_2 levels. For example, the low pH of gastric juices activates urea transport in *Helicobacter pylori*, resulting in high urease activity and CO_2 production. *H. pylori* buffers periplasmic pH by relying on the conversion of CO_2 to HCO_3^- via CA activity[227,228], providing an example of indirect CO_2 sensing by maintaining pH homeostasis. Mtb encodes for three of these carbonic anhydrases: Rv1284 (*canA*), Rv3588c (*canB*), and Rv3273 (*canC*). Based on global phenotypic profiling with transposon mutants, two of these CA (*canA* and *canB*) are predicted to be required for virulence in mice, suggesting that CO_2 sensing may be important for Mtb virulence[229].

ETZ is a potent inhibitor (~27 nM) of the most active recombinant CA protein in Mtb, CanB, and shows inhibitory activity in the low micromolar (~1.03 μM) and submicromolar (0.594 μM) range for recombinant CanA and CanC, respectively[220,230,231]. Our lab has previously confirmed that ETZ does indeed fully inhibit Mtb CA activity within cells, while also inhibiting the PhoPR regulon[50]. This suggests that a physiological link exists between CA activity and PhoPR signaling, and we hypothesize that ETZ may indirectly inhibit the PhoPR regulon by disrupting CA activity. Our lab has previously proposed a model where the interconversion of CO_2 into HCO_3^- and a H^+ may promote acidification of the pseudoperiplasm leading to activation of the PhoPR regulon[50]. ETZ would effectively block this process, causing the observed inhibition of PhoPR signaling. The goal of this study is to define interactions between CO_2 concentrations, pH, CA and PhoPR-dependent gene regulation and define their functions in macrophage virulence.

Materials and Methods

Bacterial Culture Conditions

Experiments were performed with *M. tuberculosis* strain CDC1551, unless otherwise stated. Mtb was maintained in vented T-25 culture flasks in 7H9 Middlebrook medium supplemented with 10% oleic acid-albumin-dextrose-catalase (OADC), 0.05% Tween-80, and 0.2% glycerol and incubated at 37 °C with 5% CO_2, unless noted otherwise. For experiments requiring buffered medium, 100 mM 3-(N-morpholino)propanesulfonic acid (MOPS) or 100 mM 2-(N-morpholino)ethanesulfonic acid (MES) was added to 7H9 medium for buffering to pH 7.0 or pH 5.7, respectively. Cultures were grown to mid-late log phase (OD_{600} 0.5-1.0) for use in experiments described below.

Flow cytometry and fluorescence analysis

For flow cytometry experiments, *M. tuberculosis* CDC1551 (*aprA*'::GFP) was grown to mid-late log phase (OD_{600} 0.6-1.0) in non-inducing 7H9 medium buffered to pH 7.0. Cultures were pelleted, resuspended, and seeded at an initial OD_{600} of 0.2 into 8 mL of either non-inducing medium (7H9 [pH 7.0]) or GFP-inducing medium (7H9 [pH 5.7]). High (15%), medium (5%), or low (0.5%) CO_2 concentration was applied to biological replicates of each culture condition. Cultures were incubated for six days after which samples were pelleted and fixed with 4% PFA. GFP fluorescence was measured using methods previously described by Abramovitch *et al.* [39]

Transcriptional profiling and data analysis

High-throughput RNA sequencing (RNA-seq) experiments were performed with Mtb CDC1551. Cultures were seeded at a starting OD_{600} of 0.2 in 8 mL of 7H9 buffered media and grown at 37°C in standing T-25 culture flasks. Biological replicates of the following culture conditions were examined: i) 0.5% CO_2 at pH 5.7, ii) 5% CO_2 at pH 5.7, iii) 15% CO_2 at pH 5.7, iv) 0.5% CO_2 at pH 7.0, v) 5% CO_2 at pH 7.0, and vi) 15% CO_2 at pH 7.0. Cultures were incubated for six days, after which total bacterial RNA was extracted as previously described [46]. The SPARTA (ver. 1.0) software package was used to analyze raw sequencing

data[146]. Differentially expressed genes were determined to have a differential gene expression > 1.5-fold and filtered based on $\log_2$CPM < 5. Gene enrichment was performed for Figure 4.4C and A.4.4 using the hypergeometric distribution to determine statistical significance of gene overlap. Enrichment analysis for Figure 4.5A and 4.5B was performed using a Chi-Square analysis with Yates Correction.

Construction of carbonic anhydrase CRISPRi targeting constructs and ORBIT knockout.

To investigate the role of carbonic anhydrases in Mtb pathogenesis, we silenced expression of *Rv1284* and *Rv3588c* using the dCas9$_{Sth1}$ CRISPRi system[232]. Single guide RNAs (sgRNAs) were designed with 20-22 nucleotides of complementarity to the target carbonic anhydrase (Table A.4.1). To achieve total disruption of carbonic anhydrase activity, we generated a Δ*canC* knockout mutant using the ORBIT (oligonucleotide-mediated recombineering followed by Bxb1 integrase targeting) system and replaced *canC* with a hygromycin (Hyg^R) resistance cassette. The ORBIT recombineering plasmid, pKM444, was electroporated into Mtb, and anhydrotetracycline (ATc) was added to induce expression of the RecT annealase and Bxb1 integrase. Electrocompetent cells were made from the pKM444 transformants and subsequently electroporated with the knockout integration plasmid, pKM464, and the *canC* targeting oligonucleotide. The *canC* knockout mutant was confirmed by sequencing the 5' and 3' junction sites using ORBIT target-specific and *canC*-specific primers (Table A.4.1). Semi-quantitative, real-time reverse transcription PCR (qRT-PCR) was used to confirm loss of functional *canC*. Electrocompetent Δ*canC* was used to transform the CRISPRi *canA* and *canB* and generate a knockdown or knockout of all three Mtb carbonic anhydrases.

Macrophage infections

Bone Marrow-derived macrophages (BMDMs) were extracted from mouse femurs and tibiae and cultivated at 37 °C with 5% CO_2 in 24-well tissue culture plates as previously described[200]. BMDMs were infected at a multiplicity of infection (MOI) of 1:1 with the panel of CDC1551 CRISPRi strains unless otherwise stated. Fresh media was exchanged every two days and infected BMDMs were exposed to the following treatment conditions: a) bone marrow macrophage medium [BMMO], b) BMMO + 250 ng/μL

Anhydrotetracycline (Atc), c) BMMO + 100 μM Ethoxzolamide (ETZ), and d) BMMO + 250 ng/μL Atc + 100 μM ETZ. Infected BMDMs were lysed by 0.1% v/v Tween 80 in distilled deionized water. Intracellular bacterial lysates were plated for days 0, 3, 6, and 9. Lysates were serially diluted and enumerated on 7H10 + 10% OADC agar plates and counted following 21 days of incubation at 37 °C. Each strain was performed in triplicate at the indicated timepoints.

Quantitative RT-PCR

CRISPRi samples were incubated at ambient CO_2 and 5%. CO_2 levels with or without 250 ng/mL ATc and/or 100 μM ETZ . After six days of treatment, total RNA was extracted as previously described[46]. cDNA was generated using 1 μg of Dnase-treated RNA with the High-Capacity cDNA Reverse Transcription Kit (Applied Biosystems) and kit protocol. A reaction mix of 2 μL cDNA, 2 μL of forward and reverse qRT-PCR primer, 4 μL of Dnase-free H_2O, and 10 μL of Power SYBR Green PCR Master Mix (Applied Biosystems) was made for each sample tested. All experiments were performed with two biological replicates separated into three technical replicates. The Quantstudio3 was used to perform the following qRT-PCR reaction: 95°C for 2 minutes followed by 40 2-step cycles of 95°C for 15 s and 60°C for 30 s . All samples were normalized to *sigA* signal and quantified using the ΔΔCT calculation.

Results

Carbon dioxide modulates the phoPR pathway independent of medium pH

The discovery of ETZ as an inhibitor of Mtb carbonic anhydrase activity and the PhoPR regulon suggested a potential link between CA activity and PhoPR signaling[50]. CO_2 interacts with water to form carbonic acid (H_2CO_3), which quickly dissociates into a proton (H^+) and bicarbonate (HCO_3^-). Therefore, when CO_2 levels rise it causes a decrease in pH[233]. We hypothesized that if we modulated CO_2 concentrations, much like how Mtb experiences differences in in CO_2 in the environment as compared to the lung, we may observe a subsequent modulation of the PhoPR regulon if it is indeed sensing the proton from CO_2 dissolution. To investigate this, PhoPR signaling was monitored using the CDC1551

(*aprA*'::GFP) reporter strain in GFP-inducing (7H9, pH 5.7) and non-inducing (7H9, pH 7.0) media in ambient CO_2 and 5% CO_2 concentrations. We also treated flasks with 40 μM ETZ or DMSO. Notably, the media are strongly buffered with 100 mM MOPS or MES (pH 7.0 or 5.7 respectively), and changes in CO_2 have no impact on the pH of the extracellular medium. Cultures were incubated for six days, GFP fluorescence was normalized to optical density (OD), and samples were analyzed using a plate reader. We found that fluorescence of *aprA* at ambient CO_2 in pH 5.7 medium with DMSO was ~1.5-fold lower compared to 5% (Figure 4.1A)[234]. Interestingly, ETZ causes an overall reduction in *aprA* fluorescence at pH 5.7; however, 5% CO_2 does cause slightly higher fluorescence (Figure 4.1A)[234]. This observation is consistent with the disruption of PhoPR signaling by ETZ and hints that higher CO_2 concentration may overcome some of the inhibitory activity.

To further analyze the impact of CO_2 concentration on PhoPR signaling, we repeated the experiment using a glove-box with well controlled levels of 0.5%, 5%, and 15% CO_2 in buffered medium at pH 5.7 or 7.0. To address potential impacts of CO_2 on growth that could impact normalized readings on a plate reader, we analyzed fluorescence of individual cells using flow cytometry. In all of these culture conditions, the pH of the medium did not change due to the high levels of 100 mM buffer in the media. Following six days of incubation, exposure to 5% CO_2 at pH 5.7 resulted in significant induction of PhoPR reporter fluorescence compared to 0.5% CO_2 (Figure 4.1B). This level of induction was maintained at 15% CO_2 at pH 5.7. Similarly, PhoPR reporter fluorescence was induced at neutral pH by increasing CO_2 concentrations. As in our previous studies, with CO_2 at 5%, we observed the strong pH-dependent induction of the reporter. These finding reveal that PhoPR can be regulated independent of the pH of the medium and is in fact responsive to CO_2 concentrations.

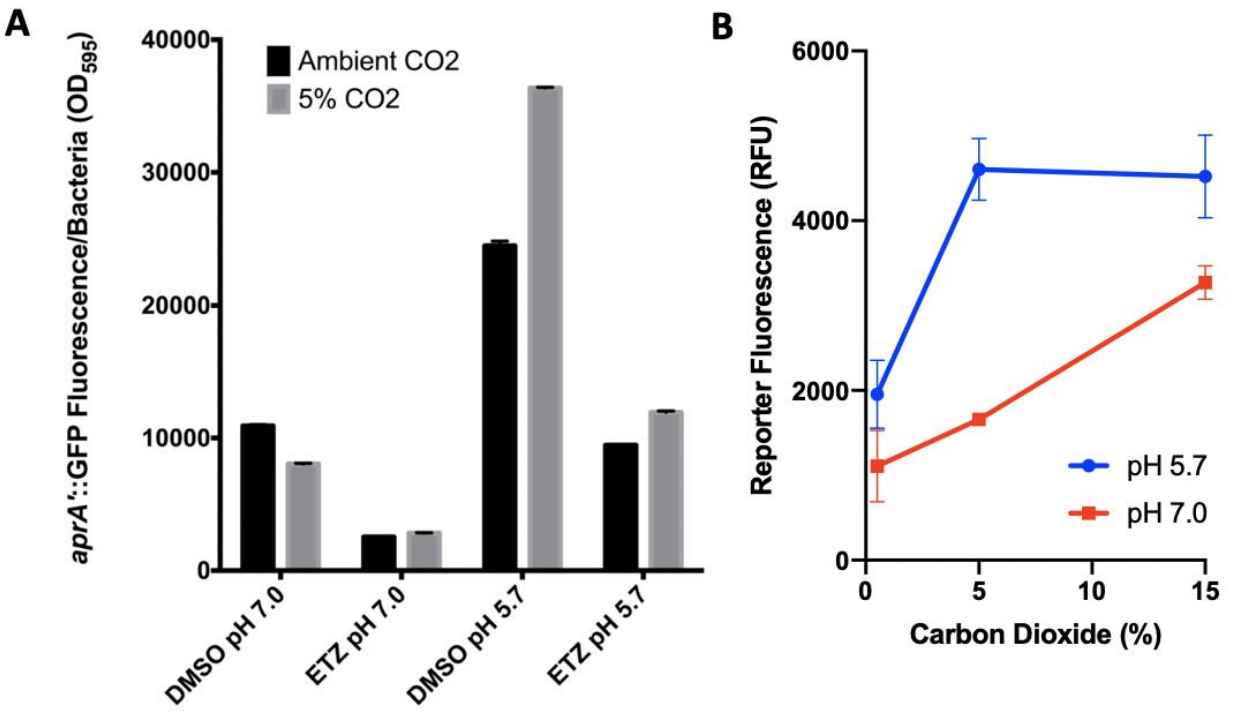

Figure 4.1. Changes in carbon dioxide concentration directly modulate *phoPR*-regulated gene expression. A) PhoPR-dependent CDC1551(*aprA*'::GFP) fluorescent reporter is responsive to changes in environmental carbon dioxide. CDC1551(*aprA*'::GFP) was grown in 7H9 rich medium buffered to pH 5.7 or 7.0 and exposed to ambient or 5% CO_2 for six days. Conditions were performed in duplicate. The error bars represent the standard deviation. Figure and data were derived from Johnson (2016)[234]. **B)** PhoPR-regulated *aprA* is modulated by CO2 independent of pH. CDC1551(*aprA*'::GFP) was grown in 7H9 rich medium buffered to pH 5.7 or 7.0 and exposed to high (15%), medium (5%), or low (0.5%) carbon dioxide concentrations for six days. Conditions were performed in duplicate and results are representative of two independent experiments. The error bars represent the standard deviation.

CanB is essential for survival in macrophages

The Mtb genome encodes for three carbonic anhydrases, Rv1284 (CanA), Rv3588c (CanB), and Rv3273 (CanC) of which CanA and CanB are required for virulence in mice[229]. Biochemical studies show that CanB has the highest catalytic activity of all three carbonic anhydrases and that ETZ is a very effective inhibitor of CanB activity (K_I = 27 nM)[220]. Based on this, we hypothesized that ETZ is targeting CanB, and the subsequent downregulation of the PhoPR regulon, is driving the previously described inhibition of Mtb growth in infected macrophages and mice treated with ETZ[50]. To further investigate the function of CanA, CanB, and CanC during infection, we created CRISPRi knockdowns of *canA*, *canB*, and *canAB* and a knockout mutant of *canC* to achieve disruption strains of all three CA. Successful Anhydrotetracycline (ATc)-induced CRISPRi knockdown in WT CDC1551 background was confirmed through qRT-PCR (Figure A.4.1A-C), with approximately 10-fold and 7-fold reduction of *canA* and *canB*, respectively. CRISPRi of *canC* was not observed, despite attempts with three different CRISPRi constructs, so we generated a Δ*canC* knockout strain in WT CDC1551 using the ORBIT system[197]. Δ*canC* was then confirmed by sequencing the 5' and 3' junction sites, PCR amplification of the knockout region, and qRT-PCR (Figure A.4.2A-C). The CRISPRi strains were introduced into WT CDC1551 and the Δ*canC* strain to achieve different combinations of *canABC* functional disruption and were confirmed with qRT-PCR (Figure A.4.2D). Bone marrow derived macrophages (BMDMs) were infected initially with the WT CDC1551 CRISPRi panel (CRISPRi-*canA*, CRISPRi-*canB*, CRISPRi-*canAB*). The empty CRISPRi vector, pLJR965, was also electroporated into WT CDC1551 and used to infect BMDMs. The infected macrophages were treated with either ATc, ETZ, both ATc and ETZ, or had no treatment applied. At the end of a 9-day macrophage survival assay, we observed ~0.25-0.5-log decrease in growth in all strains treated only with ETZ (Figure 4.2A-E). In the CRISPRi-EV and CRISPRi-*canA*, we observe inhibition of growth by ETZ treatment, but no impact of ATc treatment, suggesting a limited role of *canA* in Mtb virulence in macrophages. In contrast, when ATc is applied to infected cells containing CRISPRi-*canB* and CRISPRi-*canAB*, we observe ~ 1-log decrease in bacterial growth. This indicates that CanB is required for Mtb virulence in macrophages. Notably, there were no CFU differences in ATc-only treated CRISPRi-

canB and ATc+ETZ-treated CRISPRi-*canB*, an observation consistent with CanB potentially being the target of ETZ. We also examined the role of CanC using the knockout strain. Following a 9-day macrophage survival assay, we observed similar ~0.5-log decrease in Mtb growth in strains treated only with ETZ, but no impact on virulence in cells missing *canC* (Figure 4.2F and Figure A.4.3). Notably, in the Δ*canC*-CRISPRi-*canB* and Δ*canC*-CRISPRi-*canAB* we observed a significant reduction of virulence, with a loss of activity for ETZ treatment. Together, these data support that CanB is required for virulence in macrophages and that ETZ activity may be driven by targeting CanB.

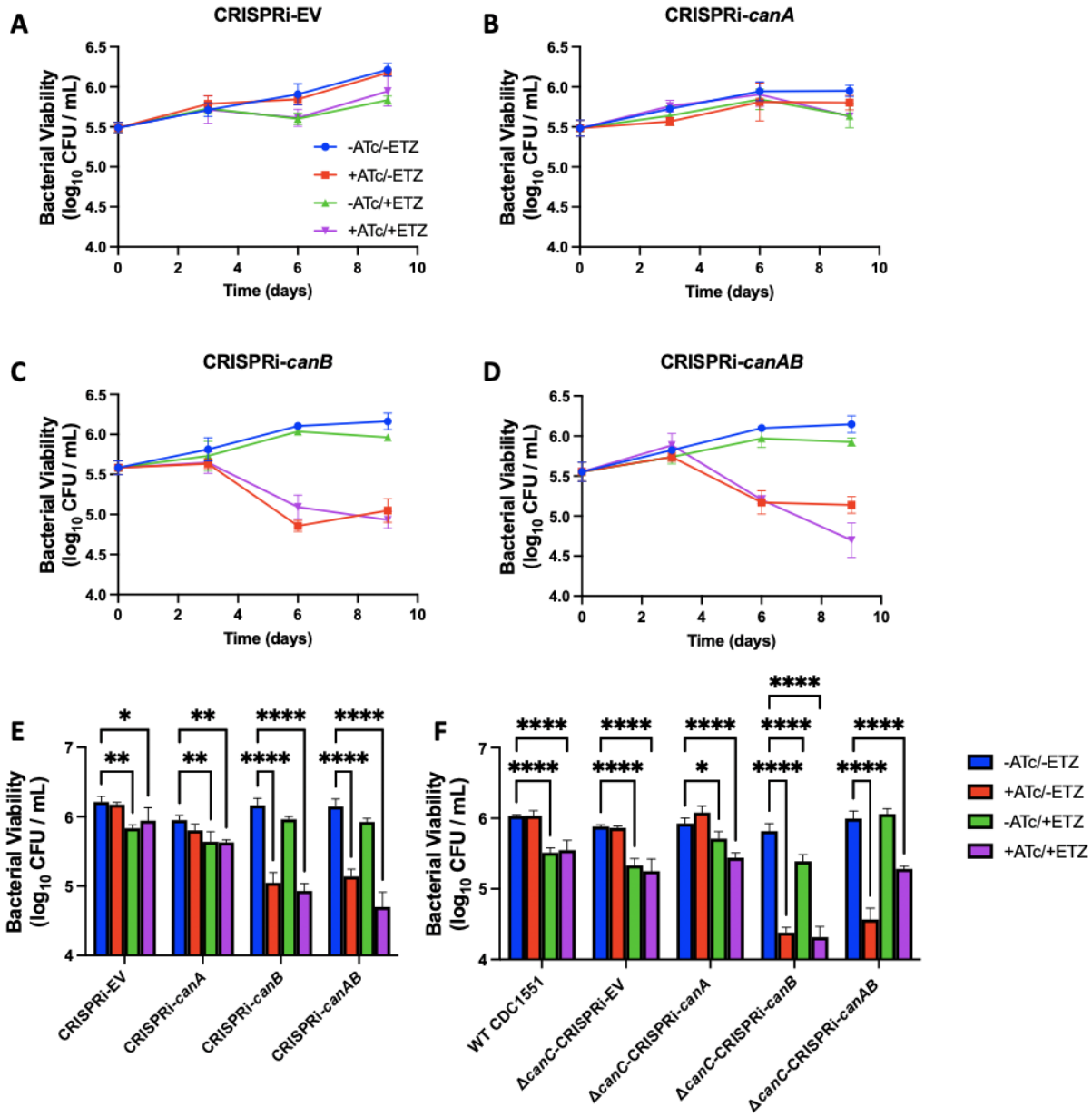

Figure 4.2. CRISPRi-*canB* exhibits reduced survival in macrophages. BMDMs infected with the CRISPRi strains in WT CDC1551: **A)** CRISPRi-EV, **B)** CRISPRi-*canA*, and **C)** CRISPRi-*canB*, and **D)** CRISPRi-*canAB*. All strain treatments were performed in triplicate over the course of 9 days and representative of multiple independent experiments. Error bars indicate standard deviation. Statistical analysis of growth differences between CRISPRi strains in the **E)** WT CDC1551 background and the **F)** Δ*canC* background at Day 9 in resting BMDMs. Significance was determined by one-way ANOVA (Tukey's multiple comparisons test; *P < 0.05, **P < 0.01, ***P < 0.001, ****P < 0.0001). Mean ± SD are shown in the bar graph.

***canB* expression is not associated with changes in *aprA* expression**

Based on our finding that *aprA* fluorescence is lower when incubated with ETZ at both pH 7.0 and pH 5.7 and that CanB is essential for pathogenesis, we wanted to compare *aprA* gene expression levels, and by proxy PhoPR regulation, between ETZ treated Mtb and the *canB* knockdown. To test the hypothesis that CanB is required for PhoPR signaling, we conducted an experiment where we incubated CDC1551 CRISPRi-EV and CRISPRi-*canB* in rich media buffered to pH 5.7 or pH 7.0 at 5% CO_2 levels for six days in the presence of either 250 ng/mL ATc or 100 μM ETZ, both ATc and ETZ, or no treatment. *aprA* gene expression response under each treatment condition for each strain were quantified using semi-quantitative, real-time RT-PCR (qRT-PCR) relative to the no treatment CRISPRi-EV control. Interestingly, we did not observe repression of *aprA* gene expression when CanB was knocked down with ATc treatment at either pH 5.7 or pH 7.0 (Figure 4.3A and 4.3B). *aprA* gene expression was, however, repressed ~10-fold when ETZ treatment was applied, which is consistent with the previous reporter fluorescence data and published RNAseq data[50] (Figure 4.1A). We also checked to see whether *canB* was appropriately knocked down by ATc, and indeed did see ~100-fold repression of *canB* transcript in the CRISPRi-*canB* treated with ATc (Figure 4.3C) compared to CRISPRi-*canB* with no treatment. Additionally, we also do not see inhibition of *canB* expression in either the CRISPRi-EV control or CRISPRi-*canB* when treated with ETZ, which indicates that ETZ is altering the expression of *canB* in intact Mtb cells.

Since there are two additional CA genes in Mtb, we hypothesized that we may see inhibition of *aprA* expression if we knocked down or knocked out all three CA genes at once. To test this, we incubated WT CDC1551, Δ*canC*-CRISPRi-EV, Δ*canC*-CRISPRi-*canA,* Δ*canC*-CRISPRi-*canB,* and Δ*canC*-CRISPRi-*canAB,* in 7H9 buffered to pH 5.7 in the presence of absence of 250 ng/mL ATc for six days. *aprA* gene expression was quantified for each strain and treatment condition relative to the no treatment WT CDC1551 control. Again, we did not observe repression of *aprA* expression in double or triple knockdown and knockout strains of CA (Figure 4.3D). These data do not support our hypothesis that CA activity is modulating PhoPR signaling and suggest that ETZ inhibits PhoPR signaling *in vitro* by a mechanism that is independent of *canA*, *canB* or *canC*.

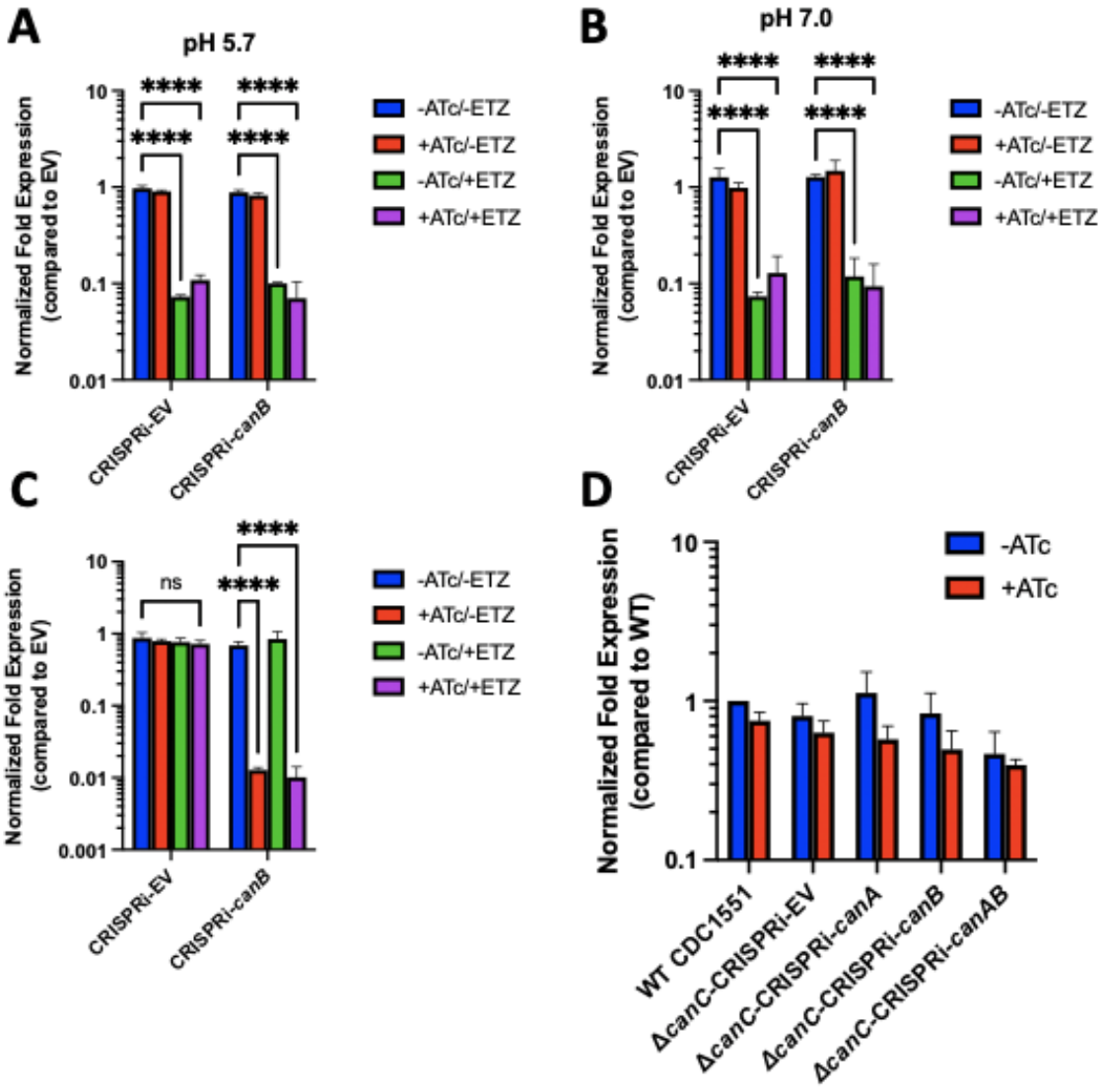

Figure 4.3. *aprA* expression is repressed in a CA-independent, ETZ-dependent manner. qRT-PCR comparing *aprA* expression of CRISPRi-EV and CRISPRi-*canB* in the WT CDC1551 background treated with either ATc, ETZ, both ATc and ETZ, or no treatment at **A)** pH 5.7 or **B)** pH 7.0 relative to the CRISPR-EV strain with no treatment. Data are shown as mean ± SD of three replicates. Statistical significance was determined using a two-way ANOVA (Tukey's multiple comparisons test; ****P < 0.0001). **C)** qRT-PCR confirmation of *canB* expression knocked down in CRISPRi-*canB* when ATc treatment was applied compared to CRISPRi-EV. Data are shown as mean ± SD of three replicates. Two-way ANOVA was applied (Tukey's multiple comparisons test; ****P < 0.0001, ns, not significant). **D)** qRT-PCR of *aprA* expression at pH 5.7 with Δ*canC* CRISPRi panel confirms that *aprA* is not repressed in a triple knockdown/knockout strain of Mtb CA. Data are shown as mean ± SD of three replicates.

Genes induced by CO_2 share significant overlap with the phoPR-regulon

Because increasing CO_2 concentrations at pH 5.7 causes significant induction of PhoPR-regulated *aprA* promoter, we sought to investigate the extent to which the PhoPR regulon might be regulated by CO_2. To more clearly define a CO_2 transcriptional response in Mtb, we performed transcriptional profiling at pH 7.0 and pH 5.7 at 0.5%, 5%, and 15% CO_2 and compared the profiles (Table S4.1A-S4.1E). Mtb grown at pH 5.7 and exposed to 5% vs. 0.5% CO_2 revealed global transcriptional changes with 183 genes induced (>1.5-fold, q <0.05) and 146 genes repressed (>1.5-fold, q < 0.05) (Figure 4.4A). The majority of differentially-expressed genes were involved in cell wall and cell processes and intermediary metabolism and respiration (Figure 4.4B), implying that the mycobacteria may be responding to and redirecting their metabolic activity due to the dynamic shift in CO_2 concentration. In addition to *aprA* induction, we also observed a total of 39 induced genes that overlapped with genes that have PhoP and acidic-pH dependent induction, as determined by induction by acidic pH in WT Mtb and lack of induction in a *phoP*::tn mutant at acidic pH (Figures 4.4C and 4.4D)[50]. Gene enrichment analysis of both transcriptional profiles revealed statistically significant overlap between the two groups of genes (p<0.0001). Notably, we observed widespread changes in gene expression in ESAT-6 secretion system-1 (ESX-1) protein secretion (*esxA, esxB, espABCDE, espL*). PE35 and PPE68, which are located directly upstream of EsxA and EsxB and are required for Mtb virulence and EsxA and EsxB secretion[229,235-237], are also differentially expressed in both profiles. ESX-1 secretion is regulated by PhoPR, and disruption of PhoP is known to negatively impact ESAT-6 secretion[48,50,238,239]. Here, we observe significant induction of ESX-1 associated genes in the 5% vs 0.5% CO_2 transcriptional profile and significant repression in the *phoP::*Tn profile at pH 5.7 (Figure 4.4D), indicating that the PhoPR TCS is induced by to the increased CO_2 concentration.

Downregulated genes in the 5% vs 0.5% CO_2 transcriptional profile at pH 5.7 include those involved predominately in iron homeostasis and intermediary metabolism and respiration (Figure 4.4A). When comparing the downregulated CO_2 profile to upregulated genes in the *phoP::*Tn profile, we see 26 differentially expressed genes that overlap (Figure A.4.4). Again, gene enrichment of this gene overlap is statistically significant (p<0.0001). These overlapping genes include the iron-scavenging mycobactins

(*mbtABCDEFGKL*) and the carboxymycobactin ABC transporter (*irtB*). In contrast, the iron storage gene (*bfrB*) is upregulated in the CO_2 transcriptional profile and down-regulated in *phoP::*Tn (Figure 4.4A), indicating that PhoPR is required for iron homeostasis. Together, roughly 20% of genes differentially regulated at 5% vs 0.5% CO_2 at pH 5.7 are also PhoPR regulated (Figure 4.4C and 4.4D, Figure A.4.4), strongly suggesting that the increased CO_2 levels are inducing PhoPR signaling.

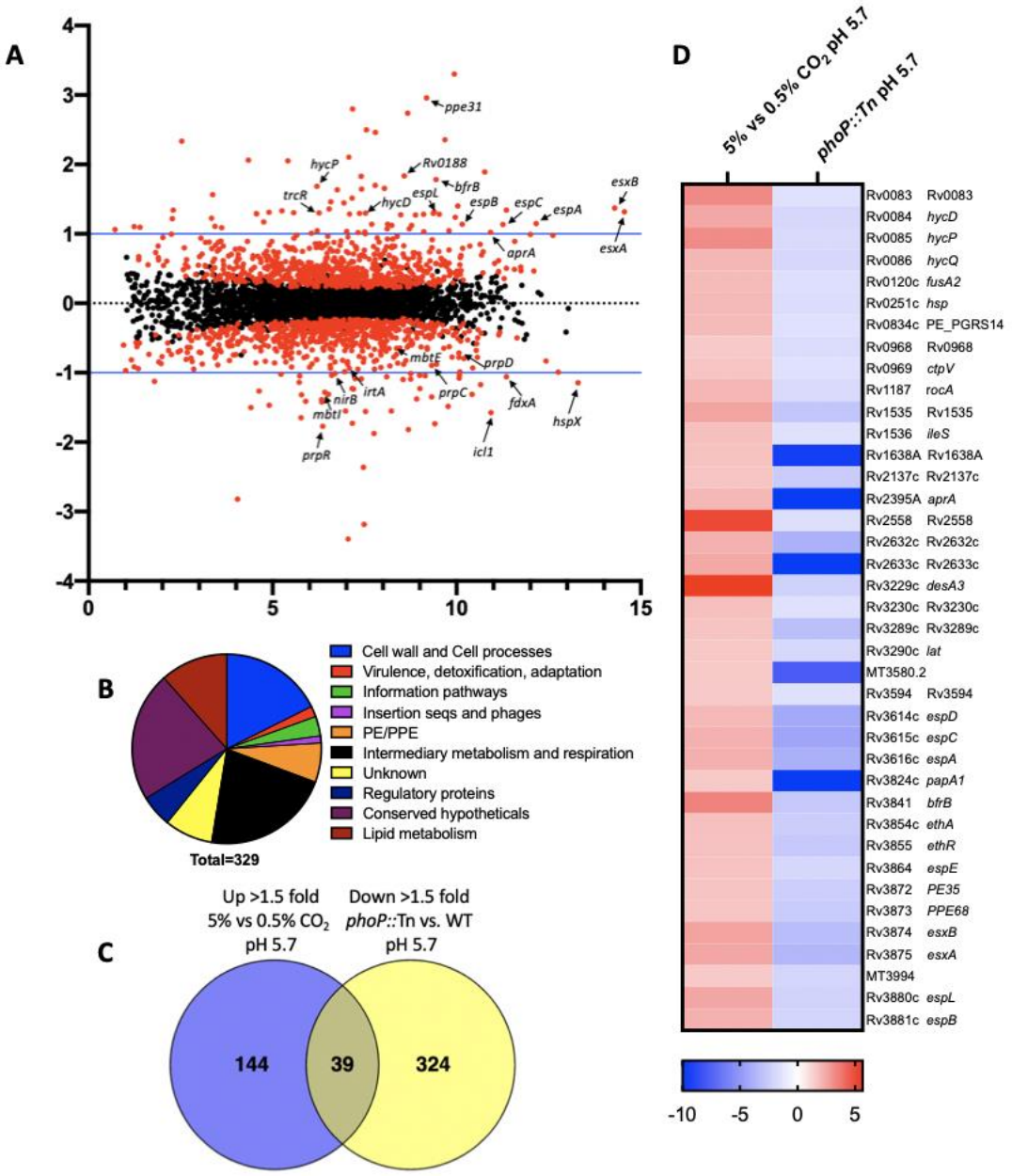

Figure 4.4. Increased CO_2 concentration induces PhoPR-regulated genes at acidic pH. A) Mtb RNAseq transcriptional profiling data following exposure to 5% CO_2 compared to 0.5% CO_2 at pH 5.7. Upregulated genes that are indicated include PhoPR-regulated ESX-1 genes, hypoxia responsive genes, and the *hyc* locus. Downregulated genes that are indicated include those involved in iron acquisition and the methylcitrate cycle. Red dots denote statistically significant genes ($q < 0.05$). **B)** Pie chart depicting the functional categories of significantly differentially expressed genes (>1.5-fold, $q < 0.05$) derived from the pH 5.7, 5% CO_2-treated Mtb RNA-seq transcriptional profile. **C)** Significant gene overlap observed between genes upregulated (Up) (>1.5-fold, $q < 0.05$) by 5% CO_2 treatment at pH 5.7 and Downregulated (Down) (>1.5-fold, $q < 0.05$) in the *phoP::*Tn mutant strain at pH 5.7[50]. **D)** A heat map of the overlapping 39 CO_2-induced (red) and the *phoP::*Tn-repressed genes (blue) (>1.5-fold, $q < 0.05$). Genes are annotated using the H37Rv genome.

RNA-seq studies define the CO_2 regulon and implicate a role for TrcRS in responding to CO_2

To define genes regulated by CO_2 independent or dependent on pH, we initially compared genes regulated by CO_2 (5% CO_2 vs 0.5% CO_2) at pH 7.0 or pH 5.7 and observed widespread changes at pH 7.0 with 78 genes induced (>1.5-fold, q <0.05) and 169 genes repressed (>1.5-fold, q < 0.05) and at pH 5.7 with 183 genes induced (>1.5-fold, q <0.05) and 146 genes repressed (>1.5-fold, q < 0.05) (Figure 4.4A). We then sought to look specifically for CO_2-regulated genes independent of pH regulation. In doing so, we compared the up-regulated transcriptional profiles of 5% CO_2 vs 0.5% CO_2 at both pH 7.0 and pH 5.7 with the acidic pH up-regulated and down-regulated genes (>1.5-fold, q <0.05) described in a previous RNA-seq study (that was conducted at 5% CO_2)[50]. Forty-three genes are both acidic pH and CO_2-upregulated of which 20 genes are controlled by PhoP including ESX-1 secretion genes (*esxAB, espABCDE*) and *aprA* (Figure 4.5A and Table A.4.4). In the 24 genes downregulated by pH and CO_2, we see genes that are repressed by high iron conditions (*mbtBCF*) or involved in intermediary metabolism (*leuCD, pfkB*) (Figure 4.5B and Table A.4.5). This finding is consistent with our conclusion that CO_2 and acidic pH regulate a shared set of genes through PhoPR.

For the CO_2 regulated genes, independent of acidic pH, we observed 21 overlapping genes that were up-regulated (Figure 4.5A and Table A.4.2) and 46 overlapping genes that were down-regulated (Figure 4.5B and Table A.4.3) specifically in response to increased CO_2 levels independent of pH. Genes that responded to CO_2, independent of pH, include intermediary metabolism genes (*icl1*, *prpR, frdA*), lipid metabolism genes (*desA3, ppsA, ppsE*), iron homeostasis genes (*irtB, mbtI, mbtL*), and hypoxia-induced genes (*Rv0081, Rv0188*) (Figure 4.5C, Table A.4.2 and Table A.4.3). Interestingly, we also see PE and PPE genes modulated that have been previously described and their functions resolved. These include PPE51, a putative glycerol transporter, and the PE20/PPE31 complex, which has been shown to mediate Mg^{2+} transport across the outer membrane[54]. Notably, we also observed the induction of *trcR*, the response regulator of the *trcRS* two-component regulatory system (TCS). Further analysis of all CO_2 transcriptional profiles revealed a pattern of up-regulation or down-regulation of the *trcRS* TCS in response to changing CO_2 levels (Figure 4.6, Table S4.1A-4.1E). The pattern of transcriptional changes in *trcRS* were

independent of pH, however, trcRS is more highly induced overall at pH 7.0 compared to pH 5.7. Interestingly, *trcR* is the most highly up-regulated gene with a fold induction of ~13-fold when comparing 5% CO_2 to 0.5% CO_2 at pH 7.0 (Table S.4.1E). CHiP-seq data is published showing the promoters directly bound by TrcR[240]. Comparing genes from the TrcR CHiP-seq study with RNA-seq of CO_2-dependent, pH-independent regulated genes (Figure 4.5A and B) shows that 13 of the CO_2-responsive genes are directly regulated by *trcR* (Table 4.1 and Table S4.2)[240]. This finding supports that TrcRS may also play a role in responding to CO_2. Overall, we observe a general trend where either *trcR* or both *trcRS* are significantly up-regulated when CO_2 levels increase (Figure 4.6). These data suggest that certain genes are directly responsive to changes in CO_2 levels independent of pH and that CO_2 may be a putative input signal for the *trcRS* TCS.

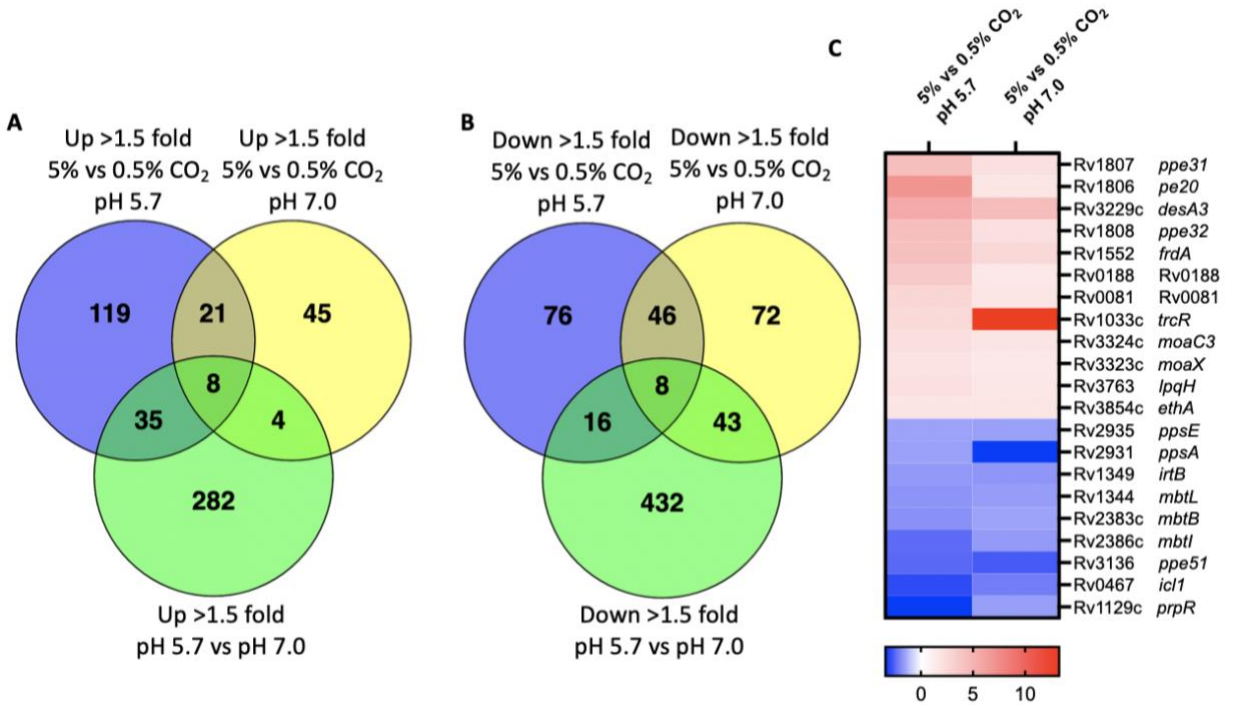

Figure 4.5. Significant overlap observed between expression profiles of increasing CO_2 pressure at both pH 5.7 and pH 7.0. Venn diagrams comparing **A)** up-regulated or **B)** down-regulated genes (> 1.5 fold) modulated by 5% CO_2 at pH 5.7 or 5% CO_2 at pH 7.0 against the pH-induced or repressed regulon, respectively[50]. **C)** A heat map summarizing 21 of the 67 overlapping CO_2-dependent, pH-independent regulated genes (>1.5-fold, $q < 0.05$). Induced genes (Up > 1.5-fold, 5% vs 0.5% CO_2 at pH 5.7 and pH 7.0) are highlighted red and repressed genes (Down > 1.5-fold, 5% vs 0.5% CO_2 at pH 5.7 and pH 7.0) are highlighted blue. Genes are annotated using the H37Rv genome.

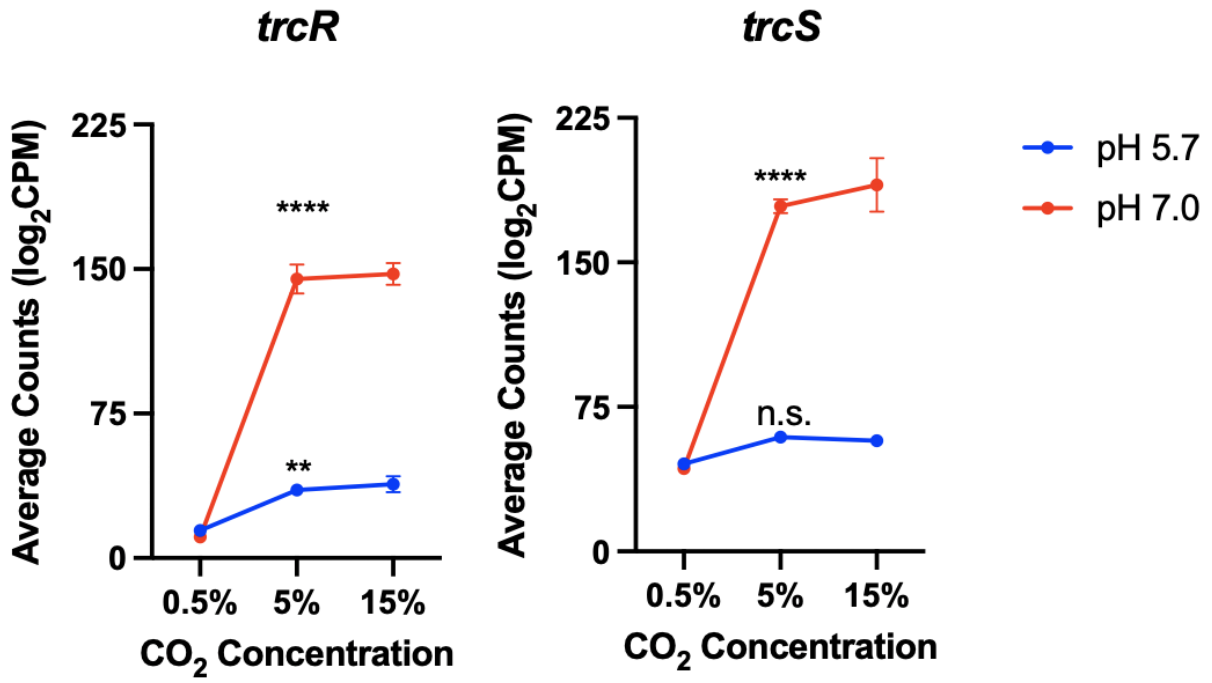

Figure 4.6. Regulatory pattern of *trcR and trcS* in response to CO_2 and pH changes. *trcR* and *trcS* are responsive to changes in environmental carbon dioxide. Average counts per million (CPM) were plotted against CO_2 concentration for *trcR* and *trcS* at both pH 5.7 and pH 7.0. Data is derived from the comparative profiles of global transcriptional response RNA-seq previously described. Conditions were performed in duplicate. Significance was determined by two-way ANOVA (Šídák's multiple comparisons test; **P < 0.01, ****P < 0.0001, n.s., not significant). Mean ± SD are shown in the line graph.

Table 4.1. Overlap of 13 genes shared between TrcR ChiP-Seq and RNA-seq data of CO_2-dependent, pH-independent regulated genes (>1.5-fold, q < 0.05)

Rv Number	Gene Name	Description	ChiP-Seq Score[a]
Rv0244c	*fadE5*	Acyl-CoA dehydrogenase	0.915964
Rv0458	Rv0458	Probable aldehyde dehydrogenase	0.928398
Rv1033c	*trcR*	Two-component response regulator	0.995841
Rv1808	*ppe32*	PPE-family protein	0.863607
Rv2329c	*narK1*	Probable nitrite extrusion protein	0.971408
Rv2949c	Rv2949c	Chorismate pyruvate lyase	0.786824
Rv2950c	*fadD29*	Acyl-CoA synthase	0.733614
Rv2958c	Rv2958c	Possible glycosyltransferases	0.970728
Rv3092c	Rv3092c	Probable conserved integral membrane protein	0.86488
Rv3229c	*desA3*	Possible linoleoyl-CoA desaturase	0.80729
Rv3230c	Rv3230c	Hypothetical oxidoreductase	0.963317
Rv3252c	Rv3252c	Possible alkane-1 monooxygenase	0.912746
Rv3921c	*yidC*	Putative translocase	0.973085

[a] quality score derived from peak calling algorithm. Based on a 0–1 scale, with 1 being a 'perfect' score.

Discussion

Here, we have demonstrated that increasing CO_2 concentration induces PhoPR signaling, and its induction is independent of medium pH (Figure 4.1A and B, Table S4.1A-4.1E). We also show that at acidic pH 5.7, a normally strong inducer of PhoPR signaling[37,46,50], that increasing CO_2 from 0.5% to 5% further induces the pathway (Figure 4.4C and 4.4D). Given that PhoPR signaling is dependent on CO_2, we propose that PhoPR functions as a CO_2 sensor. During infection, Mtb can encounter a variety of changing CO_2 conditions that might be important for PhoPR-dependent virulence. For example, as Mtb infects humans from respiratory droplets or aerosols in the environment (low environmental CO_2 concentrations) into the host lung environment (moderate, physiological CO_2 concentrations), CO_2 could provide a key cue that the bacterium has entered the host. PhoPR is required for key steps of initial macrophage infection (*e.g.* ESX-1 secretion), therefore, inducing these pathways at the onset of infection, prior to macrophage infection, could enhance virulence. PhoPR also induces the synthesis of sulfolipid, a cell envelope lipid that causes animals to cough[241]. As TB infection progresses lung damage can obstruct airflow and cause hypercapnic environments[242,243]. These high levels of CO_2 could trigger Mtb to generate more sulfolipid and drive the cough response and transmission. As such, CO_2 may play a critical role in both inducing signaling cascades for survival during macrophage infection and transmission to new hosts. Thus, studying CO_2 as an environmental cue may provide important new insights into Mtb pathogenesis.

PhoPR is strongly induced by acidification of the host macrophage early in infection[46]. We hypothesized that the proton produced during the catalysis of CO_2 hydration by CA is a possible mechanism linking CO_2 and PhoPR[221]. This model is further supported by the carbonic anhydrase inhibitor, ETZ, modulating the PhoPR regulon. Using knockdowns or knockouts of the three CA, we found that only *canB* was required for virulence. We reasoned that since both *canB* and *phoPR* are required for virulence in macrophages, that the virulence phenotype of *canB* knockdown may be related to loss of PhoPR signaling and that *canB* is required for PhoPR induction. However, under conditions that stimulate PhoPR signaling (5% CO2 and pH 5.7), we observed no impact on *aprA* regulation (a PhoPR signaling biomarker) in the *canB* knockdown. Thus, the link between CA, CO_2 and PhoPR signaling remains unresolved. Additionally,

the mechanism by which *canB* has reduced virulence in macrophages is similarly unresolved. It is possible that residual CA activity present in the CRISPRi knockdowns is sufficient to promote PhoPR signaling at acidic pH. Indeed, our prior study of ETZ in whole cell Mtb, shows ETZ completely inhibits CA activity at the concentrations tested[50]. CAs are very efficient enzymes, so residual activity is a plausible explanation, given we only caused a 10-fold reduction of CA activity in the knock-downs. Knockout strains in *canA*, *canB* or in combination would be needed to test this hypothesis. It is also possible that *canB* knockdown in macrophages may result in downregulation of PhoPR signaling, given the different cues present in macrophages as compared to *in vitro*. Therefore, further experiments are needed to definitively refute our hypothesis that CO_2 modulates PhoPR signaling through a CA dependent mechanism, although, the data presented here support that other pathways, independent of CA, link CO_2 to PhoPR signaling.

The specific induction of the TrcRS TCS in response to changing CO_2 levels is interesting because it may indicate a previously unknown CO_2-dependent signaling pathway. *trcR* encodes for the response regulator which is located directly upstream of the sensor kinase, *trcS*[244]. To our knowledge, there is no defined function for TrcRS in Mtb[245]. While little is known about the conditions under which *trcRS* may be expressed, it is induced during early to mid-logarithmic growth phase under aerobic conditions *in vitro* and following initial macrophage infection at 18 hours but not after 48 hours[244]. Additionally, only one member of the TrcRS regulon has been defined, Rv1057. Rv1057 is a β propeller protein of unknown function, and its expression is repressed by TrcR[246,247]. Interestingly, TrcRS is not the only regulator of Rv1057, which is shown to also be directly regulated by MprAB, another TCS that is associated with cell envelope stress[245,246]. Similarly, loss of *mtrB* in *Mycobacterium smegmatis* leads to defects in cell morphology and cell division, which can be reversed by *trcS* overexpression. Based on these results and ours, it is possible that TrcRS is responding to changes in CO_2 early on during macrophage infection and supports a model of cross-talk between other Mtb TCS. Seeing as TrcRS is not pH-inducible, but is induced when CO_2 levels increase, we propose a model where TrcRS may be sensing CO_2 or bicarbonate and engaging in cross-talk with other TCS pathways to modulate expression in response to CO_2. Future considerations must be made to examine TrcRS' role in CO_2 sensing. One approach is to create a knockout mutant of *trcRS* and conduct

RNA-seq to assess transcriptional modulation of CO_2-dependent genes by exposing the knockout mutant to varying CO_2 levels and comparing that to a wild type transcriptional response. It is possible that if TrcS is able to sense CO_2 using bicarbonate as a proxy, we could elucidate more genes in its regulon besides *Rv1057*. Additionally, this would provide insight into whether there are additional regulators of CO_2 responsive genes if not all are modulated by TrcRS.

When defining genes regulated by CO_2 independent of pH, we found widespread differential expression of genes involved in intermediary metabolism and respiration or lipid metabolism. For example, genes induced by CO_2 in a pH-independent manner include *ethA*, *moaX*, *moaC3*, *frdA*, *Rv3230c*, and *desA3* (Table A.4.2). *moaX* and *moaC3* are involved in molybdenum cofactor biosynthesis which is required for oxidoreductase and nitrate reductase function[248]. *desA3* and the oxidoreductase, *Rv3230c*, interact to produce oleic acid which is essential for mycobacterial membrane phospholipids and triglycerides[249]. *desA3* is also essential for Mtb survival during infection[229]. We also see that half of CO_2-repressed genes are involved in metabolic processes, (Table A.4.3) Notably, these include methylcitrate genes (*icl1*, *prpR*), pthiocerol dimycocerosate (PDIM) biosynthesis (*ppsAE*, *fadD22*, and *fadD29*), and hydrocarbon degradation (*Rv3249c*, *rubA*, *alkB*). Together, these expressional changes indicate that CO_2 induces metabolic shifts that could be required for its survival in the host. One interesting observation is the induction of the *pe20-ppe33* locus by CO_2 (Figure 4.5A and 4.5C, Table A.4.2, Table A.4.4). We see *pe20*, *ppe31*, and *ppe32* induced in a CO_2-dependent, pH-independent manner while *ppe33* is induced both by CO_2 and pH. This locus has been shown to be upregulated during Mg^{2+} starvation, clusters with the Mg^{2+} transporter *mgtC*, and possibly play a role in magnesium homeostasis[48,250,251]. Wang and colleagues recently showed that knockout mutants of this locus exhibit a growth defect in Mg^{2+}-limiting media, especially at mildly acidic pH[54]. Likewise, Piddington *et al.* demonstrated that Mtb requires higher levels of Mg^{2+} for growth at acidic pH[38]. The phagosome is thought to be a Mg^{2+}-limiting environment[252]. Induction of this locus, specifically at higher CO_2 levels, supports Mtb may be sensing the higher CO_2 in the lungs and adapting its physiology accordingly for the nutrient-limiting environment of the alveolar macrophages, possibly priming itself for survival during infection. In support of this, we see a 13-gene overlap with TrcR

ChIP-Seq data and CO_2 RNA-Seq, notably *desA3* and *ppe32* (Table 4.1). These data support a model where CO_2, via TrcR, induces metabolic changes in Mtb that prime Mtb for the nutrient-restricted environment of the host phagosome.

In conclusion, we report here experimental evidence that strongly supports a link between CO_2 levels and pH-sensing and PhoPR signaling. The impetus of this study was to define the mechanism by which the CA inhibitor ETZ inhibits PhoPR signaling. However, the overarching hypothesis driving this study, that CO_2 regulates PhoPR in an CA dependent manner, remains unresolved. It is possible that the CRISPRi knockdown of *canAB* is not sufficient to elicit a change in PhoPR signaling and that CA knockouts are required to replicate the ETZ-dependent inhibition of PhoPR signaling. There may also be additional CA not annotated in the Mtb genome that ETZ could be inhibiting. Or, potentially, ETZ could be targeting something else altogether, even directly inhibiting PhoPR. Further studies will be required to resolve these questions. Nevertheless, important new discoveries have resulted from these studies. Our finding strongly support that PhoPR functions as a CO_2 sensor, including regulation of the central regulator of Mtb virulence, the ESX-1 system, by CO_2 . We also found that increasing CO_2 concentrations elicit a core CO_2-expression profile and that includes changes in metabolism and regulation of the TrcRS regulon. In addition, we confirm that *canB* is required for virulence in whole-cell macrophage infection studies, while *canA* and *canC* are dispensable. Thus, we have defined a complex interplay between CO_2, acidic pH and PhoPR in regulating Mtb gene expression and virulence that supports further investigation of the mechanisms linking these physiologies and defining their role in pathogenesis.

Acknowledgements

We thank the MSU RTSF for providing technical support for the RNA-seq library preparation and sequencing and the MSU Flow Cytometry Core for help with analysis and sorting. This work was supported by a grant from the NIH NIAID (R01AI116605) and AgBioResearch.

CHAPTER 5 – Conclusion

Introduction

When Mtb is phagocytosed by macrophages, it resides in a mildly acidic phagosomal compartment where acidic pH is one of the initial environmental cues that Mtb senses. However, studying mechanisms of acid adaptation inside the host environment is complicated by the combination of multiple accompanying host stresses in addition to acidic pH. *in vitro* acid stress assays seek to piece apart exactly how Mtb senses and adapts to host-relevant pH levels. These assays have been instrumental in deciphering genetic requirements for acid adaption including *marP* (acid resistance)[9], *phoPR* (regulon induction by acidic pH)[37,46], and *aprABC* (induced by acidic pH and *phoP*)[39]. Other pH adaptive requirements include physiological adaptations. Work from our lab has shown that slow growth observed at acidic pH is an adaptive phenotype, and when provided a carbon source that feeds the anaplerotic node, Mtb can grow equally well at acidic pH compared to neutral pH[37]. These observations emphasize that acid adaptation is comprised of both genetic and physiological elements that drive metabolism, growth, and pathogenesis of Mtb. Furthermore, genetic disruption of these adaptations and subsequent sensitization of Mtb to antibiotic treatment shows that chemically targeting acid adaptation can aid in the development of future TB therapies. Therefore, using chemical probes and variations of acid stress assays, with a focus on altering the nutrient composition of the media, enables the identification of novel, previously unrecognized physiological and genetic adaptations to acidic pH.

Summary and additional studies for the AC2P20/thiol-oxidative stress project

Compounds that exhibit pH-dependent activity (Chapter 2) or target known pH-regulated physiologies (Chapter 4) are useful tools to probe new mechanisms of pH-driven adaptation. Using a fluorescent reporter CDC1551 (*aprA'*::GFP), a whole-cell phenotypic screen conducted by our lab uncovered a pH-dependent, growth inhibitory hit compound, AC2P20 (Chapter 2). Transcriptional profiling of AC2P20 treatment at acidic pH established a role in targeting redox- and thiol-homeostasis pathways, similar to a previously characterized pH-dependent compound, AC2P36[69]. Despite these compounds being biochemically and structurally distinct, AC2P20 and AC2P36's shared overlap of pathways and genes

modulated by treatment suggested a similar mechanism of action (Figure 2.2D). I have shown that indeed, AC2P20 targets redox-and thiol-homeostasis in Mtb by sequestering free thiols, resulting in increased ROS accumulation and sensitization of Mtb to acid and redox stress. Therefore, my identification of the shared similarities in regulation of redox- and thiol-homeostasis and regulatory genes between AC2P36 and AC2P20 supports the classification of an entirely new class of thiol-targeting compounds in Mtb.

We still have yet to answer why Mtb is selectively sensitive to thiol oxidative stress at acidic pH. We attempted to address this in part by screening for potential AC2P20 targets but were never able to acquire resistant mutants to AC2P20, which also occurred during the study of AC2P36. This is likely due to both compounds targeting thiols in general and not a specific protein target. It is still possible that we might be able to find resistant mutants by adjusting our screening methods. One approach could be examining the potential for sub-inhibitory concentrations of AC2P20 to select for resistant mutants. In my initial screening approach, I selected for mutants at a concentration causing 100% growth inhibition (Figure 2.1B), and it is possible that this killed the entire susceptible population of Mtb too quickly, not allowing for selection of weakly resistant mutants. To address this problem, an experimental evolutionary approach could be applied. Starting at sub-inhibitory concentrations, Mtb could be serially passaged for multiple generations over a period of time while being exposed to increasing concentrations of AC2P20 or AC2P36. Furthermore, all of my screening work with AC2P20 was conducted primarily at acidic pH. One aspect to explore is the potential for mutants to arise at pH 7.0, using lethal concentrations of compound and assessing their resistance later in acidic conditions. Possible mutations that might arise include those with increased expression of proteins important for regulating thiol-oxidative stress response (i.e. SigH) or protective against oxidative stress.

Another approach to characterize why Mtb is sensitive to thiol-oxidative stress at acidic pH is transposon sequencing (TN-seq)[253]. Using TN-seq, we could identify genes that are essential for survival or have enhanced resistance to AC2P20 or AC2P36 treatment at acidic or neutral pH. Notably, it may be possible to discover mutants that become hypersusceptible to these compounds at neutral pH or acidic pH when treated at a sub-lethal concentration, possibly identifying mechanisms underlying the pH-selectivity

of the compounds. Furthermore, our lab has recently developed new thiol stress reporters using GFP as a signal to probe thiol stress pathways and identify potentially new redox stress-inducing compounds. So far 11 such reporters have been developed and are in different stages of testing. These reporters could be useful for screening for mutants that exhibit differential induction following AC2P20 or AC2P36 treatment. Taken together, these findings could help us define new underlying physiology that links sensitivity or resistance to thiol-oxidative stress and potentially the mechanism driving the dependence on acidic pH.

Summary and additional studies for the PPE51 project

While transposon mutagenesis is a useful approach for generating gene-inactivating mutations across the entire Mtb genome, it overlooks the formation of spontaneous mutations in the genome unless whole genome sequencing is applied. The discovery that mutants exhibiting enhanced growth at acidic pH had spontaneous point mutations driving the selected growth phenotype, independently of the identified transposon mutation, supported additional screening for spontaneous mutants[12]. My work here (Chapter 3) was a continuation of this previous discovery, where I performed a forward genetic selection for spontaneous *eag* mutants in the absence of Tn mutagenesis, utilizing an entirely different strain of Mtb – Erdman. I discovered the same single nucleotide variants in my *ppe51* WT Erdman selection, S211R and A228D, as well as a single novel mutation, E215K. Mtb, CDC1551 or Erdman, harboring an *eag* variant specifically promote growth at pH 5.7 on glycerol and no other tested carbon sources that are non-permissive for growth at acidic pH, supporting a direct role for PPE51 in glycerol utilization. Indeed, PPE51 variants exhibited enhanced uptake of radiolabeled glycerol and accumulation of triacylglycerol (TAG) (Figure 3.6C). These results were consistent with my observation that Mtb specifically restricts its growth on glycerol unless provided a high concentration of glycerol at acidic pH (Figure 3.5) and supports a mechanism whereby PPE51 variants are unable to restrict growth on glycerol. Furthermore, because PPE51 variants are unable to restrict their growth on glycerol, they are significantly attenuated for virulence in macrophages. I also uncovered novel mutants that exhibit enhanced growth on glycerol at acidic pH in a

Δ*ppe51* background, in PPE60 and EccC5, showing that other genetic components may also play a role in Mtb acid adaptation.

While this study mainly focused on the physiological and pathogenic requirements for PPE51 and PPE51 *eag* variants during acid growth arrest, additional experiments are needed to better define the mechanism by which PPE51 acquires or interacts with glycerol. An outstanding question that we have yet to answer is exactly how Mtb acquires glycerol in the macrophage/host and subsequently metabolizes it. We postulate that glycerol could be released from host-acquired TAG during infection through hydrolysis of TAG to glycerol and free fatty acids by a lipase. To examine this, we would need to test whether Mtb can utilize host-acquired TAG. A radiolabeling experiment would be appropriate for probing this question. A radiolabeled triacylglycerol specifically with the carbons of the glycerol backbone radiolabeled (i.e. Triolein [glycerol-^{14}C(U)]) could be employed in such experiment. WT Mtb and a knockout mutant of PPE51 would be incubated with radiolabeled TAG as the sole carbon source. TAG would then be purified from total lipid extracts and quantified using thin-layer chromatography. If we see exogenous ^{14}C being incorporated into mycobacterial lipids, this would tell us that (1) Mtb is breaking down TAG and utilizing it , and (2) that Mtb is utilizing the glycerol directly from TAG. If PPE51 is required for utilizing glycerol derived from TAG, then we should also see ^{14}C-labeled lipids absent from the knockout mutant. Additionally, our lab has not looked at Mtb growth on TAG at acidic pH. An interesting follow-up experiment would be to see whether the *eag* variants exhibit enhanced growth on TAG at acidic pH, and if so, this would further support a role whereby Mtb metabolizes and incorporates carbons from TAG, specifically from TAG's glycerol backbone.

LipY, a PE protein, is a TAG lipase that could be acting to release this glycerol from TAG[254]. To examine whether there is an interaction between LipY's hydrolysis of TAG and PPE51's transport of glycerol, a possible experiment to perform would be to knockout out LipY in an *eag* variant and then transform the pBP10 replication clock plasmid. I would then infect activated macrophages with this mutant strain and observe whether the *eag* virulence defect is still present and whether a lack of enhanced replication in the *lipY* knockout-*eag* variant occurs. This experiment would be key in telling us if there is a

connection between LipY's role in TAG hydrolysis and PPE51's putative role as a glycerol transporter. To further probe if a mechanistic connection exists between TAG breakdown and glycerol metabolism, TN-seq using a saturating transposon library in an *eag* variant background could be employed. This library could be plated on minimal media agar plates (pH 5.7) with TAG or glycerol as the carbon source and used to identify genes essential for TAG and glycerol metabolism. Furthermore, if we see similar genes that are essential to both screens, this would again support a link between TAG hydrolysis and glycerol metabolism. Altogether, we propose that future studies involving PPE51 and *eag* variant PPE51 will involve targeted approaches to assess the requirement for host-derived glycerol stores and help to elucidate whether other physiologies exist in Mtb that interact with glycerol.

My discovery of novel *eag* mutants in the Δ*ppe51* background of both CDC1551 and Erdman strains revealed the *eag* phenotype can be re-established in the *ppe51* mutant background with point mutations in *ppe60* and *eccC*$_5$. I found that all SNPs in *ppe60* occurred within a conserved 20 bp region and that the same mutation in *eccC*$_5$ occurred in both CDC1551 and Erdman strains. We have not yet tested whether these mutants would exhibit the *eag* phenotype specifically on glycerol or on other non-permissive carbon sources at acidic pH. It is interesting that we uncovered a novel *eag* mutant in a secondary PPE protein, and it is plausible that PPE60 could be potentially interacting with glycerol as well. Moreover, PPE60 is secreted through ESX-5[186,190], of which EccC$_5$ forms the central pore of this secretion system[255]. One hypothesis is that the P172L mutation in *eccC*$_5$ may be functioning as a hypersecreter of PPE60, leading to the *eag* phenotype seen with the *eccC*$_5$ mutant. To test this, a PPE60 knockout could be introduced into the *eccC*$_5$-P172L mutant and observed for loss of the *eag* phenotype. Additionally, I have acquired a PE/PPE antibody that would allow us to test the hypersecreter hypothesis directly. In all, our discovery of these novel point mutations that lead to the *eag* phenotype in a Δ*ppe51* background could help us elucidate a functional role for PPE60 in acid adaptation and allow us to probe ESX-5 secretion of PE/PPE proteins.

Summary and additional studies for the carbonic anhydrase project

Despite numerous studies describing a role for PhoPR as a pH-sensing TCS, we do not know how Mtb's PhoPR responds to pH biochemically. Previous work from our lab with the carbonic anhydrase inhibitor, ETZ, proposed that a previously unrecognized link exists between CO_2 sensing, carbonic anhydrase activity, and PhoPR signaling[50]. It is hypothesized PhoPR may be sensing the proton produced from the dissolution of CO_2 by carbonic anhydrase, and that the proton may promote acidification of the Mtb pseudoperiplasm, leading to activation of the PhoPR regulon. Furthermore, increasing CO_2 concentrations could result in greater PhoPR induction. In this study (Chapter 4), I show that PhoPR is induced by higher concentrations of CO_2 independent of pH. Furthermore, transcriptional profiling studies at pH 5.7 and pH 7.0 with increasing concentrations of CO_2 showed that a subset of core PhoPR regulon genes are significantly induced by higher CO_2 at acidic pH. I also uncovered the induction of an undefined TCS, TrcRS, which is slightly induced by higher concentrations of CO_2 at pH 5.7 and greatly induced by higher CO_2 concentrations at pH 7.0, suggesting that it may be sensing CO_2 concentrations. This study also sought to better understand the role of the three Mtb CA in Mtb pathogenesis. Using the CRISPRi knockdown system, I observed that only functional CanB is required for virulence in macrophages. However, knockdown of *canB* did not alter the induction of a PhoPR regulated gene, *aprA*, suggesting that *canB* alone is not responsible for linking PhoPR induction to CO_2 concentration.

While these experiments strongly support a role whereby PhoPR is directly responding to changes in CO_2 concentrations, attempts to develop an Mtb tat-secreted pH-sensitive GFP (pHluorin[72]) to monitor pseudoperiplasmic pH, and thereby biochemically support the proposed function for PhoPR as an integrated pH and CO_2 sensor, were unsuccessful. It is known that expressing fluorescent proteins in oxidizing environments like the bacterial periplasm can cause misfolding and disruption of fluorescence[256,257], however, we can only speculate if similar conditions exist in the Mtb pseudoperiplasm. To overcome this potential problem in the future, new superfolder variants of pHluorin could be employed to determine periplasmic pH[258]. In addition to better understanding the biochemical interactions of PhoPR and pH, we have yet to define the physiological implications of CO_2 during infection and how or why Mtb may be

sensing changes in environmental CO_2 concentration overall. My discovery that TrcRS is induced directly in response to higher CO_2 implicates this TCS in a possible CO_2-sensing role. Generating a *trcRS* knockout mutant would allow further probing of this hypothesis. Transcriptional profiling with Δ*trcRS* could help identify a core TrcRS regulon by comparing a Δ*trcRS* transcriptional response at 0.5% and 5% CO_2 (pH 5.7 and pH 7.0) with the transcriptional data presented here in Chapter 4.

While my study begins to probe this interaction, further consideration is needed for exploring Mtb's ability to sense differences in CO_2 *in vivo*. TrcRS and PhoPR are both implicated in sensing CO_2 by the studies presented here. Despite there being no cross-talk observed between either TCS[259], it is possible that both of these TCS work in concert with each other to induce a transcriptional response influenced by changes in environmental CO_2. However, we still have yet to determine why Mtb needs to sense CO_2 in the first place. It is plausible that CO_2 acts as an environmental cue that allows Mtb to discern when it has entered the host, thereby inducing TrcRS and PhoPR to elicit a transcriptional response. We know that PhoPR genes are turned on within two hours following a macrophage infection and that acidification is an important trigger for PhoPR-regulated differential gene expression[46]. Interestingly, the PhoPR regulon is induced ~pH 6.4[39], which is consistent with the pH range of the phagosome in resting macrophages[21]. It is possible that CO_2 may elicit a similar effect, in that TrcRS and PhoPR regulons could be induced when CO_2 levels reach a certain threshold within the host. An experiment could be conducted *in vitro* looking at increasing CO_2 concentrations from ambient to 5% CO_2, using fluorescence reporters of the TrcRS and PhoPR regulons. If we see induction of both TCS occurring at a threshold consistent with CO_2 levels normally found in the lungs, this could suggest that CO_2 is playing an important role in inducing a targeted transcriptional response. Additional consideration for *in vivo* studies is that Mtb causes damage to lung tissue and forms granulomas that can lead to hypercapnic regions of the lungs. Animal models that are incapable of forming obstructions could be harnessed to assess Mtb differential gene expression during an infection period and compared to animal models that are capable of forming lung obstructions. Again, induction of CO_2-responsive genes and the PhoPR regulon in animal models that can form granulomas, in areas associated with lung damage and disrupted lung function, may indicate a connection for Mtb to sense

CO_2 in the host. Thus, future studies of integrated CO_2-and-pH-inducible PhoPR signaling will focus on developing and improving biochemical and physiological experimental methods to elucidate the exact inputs and host-relevant environments sensed by PhoPR.

Concluding remarks

Understanding what pathways and physiologies are important for Mtb to survive acid stress are crucial for developing new TB therapies and increasing our understanding of Mtb pathogenesis in the host. In this study, I have characterized a new compound with pH-dependent activity and shown that it selectively kills Mtb at acidic pH by depleting free thiols. As a result, AC2P20, in combination with AC2P36, can be classified as an entirely new class of compounds that render Mtb especially sensitive to changes in thiol homeostasis at acidic pH. Additionally, I have further defined the role of PPE51 in acid growth arrest and shown that Mtb specifically restricts its growth on glycerol through an adaptive and regulated process. Furthermore, I have demonstrated that pH-dependent metabolic adaptation is required for pathogenesis and that loss of acid growth arrest leads to reduced Mtb survival in macrophages. This work has also elucidated the possible biochemical inputs required for PhoPR activation and established a role for carbonic anhydrases and CO_2 sensing in Mtb pathogenesis. Taken together, this work has furthered our understanding of novel or poorly defined physiologies important for acid adaptation in Mtb, demonstrated their susceptibility to therapeutic treatment or host-relevant stress, and prompted future studies of pH-dependent adaptation.

APPENDICES

APPENDIX A:

Supplemental Figures

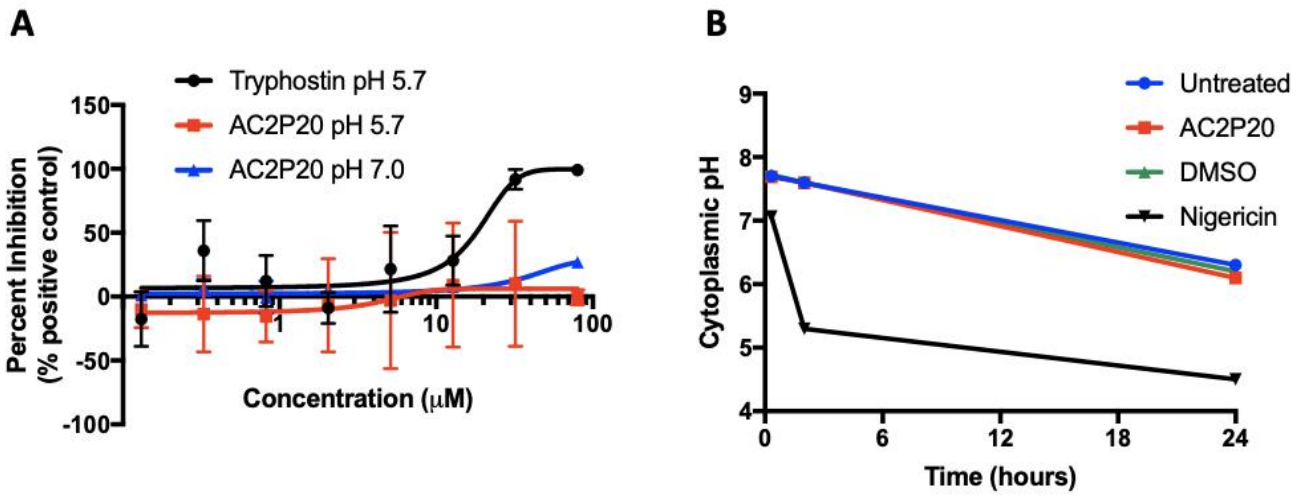

Figure A.2.1. AC2P20 does not inhibit *M. smegmatis* growth or Mtb pH homeostasis. A) Dose-response curve for AC2P20 inhibition of M. smegmatis GFP fluorescence. **B)** AC2P20 does not modulate Mtb cytoplasmic pH at pH 5.7. DMSO and Nigericin served as negative and positive controls, respectively.

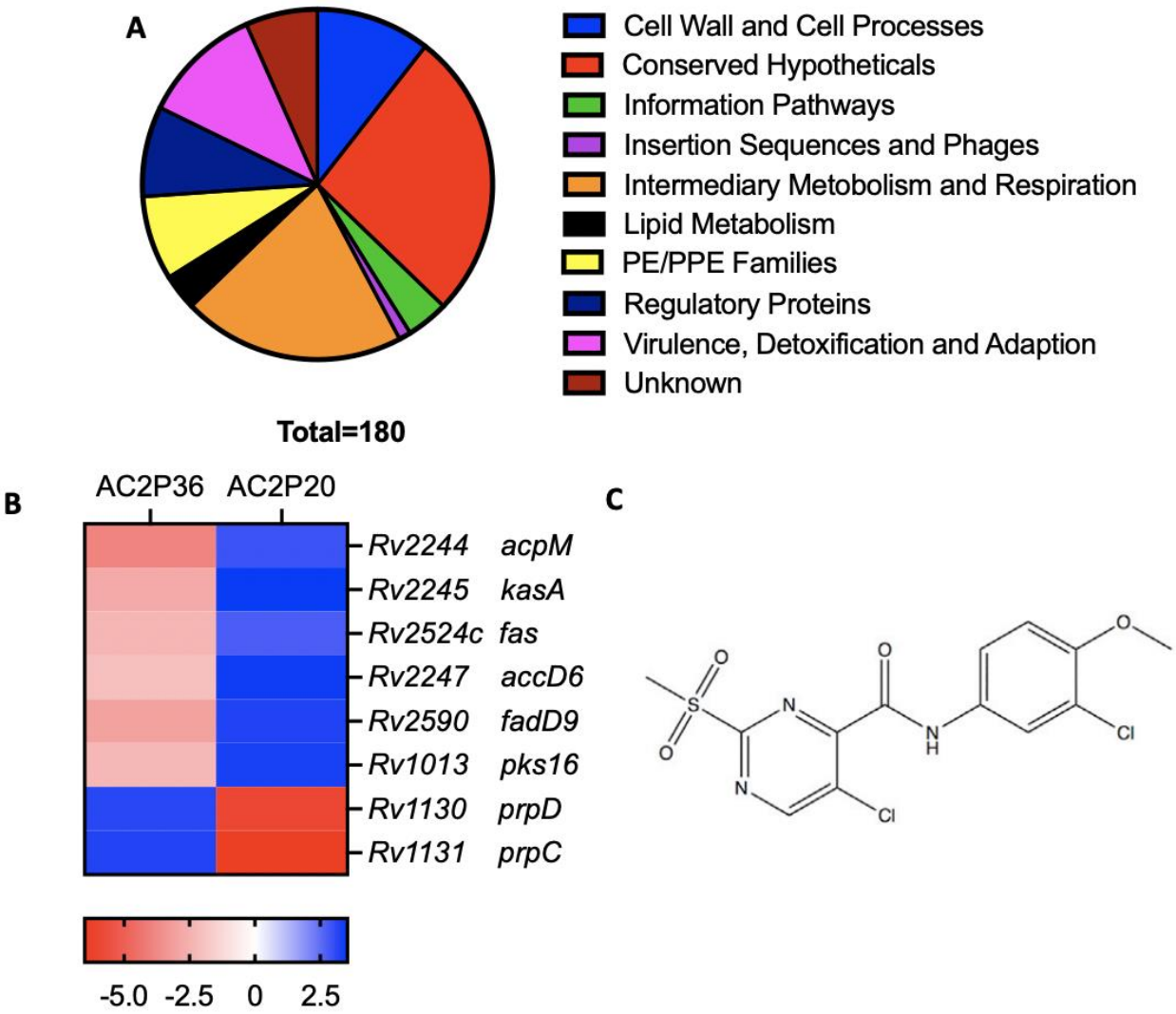

Figure A.2.2. AC2P36 transcriptional profile and structure is distinct from AC2P20. A) A pie chart depicting the functional classification breakdown of significantly induced genes (>2-fold, $q < 0.05$) following the analysis of AC2P36-treated Mtb RNA-seq profile. **B)** Heatmap comparing the contrast between 8 differentially-regulated genes (between AC2P20 and AC2P36 at pH 5.7) that are involved in lipid metabolism and central metabolism. Genes were annotated with the H37Rv genome. **C)** The chemical structure of AC2P36 (5-chloro-N-(3-chloro-4-methoxyphenyl)-2-methylsulfonylpyrimidine-4-carboxamide) [69].

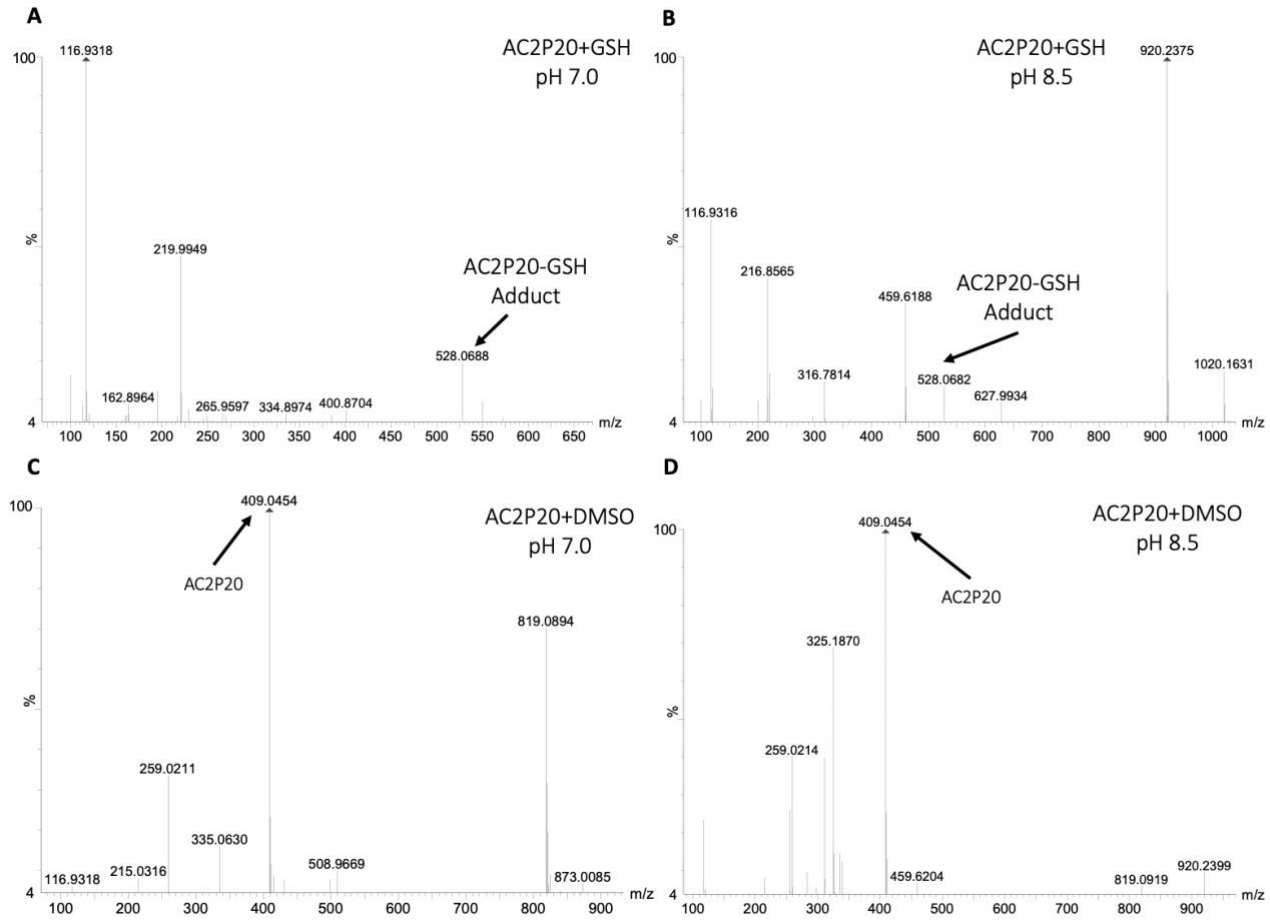

Figure A.2.3. AC2P20 forms adducts with GSH and remains stable at neutral and basic pH. A) Mass spectrometry data showing adduct formation between AC2P20 and GSH at pH 7.0. Spectra were analyzed in negative ESI mode. **B)** Mass spectrometry data showing adduct formation between AC2P20 and GSH at pH 8.5. Spectra were analyzed in negative ESI mode. **C)** AC2P20 incubated with DMSO does not fragment in the absence of GSH at pH 7.0. Spectra were analyzed in negative ESI mode. **D)** AC2P20 incubated with DMSO does not fragment in the absence of GSH at pH 8.5. Spectra were analyzed in negative ESI mode.

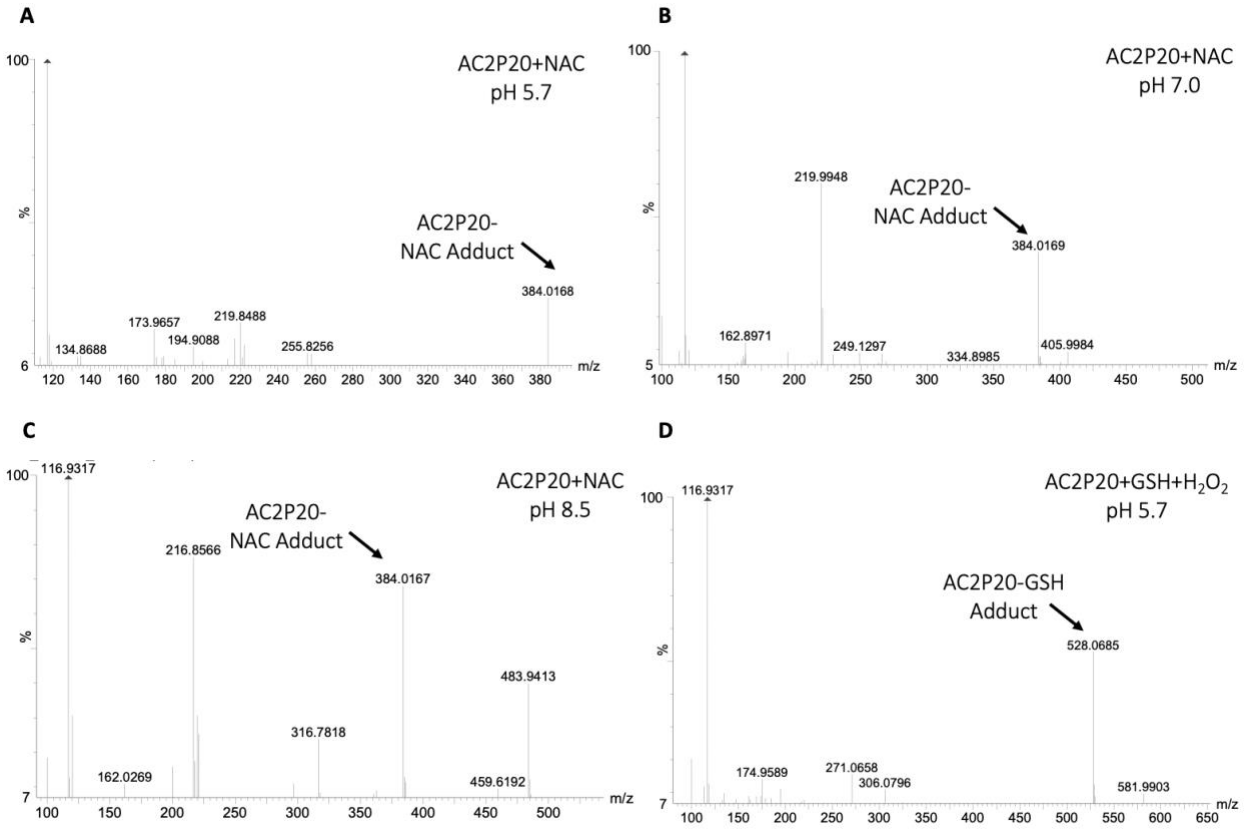

Figure A.2.4. AC2P20 is able to form adducts with N-acetylcysteine and in the presence of an oxidant. **A)** Mass spectrometry data showing adduct formation between AC2P20 and N-acetylcysteine at pH 5.7. Spectra were analyzed in negative ESI mode. **B)** Mass spectrometry data showing adduct formation between AC2P20 and N-acetylcysteine at pH 7.0. Spectra were analyzed in negative ESI mode. 20 +NAC 7.0 **C)** Mass spectrometry data showing adduct formation between AC2P20 and N-acetylcysteine at pH 8.5. Spectra were analyzed in negative ESI mode. **D)** AC2P20 is still able to form an adduct with GSH in the presence of the oxidant, H_2O_2. Spectra were analyzed in negative ESI mode.

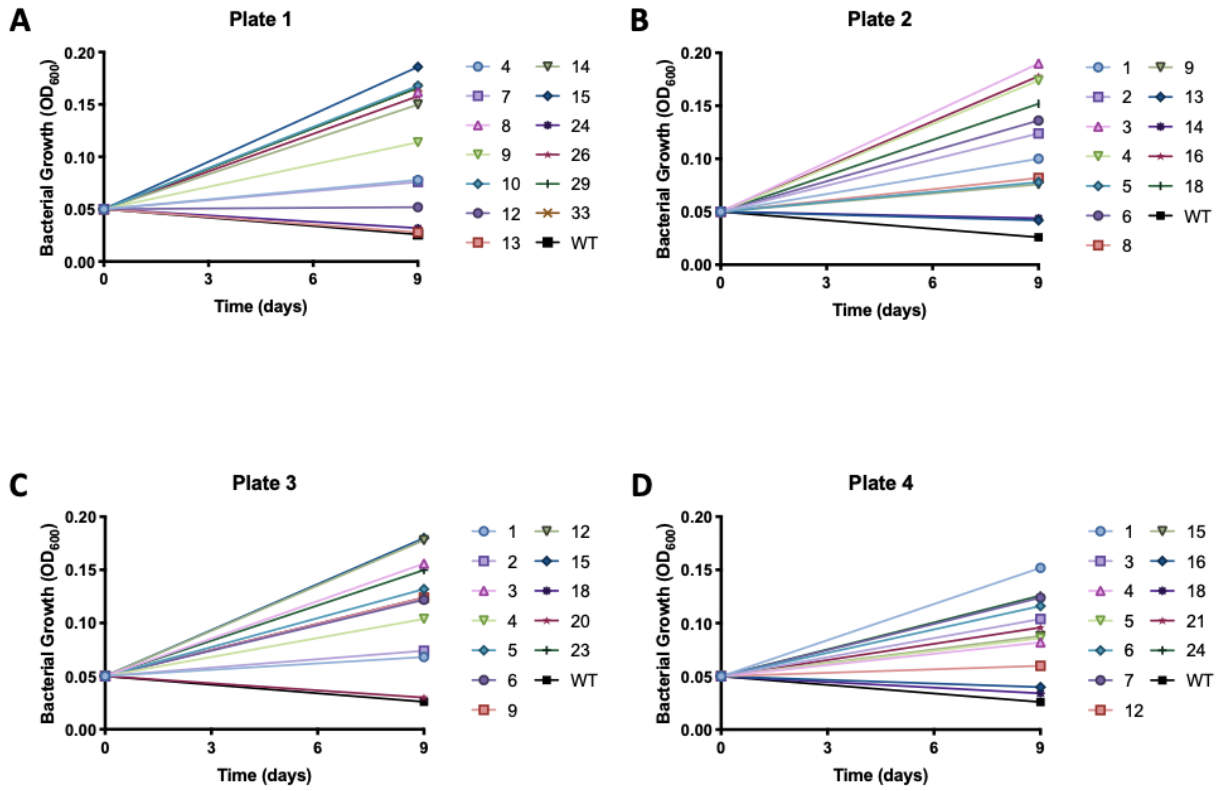

Figure A.3.1. Enhanced acid growth confirmation of mutants isolated from WT Erdman genetic screen. Single colony isolates from Plate 1 **(A)**, Plate 2 **(B)**, Plate 3 **(C)**, and Plate 4 **(D)** were grown in liquid MMAT (pH 5.7) with glycerol and compared to the WT for the enhanced acid growth phenotype. Each symbol represents the numbered colony isolated from the acid growth arrest plates.

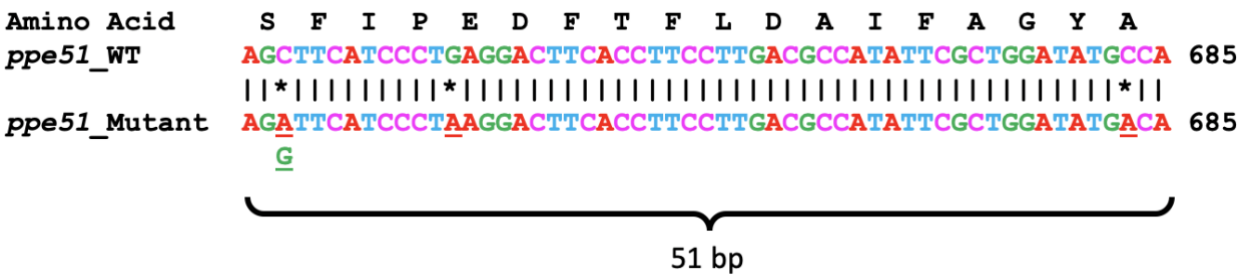

Figure A.3.2. SNP sites in *ppe51*. SNP mapping identified three separate mutations within a 50 bp region of *ppe51*. Underlined and starred bases represent the SNP position (bp). S211R substitution had two SNPs as denoted by the guanine (G) underneath.

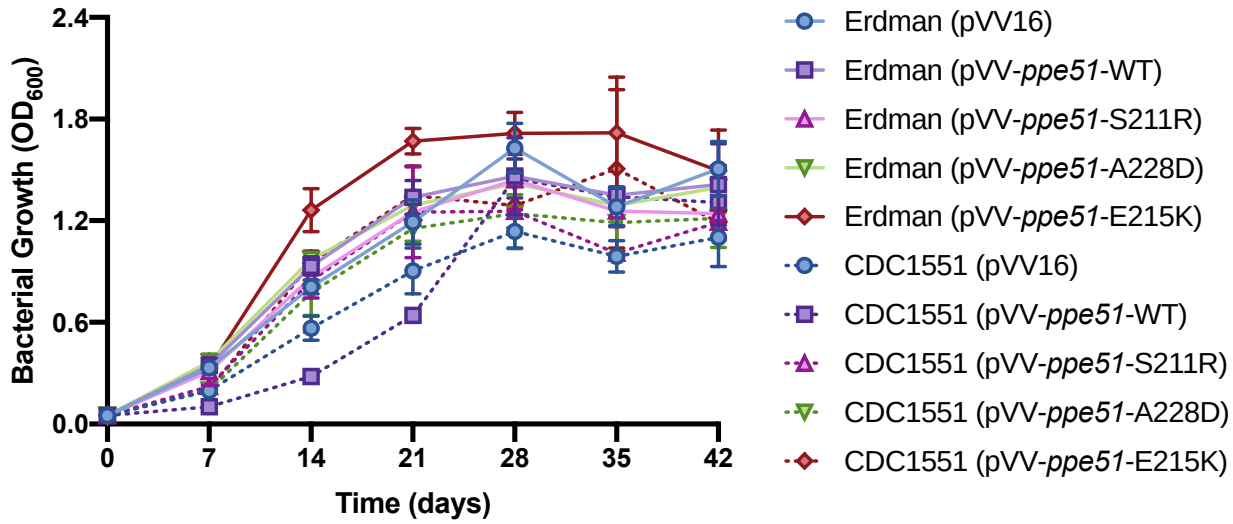

Figure A.3.3. Growth curve of pVV16 overexpression constructs (CDC1551 and Erdman) in minimal media at pH 7.0 with 10 mM glycerol. Expression of *eag* mutant alleles in WT Mtb does not result in significantly enhanced growth under neutral conditions. This experiment was repeated three times in duplicate. Error bars indicate standard deviation.

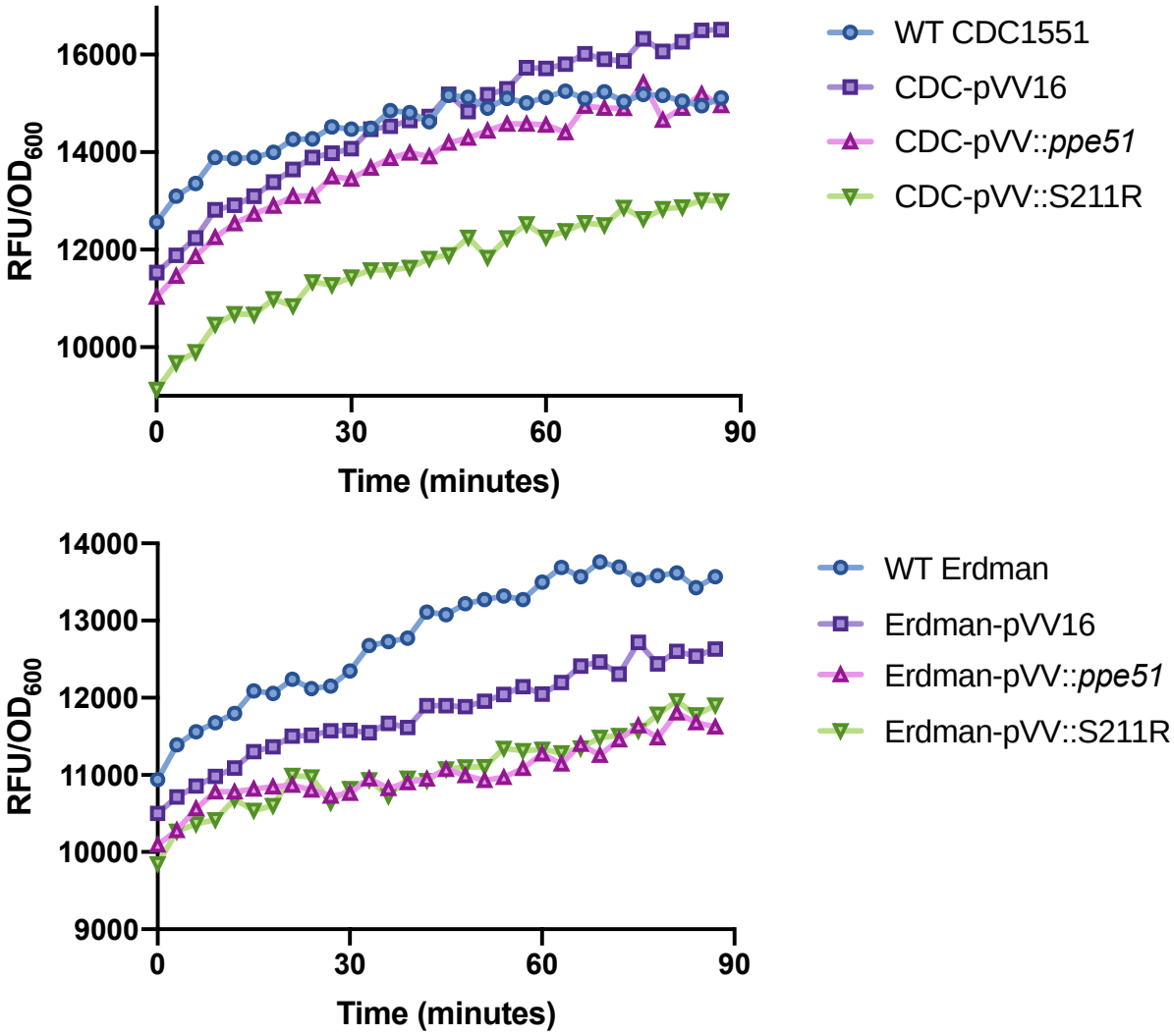

Figure A.3.4. Accumulation of EtBr by Mtb and pVV16 overexpression constructs. pVV16 overexpression constructs (CDC1551 and Erdman) were incubated with Ethidium bromide (EtBr) for 90 minutes. EtBr fluorescence was measured every 3 minutes using the excitation wavelength (530 nm) and emission wavelength (590 nm). Samples were measured in triplicate.

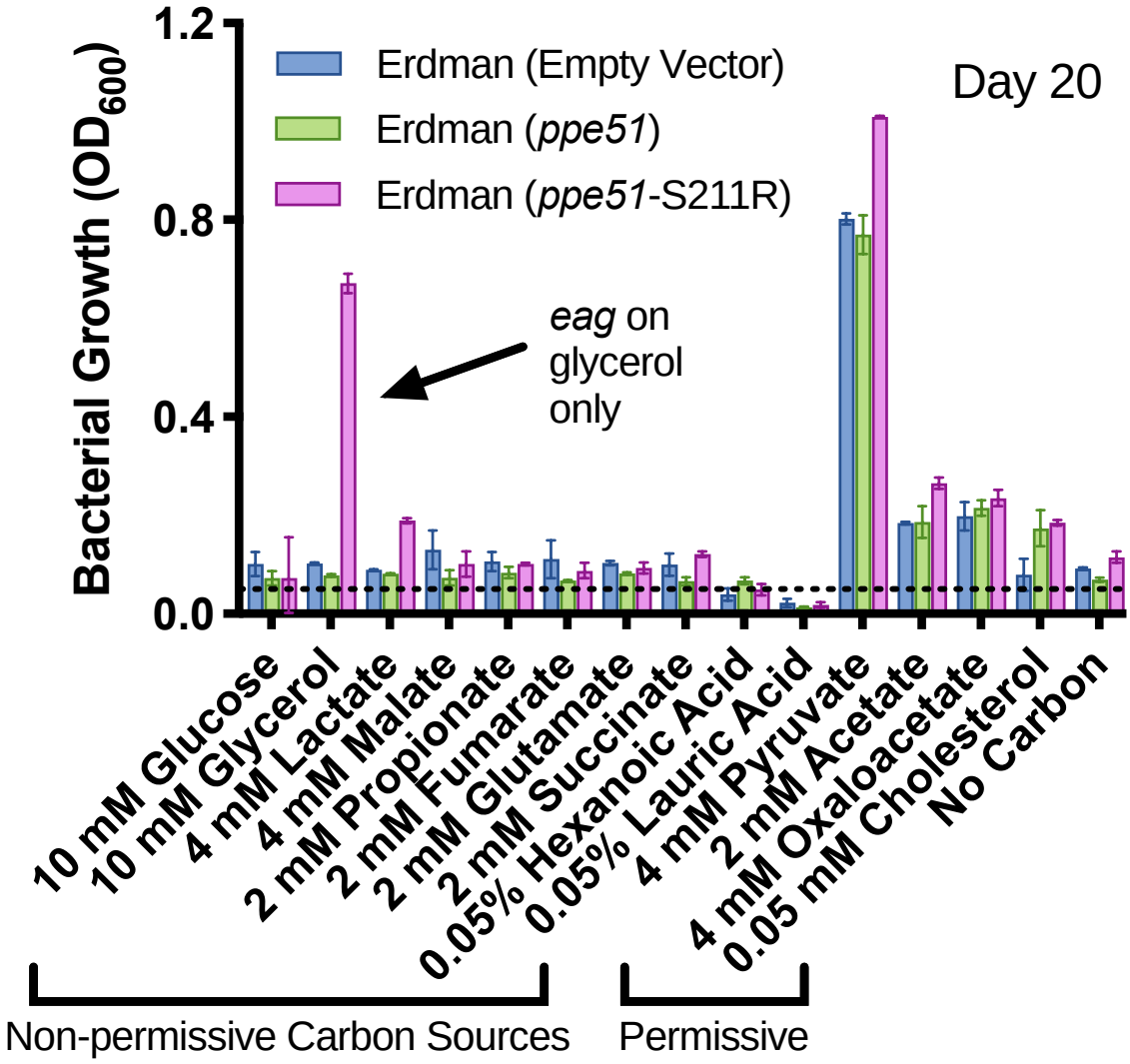

Figure A.3.5. Analysis of the Erdman S211R variant growth on various carbon sources. Erdman overexpression strains were grown in MMAT medium (pH 5.7) in the presence of various growth-permissive (i.e. pyruvate acetate, OA) and non-permissive (i.e. glucose, propionate, lactate) carbon sources. *ppe51*-S211R (pink bars) growth is carbon source specific and only exhibits enhanced growth on glycerol, a normally non-permissive carbon source at pH 5.7. Growth on permissive carbon sources is not impacted by *ppe51*-S211R. The horizontal dotted line indicates the starting density of 0.05 OD_{600}.

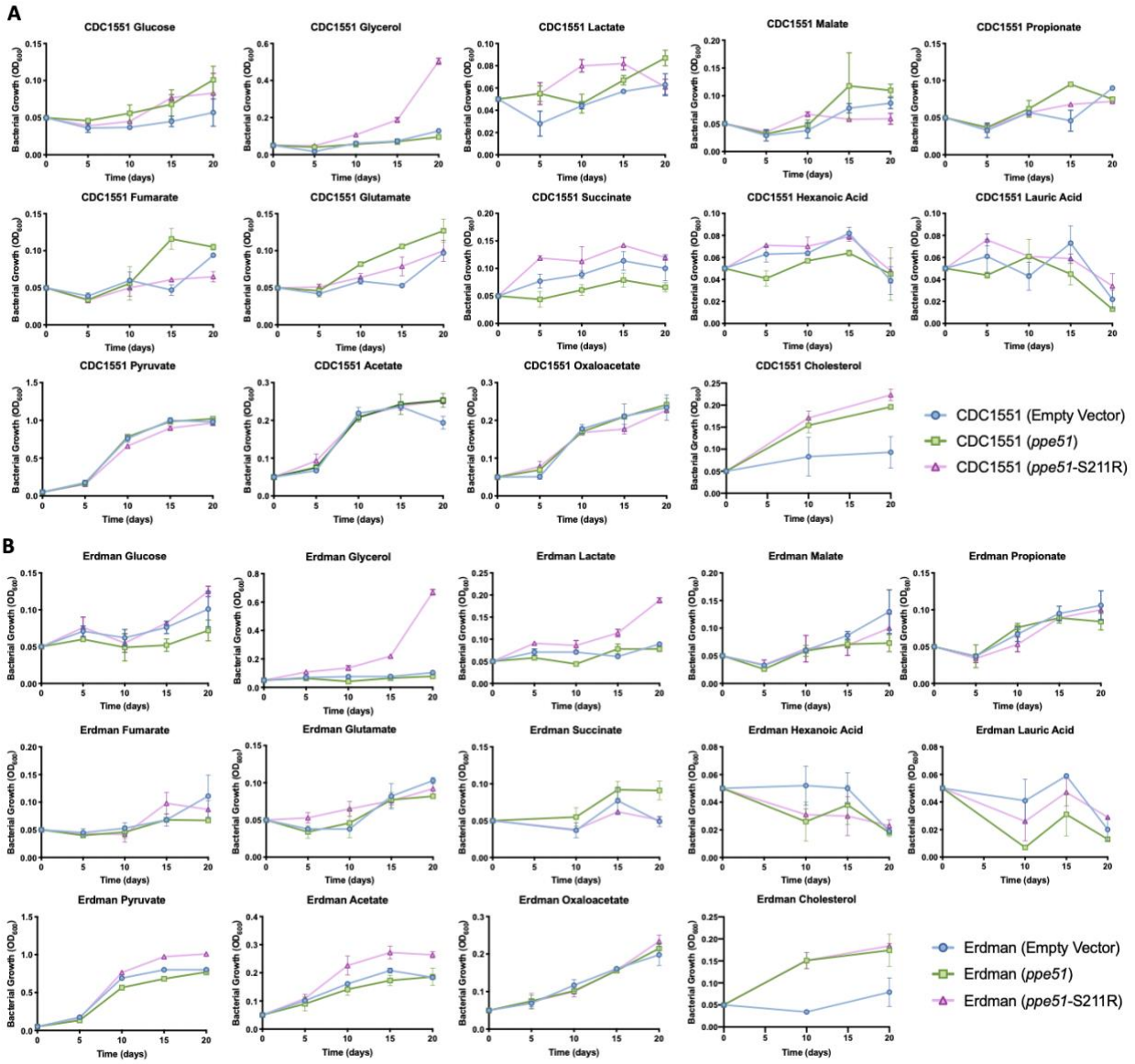

Figure A.3.6. Growth curves of expression strains on individual carbon sources. A) Mtb CDC1551 expression strains. Each strain was grown in duplicate for 20 days on their respective carbon source in minimal media buffered to pH 5.7. **B)** Mtb Erdman expression strains. Each strain was grown in duplicate for 20 days on their respective carbon source in minimal media buffered to pH 5.7.

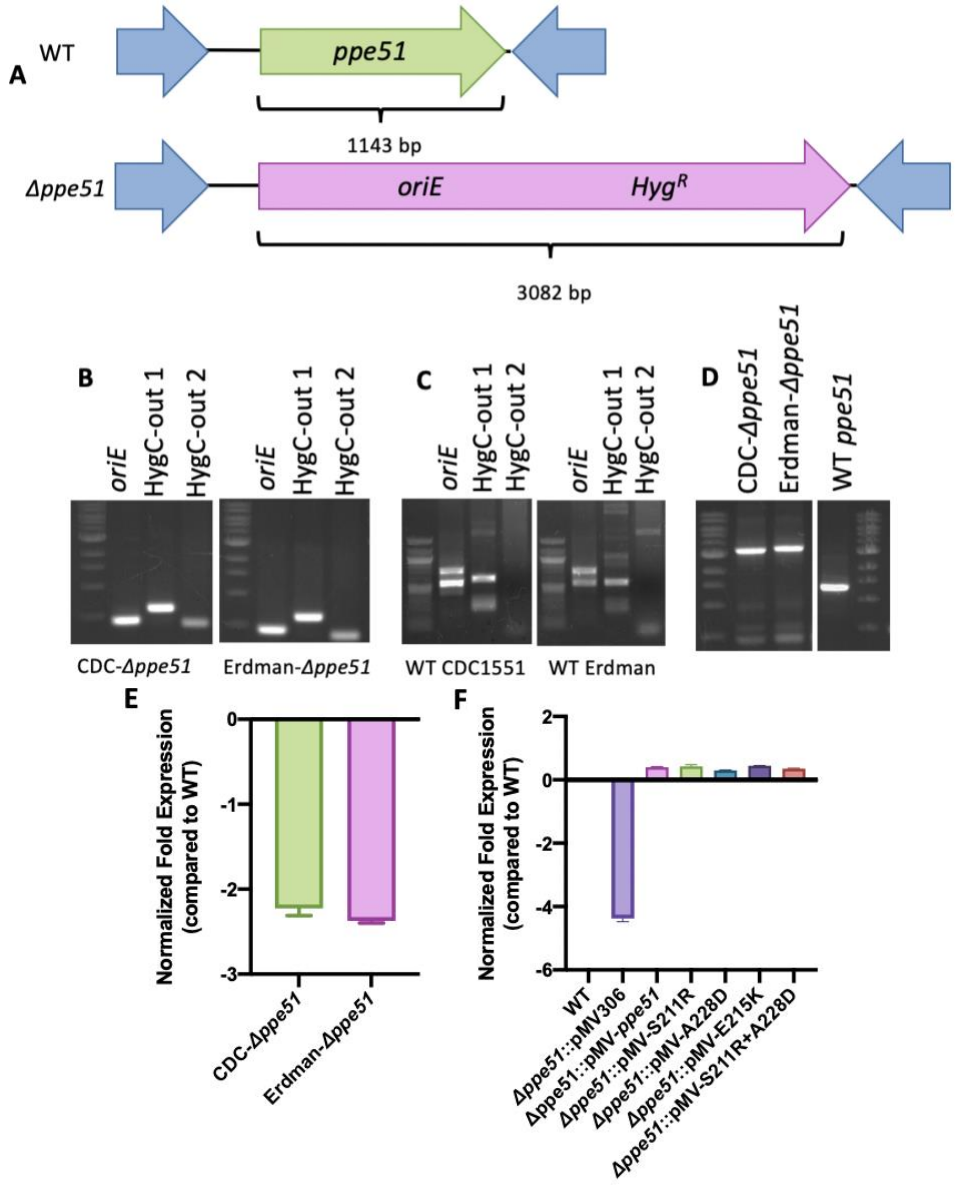

Figure A.3.7. Construction of ppe51 deletion mutant in Mtb CDC1551 and Erdman. A) Schematic of chromosomal *ppe51* and the subsequent ORBIT[197]-promoted deletion of the *ppe51* target gene, *attP* replacement, and plasmid integration containing hygromycin resistance for selection. **B)** PCR amplification of the 5'(oriE) and 3' (HygC-out1/2) junctions of CDC1551 and Erdman *Δppe51*. Positive bands were confirmed by sanger sequencing. **C)** WT control for PCR showing non-specific oriE and HygC-out1/2 primer binding. **D)** PCR analysis of the integration site of the payload plasmid (pKM464). pKM464 is 3082 bp which is consistent with the size of the bands observed in the *ppe51* deletion mutants compared to WT *ppe51* which is 1143 bp. **E)** qRT-PCR analysis confirming the *ppe51* knockout in CDC1551 and Erdman. Total RNA was collected after samples were grown for six days in minimal media buffered to pH 5.7. Fold expression was normalized to the respective WT strains. Error bars represent the standard deviation of three technical replicates. Deletion mutants typically exhibited a non-specific primed Ct ~30 cycles compared to WT which had a Ct of ~20 cycles. **F)** qRT-PCR analysis confirming the presence of the *ppe51* gene in complemented *Δppe51*. Fold expression was normalized to WT Mtb. Error bars represent the standard deviation of three technical replicates. Complemented strains had Ct ~14 cycles compared to *Δppe51* which had non-specific primed Ct ~30 cycles.

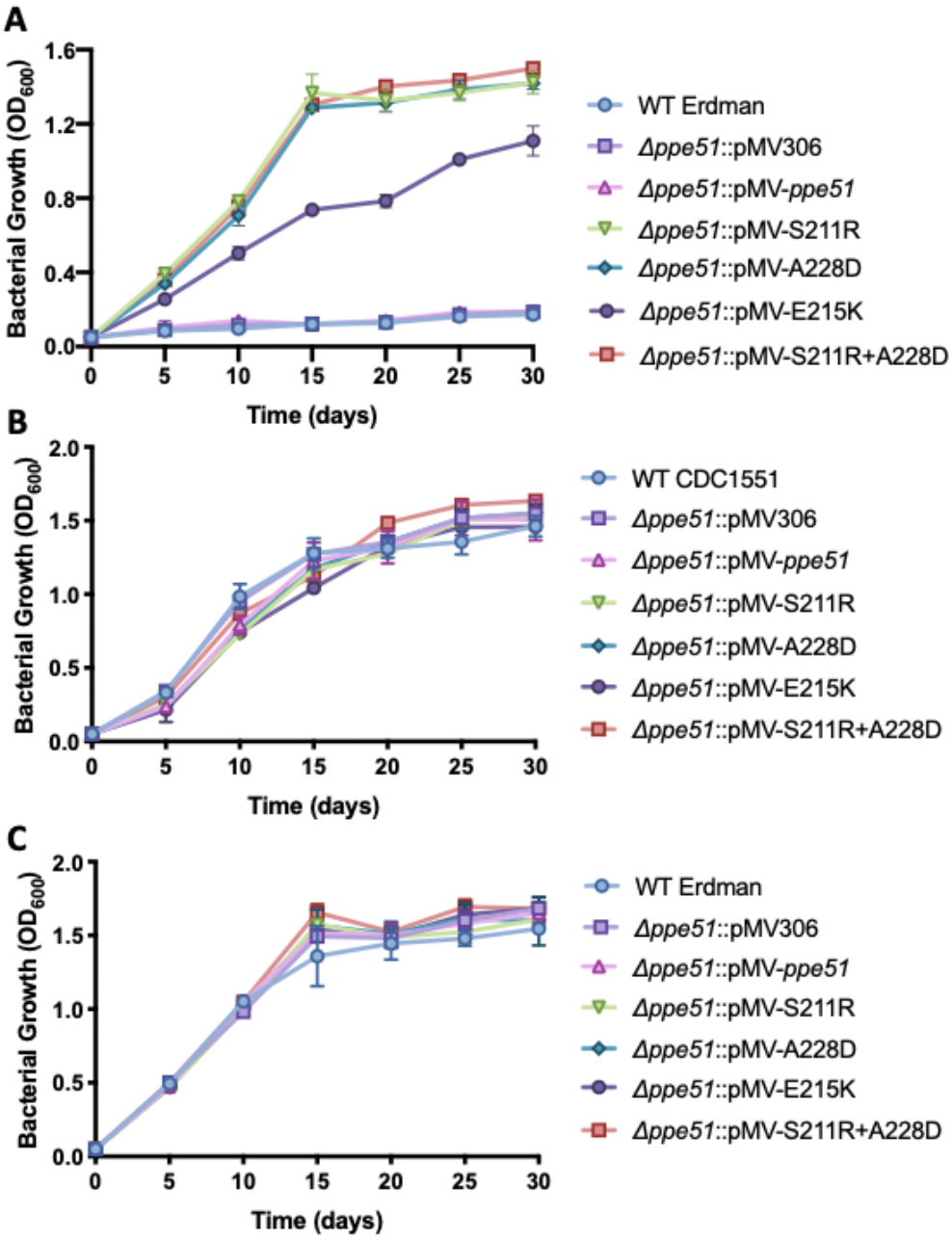

Figure A.3.8. Growth of complemented *Δppe51* strains. Growth curves of *Δppe51* complemented strains in minimal media at **A)** pH 5.7 with 10 mM glycerol (Erdman), **B)** minimal media at pH 7.0 with 10 mM glycerol (CDC1551) and **C)** minimal media at pH 7.0 with 10 mM glycerol (Erdman). Error bars represent standard deviation of three technical replicates.

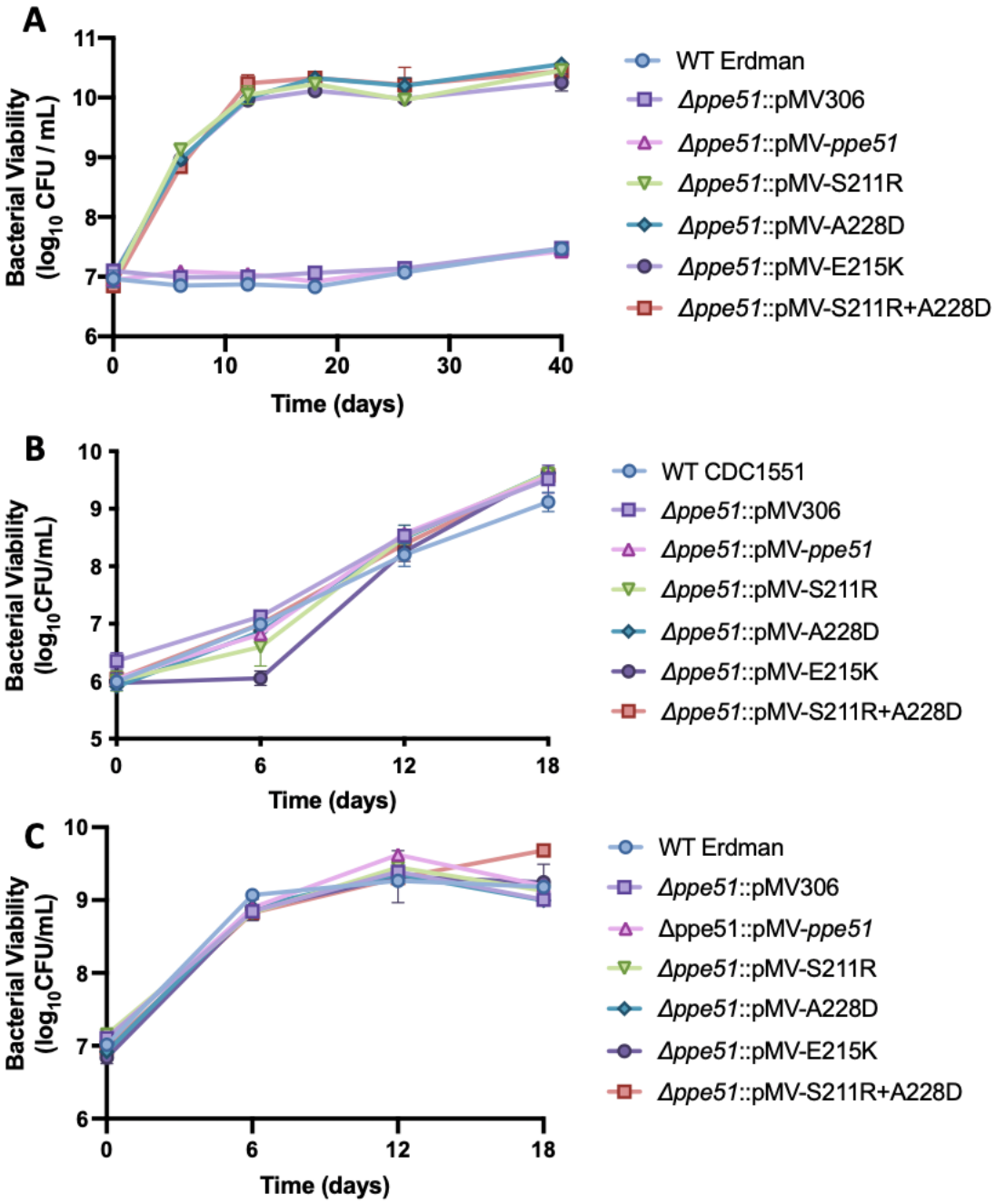

Figure A.3.9. Viability of complemented *Δppe51* strains. Viability assays of *Δppe51* complemented strains in minimal media at **A)** pH 5.7 with 10 mM glycerol (Erdman), **B)** minimal media at pH 7.0 with 10 mM glycerol (CDC1551) and **C)** minimal media at pH 7.0 with 10 mM glycerol (Erdman). Error bars represent standard deviation of three technical replicates.

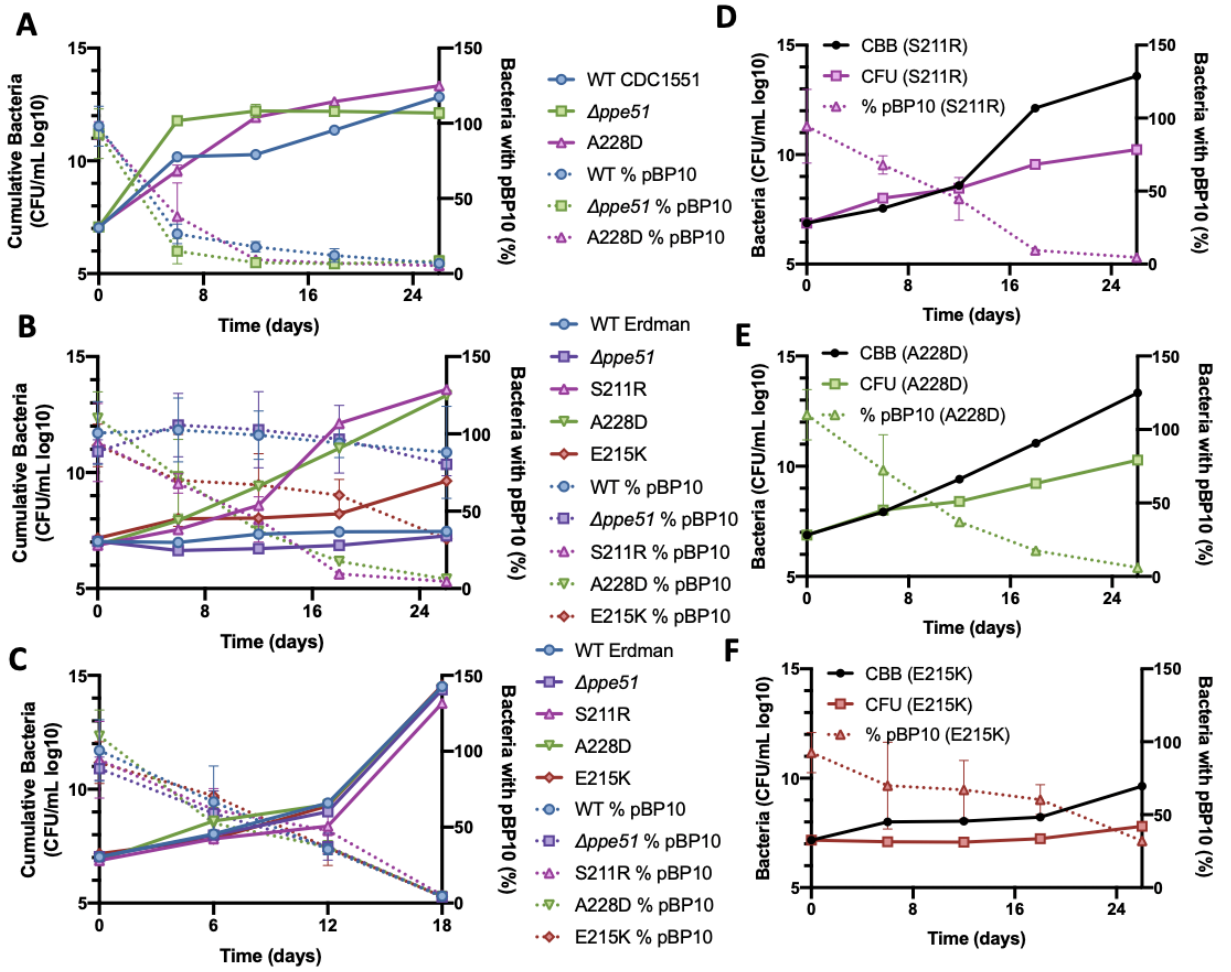

Figure A.3.10. ***In vitro*** **replication dynamics of CDC1551** ***eag*** **variants (pH 7.0) and Erdman** ***eag*** **variants (pH 5.7 and pH 7.0). A)** All CDC1551 Mtb strains, WT, *Δppe51*, and the native variant allele, A228D, continues to replicate at neutral pH in minimal media. To estimate replication dynamics of the indicated strains, plasmid frequency data was obtained from CFU counts (right axis, dotted lines). CFUs of plasmid-free and plasmid-bearing strains were then used to calculate cumulative bacterial burden (CBB) of total live, dead, or degraded Mtb (left axis, solid lines). **B)** Erdman strains containing the native variant alleles, S211R, A228D, and E215K continue to replicate at pH 5.7 in minimal media, albeit E215K exhibits a more reduced capacity for replication compared to S211R and A228D. WT and *Δppe51* cease replication. Plasmid frequency (right axis, dotted lines) and cumulative bacterial burden (CBB) (left axis, solid lines) are shown. **C)** All Erdman Mtb strains, WT, *Δppe51*, and the native variant alleles (S211R, A228D, and E215K), continue to replicate at neutral pH in minimal media. Plasmid frequency (right axis, dotted lines) and cumulative bacterial burden (CBB) (left axis, solid lines) are shown. Replication dynamics of the native Erdman **D)** S211R variant, **E)** A228D variant, and **F)** E215K variant (comparing CBB (cumulative bacterial burden), CFU (total CFUs from nonselective plating), and % pBP10 (percentage of bacteria carrying plasmid).

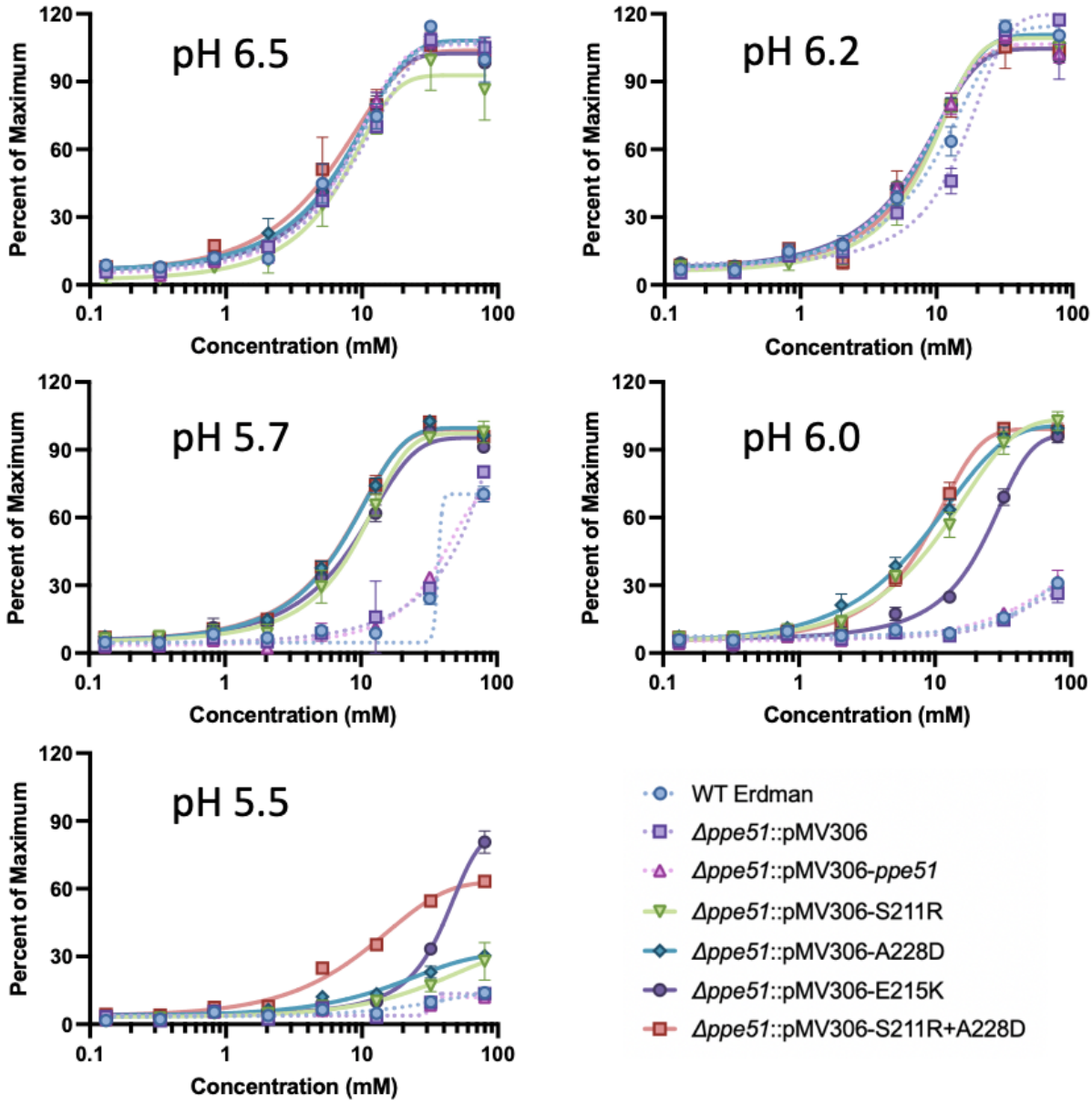

Figure A.3.11. Mtb shows growth restriction at low pH in Erdman. Growth of WT Erdman, *Δppe51* (empty vector), and *Δppe51* complemented strains in minimal media supplemented in a dose-dependent manner with glycerol and buffered to one of five pH levels (pH 6.5, 6.2, 6.0, 5.7, or 5.5). All strains exhibit a reduced capacity for growth starting ~2 mM glycerol compared to higher glycerol concentrations. At decreasing pH, WT, *Δppe51*(empty vector), and *Δppe51*::pMV-WT restrict their ability to uptake glycerol, whereas any variant complement is able to maintain glycerol uptake. However, restricted growth can be rescued at high concentrations of glycerol (~80 mM) at pH 5.7 for WT, *Δppe51*(empty vector), and *Δppe51*::pMV-*ppe51*, and pH 5.5 for variant complements. Growth analyses were performed at Day 14 following initial inoculation with data being shown as percent of the maximum well-growth. All conditions were conducted in triplicate and representative of multiple independent experiments.

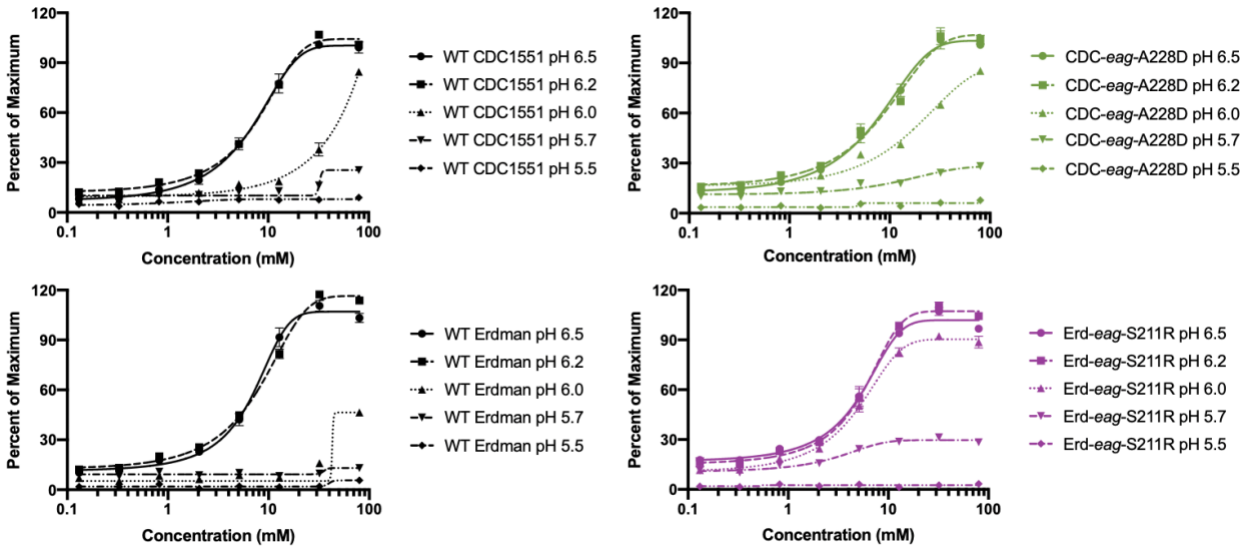

Figure A.3.12. Mtb growth restriction and rescue at low pH is also observed in the native *eag* variants in CDC1551 and Erdman. WT CDC1551 and Erdman exhibit a slight rescuing of growth at high glycerol concentrations (~80 mM) in minimal media buffered to pH 5.7, consistent with what has been observed in the *Δppe51* complemented strains. The native CDC1551 *eag* variant, A228D, and native Erdman *eag* variant exhibit a greater capacity for growth at pH 5.7 at lower concentrations of glycerol (~5mM) compared to their respective WT strains. Growth analyses were performed at Day 14 following initial inoculation with data being shown as percent of the maximum well-growth. All conditions were conducted in duplicate and representative of multiple independent experiments.

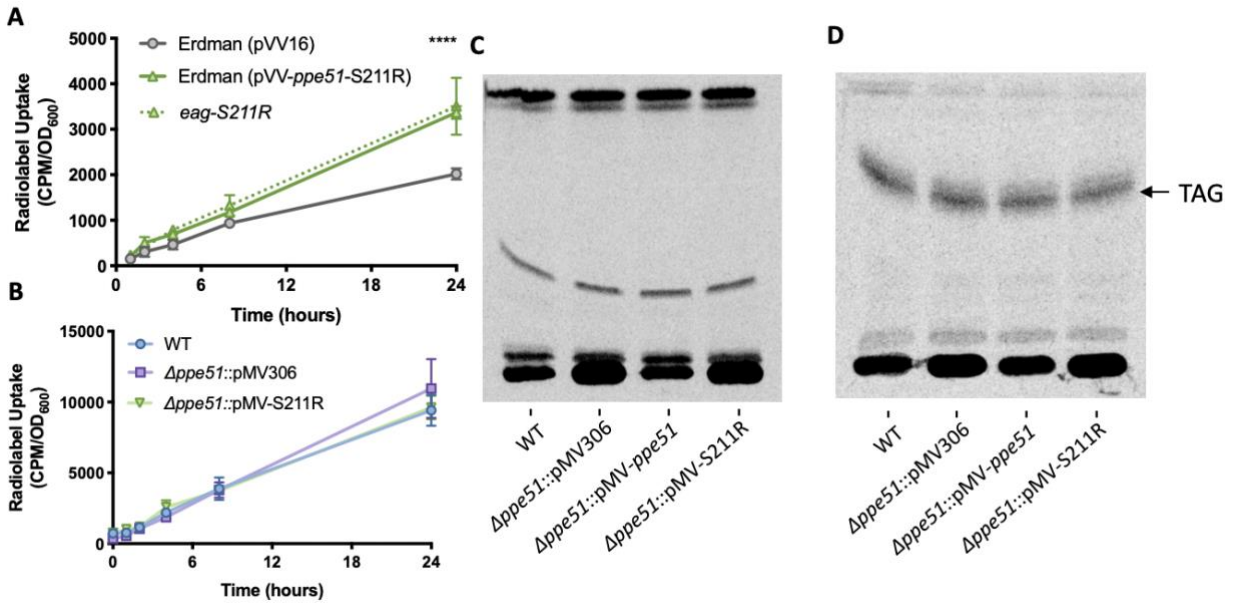

Figure A.3.13. Glycerol uptake in native *eag* variants (pH 5.7), and radiolabeled uptake and incorporation into lipids at pH 7.0. A) The Erdman native *eag* S211R variant and the overexpressing pVV16-S211R variant uptake ^{14}C-glycerol at a similar enhanced rate compared to WT Erdman which exhibits a more reduced capacity for radiolabeled uptake. Mtb was pre-adapted for 3 days in minimal media (pH 5.7) with 10 mM glycerol and subsequently washed prior to the additional of radiolabeled glycerol. ^{14}C-glycerol uptake was measured at various timepoints using Scintillation counting over 24 hours. Significance was determined by two-way ANOVA (Tukey's multiple comparisons test; ****P < 0.0001)**. B)** Erdman WT, *Δppe51* (empty vector) and, *Δppe51*::pMV-S211R were assessed for ^{14}C-glycerol uptake in minimal media buffered to pH 7.0. Strains were pre-adapted for 3 days in minimal media buffered to pH 7.0 with 10 mM glycerol. All strains showed similar rates of glycerol uptake. **C)** Incorporation of ^{14}C-glycerol into sulfolipids at neutral pH. For each strain, 10,000 CPM was spotted at the origin on 100 cm^2 silica gel 60 aluminum sheets. Sulfolipids were separated using a chloroform:methanol:water (90:10:1 v/v/v) solvent system. Sulfolipid is absent at pH 7.0 which is consistent with previous observations made by Baker *et al*. Strains were analyzed in duplicate with representative results being shown. **D)** Incorporation of ^{14}C-glycerol into TAG at acidic pH. For each strain, 10,000 CPM was spotted at the origin on 100 cm^2 silica gel 60 aluminum sheets. TAG were separated using a hexane:diethyl ether:acetic acid (80:20:1, v/v/v) solvent system. TAG are indicated with an arrow and are present in all strains. Strains were analyzed in duplicate with representative results being shown.

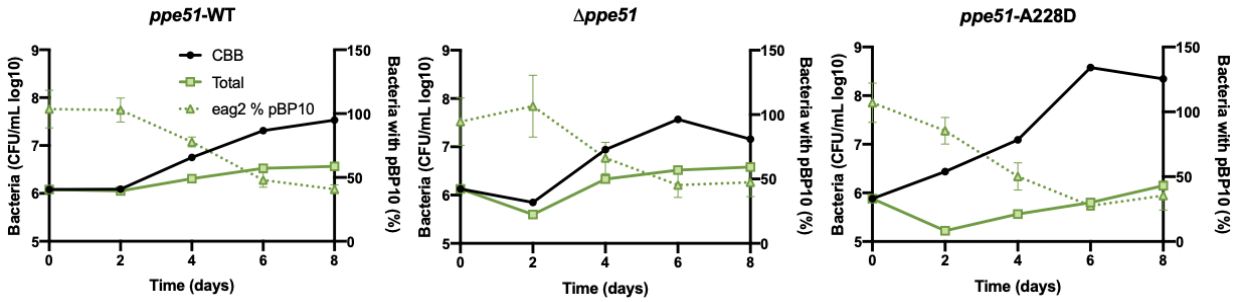

Figure A.3.14. Resting BMDMs infected with native WT CDC1551, *Δppe51*, and A228D variant strains containing the pBP10 replication clock plasmid. CFUs on selective plates were compared to CFUs on nonselective plates and used to calculated frequency of plasmid-bearing bacteria (% pBP10), cumulative bacterial burden (CBB) of total live and dead bacteria, and total enumerated colonies on nonselective plates (CFU).

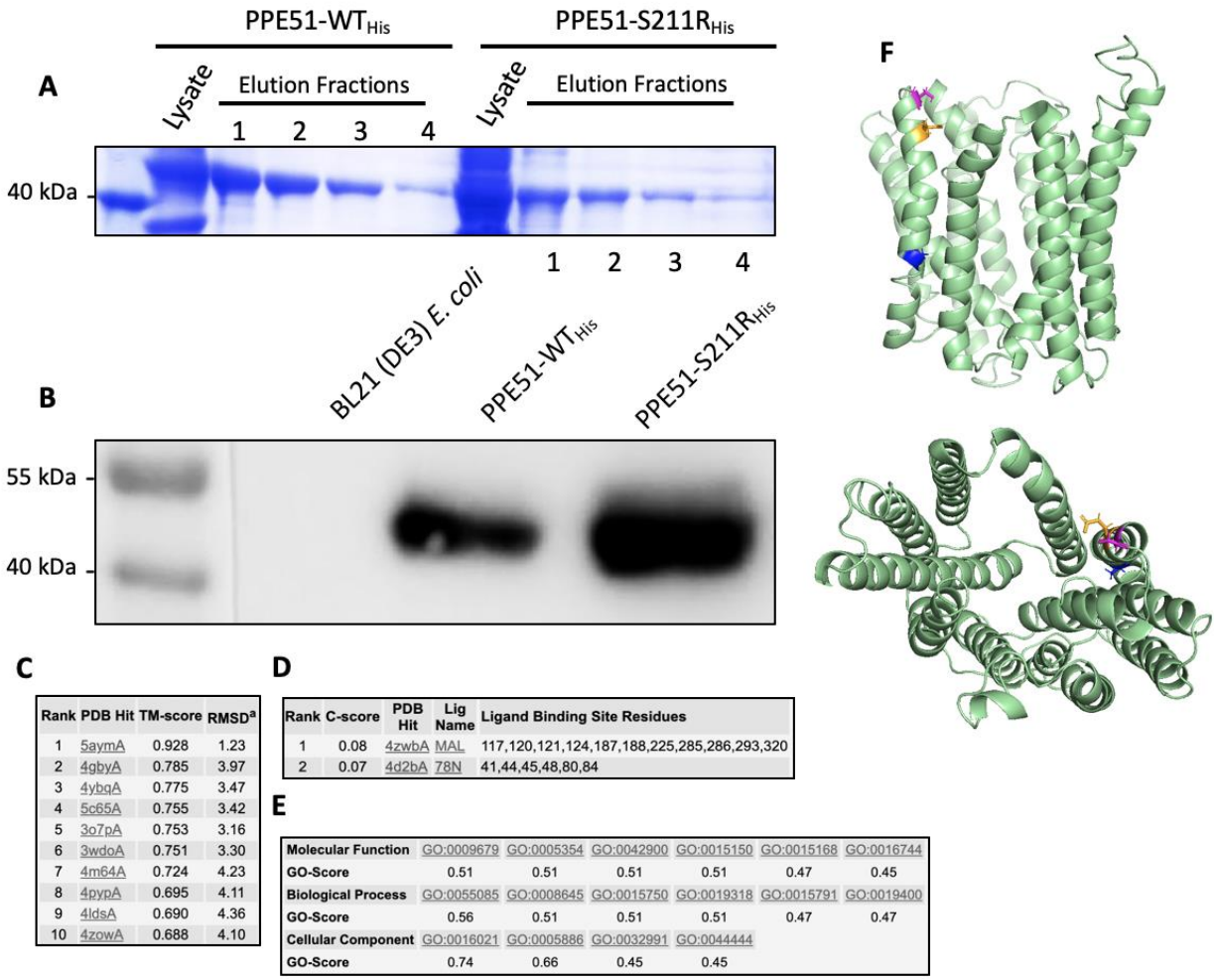

C

Rank	PDB Hit	TM-score	RMSD[a]
1	5aymA	0.928	1.23
2	4gbyA	0.785	3.97
3	4ybqA	0.775	3.47
4	5c65A	0.755	3.42
5	3o7pA	0.753	3.16
6	3wdoA	0.751	3.30
7	4m64A	0.724	4.23
8	4pypA	0.695	4.11
9	4ldsA	0.690	4.36
10	4zowA	0.688	4.10

D

Rank	C-score	PDB Hit	Lig Name	Ligand Binding Site Residues
1	0.08	4zwbA	MAL	117,120,121,124,187,188,225,285,286,293,320
2	0.07	4d2bA	78N	41,44,45,48,80,84

E

Molecular Function	GO:0009679	GO:0005354	GO:0042900	GO:0015150	GO:0015168	GO:0016744
GO-Score	0.51	0.51	0.51	0.51	0.47	0.45
Biological Process	GO:0055085	GO:0008645	GO:0015750	GO:0019318	GO:0015791	GO:0019400
GO-Score	0.56	0.51	0.51	0.51	0.47	0.47
Cellular Component	GO:0016021	GO:0005886	GO:0032991	GO:0044444		
GO-Score	0.74	0.66	0.45	0.45		

Figure A.3.15. Protein expression of PPE51$_{His}$ and *in silico* modeling. Lysates of overexpressed His-tagged PPE51-WT and PPE51-S211R were run on a Talon resin column, and fractions were collected in (4) 1 mL aliquots. PPE51-WT and PPE51-S211R proteins were separated on 12% SDS-PAGE gels , which were either stained with Coomassie Blue dye **(A)** or used for western blots **(B)**. Western blots were incubated with mouse anti-His tag monoclonal antibody followed by HRP-conjugated anti-mouse IgG secondary antibody. The molecular weights of the protein standards are shown on the left. **C)** Top ten PDB structures close to the target protein. TM-scores are a measurement of the structural similarity between the query structure and known structures in the PDB library in the range [0,1]. TM-scores >0.5 indicate a more correct topology. RMSD is the measurement of the average distance of residues between two structures. **D)** Ligand binding site prediction. C-score is the confidence score of the prediction in the range [0,1]. A higher score indicates a more reliable prediction. Ligand names are possible binding ligands found in the BioLiP database. **E)** Gene ontology (GO) term prediction. Summary prediction of the most common GO terms occurring in three functional aspects (molecular function, biological process, and cellular component). GO-Score is a confidence score of the predicted GO term. A GO-Score >0.5 indicates a more reliable prediction. **F)** Modeling of the *eag* mutation sites in PPE51 shows that S211R (pink), E215K (orange), and A228D (blue) all occur on the same alpha helix.

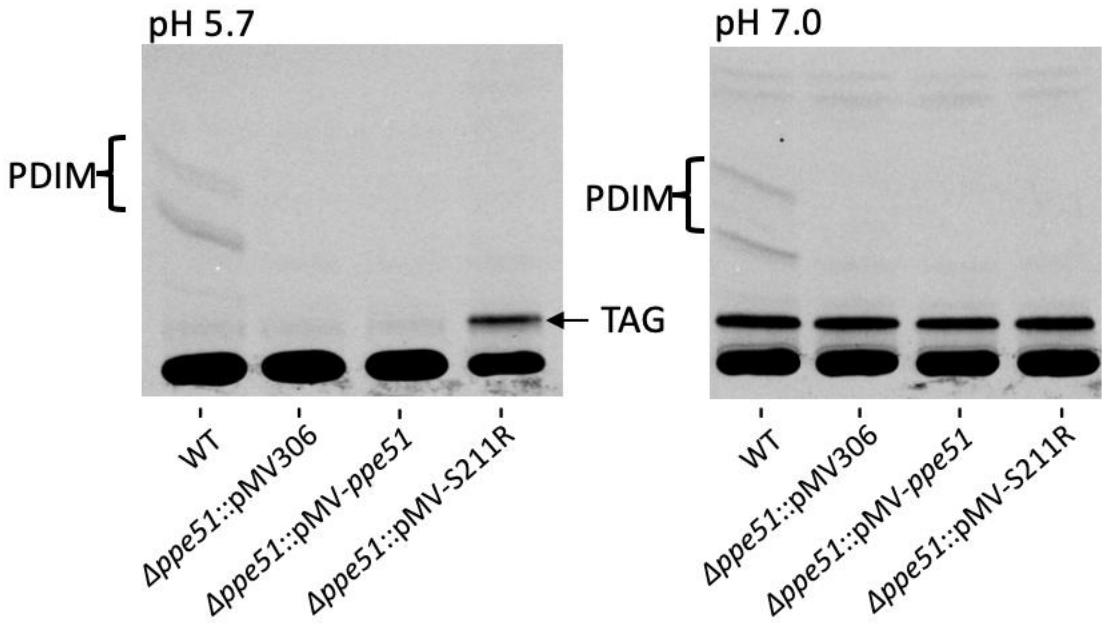

Figure A.3.16. Incorporation of ^{14}C-glycerol into PDIM at acidic and neutral pH. For each strain, 5,000 CPM was spotted at the origin on 100 cm^2 silica gel 60 aluminum sheets. PDIM were separated using a petroleum ether:acetone (98:2 v/v) solvent system. PDIM is indicated with a bracket and accumulates in the WT strain at both pH 5.7 and pH 7.0 but is absent in the *ppe51* knockout mutant. A band consistent with TAG appears in *Δppe51*::pMV-S211R and is indicated by an arrow. Strains were analyzed in duplicate with representative results being shown

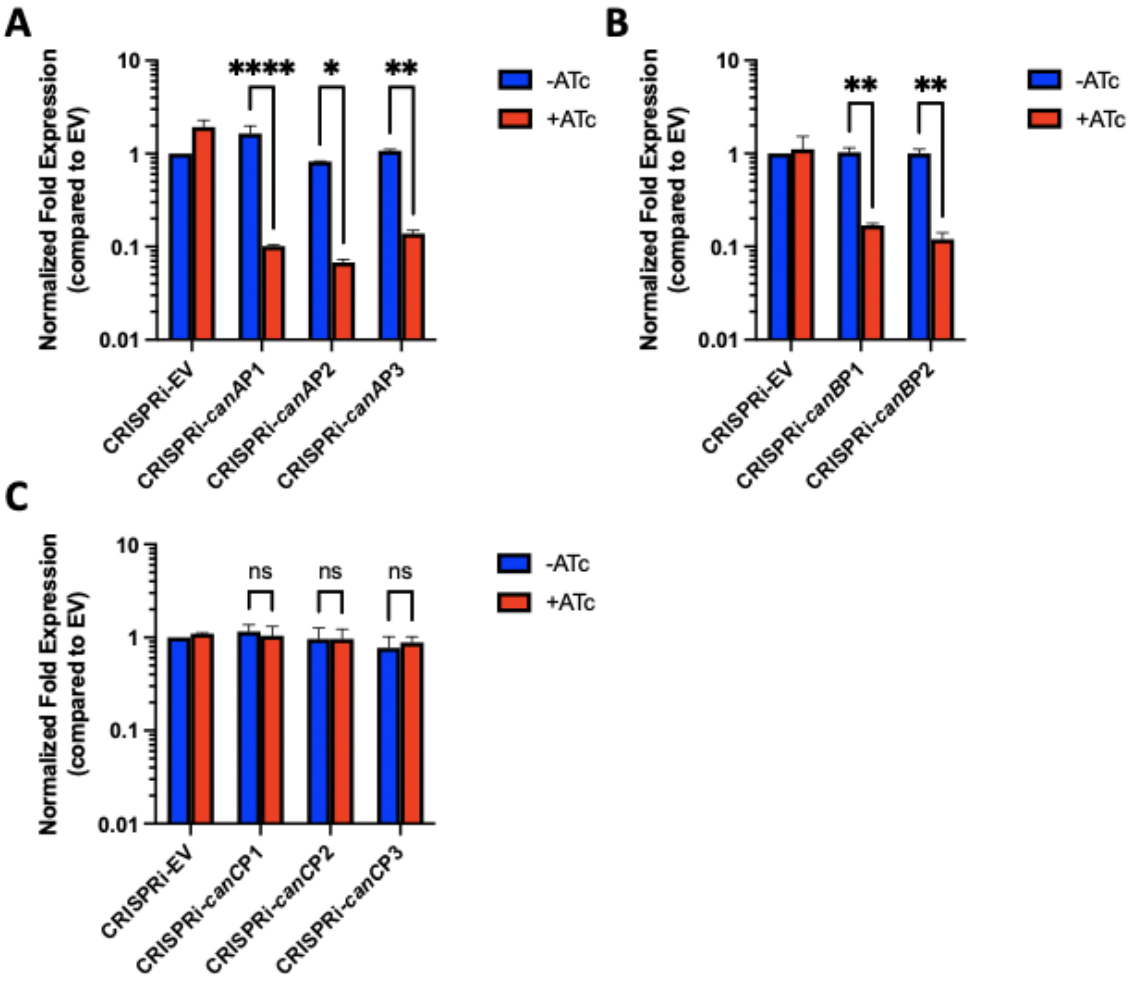

Figure A.4.1. qRT-PCR confirmation of *canA* and *canB* CRISPRi in WT CDC1551. A) $dCas9_{Sth1}$ knockdown of *canA* target in Mtb. Three sgRNAs targeting *canA* were co-expressed with $dCas9_{Sth1}$ (+ATc). After 6 days of incubation in 7H9 media, total RNA was extracted, and *canA* knockdown was quantified by qRT-PCR. **B)** Two sgRNAs targeting *canB* were co-expressed with $dCas9_{Sth1}$ (+ATc) and *canB* knockdown was quantified by qRT-PCR. **C)** Three sgRNAs targeting *canC* were co-expressed with $dCas9_{Sth1}$ (+ATc). *canC* knockdown was quantified by qRT-PCR but lacked knockdown efficiency. Error bars in all three figures represent the standard deviation of three technical replicates. Significance was determined by two-way ANOVA (Šídák's multiple comparisons test; ****$P < 0.0001$). Mean ± SD are shown in the bar graph.

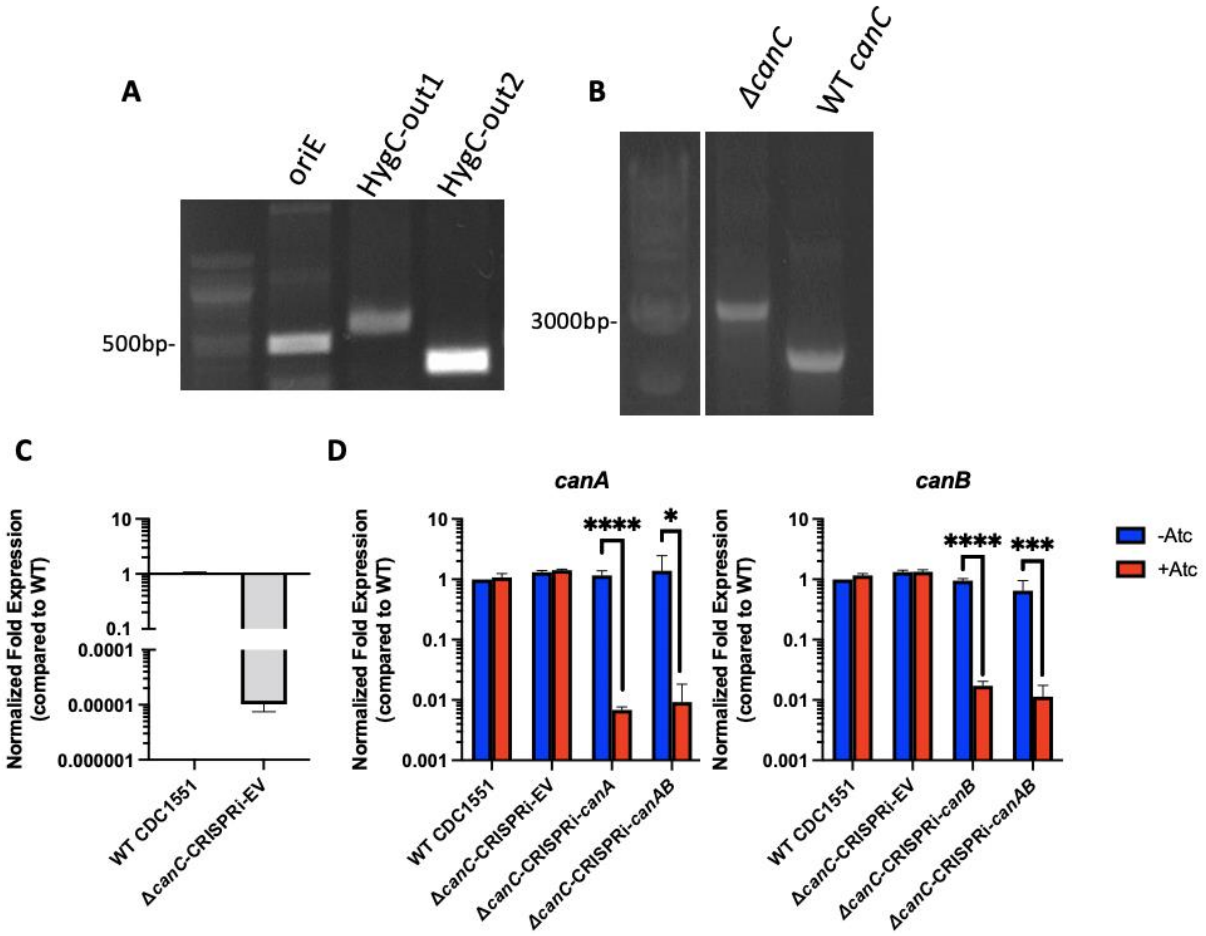

Figure A.4.2. PCR and qRT-PCR confirmation of *canC* ORBIT knockout and CRISPRi. A) PCR amplification of the 5'(oriE) and 3' (HygC-out1/2) junctions of CDC1551 *ΔcanC*. **B)** PCR analysis of the integration site of the payload plasmid (pKM464). pKM464 is 3082 bp which is consistent with the size of the bands observed in the *canC* deletion mutants compared to WT *canC* which is 2295 bp. **C)** qRT-PCR analysis confirming the *canC* knockout. Total RNA was collected after samples were grown for six days in 7H9 media buffered to pH 7.0. Fold expression was normalized to WT. Error bars represent the standard deviation of three technical replicates. Deletion mutant of *canC* typically exhibited a non-specific primed Ct ~35 cycles compared to WT which had a Ct of ~16 cycles. **D)** qRT-PCR confirmed gene knockdown of *canA*, *canB*,and *canAB* in the *canC* deletion mutation background. Fold expression was normalized to WT Mtb. Error bars represent the standard deviation of three technical replicates. Significance was determined by student's t-test. (*P < 0.05, ***P < 0.001, ****P < 0.0001).

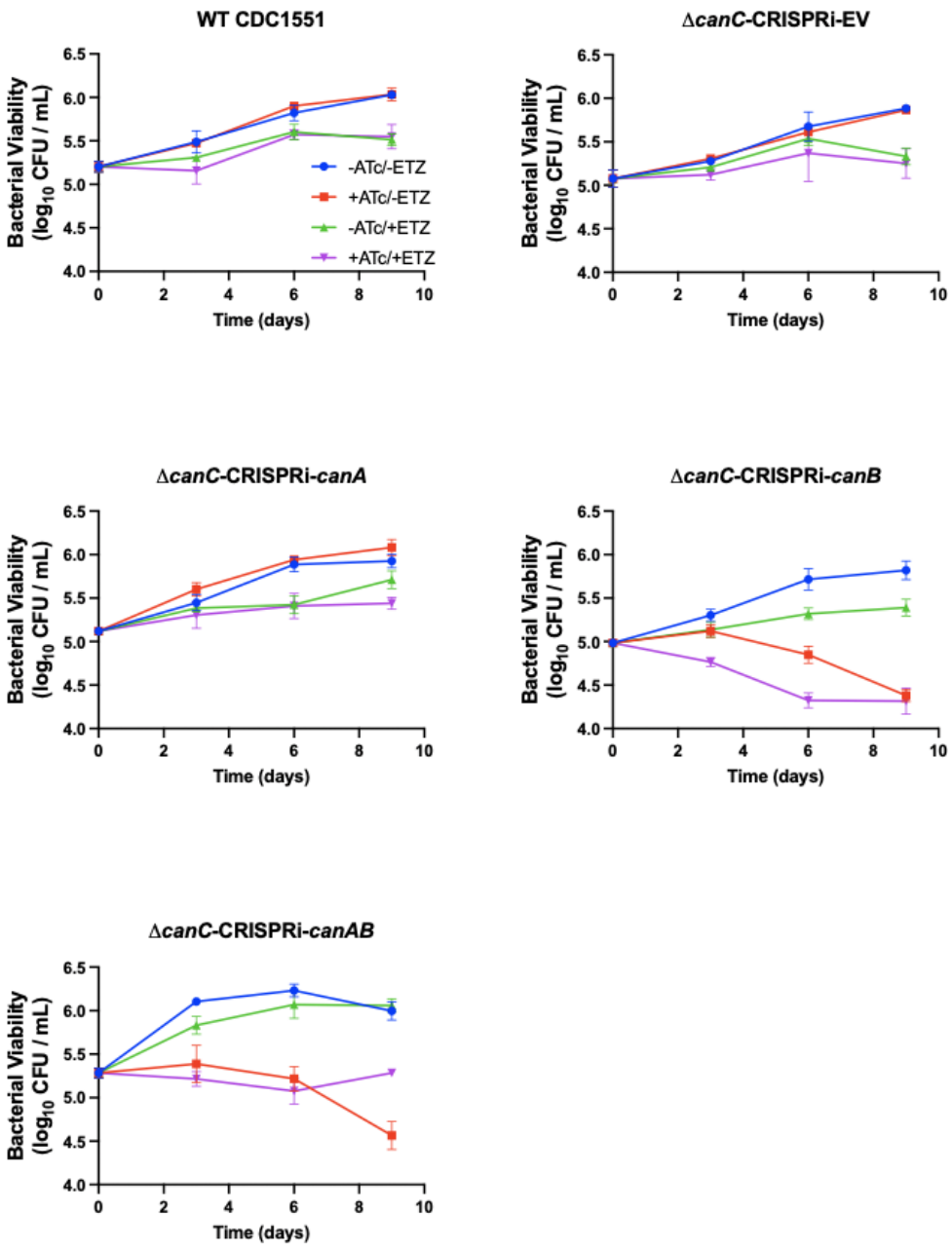

Figure A.4.3. Nine day bacterial viability CFUs that correspond to the endpoint data summarized in Figure 4.2E. BMDMs infected with the CA CRISPRi strains in the CDC1551 Δ*canC* background. All strain treatments were performed in triplicate. Error bars indicate standard deviation.

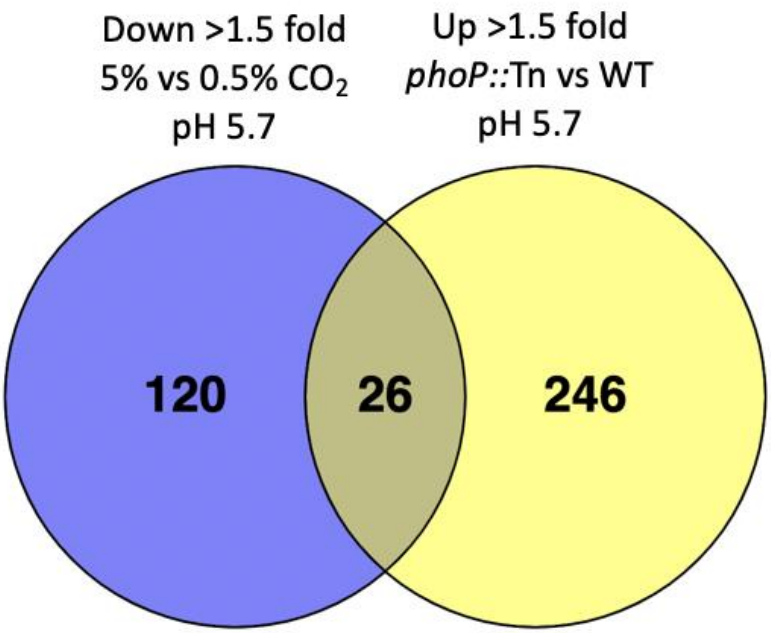

Figure A.4.4. Venn diagram of down-regulated genes 5% CO_2 vs 0.5% CO_2, pH 5.7 compared to up-regulated *phoP::*Tn profile. Significant gene overlap observed between genes downregulated (Down) (>1.5-fold, q < 0.05) by 5% CO_2 treatment at pH 5.7 and Upregulated (Up) (>1.5-fold, q < 0.05) in the *phoP::*Tn mutant strain at pH 5.7[50].

APPENDIX B:

Supplemental Tables

Table A.2.1. Labeled mass spectrometry peaks with their corresponding hypothetical chemical scaffolds.

Peak (Da)	Possible Chemical Scaffold	Figure No.
130.16	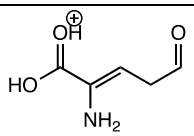	2.3C
178.12	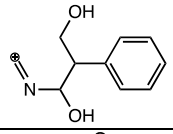	2.3C
194.12	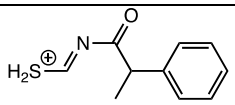	2.3C
206.15	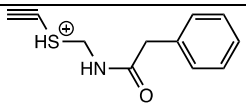	2.3C
222.11	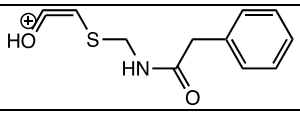	2.3C
384.02	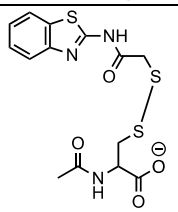	A.2.4A, A.2.4B, A.2.4C
391.28	Phthalate Plasticizer	2.3C
401.26	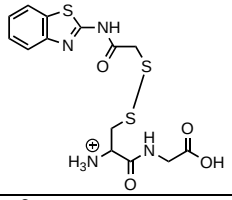	2.3C
409.04, 409.05	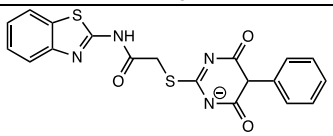	2.3B, A.2.3C, A.2.3D
528.06, 528.07	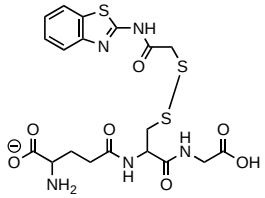	2.3A, A.2.3A, A.2.3B, A.2.4D
530.08	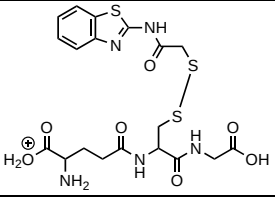	2.3C

Table A.3.1. Plasmids and primers used in this study.

Plasmid or Primer Name	Characteristics or Sequence (5'→ 3')	Reference
Plasmids		
pVV16	Kan^R, Hyg^R; *E. coli*-mycobacterial shuttle vector containing the *hsp60* promoter	BEI Resources, NIAID, NIH
pKM444	Kan^R; Mycobacterial shuttle vector expressing the Che9c phage RecT annealase and the Bxb1 phage integrase from the P_{tet} promoter	Murphy *et al.* (2018)
pKM464	Hyg^R; Mycobacterial integration vector for deleting target gene, insertion of Bxb1 *attB* site from the P_{Hyg} promoter	Murphy *et al.* (2018)
pMV306	Kan^R; Mycobacterial integration vector	Stover *et al.* (1991)
pBP10	Amp^R, Kan^R; Mycobacterial shuttle vector, used as a replication clock plasmid	Bachrach *et al.* (2000)
pET-23a(+)	Amp^R; Bacterial expression vector carrying an N-terminal T7-Tag sequence and a C-terminal His-Tag sequence from the T7 promoter	Rosenberg *et al.* (1987); Studier *et al.* (1990)
pVV-*ppe51*-WT	*ppe51* PCR product ligated into *Bam*HI and *Hind*III sites of pVV16	Baker *et al.* (2018)
pVV-*ppe51*-S211R	*ppe51* PCR product ligated into *Bam*HI and *Hind*III sites of pVV16	Baker *et al.* (2018)
pVV-*ppe51*-A228D	Ligated site-directed mutagenesis product of pVV16 and *ppe51*	This study
pVV-*ppe51*-E215K	Ligated site-directed mutagenesis product of pVV16 and *ppe51*	This study
pMV::*ppe51*	*ppe51*+ its native promoter PCR product ligated into *Xba*I and *Eco*RI sites of pMV306	This study
pMV::*ppe51*-S211R	Ligated site-directed mutagenesis product of pMV306 and *ppe51*	This study
pMV::*ppe51*-A228D	Ligated site-directed mutagenesis product of pMV306 and *ppe51*	This study
pMV::*ppe51*-E215K	Ligated site-directed mutagenesis product of pMV306 and *ppe51*	This study
pMV::*ppe51*-S211R+A228D	Ligated site-directed mutagenesis product of pMV306 and *ppe51*-S211R	This study
pET::*ppe51*-WT	*ppe51* PCR product ligated into *Bam*HI and *Hind*III sites of pET23a(+)	This study
pET::*ppe51*-S211R	Ligated site-directed mutagenesis product of pET32a(+) and *ppe51*	This Study
ORBIT Oligonucleotide		
ppe51 (oligomer)	ACGACACCGTATCCGCACAAATGTAAGGAGCTGAGACACAA TGGATTTCGCACTGTTACCACCGGAAGTC**GGTTTGTCTGGT CAACCACCGCGGTCTCAGTGGTGTACGGTACAAACC**GTG ATGGCCCACCCACCCGCGGCAGGGTAACCCGGCGCCTAACC GACAGGCGGCCCGTTGGGCGTAAACG	This Study

Table A.3.1. (cont'd)

ORBIT primers		
oriE	cctggtatctttatagtcctgtcg	Murphy *et al.* (2018)
HygC-out	(1) tgcacgggaccaacaccttcgtgg (2) gaggaactggcgcagttcctctgg	Murphy *et al.* (2018)
PCR primers		
Seq-*ppe51*-For	atggatttcgcactgttaccaccgga	Baker *et al.* (2018)
Seq-*ppe51*-Rev	ctgtcggttagttaccctgccgc	Baker *et al.* (2018)
pMV306::*ppe51*-Fwd	ggtaccagatctttaaatgcctgccgcacagaacctc	This study
pMV306::*ppe51*-Rev	gtcgacatcgataagcttcgttaccctgccgcgggtg	This study
pET23a::*ppe51*-Fwd	atatatggatccatggatttcgcactgttaccaccggaag	This study
pET23a::*ppe51*-Rev	atataagctttgggtgggccatcaccgtga	This study
pMV306-conf-Fwd	cgtattaccgcctttgagtgag	This study
pMV306-conf-Rev	gcagtgaagagaatagaccgg	This study
Site-directed mutagenesis primers		
ppe51-S211R-1-Fwd	gctgacgattccgag**a**ttcatccctgaggac	This study
ppe51-S211R-1-Rev	gtcctcagggatgaa**t**ctcggaatcgtcagc	This Study
ppe51-S211R-2-Fwd	gctgacgattccgag**g**ttcatccctgaggac	This study
ppe51-S211R-2-Rev	gtcctcagggatgaa**c**ctcggaatcgtcagc	This study
ppe51-A228D-Fwd	cgattccgagcttcatccct**a**aggacttcaccttc	This study
ppe51-A228D-Rev	gaaggtgaagtccttagggat**t**gaagctcggaatcg	This study
ppe51-E215K-Fwd	catattcgctggatatg**a**cacggtaggtgtgacg	This study
ppe51-E215K-Rev	cgtcacacctaccgtg**t**catatccagcgaatatg	This study
qRT-PCR primers		
RTpcr-*ppe51*-Fwd	gagcaagcatacgcaatgac	This study
RTpcr-*ppe51*-Rev	agtgttctggccgaagaag	This study

The Bxb1 phage *attP* sequence is in bold. Enzyme restriction cut sites are underlined. Site-directed mutagenesis sites are bold and underlined.

Table A.3.2. Mass Spectrometry results for bands associated with PPE51 induction.

Sample Name	Cluster	Protein Name	Protein accession numbers	Protein molecular weight (Da)	Protein identification probability	Exclusive unique peptide count	Exclusive unique spectrum count	Total spectrum count
Induced	Cluster of PPE family protein [Mycobacterium tuberculosis CDC1551] (AAK47561.1)	PPE family protein [Mycobacterium tuberculosis CDC1551]	AAK47561.1,KBN10067.1,WP_003416381.1,sp|P9WHY2.1|PPE51_MYCTO	37,979.90	100.00%	5	13	32
Pellet	Cluster of PPE family protein [Mycobacterium tuberculosis CDC1551] (AAK47561.1)	PPE family protein [Mycobacterium tuberculosis CDC1551]	AAK47561.1,KBN10067.1,WP_003416381.1,sp|P9WHY2.1|PPE51_MYCTO	37,979.90	100.00%	7	17	54

Table A.4.1. Plasmids and primers used in this study.

Plasmid or Primer Name	Characteristics or Sequence (5'→ 3')	Reference
pKM444	Kan^R; Mycobacterial shuttle vector expressing the Che9c phage RecT annealase and the Bxb1 phage integrase from the P_{tet} promoter	Murphy *et al.* (2018)
pKM464	Hyg^R; Mycobacterial integration vector for deleting target gene, insertion of Bxb1 *attB* site from the P_{Hyg} promoter	Murphy *et al.* (2018)
canC (ORBIT oligomer)[a]	ggcgaacacaatgccgtgtttctggcccggccctgacgctgtgaccattccgaggagt caacacatgagc**GGTTTGTCTGGTCAACCACCGCGGTCT CAGTGGTGTACGGTACAAACC**cgccccgtcgaccacgaatca gcgcagtagcgcccgcgacatcactacccgctgaatctgattggtgccc	This Study
oriE	cctggtatctttatagtcctgtcg	Murphy *et al*. (2018)
HygC-out	tgcacgggaccaacaccttcgtgg OR gaggaactggcgcagttcctctgg	Murphy *et al*. (2018)
Seq-*canC*-For	agaacgacctcaccctggaagtcg	This Study
Seq-*canC*-Rev	gaggtcaccaccgatgccgtacaa	ThisStudy
PLJR965	Kan^R; Plasmid co-expressing $dCas9_{Sth1}$ and targeting sgRNA under the control TetR-regulated *dcas9* promoter	Rock *et al.* (2017)
canA Pam1-FWD	gggagtgcctcgccctccttgatgc	This Study
canA Pam1-REV	aaacgcatcaaggagggcgaggcac	This Study
canA Pam2-FWD	gggagaagtcgtcgtcggtgaaag	This Study
canA Pam2-REV	aaacctttcaccgacgacgacttc	This Study
canA Pam3-FWD	gggaatcccacagtcggtgtggtgca	This Study
canA Pam3-REV	aaactgcaccacaccgactgtgggat	This Study
canB Pam1-FWD	gggagatggccgatgaacgcgcca	This Study
canB Pam1-REV	aaactggcgcgttcatcggccatc	This Study
canB Pam2-FWD	gggaactcagaccgtcacggcggc	This Study
canB Pam2-REV	aaacgccgccgtgacggtctgagt	This Study
canC Pam1-FWD	gggagtttgggcaagccaatcgcgtc	This Study
canC Pam1-REV	aaacgacgcgattggcttgcccaaac	This Study
canC Pam2-FWD	gggagctggcggtgatgacgttcg	This Study
canC Pam2-REV	aaaccgaacgtcatcaccgccagc	This Study
canC Pam3-FWD	gggaagcgaaagtggcaacgcaac	This Study
canC Pam3-REV	aaacgttgcgttgccactttcgct	This Study
RTpcr-*canA*-FWD	acgactacctggccaacaac	This Study
RTpcr-*canA*-REV	cagtgaacggatcacatcgt	This Study
RTpcr-*canB*-FWD	tgagtcgtgtcgacgagttc	This Study
RTpcr-*canB*-REV	gcccatcgtcgagttgatag	This Study
RTpcr-*canC*-FWD	ctgatccgattggactggtt	This Study
RTpcr-*canC*-REV	cacaggtgaggaacagctca	This Study

[a]The Bxb1 phage *attP* sequence is in bold

Table A.4.2. Genes induced at 5% CO_2 vs 0.5% CO_2 (> 1.5 fold, q<0.05) at pH 5.7 and pH 7.0 as determined by Venn diagram overlap.

Rv Number	Gene Name	Fold Change (pH 5.7)	Fold Change (pH 7.0)	Description
MT3426		2.753243942	1.778110193	
MT3762		5.505328015	2.45684967	
Rv0077c	Rv0077c	2.011314531	1.788057531	Probable oxidoreductase
Rv0081	Rv0081	2.753243942	1.717336216	Predicted to response to early hypoxia responses, is a regulatory hub, transcriptional regulator (ArsR family)
Rv0188	Rv0188	3.571535759	1.598608345	Early hypoxia induced antigen, probable conserved transmembrane protein
Rv0458	Rv0458	2.199277737	1.564036375	Probable aldehyde dehydrogenase
Rv0459	Rv0459	1.773505357	1.773094475	Conserved hypothetical protein
Rv1033c	*trcR*	2.466853742	13.24060216	Two-component response regulator
Rv1552	*frdA*	4.150631455	2.576019619	Fumarate reductase flavoprotein subunit
Rv1806	*pe20*	6.959283454	1.724457405	PE-family protein
Rv1807	*ppe31*	7.778629224	3.172502085	PPE-family protein
Rv1808	*ppe32*	4.302656374	2.132283225	PPE-family protein
Rv1926c	*mpt63*	3.149693231	1.591459529	Immunogenic protein
Rv2557	Rv2557	9.857833371	1.771311623	Conserved hypothetical protein
Rv2558	Rv2558	5.111890216	1.509389446	Conserved hypothetical protein
Rv3196A	Rv3196A	1.517727195	1.579298182	Hypothetical protein
Rv3229c	*desA3*	5.647648564	4.423655087	Possible linoleoyl-CoA desaturase
Rv3230c	Rv3230c	1.822523912	2.44875638	Hypothetical oxidoreductase
Rv3323c	*moaX*	1.900813486	1.591597104	Probable MoaD-MoaE fusion protein MoaX
Rv3324c	*moaC3*	2.178018167	1.73271074	Molybdenum cofactor biosynthesis, protein C
Rv3854c	*ethA*	1.771201446	1.716961024	Monooxegenase/ activates prodrug ethionamide

Table A.4.3. Genes repressed at 5% CO_2 vs 0.5% CO_2 (> 1.5 fold, q<0.05) at pH 5.7 and pH 7.0 as determined by Venn diagram overlap.

Rv Number	Gene Name	Fold Change (pH 5.7)	Fold Change (pH 7.0)	Description
MT1924.1		-3.6684033	-1.7487523	
MT3846		-1.8292278	-1.9523891	
Rv0113 / Rv0114	*gmhA/ gmhB*	-1.6102557	-1.7951531	Phosphoheptose isomerase
Rv0196	Rv0196	-2.4923411	-2.2236991	Transcriptional regulator (TetR/AcrR family)
Rv0197	Rv0197	-1.8021954	-1.5465353	Possible oxidoreductase
Rv0244c	*fadE5*	-1.982132	-1.725153	Acyl-CoA dehydrogenase
Rv0467	*iclI*	-2.9811836	-2.1711127	Isocitrate lyase
Rv0468	*fadB2*	-2.9304622	-1.6344645	3-hydroxybutyryl-CoA dehydrogenase
Rv0694	*lldD1*	-1.8384573	-2.0743212	L-lactate dehydrogenase (cytochrome)
Rv0695	Rv0695	-1.5141984	-1.5953014	Probable mycofactonin system creatinine amidohydrolase family protein MftE
Rv1057	Rv1057	-1.8382357	-1.8296267	B-propeller gene
Rv1128c	Rv1128c	-1.8961871	-1.6932342	Hypothetical protein
Rv1129c	*prpR*	-3.4181997	-1.632647	Probable PrpCD transcriptional regulator (PbsX/Xre family)
Rv1168c	*ppe17*	-1.615023	-1.7580494	PPE-family protein
Rv1196	*ppe18*	-1.7158895	-2.4923359	PPE-family protein
Rv1344	*mbtL*	-1.7902261	-1.6490043	Acyl carrier protein involved in mycobactin synthesis
Rv1349	*irtB*	-1.7211027	-1.7660285	Iron regulated transporter, probable membrane protein
Rv1505c	Rv1505c	-1.5017694	-1.5683214	Conserved hypothetical protein
Rv1644	*tsnR*	-1.8184345	-1.8746149	Putative 23S rRNA methyltransferase
Rv1979c	Rv1979c	-1.5697631	-1.5614064	Possible permease/ involved in clofazamin resistance
Rv2189c	Rv2189c	-3.3102287	-1.6934025	Hypothetical protein
Rv2329c	*narK1*	-1.5663419	-2.2888819	Probable nitrite extrusion protein
Rv2386c	*mbtI*	-2.4318689	-1.7085145	Mycobactin/exochelin synthesis (isochorismate synthase)
Rv2645	Rv2645	-1.5251948	-1.5191805	Hypothetical protein
Rv2931	*ppsA*	-1.5990587	-3.3959071	Phenolpthiocerol synthesis (pksB)
Rv2935	*ppsE*	-1.5563521	-1.6058716	Phenolpthiocerol synthesis (pksF)
Rv2948c	*fadD22*	-1.663901	-2.1072725	P-hydroxybenzoyl-AMP ligase
Rv2949c	Rv2949c	-1.7653822	-2.2946056	Chorismate pyruvate lyase
Rv2950c	*fadD29*	-1.7369432	-1.6621187	Acyl-CoA synthase
Rv2958c	Rv2958c	-1.928179	-2.2607948	Possible glycosyltransferases
Rv3084	*lipR*	-2.0848742	-1.6080043	Probable acetyl-hydrolase
Rv3085	Rv3085	-1.8684076	-1.5942201	Short chain alcohol dehydrogenase
Rv3092c	Rv3092c	-3.5242887	-1.5899468	Probable conserved integral membrane protein
Rv3135	*ppe50*	-2.1327559	-2.1218846	PPE-family protein
Rv3136	*ppe51*	-2.4821091	-2.7104901	PPE-family protein
Rv3137	Rv3137	-2.4840015	-2.7223984	Probable monophosphatase
Rv3249c	Rv3249c	-2.1429063	-2.1664398	Transcriptional regulator (TetR/AcrR family)
Rv3251c	*rubA*	-3.1358253	-3.7881419	Rubredoxin A
Rv3252c	*alkB*	-3.328656	-2.876874	Possible alkane-1 monooxygenase
Rv3453 / Rv3454	Rv3453 / Rv3454	-2.0682255	-1.8513195	Hypothetical protein
Rv3740c	Rv3740c	-5.1395159	-3.4196278	Putative diacylglycerol o-acyltransferase
Rv3741c	Rv3741c	-10.507792	-3.506946	Possible oxidoreductase
Rv3742c	Rv3742c	-9.0868131	-2.6889642	Possible monooxygenase-b
Rv3919c	*gid*	-1.5628553	-1.7456093	Probable glucose-inhibited division protein B Gid
Rv3920c	Rv3920c	-1.7098621	-2.2708554	Jag like protein involved in cell divison
Rv3921c	*yidC*	-1.5832739	-1.6413533	Putative translocase

Table A.4.4. Genes induced at 5% CO_2 vs 0.5% CO_2 at pH 5.7 (> 1.5 fold, q<0.05) compared to genes in the pH-induced regulon (> 1.5 fold, q<0.05)[50] as determined by Venn diagram overlap.

Rv Number	Gene Name	Fold Change (CO_2)	Fold Change (pH regulon)	Description
MT1178		1.61017777	1.74288483	
MT2042.1		1.78287046	1.72382925	
MT3427		2.45654718	1.58212572	
MT3580.2*		1.53712592	5.20550219	
MT3953		1.819035	2.02925568	
Rv0120c*	*fusA2*	1.94679133	2.13087942	Elongation factor G
Rv0208c	Rv0208c	1.89671423	1.77006516	Hypothetical methytransferase
Rv0223c	Rv0223c	1.74752112	1.5318152	Aldehyde dehydrogenase (possible betb)
Rv0251c*	*hsp*	2.00294935	3.59004318	Heat shock protein Hsp (heat-stress-induced ribosome-binding protein A)
Rv0263c	Rv0263c	1.76417163	1.75020752	Conserved hypothetical protein
Rv0264c	Rv0264c	1.65398066	1.89095463	Conserved hypothetical protein
Rv0806c	*cpsY*	1.54541702	1.57771772	Probable UDP-glucose-4-epimerase
Rv0888	Rv0888	2.10094033	3.98240586	Probable extracellular nuclease
Rv1239c	*corA*	1.5961507	1.69400197	Possible magnesium and cobalt transport transmembrane protein
Rv1265	Rv1265	1.58042259	1.50182124	Camp regulated protein
Rv1535*	Rv1535	2.53595705	8.84006393	Predicted to have nucleoid associated protein homology
Rv1536*	*ileS*	1.80085137	1.55823556	Isoleucyl-tRNA synthase
Rv1638A*	Rv1638A	1.70827347	10.1711742	Conserved hypothetical protein
Rv1646	*pe17*	2.41950428	1.74198666	PE-family protein
Rv1690	*lprJ*	2.45346233	2.09355253	Lipoprotein
Rv1809	*ppe33*	1.88690596	2.66860728	PPE-family protein
Rv1875	Rv1875	1.57529174	2.08326312	Hypothetical protein
Rv1920	Rv1920	1.64769328	1.57703447	Probable membrane protein
Rv2395A*	*aprA*	2.0296914	11.4208153	Acid and phagosome regulated protein A
Rv2632c*	Rv2632c	2.20247671	2.86784453	Conserved hypothetical protein
Rv2633c*	Rv2633c	2.43252942	3.12205054	Hypothetical protein
Rv2638	Rv2638	2.86070656	1.63584203	Putative anti-sigma factor
Rv3614c*	*espD*	1.98988522	1.79620859	ESX-1 secretion associated
Rv3615c*	*espC*	2.1955695	1.86802708	ESX-1 secretion associated
Rv3616c*	*espA*	2.21804186	1.58641301	ESX-1 secretion associated
Rv3633	Rv3633	2.36123794	1.89856682	Conserved hypothetical protein
Rv3675	Rv3675	2.43695043	1.66624442	Possible membrane protein
Rv3763	*lpqH*	2.0617702	1.89796301	19 kda lipoprotein antigen precursor lpqh
Rv3824c*	*papA1*	1.53525164	13.6840266	PKS-associated protein, unknown function
Rv3864*	*espE*	1.72937794	1.51523716	ESX1 associated
Rv3872*	*pe35*	1.67550172	2.24423035	PE-family protein
Rv3873*	*ppe68*	1.67218108	2.21838674	PPE-family protein
Rv3874*	*esxB*/CFP-10	2.58749199	3.33156797	Conserved hypothetical protein
Rv3875*	*esxA/esat6*	2.49227331	3.5729886	Early secretory antigen target
Rv3880c*	*espL*	2.4957492	1.54113981	ESX-1 secretion associated protein
Rv3881c*	*espB*	2.20071928	1.51062142	Secreted esx-1 protein
Rv3890c	*esxC*	1.62329621	2.40192671	ESAT-6 paralogue
Rv3891c	*esxD*	1.77562298	1.92094002	CFP-10 paralogue

Table A.4.5. Genes repressed at 5% CO2 vs 0.5% CO2 at pH 5.7 (> 1.5 fold, q<0.05) compared to genes in the pH-repressed regulon (> 1.5 fold, p<0.05) [50] as determined by Venn diagram overlap.

Rv Number	Gene Name	Fold Change (CO_2)	Fold Change (pH regulon)	Description
MT0600		-1.7844415	-2.5823826	
MT1775		-1.5476337	-2.2664654	
MT2617		-1.7550134	-1.6679183	
Rv0972c	*fadE12*	-1.5709961	-3.2552682	Acyl-CoA dehydrogenase
Rv1169c	*lipX*	-1.7659147	-1.7374021	Possible lipase/ PE-family protein
Rv1195	*pe13*	-2.7993255	-2.3086343	PE-family protein
Rv1297	*rho*	-1.7808529	-1.7372071	Transcription termination factor rho
Rv1733c	Rv1733c	-2.0523501	-2.1026705	Probable conserved transmembrane protein
Rv1737c	*narK2*	-1.7711458	-3.3817382	Nitrite extrusion protein
Rv1738	Rv1738	-1.5658166	-3.9004149	Possibly interact with ribosome structural prection
Rv2007c	*fdxA*	-2.081072	-2.4900084	Ferredoxin
Rv2028c	Rv2028c	-2.5482444	-1.8673765	Universal stress protein family protein
Rv2029c	*pfkB*	-1.9083496	-3.0697337	Phosphofructokinase
Rv2030c	Rv2030c	-1.9899349	-2.4777995	Conserved protein
Rv2031c	*hspX*	-2.2091578	-1.935502	Heat shock protein
Rv2032	*acg*	-1.5467977	-2.3186279	Conserved protein
Rv2379c	*mbtF*	-1.5463819	-1.567989	Mycobactin/exochelin synthesis (lysine ligation)
Rv2382c	*mbtC*	-1.7959495	-1.5139581	Mycobactin/exochelin synthesis
Rv2383c	*mbtB*	-1.8377144	-1.5074697	Mycobactin/exochelin synthesis (serine/threonine
Rv2450c	*rpfE*	-2.6194638	-1.8434405	Probable resuscitation promoting factor
Rv2987c	*leuD*	-2.032139	-2.5654292	3-isopropylmalate dehydratase small subunit
Rv2988c	*leuC*	-2.9299457	-1.9645698	3-isopropylmalate dehydratase large subunit
Rv2989	Rv2989	-2.2003943	-1.7051843	Transcriptional regulator (iclr family)
Rv3402c	Rv3402c	-2.1194352	-1.6791906	Conserved protein

REFERENCES

REFERENCES

1 WHO. Global Tuberculosis Report 2020. (2020).

2 Riley, R. L. Aerial dissemination of pulmonary tuberculosis. *Am Rev Tuberc* **76**, 931-941, doi:10.1164/artpd.1957.76.6.931 (1957).

3 Ehrt, S. & Schnappinger, D. Mycobacterial survival strategies in the phagosome: defence against host stresses. *Cell Microbiol* **11**, 1170-1178, doi:10.1111/j.1462-5822.2009.01335.x (2009).

4 Zheng, H. *et al.* Inhibitors of Mycobacterium tuberculosis DosRST signaling and persistence. *Nat Chem Biol* **13**, 218-225, doi:10.1038/nchembio.2259 (2017).

5 Gengenbacher, M., Rao, S. P., Pethe, K. & Dick, T. Nutrient-starved, non-replicating Mycobacterium tuberculosis requires respiration, ATP synthase and isocitrate lyase for maintenance of ATP homeostasis and viability. *Microbiology* **156**, 81-87, doi:10.1099/mic.0.033084-0 (2010).

6 Baek, S.-H., Li, A. H. & Sassetti, C. M. Metabolic regulation of mycobacterial growth and antibiotic sensitivity. *PLoS Biol* **9**, e1001065-e1001065, doi:10.1371/journal.pbio.1001065 (2011).

7 Gold, B. & Nathan, C. Targeting Phenotypically Tolerant Mycobacterium tuberculosis. *Microbiology spectrum* **5**, 10.1128/microbiolspec.TBTB1122-0031-2016, doi:10.1128/microbiolspec.TBTB2-0031-2016 (2017).

8 Vandal, O. H. *et al.* Acid-susceptible mutants of Mycobacterium tuberculosis share hypersusceptibility to cell wall and oxidative stress and to the host environment. *J Bacteriol* **191**, 625-631, doi:10.1128/JB.00932-08 (2009).

9 Vandal, O. H., Pierini, L. M., Schnappinger, D., Nathan, C. F. & Ehrt, S. A membrane protein preserves intrabacterial pH in intraphagosomal Mycobacterium tuberculosis. *Nat Med* **14**, 849-854, doi:10.1038/nm.1795 (2008).

10 Perez, E. *et al.* An essential role for phoP in Mycobacterium tuberculosis virulence. *Mol Microbiol* **41**, 179-187, doi:10.1046/j.1365-2958.2001.02500.x (2001).

11 Levitte, S. *et al.* Mycobacterial Acid Tolerance Enables Phagolysosomal Survival and Establishment of Tuberculous Infection In Vivo. *Cell host & microbe* **20**, 250-258, doi:10.1016/j.chom.2016.07.007 (2016).

12 Baker, J. J. & Abramovitch, R. B. Genetic and metabolic regulation of Mycobacterium tuberculosis acid growth arrest. *Sci Rep* **8**, 4168, doi:10.1038/s41598-018-22343-4 (2018).

13 Wayne, L. G. & Sohaskey, C. D. Nonreplicating persistence of mycobacterium tuberculosis. *Annu Rev Microbiol* **55**, 139-163, doi:10.1146/annurev.micro.55.1.139 (2001).

14 Dannenberg, J. A. M. *Pathogenesis of Human Pulmonary Tuberculosis: Insights from the Rabbit Model*. (2006).

15 MacMicking, J. D., Taylor, G. A. & McKinney, J. D. Immune control of tuberculosis by IFN-gamma-inducible LRG-47. *Science* **302**, 654-659, doi:10.1126/science.1088063 (2003).

16 Hackam, D. J. *et al.* Regulation of phagosomal acidification. Differential targeting of Na+/H+ exchangers, Na+/K+-ATPases, and vacuolar-type H+-atpases. *Journal of Biological Chemistry* **272**, 29810-29820, doi:10.1074/jbc.272.47.29810 (1997).

17 Bach, H., Papavinasasundaram, K. G., Wong, D., Hmama, Z. & Av-Gay, Y. Mycobacterium tuberculosis virulence is mediated by PtpA dephosphorylation of human vacuolar protein sorting 33B. *Cell Host Microbe* **3**, 316-322, doi:10.1016/j.chom.2008.03.008 (2008).

18 Wong, D., Bach, H., Sun, J., Hmama, Z. & Av-Gay, Y. Mycobacterium tuberculosis protein tyrosine phosphatase (PtpA) excludes host vacuolar-H+–ATPase to inhibit phagosome acidification. *Proceedings of the National Academy of Sciences* **108**, 19371, doi:10.1073/pnas.1109201108 (2011).

19 Sibley, L. D., Franzblau, S. G. & Krahenbuhl, J. L. Intracellular fate of Mycobacterium leprae in normal and activated mouse macrophages. *Infection and Immunity* **55**, 680-685 (1987).

20 Via, L. E. *et al.* Arrest of mycobacterial phagosome maturation is caused by a block in vesicle fusion between stages controlled by rab5 and rab7. *Journal of Biological Chemistry* **272**, 13326-13331 (1997).

21 Sturgill-Koszycki, S. *et al.* Lack of acidification in Mycobacterium phagosomes produced by exclusion of the vesicular proton-ATPase. *Science* **263**, 678-681 (1994).

22 Beauregard, K. E., Lee, K.-D., Collier, R. J. & Swanson, J. A. pH-dependent perforation of macrophage phagosomes by listeriolysin O from Listeria monocytogenes. *The Journal of experimental medicine* **186**, 1159-1163 (1997).

23 Rathman, M., Sjaastad, M. D. & Falkow, S. Acidification of phagosomes containing Salmonella typhimurium in murine macrophages. *Infection and immunity* **64**, 2765-2773 (1996).

24 Hackstadt, T. & Williams, J. C. Biochemical stratagem for obligate parasitism of eukaryotic cells by Coxiella burnetii. *Proceedings of the National Academy of Sciences* **78**, 3240-3244 (1981).

25 Via, L. *et al.* Effects of cytokines on mycobacterial phagosome maturation. *Journal of cell science* **111**, 897-905 (1998).

26 Yates, R. M., Hermetter, A., Taylor, G. A. & Russell, D. G. Macrophage activation downregulates the degradative capacity of the phagosome. *Traffic* **8**, 241-250 (2007).

27 Manzanillo, Paolo S., Shiloh, Michael U., Portnoy, Daniel A. & Cox, Jeffery S. Mycobacterium Tuberculosis Activates the DNA-Dependent Cytosolic Surveillance Pathway within Macrophages. *Cell Host & Microbe* **11**, 469-480, doi:https://doi.org/10.1016/j.chom.2012.03.007 (2012).

28 Jonge, M. I. d. *et al.* ESAT-6 from *Mycobacterium tuberculosis* Dissociates from Its Putative Chaperone CFP-10 under Acidic Conditions and Exhibits Membrane-Lysing Activity. *Journal of Bacteriology* **189**, 6028-6034, doi:doi:10.1128/JB.00469-07 (2007).

29 Abdallah, A. M. *et al.* Type VII secretion — mycobacteria show the way. *Nature Reviews Microbiology* **5**, 883-891, doi:10.1038/nrmicro1773 (2007).

30 Augenstreich, J. *et al.* ESX-1 and phthiocerol dimycocerosates of Mycobacterium tuberculosis act in concert to cause phagosomal rupture and host cell apoptosis. *Cell Microbiol* **19**, doi:10.1111/cmi.12726 (2017).

31 Baker, J. J., Dechow, S. J. & Abramovitch, R. B. Acid Fasting: Modulation of Mycobacterium tuberculosis Metabolism at Acidic pH. *Trends Microbiol* **27**, 942-953, doi:10.1016/j.tim.2019.06.005 (2019).

32 Gill, W. P. *et al.* A replication clock for Mycobacterium tuberculosis. *Nature medicine* **15**, 211-214, doi:10.1038/nm.1915 (2009).

33 Rohde, K. H., Veiga, D. F. T., Caldwell, S., Balázsi, G. & Russell, D. G. Linking the Transcriptional Profiles and the Physiological States of Mycobacterium tuberculosis during an Extended Intracellular Infection. *PLoS Pathogens* **8**, e1002769, doi:10.1371/journal.ppat.1002769 (2012).

34 Loebel, R. O., Shorr, E. & Richardson, H. B. The Influence of Foodstuffs upon the Respiratory Metabolism and Growth of Human Tubercle Bacilli. *Journal of bacteriology* **26**, 139--166 (1933).

35 Loebel, R. O., Shorr, E. & Richardson, H. B. The Influence of Adverse Conditions upon the Respiratory Metabolism and Growth of Human Tubercle Bacilli. *Journal of bacteriology* **26**, 167-200, doi:10.1128/JB.26.2.167-200.1933 (1933).

36 Galagan, J. E. *et al.* The Mycobacterium tuberculosis regulatory network and hypoxia. *Nature* **499**, 178-183, doi:10.1038/nature12337 (2013).

37 Baker, J. J., Johnson, B. K. & Abramovitch, R. B. Slow growth of Mycobacterium tuberculosis at acidic pH is regulated by phoPR and host-associated carbon sources. *Mol Microbiol* **94**, 56-69, doi:10.1111/mmi.12688 (2014).

38 Piddington, D. L. a. K. A. a. B. N. A. Growth of Mycobacterium tuberculosis in a defined medium is very restricted by acid pH and Mg(2+) levels. *Infection and immunity* **68**, 4518--4522 (2000).

39 Abramovitch, R. B., Rohde, K. H., Hsu, F. F. & Russell, D. G. aprABC: a Mycobacterium tuberculosis complex-specific locus that modulates pH-driven adaptation to the macrophage phagosome. *Mol Microbiol* **80**, 678-694, doi:10.1111/j.1365-2958.2011.07601.x (2011).

40 McKinney, J. D. *et al.* Persistence of Mycobacterium tuberculosis in macrophages and mice requires the glyoxylate shunt enzyme isocitrate lyase. *Nature* **406**, 735-738, doi:10.1038/35021074 (2000).

41 Upton, A. M. & McKinney, J. D. Role of the methylcitrate cycle in propionate metabolism and detoxification in Mycobacterium smegmatis. *Microbiology (Reading)* **153**, 3973-3982, doi:10.1099/mic.0.2007/011726-0 (2007).

42 Munoz-Elias, E. J., Upton, A. M., Cherian, J. & McKinney, J. D. Role of the methylcitrate cycle in Mycobacterium tuberculosis metabolism, intracellular growth, and virulence. *Mol Microbiol* **60**, 1109-1122, doi:10.1111/j.1365-2958.2006.05155.x (2006).

43 Lee, W., VanderVen, B. C., Fahey, R. J. & Russell, D. G. Intracellular Mycobacterium tuberculosis exploits host-derived fatty acids to limit metabolic stress. *J Biol Chem* **288**, 6788-6800, doi:10.1074/jbc.M112.445056 (2013).

44 Van der Geize, R. *et al.* A gene cluster encoding cholesterol catabolism in a soil actinomycete provides insight into Mycobacterium tuberculosis survival in macrophages. *Proceedings of the National Academy of Sciences of the United States of America* **104**, 1947-1952, doi:10.1073/pnas.0605728104 (2007).

45 Cole, S. T. *et al.* Deciphering the biology of Mycobacterium tuberculosis from the complete genome sequence. *Nature* **393**, 537-544, doi:10.1038/31159 (1998).

46 Rohde, K. H., Abramovitch, R. B. & Russell, D. G. Mycobacterium tuberculosis invasion of macrophages: linking bacterial gene expression to environmental cues. *Cell Host Microbe* **2**, 352-364, doi:10.1016/j.chom.2007.09.006 (2007).

47 Fisher, M. A., Plikaytis, B. B. & Shinnick, T. M. Microarray analysis of the Mycobacterium tuberculosis transcriptional response to the acidic conditions found in phagosomes. *J Bacteriol* **184**, 4025-4032, doi:10.1128/jb.184.14.4025-4032.2002 (2002).

48 Walters, S. B. *et al.* The Mycobacterium tuberculosis PhoPR two-component system regulates genes essential for virulence and complex lipid biosynthesis. *Mol Microbiol* **60**, 312-330, doi:10.1111/j.1365-2958.2006.05102.x (2006).

49 Gonzalo-Asensio, J. *et al.* PhoP: A Missing Piece in the Intricate Puzzle of Mycobacterium tuberculosis Virulence. *PLOS ONE* **3**, e3496, doi:10.1371/journal.pone.0003496 (2008).

50 Johnson, B. K. *et al.* The Carbonic Anhydrase Inhibitor Ethoxzolamide Inhibits the Mycobacterium tuberculosis PhoPR Regulon and Esx-1 Secretion and Attenuates Virulence. *Antimicrob Agents Chemother* **59**, 4436-4445, doi:10.1128/AAC.00719-15 (2015).

51 Segovia-Juarez, J. L., Ganguli, S. & Kirschner, D. Identifying control mechanisms of granuloma formation during M. tuberculosis infection using an agent-based model. *Journal of Theoretical Biology* **231**, 357-376, doi:https://doi.org/10.1016/j.jtbi.2004.06.031 (2004).

52 Betts, J. C., Lukey, P. T., Robb, L. C., McAdam, R. A. & Duncan, K. Evaluation of a nutrient starvation model of Mycobacterium tuberculosis persistence by gene and protein expression profiling. *Mol Microbiol* **43**, 717-731, doi:10.1046/j.1365-2958.2002.02779.x (2002).

53 Dechow, S. J., Baker, J. J., Murto, M. R. & Abramovitch, R. B. *ppe51* variants promote non-replicating *Mycobacterium tuberculosis* to grow at acidic pH by selectively promoting glycerol uptake. *bioRxiv*, 2021.2005.2019.444820, doi:10.1101/2021.05.19.444820 (2021).

54 Wang, Q. *et al.* PE/PPE proteins mediate nutrient transport across the outer membrane of *Mycobacterium tuberculosis*. *Science* **367**, 1147, doi:10.1126/science.aav5912 (2020).

55 Bellerose, M. M. *et al.* Common Variants in the Glycerol Kinase Gene Reduce Tuberculosis Drug Efficacy. *mBio* **10**, e00663-00619, doi:10.1128/mBio.00663-19 (2019).

56 Korycka-Machała, M. *et al.* PPE51 Is Involved in the Uptake of Disaccharides by Mycobacterium tuberculosis. *Cells* **9**, 603, doi:10.3390/cells9030603 (2020).

57 Gouzy, A., Healy, C., Black, K. A., Rhee, K. Y. & Ehrt, S. Growth of *Mycobacterium tuberculosis* at acidic pH depends on lipid assimilation and is accompanied by reduced GAPDH activity. *Proceedings of the National Academy of Sciences* **118**, e2024571118, doi:10.1073/pnas.2024571118 (2021).

58 Rustad, T. R., Harrell, M. I., Liao, R. & Sherman, D. R. The Enduring Hypoxic Response of Mycobacterium tuberculosis. *PLOS ONE* **3**, e1502, doi:10.1371/journal.pone.0001502 (2008).

59 Tischler, A. D., Leistikow, R. L., Ramakrishnan, P., Voskuil, M. I. & McKinney, J. D. Mycobacterium tuberculosis Phosphate Uptake System Component PstA2 Is Not Required for Gene Regulation or Virulence. *PLOS ONE* **11**, e0161467, doi:10.1371/journal.pone.0161467 (2016).

60 Wanner, B. L. Phosphorus assimilation and control of the phosphate regulon. *Escherichia coli and Salmonella: cellular and molecular biology* **1**, 1357-1381 (1996).

61 Jackett, P., Aber, V. & Lowrie, D. Virulence and resistance to superoxide, low pH and hydrogen peroxide among strains of Mycobacterium tuberculosis. *Microbiology* **104**, 37-45 (1978).

62 Dubos, R. J. THE EFFECT OF LIPIDS AND SERUM ALBUMIN ON BACTERIAL GROWTH. *J Exp Med* **85**, 9-22, doi:10.1084/jem.85.1.9 (1947).

63 Davis, B. D. & Dubos, R. J. THE BINDING OF FATTY ACIDS BY SERUM ALBUMIN, A PROTECTIVE GROWTH FACTOR IN BACTERIOLOGICAL MEDIA. *J Exp Med* **86**, 215-228, doi:10.1084/jem.86.3.215 (1947).

64 Kanai, K. & Kondo, E. Antibacterial and cytotoxic aspects of long-chain fatty acids as cell surface events: selected topics. *Jpn J Med Sci Biol* **32**, 135-174, doi:10.7883/yoken1952.32.135 (1979).

65 Lynn, M., Wilson, A. R. & Solotorovsky, M. Role of bovine serum albumin in the nutrition of Mycobacterium tuberculosis. *Appl Environ Microbiol* **38**, 806-810, doi:10.1128/aem.38.5.806-810.1979 (1979).

66 Kondo, E. & Kanai, K. The lethal effect of long-chain fatty acids on mycobacteria. *Jpn J Med Sci Biol* **25**, 1-13, doi:10.7883/yoken1952.25.1 (1972).

67 Lampe, D. J., Churchill, M. E. & Robertson, H. M. A purified mariner transposase is sufficient to mediate transposition in vitro. *EMBO J* **15**, 5470-5479 (1996).

68 Dechow, S. J., Coulson, G. B., Wilson, M. W., Larsen, S. D. & Abramovitch, R. B. AC2P20 selectively kills Mycobacterium tuberculosis at acidic pH by depleting free thiols. *RSC Advances* **11**, 20089-20100, doi:10.1039/D1RA03181C (2021).

69 Coulson, G. B. *et al.* Targeting Mycobacterium tuberculosis Sensitivity to Thiol Stress at Acidic pH Kills the Bacterium and Potentiates Antibiotics. *Cell Chem Biol* **24**, 993-1004 e1004, doi:10.1016/j.chembiol.2017.06.018 (2017).

70 Darby, C. M. *et al.* Whole cell screen for inhibitors of pH homeostasis in Mycobacterium tuberculosis. *PLoS One* **8**, e68942, doi:10.1371/journal.pone.0068942 (2013).

71 Early, J. *et al.* Identification of Compounds with pH-Dependent Bactericidal Activity against Mycobacterium tuberculosis. *ACS Infect Dis* **5**, 272-280, doi:10.1021/acsinfecdis.8b00256 (2019).

72 Miesenböck, G., De Angelis, D. A. & Rothman, J. E. Visualizing secretion and synaptic transmission with pH-sensitive green fluorescent proteins. *Nature* **394**, 192-195 (1998).

73 Gold, B., Warrier, T. & Nathan, C. in *Mycobacteria protocols* 293-315 (Springer, 2015).

74 Solans, L. *et al.* The PhoP-Dependent ncRNA Mcr7 Modulates the TAT Secretion System in Mycobacterium tuberculosis. *PLOS Pathogens* **10**, e1004183, doi:10.1371/journal.ppat.1004183 (2014).

75 Zhao, N. *et al.* Target-based screen against a periplasmic serine protease that regulates intrabacterial pH homeostasis in Mycobacterium tuberculosis. *ACS Chem Biol* **10**, 364-371, doi:10.1021/cb500746z (2015).

76 Kugadas, A. *et al.* A Mycobacterium avium subsp. paratuberculosis Predicted Serine Protease Is Associated with Acid Stress and Intraphagosomal Survival. *Frontiers in Cellular and Infection Microbiology* **6**, doi:10.3389/fcimb.2016.00085 (2016).

77 Cravatt, B. F., Wright, A. T. & Kozarich, J. W. Activity-based protein profiling: from enzyme chemistry to proteomic chemistry. *Annu. Rev. Biochem.* **77**, 383-414 (2008).

78 Wang, S. *et al.* Advanced Activity-Based Protein Profiling Application Strategies for Drug Development. *Frontiers in Pharmacology* **9**, doi:10.3389/fphar.2018.00353 (2018).

79 Zhao, N. *et al.* Identification of Rv3852 as an Agrimophol-Binding Protein in Mycobacterium tuberculosis. *PloS one* **10**, e0126211-e0126211, doi:10.1371/journal.pone.0126211 (2015).

80 Schaible, U. E., Sturgill-Koszycki, S., Schlesinger, P. H. & Russell, D. G. Cytokine activation leads to acidification and increases maturation of Mycobacterium avium-containing phagosomes in murine macrophages. *The Journal of Immunology* **160**, 1290-1296 (1998).

81 Vandal, O. H., Nathan, C. F. & Ehrt, S. Acid resistance in Mycobacterium tuberculosis. *J Bacteriol* **191**, 4714-4721, doi:10.1128/JB.00305-09 (2009).

82 Andries, K. *et al.* A diarylquinoline drug active on the ATP synthase of Mycobacterium tuberculosis. *Science* **307**, 223-227 (2005).

83 de Carvalho, L. P. S., Darby, C. M., Rhee, K. Y. & Nathan, C. Nitazoxanide Disrupts Membrane Potential and Intrabacterial pH Homeostasis of Mycobacterium tuberculosis. *ACS Medicinal Chemistry Letters* **2**, 849-854, doi:10.1021/ml200157f (2011).

84 O'Malley, T. *et al.* Imidazopyridine Compounds Inhibit Mycobacterial Growth by Depleting ATP Levels. *Antimicrobial Agents and Chemotherapy* **62**, e02439-02417, doi:doi:10.1128/AAC.02439-17 (2018).

85 Moraski, G. C. *et al.* Advancement of Imidazo[1,2-a]pyridines with Improved Pharmacokinetics and nM Activity vs. Mycobacterium tuberculosis. *ACS Medicinal Chemistry Letters* **4**, 675-679, doi:10.1021/ml400088y (2013).

86 Zhang, Y., Wade, M. M., Scorpio, A., Zhang, H. & Sun, Z. Mode of action of pyrazinamide: disruption of Mycobacterium tuberculosis membrane transport and energetics by pyrazinoic acid. *Journal of Antimicrobial Chemotherapy* **52**, 790-795, doi:10.1093/jac/dkg446 (2003).

87 Lam, K. K. *et al.* Nitazoxanide stimulates autophagy and inhibits mTORC1 signaling and intracellular proliferation of Mycobacterium tuberculosis. *PLoS pathogens* **8**, e1002691 (2012).

88 de Carvalho, L. P. S., Lin, G., Jiang, X. & Nathan, C. Nitazoxanide kills replicating and nonreplicating Mycobacterium tuberculosis and evades resistance. *Journal of medicinal chemistry* **52**, 5789-5792 (2009).

89 Smith, J. *et al.* Anthranilic amide and imidazobenzothiadiazole compounds disruptMycobacterium tuberculosismembrane potential. *MedChemComm* **10**, 934-945, doi:10.1039/c9md00088g (2019).

90 Hendrick, S. H. *et al.* Efficacy of monensin sodium for the reduction of fecal shedding of Mycobacterium avium subsp. paratuberculosis in infected dairy cattle. *Preventive veterinary medicine* **75**, 206-220 (2006).

91 Brumbaugh, G., Frelier, P., Roussel Jr, A. & Thomson, T. Prophylactic effect of monensin sodium against experimentally induced paratuberculosis in mice. *American journal of veterinary research* **53**, 544-546 (1992).

92 Flentie, K. *et al.* Chemical disarming of isoniazid resistance in Mycobacterium tuberculosis. *Proc Natl Acad Sci U S A* **116**, 10510-10517, doi:10.1073/pnas.1818009116 (2019).

93 Ruth, M. M. *et al.* Auranofin Activity Exposes Thioredoxin Reductase as a Viable Drug Target in Mycobacterium abscessus. *Antimicrob Agents Chemother* **63**, doi:10.1128/AAC.00449-19 (2019).

94 Harbut, M. B. *et al.* Auranofin exerts broad-spectrum bactericidal activities by targeting thiol-redox homeostasis. *Proc Natl Acad Sci U S A* **112**, 4453-4458, doi:10.1073/pnas.1504022112 (2015).

95 Gold, B. *et al.* Nonsteroidal anti-inflammatory drug sensitizes Mycobacterium tuberculosis to endogenous and exogenous antimicrobials. *Proceedings of the National Academy of Sciences* **109**, 16004-16011 (2012).

96 Advani, M. J., Siddiqui, I., Sharma, P. & Reddy, H. Activity of trifluoperazine against replicating, non-replicating and drug resistant M. tuberculosis. (2012).

97 Bryk, R. *et al.* Selective Killing of Nonreplicating Mycobacteria. *Cell Host & Microbe* **3**, 137-145, doi:https://doi.org/10.1016/j.chom.2008.02.003 (2008).

98 Lin, G. *et al.* N, C-Capped dipeptides with selectivity for mycobacterial proteasome over human proteasomes: role of S3 and S1 binding pockets. *Journal of the American Chemical Society* **135**, 9968-9971 (2013).

99 Darby, C. M. & Nathan, C. F. Killing of non-replicating Mycobacterium tuberculosis by 8-hydroxyquinoline. *Journal of antimicrobial chemotherapy* **65**, 1424-1427 (2010).

100 Olaleye, O. *et al.* Characterization of clioquinol and analogues as novel inhibitors of methionine aminopeptidases from Mycobacterium tuberculosis. *Tuberculosis* **91**, S61-S65 (2011).

101 Olaleye, O. *et al.* Methionine aminopeptidases from Mycobacterium tuberculosis as novel antimycobacterial targets. *Chemistry & biology* **17**, 86-97, doi:10.1016/j.chembiol.2009.12.014 (2010).

102 Kwai, B. X. *et al.* Itaconate is a covalent inhibitor of the Mycobacterium tuberculosis isocitrate lyase. *RSC Medicinal Chemistry* **12**, 57-61 (2021).

103 Schloss, J. V. & Cleland, W. Inhibition of isocitrate lyase by 3-nitropropionate, a reaction-intermediate analog. *Biochemistry* **21**, 4420-4427 (1982).

104 Crowle, A. J. & May, M. H. Inhibition of tubercle bacilli in cultured human macrophages by chloroquine used alone and in combination with streptomycin, isoniazid, pyrazinamide, and two metabolites of vitamin D3. *Antimicrobial agents and chemotherapy* **34**, 2217-2222 (1990).

105 Matt, U. *et al.* Chloroquine enhances the antimycobacterial activity of isoniazid and pyrazinamide by reversing inflammation-induced macrophage efflux. *International journal of antimicrobial agents* **50**, 55-62 (2017).

106 Hart, P. in *JOURNAL OF PATHOLOGY*. 55-55 (JOHN WILEY & SONS LTD BAFFINS LANE CHICHESTER, W SUSSEX, ENGLAND PO19 1UD).

107 Hart, P., Young, M., Gordon, A. & Sullivan, K. Inhibition of phagosome-lysosome fusion in macrophages by certain mycobacteria can be explained by inhibition of lysosomal movements observed after phagocytosis. *The Journal of experimental medicine* **166**, 933-946 (1987).

108 Byrd, T. F. & Horwitz, M. A. Chloroquine inhibits the intracellular multiplication of Legionella pneumophila by limiting the availability of iron. A potential new mechanism for the therapeutic effect of chloroquine against intracellular pathogens. *J Clin Invest* **88**, 351-357, doi:10.1172/JCI115301 (1991).

109 Mishra, R. *et al.* Targeting redox heterogeneity to counteract drug tolerance in replicating Mycobacterium tuberculosis. *Sci Transl Med* **11**, doi:10.1126/scitranslmed.aaw6635 (2019).

110 Martin, C. *et al.* The live Mycobacterium tuberculosis phoP mutant strain is more attenuated than BCG and confers protective immunity against tuberculosis in mice and guinea pigs. *Vaccine* **24**, 3408-3419, doi:10.1016/j.vaccine.2006.03.017 (2006).

111 Eoh, H. & Rhee, K. Y. Methylcitrate cycle defines the bactericidal essentiality of isocitrate lyase for survival of Mycobacterium tuberculosis on fatty acids. *Proceedings of the national academy of sciences* **111**, 4976-4981 (2014).

112 Eoh, H. & Rhee, K. Y. Multifunctional essentiality of succinate metabolism in adaptation to hypoxia in Mycobacterium tuberculosis. *Proceedings of the National Academy of Sciences* **110**, 6554-6559 (2013).

113 Muñoz-Elías, E. J. & McKinney, J. D. Mycobacterium tuberculosis isocitrate lyases 1 and 2 are jointly required for in vivo growth and virulence. *Nature medicine* **11**, 638-644, doi:10.1038/nm1252 (2005).

114 Bryk, R., Lima, C. D., Erdjument-Bromage, H., Tempst, P. & Nathan, C. Metabolic enzymes of mycobacteria linked to antioxidant defense by a thioredoxin-like protein. *Science* **295**, 1073-1077, doi:10.1126/science.1067798 (2002).

115 Shi, S. & Ehrt, S. Dihydrolipoamide Acyltransferase Is Critical for Mycobacterium tuberculosis Pathogenesis. *Infection and Immunity* **74**, 56-63, doi:10.1128/iai.74.1.56-63.2006 (2006).

116 Scorpio, A. & Zhang, Y. Mutations in pncA, a gene encoding pyrazinamidase/nicotinamidase, cause resistance to the antituberculous drug pyrazinamide in tubercle bacillus. *Nature medicine* **2**, 662-667 (1996).

117 Thoracic, B. Short-course chemotherapy in pulmonary tuberculosis. *Lancet* **2**, 1102-1104 (1976).

118 Society, B. T. A controlled trial of 6 months' chemotherapy in pulmonary tuberculosis Final report: Results during the 36 months after the end of chemotherapy and beyond. *British Journal of Diseases of the Chest* **78**, 330-336 (1984).

119 McDermott, W. & Tompsett, R. Activation of pyrazinamide and nicotinamide in acidic environments in vitro. *American review of tuberculosis* **70**, 748-754 (1954).

120 Zhang, Y. & Mitchison, D. The curious characteristics of pyrazinamide: a review. *The international journal of tuberculosis and lung disease* **7**, 6-21 (2003).

121 Zhang, Y., Scorpio, A., Nikaido, H. & Sun, Z. Role of acid pH and deficient efflux of pyrazinoic acid in unique susceptibility of Mycobacterium tuberculosis to pyrazinamide. *Journal of bacteriology* **181**, 2044-2049 (1999).

122 Fontes, F. L., Peters, B. J., Crans, D. C. & Crick, D. C. The Acid–Base Equilibrium of Pyrazinoic Acid Drives the pH Dependence of Pyrazinamide-Induced Mycobacterium tuberculosis Growth Inhibition. *ACS Infectious Diseases* **6**, 3004-3014, doi:10.1021/acsinfecdis.0c00507 (2020).

123 den Hertog, A. L. *et al.* Pyrazinamide is active against Mycobacterium tuberculosis cultures at neutral pH and low temperature. *Antimicrobial agents and chemotherapy* **60**, 4956-4960 (2016).

124 Peterson, N. D., Rosen, B. C., Dillon, N. A. & Baughn, A. D. Uncoupling Environmental pH and Intrabacterial Acidification from Pyrazinamide Susceptibility in Mycobacterium tuberculosis. *Antimicrobial Agents and Chemotherapy* **59**, 7320-7326, doi:doi:10.1128/AAC.00967-15 (2015).

125 Via, L. E. *et al.* Host-mediated bioactivation of pyrazinamide: implications for efficacy, resistance, and therapeutic alternatives. *ACS infectious diseases* **1**, 203-214 (2015).

126 Lanoix, J.-P. *et al.* High systemic exposure of pyrazinoic acid has limited antituberculosis activity in murine and rabbit models of tuberculosis. *Antimicrobial agents and chemotherapy* **60**, 4197-4205 (2016).

127 Gopal, P. *et al.* Pyrazinamide Resistance Is Caused by Two Distinct Mechanisms: Prevention of Coenzyme A Depletion and Loss of Virulence Factor Synthesis. *ACS Infectious Diseases* **2**, 616-626, doi:10.1021/acsinfecdis.6b00070 (2016).

128 Rosen, B. C., Dillon, N. A., Peterson, N. D., Minato, Y. & Baughn, A. D. Long-Chain Fatty Acyl Coenzyme A Ligase FadD2 Mediates Intrinsic Pyrazinamide Resistance in Mycobacterium tuberculosis. *Antimicrob Agents Chemother* **61**, doi:10.1128/aac.02130-16 (2017).

129 Asensio, J. G. *et al.* The Virulence-associated Two-component PhoP-PhoR System Controls the Biosynthesis of Polyketide-derived Lipids inMycobacterium tuberculosis. *Journal of Biological Chemistry* **281**, 1313-1316, doi:10.1074/jbc.c500388200 (2006).

130 Gopal, P., Gerhard, G., Vronique, D. & Thomas, D. Pharmacological and Molecular Mechanisms Behind the Sterilizing Activity of Pyrazinamide. *Trends in Pharmacological Sciences* **40**, 930-940, doi:10.1016/j.tips.2019.10.005 (2019).

131 Kempker, R. R. *et al.* Lung Tissue Concentrations of Pyrazinamide among Patients with Drug-Resistant Pulmonary Tuberculosis. *Antimicrob Agents Chemother* **61**, doi:10.1128/AAC.00226-17 (2017).

132 Bigger, J. TREATMENT OF STAPHYLOCOCCAL INFECTIONS WITH PENICILLIN BY INTERMITTENT STERILISATION. *The Lancet* **244**, 497-500, doi:https://doi.org/10.1016/S0140-6736(00)74210-3 (1944).

133 Hobby, G. L. & Lenert, T. F. The in vitro action of antituberculous agents against multiplying and non-multiplying microbial cells. *Am Rev Tuberc* **76**, 1031-1048, doi:10.1164/artpd.1957.76.6.1031 (1957).

134 Deb, C. *et al.* A Novel In Vitro Multiple-Stress Dormancy Model for Mycobacterium tuberculosis Generates a Lipid-Loaded, Drug-Tolerant, Dormant Pathogen. *PLoS ONE* **4**, e6077, doi:10.1371/journal.pone.0006077 (2009).

135 Liu, Y. *et al.* Immune activation of the host cell induces drug tolerance in Mycobacterium tuberculosis both in vitro and in vivo. *The Journal of experimental medicine* **213**, 809-825, doi:10.1084/jem.20151248 (2016).

136 Dutta, N. K. & Karakousis, P. C. Latent tuberculosis infection: myths, models, and molecular mechanisms. *Microbiol Mol Biol Rev* **78**, 343-371, doi:10.1128/MMBR.00010-14 (2014).

137 Song, H. *et al.* Expression of the ompATb operon accelerates ammonia secretion and adaptation of Mycobacterium tuberculosis to acidic environments. *Mol Microbiol* **80**, 900-918, doi:10.1111/j.1365-2958.2011.07619.x (2011).

138 Mehta, M., Rajmani, R. S. & Singh, A. Mycobacterium tuberculosis WhiB3 Responds to Vacuolar pH-induced Changes in Mycothiol Redox Potential to Modulate Phagosomal Maturation and Virulence. *J Biol Chem* **291**, 2888-2903, doi:10.1074/jbc.M115.684597 (2016).

139 Farhana, A. *et al.* Reductive stress in microbes: implications for understanding Mycobacterium tuberculosis disease and persistence. *Adv Microb Physiol* **57**, 43-117, doi:10.1016/B978-0-12-381045-8.00002-3 (2010).

140 Singh, A. *et al.* Mycobacterium tuberculosis WhiB3 responds to O2 and nitric oxide via its [4Fe-4S] cluster and is essential for nutrient starvation survival. *Proc Natl Acad Sci U S A* **104**, 11562-11567, doi:10.1073/pnas.0700490104 (2007).

141 Singh, A. *et al.* Mycobacterium tuberculosis WhiB3 maintains redox homeostasis by regulating virulence lipid anabolism to modulate macrophage response. *PLoS Pathog* **5**, e1000545, doi:10.1371/journal.ppat.1000545 (2009).

142 Reichlen, M. J., Leistikow, R. L., Scobey, M. S., Born, S. E. M. & Voskuil, M. I. Anaerobic Mycobacterium tuberculosis Cell Death Stems from Intracellular Acidification Mitigated by the DosR Regulon. *J Bacteriol* **199**, doi:10.1128/JB.00320-17 (2017).

143 Tan, M. P. *et al.* Nitrate respiration protects hypoxic Mycobacterium tuberculosis against acid- and reactive nitrogen species stresses. *PLoS One* **5**, e13356, doi:10.1371/journal.pone.0013356 (2010).

144 Hards, K. *et al.* Ionophoric effects of the antitubercular drug bedaquiline. *Proc Natl Acad Sci U S A* **115**, 7326-7331, doi:10.1073/pnas.1803723115 (2018).

145 Lin, K. *et al.* Mycobacterium tuberculosis Thioredoxin Reductase Is Essential for Thiol Redox Homeostasis but Plays a Minor Role in Antioxidant Defense. *PLoS Pathog* **12**, e1005675, doi:10.1371/journal.ppat.1005675 (2016).

146 Johnson, B. K., Scholz, M. B., Teal, T. K. & Abramovitch, R. B. SPARTA: Simple Program for Automated reference-based bacterial RNA-seq Transcriptome Analysis. *BMC Bioinformatics* **17**, 66, doi:10.1186/s12859-016-0923-y (2016).

147 Purdy, G. E., Niederweis, M. & Russell, D. G. Decreased outer membrane permeability protects mycobacteria from killing by ubiquitin-derived peptides. *Mol Microbiol* **73**, 844-857, doi:10.1111/j.1365-2958.2009.06801.x (2009).

148 Saini, V. *et al.* Ergothioneine Maintains Redox and Bioenergetic Homeostasis Essential for Drug Susceptibility and Virulence of Mycobacterium tuberculosis. *Cell Rep* **14**, 572-585, doi:10.1016/j.celrep.2015.12.056 (2016).

149 Williams, J. T. *et al.* Identification of New MmpL3 Inhibitors by Untargeted and Targeted Mutant Screens Defines MmpL3 Domains with Differential Resistance. *Antimicrob Agents Chemother* **63**, doi:10.1128/AAC.00547-19 (2019).

150 Kapopoulou, A., Lew, J. M. & Cole, S. T. The MycoBrowser portal: a comprehensive and manually annotated resource for mycobacterial genomes. *Tuberculosis (Edinb)* **91**, 8-13, doi:10.1016/j.tube.2010.09.006 (2011).

151 Voskuil, M. I., Bartek, I. L., Visconti, K. & Schoolnik, G. K. The response of mycobacterium tuberculosis to reactive oxygen and nitrogen species. *Front Microbiol* **2**, 105, doi:10.3389/fmicb.2011.00105 (2011).

152 Manganelli, R. *et al.* Role of the extracytoplasmic-function sigma factor sigma(H) in Mycobacterium tuberculosis global gene expression. *Mol Microbiol* **45**, 365-374, doi:10.1046/j.1365-2958.2002.03005.x (2002).

153 Raman, S. *et al.* The alternative sigma factor SigH regulates major components of oxidative and heat stress responses in Mycobacterium tuberculosis. *J Bacteriol* **183**, 6119-6125, doi:10.1128/JB.183.20.6119-6125.2001 (2001).

154 Voss, M., Nimtz, M. & Leimkuhler, S. Elucidation of the dual role of Mycobacterial MoeZR in molybdenum cofactor biosynthesis and cysteine biosynthesis. *PLoS One* **6**, e28170, doi:10.1371/journal.pone.0028170 (2011).

155 Warrier, T. *et al.* N-methylation of a bactericidal compound as a resistance mechanism in Mycobacterium tuberculosis. *Proc Natl Acad Sci U S A* **113**, E4523-4530, doi:10.1073/pnas.1606590113 (2016).

156 Sun, Z., Cheng, S. J., Zhang, H. & Zhang, Y. Salicylate uniquely induces a 27-kDa protein in tubercle bacillus. *FEMS Microbiol Lett* **203**, 211-216, doi:10.1111/j.1574-6968.2001.tb10843.x (2001).

157 Garbe, T. R. Co-induction of methyltransferase Rv0560c by naphthoquinones and fibric acids suggests attenuation of isoprenoid quinone action in Mycobacterium tuberculosis. *Can J Microbiol* **50**, 771-778, doi:10.1139/w04-067 (2004).

158 Camus, J. C., Pryor, M. J., Medigue, C. & Cole, S. T. Re-annotation of the genome sequence of Mycobacterium tuberculosis H37Rv. *Microbiology* **148**, 2967-2973, doi:10.1099/00221287-148-10-2967 (2002).

159 Motiwala, H. F., Kuo, Y. H., Stinger, B. L., Palfey, B. A. & Martin, B. R. Tunable Heteroaromatic Sulfones Enhance in-Cell Cysteine Profiling. *J Am Chem Soc* **142**, 1801-1810, doi:10.1021/jacs.9b08831 (2020).

160 Zambaldo, C. *et al.* 2-Sulfonylpyridines as Tunable, Cysteine-Reactive Electrophiles. *J Am Chem Soc* **142**, 8972-8979, doi:10.1021/jacs.0c02721 (2020).

161 Murphy, C. M., Fenselau, C. & Gutierrez, P. L. Fragmentation characteristic of glutathione conjugates activated by high-energy collisions. *J Am Soc Mass Spectrom* **3**, 815-822, doi:10.1016/1044-0305(92)80004-5 (1992).

162 Fine, Z. & Wood, T. D. Formation of Mercury(II)-Glutathione Conjugates Examined Using High Mass Accuracy Mass Spectrometry. *Int J Anal Mass Spectrom Cromatogr* **1**, 90-94, doi:10.4236/ijamsc.2013.12011 (2013).

163 Abedinzadeh, Z., Gardes-Albert, M. & Ferradini, C. Kinetic study of the oxidation mechanism of glutathione by hydrogen peroxide in neutral aqueous medium. *Canadian Journal of Chemistry* **67**, 1247-1255 (1989).

164 Small, J. L. *et al.* Substrate specificity of MarP, a periplasmic protease required for resistance to acid and oxidative stress in Mycobacterium tuberculosis. *J Biol Chem* **288**, 12489-12499, doi:10.1074/jbc.M113.456541 (2013).

165 Newton, G. L. *et al.* Distribution of thiols in microorganisms: mycothiol is a major thiol in most actinomycetes. *J Bacteriol* **178**, 1990-1995, doi:10.1128/jb.178.7.1990-1995.1996 (1996).

166 Sao Emani, C. *et al.* Gamma-glutamylcysteine protects ergothioneine-deficient Mycobacterium tuberculosis mutants against oxidative and nitrosative stress. *Biochem Biophys Res Commun* **495**, 174-178, doi:10.1016/j.bbrc.2017.10.163 (2018).

167 Via, L. E. *et al.* Tuberculous granulomas are hypoxic in guinea pigs, rabbits, and nonhuman primates. *Infect Immun* **76**, 2333-2340, doi:10.1128/IAI.01515-07 (2008).

168 Converse, P. J. *et al.* Role of the dosR-dosS two-component regulatory system in Mycobacterium tuberculosis virulence in three animal models. *Infect Immun* **77**, 1230-1237, doi:10.1128/IAI.01117-08 (2009).

169 Munoz-Elias, E. J. & McKinney, J. D. Carbon metabolism of intracellular bacteria. *Cell Microbiol* **8**, 10-22, doi:10.1111/j.1462-5822.2005.00648.x (2006).

170 Zhang, Y. Persistent and dormant tubercle bacilli and latent tuberculosis. *Frontiers in Bioscience* **9**, 1136, doi:10.2741/1291 (2004).

171 Baker, J. J., Dechow, S. J. & Abramovitch, R. B. Acid Fasting: Modulation of Mycobacterium tuberculosis Metabolism at Acidic pH. *Trends Microbiol*, doi:10.1016/j.tim.2019.06.005 (2019).

172 Vandal, O. H., Pierini, L. M., Schnappinger, D., Nathan, C. F. & Ehrt, S. A membrane protein preserves intrabacterial pH in intraphagosomal *Mycobacterium tuberculosis*. *Nat Med* **14**, 849-854 (2008).

173 Perez, E. *et al.* An essential role for *phoP* in *Mycobacterium tuberculosis* virulence. *Mol Microbiol* **41**, 179-187 (2001).

174 Karboul, A. *et al.* Frequent Homologous Recombination Events in Mycobacterium tuberculosis PE/PPE Multigene Families: Potential Role in Antigenic Variability. *Journal of Bacteriology* **190**, 7838-7846, doi:10.1128/jb.00827-08 (2008).

175 Akhter, Y., Ehebauer, M. T., Mukhopadhyay, S. & Hasnain, S. E. The PE/PPE multigene family codes for virulence factors and is a possible source of mycobacterial antigenic variation: perhaps more? *Biochimie* **94**, 110-116, doi:10.1016/j.biochi.2011.09.026 (2012).

176 Mukhopadhyay, S., Nair, S. & Ghosh, S. Pathogenesis in tuberculosis: transcriptomic approaches to unraveling virulence mechanisms and finding new drug targets. *FEMS Microbiol Rev* **36**, 463-485, doi:10.1111/j.1574-6976.2011.00302.x (2012).

177 Bhat, K. H., Ahmed, A., Kumar, S., Sharma, P. & Mukhopadhyay, S. Role of PPE18 Protein in Intracellular Survival and Pathogenicity of Mycobacterium tuberculosis in Mice. *PLoS ONE* **7**, e52601, doi:10.1371/journal.pone.0052601 (2012).

178 Strong, M. *et al.* Toward the structural genomics of complexes: crystal structure of a PE/PPE protein complex from Mycobacterium tuberculosis. *Proc Natl Acad Sci U S A* **103**, 8060-8065, doi:10.1073/pnas.0602606103 (2006).

179 Mitra, A., Speer, A., Lin, K., Ehrt, S. & Niederweis, M. PPE Surface Proteins Are Required for Heme Utilization by Mycobacterium tuberculosis. *mBio* **8**, doi:10.1128/mBio.01720-16 (2017).

180 Zhang, L. *et al.* Comprehensive analysis of iron utilization by Mycobacterium tuberculosis. *PLoS Pathog* **16**, e1008337, doi:10.1371/journal.ppat.1008337 (2020).

181 Espitia, C. *et al.* The PE-PGRS glycine-rich proteins of Mycobacterium tuberculosis: a new family of fibronectin-binding proteins? *Microbiology (Reading)* **145 (Pt 12)**, 3487-3495, doi:10.1099/00221287-145-12-3487 (1999).

182 Sultana, R., Tanneeru, K. & Guruprasad, L. The PE-PPE domain in mycobacterium reveals a serine alpha/beta hydrolase fold and function: an in-silico analysis. *PLoS One* **6**, e16745, doi:10.1371/journal.pone.0016745 (2011).

183 Garrett, C. K., Broadwell, L. J., Hayne, C. K. & Neher, S. B. Modulation of the Activity of Mycobacterium tuberculosis LipY by Its PE Domain. *PLoS One* **10**, e0135447, doi:10.1371/journal.pone.0135447 (2015).

184 Gey van Pittius, N. C. *et al.* Evolution and expansion of the Mycobacterium tuberculosis PE and PPE multigene families and their association with the duplication of the ESAT-6 (esx) gene cluster regions. *BMC Evol Biol* **6**, 95, doi:10.1186/1471-2148-6-95 (2006).

185 Simeone, R., Bottai, D., Frigui, W., Majlessi, L. & Brosch, R. ESX/type VII secretion systems of mycobacteria: Insights into evolution, pathogenicity and protection. *Tuberculosis (Edinb)* **95 Suppl 1**, S150-154, doi:10.1016/j.tube.2015.02.019 (2015).

186 Ates, L. S. *et al.* Essential Role of the ESX-5 Secretion System in Outer Membrane Permeability of Pathogenic Mycobacteria. *PLoS Genet* **11**, e1005190, doi:10.1371/journal.pgen.1005190 (2015).

187 Sani, M. *et al.* Direct Visualization by Cryo-EM of the Mycobacterial Capsular Layer: A Labile Structure Containing ESX-1-Secreted Proteins. *PLoS Pathogens* **6**, e1000794, doi:10.1371/journal.ppat.1000794 (2010).

188 Sampson, S. L. Mycobacterial PE/PPE proteins at the host-pathogen interface. *Clin Dev Immunol* **2011**, 497203-497203, doi:10.1155/2011/497203 (2011).

189 Gey Van Pittius, N. C. *et al.* The ESAT-6 gene cluster of Mycobacterium tuberculosis and other high G+C Gram-positive bacteria. *Genome Biol* **2**, Research0044, doi:10.1186/gb-2001-2-10-research0044 (2001).

190 Abdallah, A. M. *et al.* PPE and PE_PGRS proteins of Mycobacterium marinum are transported via the type VII secretion system ESX-5. *Mol Microbiol* **73**, 329-340, doi:10.1111/j.1365-2958.2009.06783.x (2009).

191 Tufariello, J. M. *et al.* Separable roles forMycobacterium tuberculosisESX-3 effectors in iron acquisition and virulence. *Proceedings of the National Academy of Sciences* **113**, E348-E357, doi:10.1073/pnas.1523321113 (2016).

192 Mitra, A., Ko, Y. H., Cingolani, G. & Niederweis, M. Heme and hemoglobin utilization by Mycobacterium tuberculosis. *Nat Commun* **10**, 4260, doi:10.1038/s41467-019-12109-5 (2019).

193 Malen, H., De Souza, G. A., Pathak, S., Softeland, T. & Wiker, H. G. Comparison of membrane proteins of Mycobacterium tuberculosis H37Rv and H37Ra strains. *BMC Microbiol* **11**, 18, doi:10.1186/1471-2180-11-18 (2011).

194 Lohse, M. *et al.* RobiNA: a user-friendly, integrated software solution for RNA-Seq-based transcriptomics. *Nucleic Acids Res* **40**, W622-627, doi:10.1093/nar/gks540 (2012).

195 Li, H. Aligning sequence reads, clone sequences and assembly contigs with BWA-MEM. *arXiv* **1303.3997v1[q-bio.GN]**, doi:arxiv:1303.3997 (2013).

196 McKenna, A. *et al.* The Genome Analysis Toolkit: a MapReduce framework for analyzing next-generation DNA sequencing data. *Genome Res* **20**, 1297-1303, doi:10.1101/gr.107524.110 (2010).

197 Murphy, K. C. *et al.* ORBIT: a New Paradigm for Genetic Engineering of Mycobacterial Chromosomes. *mBio* **9**, e01467-01418, doi:10.1128/mBio.01467-18 (2018).

198 Schneider, C. A., Rasband, W. S. & Eliceiri, K. W. NIH Image to ImageJ: 25 years of image analysis. *Nature Methods* **9**, 671-675, doi:10.1038/nmeth.2089 (2012).

199 Bachrach, G. *et al.* A new single-copy mycobacterial plasmid, pMF1, from Mycobacterium fortuitum which is compatible with the pAL5000 replicon. *Microbiology (Reading)* **146 (Pt 2)**, 297-303, doi:10.1099/00221287-146-2-297 (2000).

200 Johnson, B. K. & Abramovitch, R. B. Macrophage infection models for Mycobacterium tuberculosis. *Methods Mol Biol* **1285**, 329-341, doi:10.1007/978-1-4939-2450-9_20 (2015).

201 Park, Y. *et al.* Inhibition of CorA-Dependent Magnesium Homeostasis Is Cidal in Mycobacterium tuberculosis. *Antimicrobial Agents and Chemotherapy* **63**, doi:10.1128/aac.01006-19 (2019).

202 Sirakova, T. D. *et al.* Identification of a diacylglycerol acyltransferase gene involved in accumulation of triacylglycerol in Mycobacterium tuberculosis under stress. *Microbiology (Reading, England)* **152**, 2717-2725, doi:10.1099/mic.0.28993-0 (2006).

203 Roy, A., Kucukural, A. & Zhang, Y. I-TASSER: a unified platform for automated protein structure and function prediction. *Nature Protocols* **5**, 725-738, doi:10.1038/nprot.2010.5 (2010).

204 Daniel, J., Maamar, H., Deb, C., Sirakova, T. D. & Kolattukudy, P. E. Mycobacterium tuberculosis Uses Host Triacylglycerol to Accumulate Lipid Droplets and Acquires a Dormancy-Like Phenotype in Lipid-Loaded Macrophages. *PLoS Pathog* **7**, e1002093 (2011).

205 Guerrini, V. *et al.* Storage lipid studies in tuberculosis reveal that foam cell biogenesis is disease-specific. *PLoS Pathog* **14**, e1007223, doi:10.1371/journal.ppat.1007223 (2018).

206 Mishra, K. C. *et al.* Functional role of the PE domain and immunogenicity of the Mycobacterium tuberculosis triacylglycerol hydrolase LipY. *Infect Immun* **76**, 127-140, doi:10.1128/IAI.00410-07 (2008).

207 de Carvalho, L. P. S. *et al.* Metabolomics of Mycobacterium tuberculosis Reveals Compartmentalized Co-Catabolism of Carbon Substrates. *Chemistry & Biology* **17**, 1122-1131, doi:https://doi.org/10.1016/j.chembiol.2010.08.009 (2010).

208 Stahl, C. *et al.* MspA provides the main hydrophilic pathway through the cell wall of Mycobacterium smegmatis. *Mol Microbiol* **40**, 451-464, doi:10.1046/j.1365-2958.2001.02394.x (2001).

209 Stephan, J. *et al.* The growth rate of Mycobacterium smegmatis depends on sufficient porin-mediated influx of nutrients. *Molecular Microbiology* **58**, 714-730, doi:https://doi.org/10.1111/j.1365-2958.2005.04878.x (2005).

210 Danilchanka, O., Pavlenok, M. & Niederweis, M. Role of Porins for Uptake of Antibiotics by *Mycobacterium smegmatis*. *Antimicrobial Agents and Chemotherapy* **52**, 3127, doi:10.1128/AAC.00239-08 (2008).

211 Zambolin, S. *et al.* Structural basis for haem piracy from host haemopexin by Haemophilus influenzae. *Nature Communications* **7**, 11590, doi:10.1038/ncomms11590 (2016).

212 Mitra, A., Ko, Y.-H., Cingolani, G. & Niederweis, M. Heme and hemoglobin utilization by Mycobacterium tuberculosis. *Nature Communications* **10**, doi:10.1038/s41467-019-12109-5 (2019).

213 Bellerose, M. M. *et al.* Common variants in the glycerol kinase gene reduce tuberculosis drug efficacy. *mBio* **in press** (2019).

214 Xu, W. *et al.* Chemical Genetic Interaction Profiling Reveals Determinants of Intrinsic Antibiotic Resistance in Mycobacterium tuberculosis. *Antimicrob Agents Chemother* **61**, doi:10.1128/AAC.01334-17 (2017).

215 Wolfe, L. M., Mahaffey, S. B., Kruh, N. A. & Dobos, K. M. Proteomic definition of the cell wall of Mycobacterium tuberculosis. *J Proteome Res* **9**, 5816-5826, doi:10.1021/pr1005873 (2010).

216 McEvoy, C. R. E. *et al.* Comparative Analysis of Mycobacterium tuberculosis pe and ppe Genes Reveals High Sequence Variation and an Apparent Absence of Selective Constraints. *PLoS ONE* **7**, e30593, doi:10.1371/journal.pone.0030593 (2012).

217 Rohde, K., Yates, R. M., Purdy, G. E. & Russell, D. G. Mycobacterium tuberculosis and the environment within the phagosome. *Immunol Rev* **219**, 37-54, doi:10.1111/j.1600-065X.2007.00547.x (2007).

218 Ruhl, C. R. *et al.* Mycobacterium tuberculosis sulfolipid-1 activates nociceptive neurons and induces cough. *Cell* **181**, 293-305. e211 (2020).

219 Tan, S., Sukumar, N., Abramovitch, R. B., Parish, T. & Russell, D. G. Mycobacterium tuberculosis responds to chloride and pH as synergistic cues to the immune status of its host cell. *PLoS pathogens* **9**, e1003282 (2013).

220 Carta, F. *et al.* Carbonic anhydrase inhibitors. Characterization and inhibition studies of the most active β-carbonic anhydrase from Mycobacterium tuberculosis, Rv3588c. *Bioorganic &*

Medicinal Chemistry Letters **19**, 6649-6654, doi:https://doi.org/10.1016/j.bmcl.2009.10.009 (2009).

221 Supuran, C. T. Carbonic anhydrases: novel therapeutic applications for inhibitors and activators. *Nature Reviews Drug Discovery* **7**, 168-181, doi:10.1038/nrd2467 (2008).

222 Cummins, E. P., Selfridge, A. C., Sporn, P. H., Sznajder, J. I. & Taylor, C. T. Carbon dioxide-sensing in organisms and its implications for human disease. *Cell Mol Life Sci* **71**, 831-845, doi:10.1007/s00018-013-1470-6 (2014).

223 Tresguerres, M., Buck, J. & Levin, L. R. Physiological carbon dioxide, bicarbonate, and pH sensing. *Pflugers Arch* **460**, 953-964, doi:10.1007/s00424-010-0865-6 (2010).

224 Constantin de Magny, G. & Colwell, R. R. Cholera and climate: a demonstrated relationship. *Trans Am Clin Climatol Assoc* **120**, 119-128 (2009).

225 Shimamura, T., Watanabe, S. & Sasaki, S. Enhancement of enterotoxin production by carbon dioxide in Vibrio cholerae. *Infection and Immunity* **49**, 455-456, doi:10.1128/iai.49.2.455-456.1985 (1985).

226 Abuaita, B. H. & Withey, J. H. Bicarbonate Induces Vibrio cholerae virulence gene expression by enhancing ToxT activity. *Infect Immun* **77**, 4111-4120, doi:10.1128/iai.00409-09 (2009).

227 Marcus, E. A., Moshfegh, A. P., Sachs, G. & Scott, D. R. The periplasmic alpha-carbonic anhydrase activity of Helicobacter pylori is essential for acid acclimation. *Journal of bacteriology* **187**, 729-738, doi:10.1128/JB.187.2.729-738.2005 (2005).

228 McNulty, R., Ulmschneider, J. P., Luecke, H. & Ulmschneider, M. B. Mechanisms of molecular transport through the urea channel of Helicobacter pylori. *Nature Communications* **4**, 2900, doi:10.1038/ncomms3900 (2013).

229 Sassetti, C. M. & Rubin, E. J. Genetic requirements for mycobacterial survival during infection. *Proceedings of the National Academy of Sciences* **100**, 12989, doi:10.1073/pnas.2134250100 (2003).

230 Nishimori, I. *et al.* Carbonic Anhydrase Inhibitors. Cloning, Characterization, and Inhibition Studies of a New β-Carbonic Anhydrase from Mycobacterium tuberculosis. *Journal of Medicinal Chemistry* **52**, 3116-3120, doi:10.1021/jm9003126 (2009).

231 Minakuchi, T., Nishimori, I., Vullo, D., Scozzafava, A. & Supuran, C. T. Molecular Cloning, Characterization, and Inhibition Studies of the Rv1284 β-Carbonic Anhydrase from Mycobacterium tuberculosis with Sulfonamides and a Sulfamate. *Journal of Medicinal Chemistry* **52**, 2226-2232, doi:10.1021/jm9000488 (2009).

232 Rock, J. M. *et al.* Programmable transcriptional repression in mycobacteria using an orthogonal CRISPR interference platform. *Nat Microbiol* **2**, 16274, doi:10.1038/nmicrobiol.2016.274 (2017).

233 Pedersen, O., Colmer, T. & Sand-Jensen, K. Underwater Photosynthesis of Submerged Plants – Recent Advances and Methods. *Frontiers in Plant Science* **4**, doi:10.3389/fpls.2013.00140 (2013).

234 Johnson, B. K. *Investigating Mycobacterium tuberculosis pH-dependent adaptations*. (Michigan State University, 2016).

235 Jiang, Y. *et al.* Polymorphisms in the PE35 and PPE68 antigens in Mycobacterium tuberculosis strains may affect strain virulence and reflect ongoing immune evasion. *Mol Med Rep* **13**, 947-954, doi:10.3892/mmr.2015.4589 (2016).

236 Brodin, P. *et al.* Dissection of ESAT-6 system 1 of Mycobacterium tuberculosis and impact on immunogenicity and virulence. *Infect Immun* **74**, 88-98, doi:10.1128/iai.74.1.88-98.2006 (2006).

237 Damen, M. P. M. *et al.* Modification of a PE/PPE substrate pair reroutes an Esx substrate pair from the mycobacterial ESX-1 type VII secretion system to the ESX-5 system. *Journal of Biological Chemistry* **295**, 5960-5969, doi:10.1074/jbc.ra119.011682 (2020).

238 Frigui, W. *et al.* Control of M. tuberculosis ESAT-6 Secretion and Specific T Cell Recognition by PhoP. *PLoS Pathogens* **4**, e33, doi:10.1371/journal.ppat.0040033 (2008).

239 Lee, J. S. *et al.* Mutation in the transcriptional regulator PhoP contributes to avirulence of Mycobacterium tuberculosis H37Ra strain. *Cell Host Microbe* **3**, 97-103, doi:10.1016/j.chom.2008.01.002 (2008).

240 Minch, K. J. *et al.* The DNA-binding network of Mycobacterium tuberculosis. *Nature communications* **6**, 5829-5829, doi:10.1038/ncomms6829 (2015).

241 Ruhl, C. R. *et al.* Mycobacterium tuberculosis Sulfolipid-1 Activates Nociceptive Neurons and Induces Cough. *Cell* **181**, 293-305.e211, doi:10.1016/j.cell.2020.02.026 (2020).

242 Vadász, I., Hubmayr, R. D., Nin, N., Sporn, P. H. S. & Sznajder, J. I. Hypercapnia: a nonpermissive environment for the lung. *Am J Respir Cell Mol Biol* **46**, 417-421, doi:10.1165/rcmb.2011-0395PS (2012).

243 Ravimohan, S., Kornfeld, H., Weissman, D. & Bisson, G. P. Tuberculosis and lung damage: from epidemiology to pathophysiology. *European Respiratory Review* **27**, 170077, doi:10.1183/16000617.0077-2017 (2018).

244 Haydel, S. E., Benjamin, W. H., Jr., Dunlap, N. E. & Clark-Curtiss, J. E. Expression, autoregulation, and DNA binding properties of the Mycobacterium tuberculosis TrcR response regulator. *J Bacteriol* **184**, 2192-2203, doi:10.1128/jb.184.8.2192-2203.2002 (2002).

245 Parish, T., Hatfull, G. F. & Jr., W. R. J. Two-Component Regulatory Systems of Mycobacteria. *Microbiology Spectrum* **2**, 2.1.17, doi:doi:10.1128/microbiolspec.MGM2-0010-2013 (2014).

246 Pang, X. *et al.* The β-propeller gene Rv1057 of Mycobacterium tuberculosis has a complex promoter directly regulated by both the MprAB and TrcRS two-component systems. *Tuberculosis (Edinburgh, Scotland)* **91 Suppl 1**, S142-S149, doi:10.1016/j.tube.2011.10.024 (2011).

247 Haydel, S. E. & Clark-Curtiss, J. E. The Mycobacterium tuberculosis TrcR response regulator represses transcription of the intracellularly expressed Rv1057 gene, encoding a seven-bladed beta-propeller. *Journal of bacteriology* **188**, 150-159, doi:10.1128/JB.188.1.150-159.2006 (2006).

248 Magalon, A., Fedor, J. G., Walburger, A. & Weiner, J. H. Molybdenum enzymes in bacteria and their maturation. *Coordination chemistry reviews* **255**, 1159-1178 (2011).

249 Yang, J., Li, J., Grunewald, S. & Wan, X. F. BinAligner: a heuristic method to align biological networks. *BMC Bioinformatics* **14 Suppl 14**, S8, doi:10.1186/1471-2105-14-S14-S8 (2013).

250 Belon, C., Gannoun-Zaki, L., Lutfalla, G., Kremer, L. & Blanc-Potard, A.-B. Mycobacterium marinum MgtC plays a role in phagocytosis but is dispensable for intracellular multiplication. *PLoS One* **9**, e116052 (2014).

251 Arnvig, K. B. *et al.* Sequence-based analysis uncovers an abundance of non-coding RNA in the total transcriptome of Mycobacterium tuberculosis. *PLoS pathogens* **7**, e1002342 (2011).

252 Portillo, F. G. d., Foster, J. W., Maguire, M. E. & Finlay, B. B. Characterization of the micro-environment of Salmonella typhimurium–containing vacuoles within MDCK epithelial cells. *Molecular microbiology* **6**, 3289-3297 (1992).

253 van Opijnen, T., Bodi, K. L. & Camilli, A. Tn-seq: high-throughput parallel sequencing for fitness and genetic interaction studies in microorganisms. *Nat Methods* **6**, 767-772, doi:10.1038/nmeth.1377 (2009).

254 Mishra, K. C. *et al.* Functional role of the PE domain and immunogenicity of the Mycobacterium tuberculosis triacylglycerol hydrolase LipY. *Infection and immunity* **76**, 127-140 (2008).

255 Beckham, K. S. H. *et al.* Structure of the mycobacterial ESX-5 type VII secretion system pore complex. *Science Advances* **7**, eabg9923, doi:doi:10.1126/sciadv.abg9923 (2021).

256 JAIN, R. K., JOYCE, P. B., MOLINETE, M., Halban, P. A. & GORR, S.-U. Oligomerization of green fluorescent protein in the secretory pathway of endocrine cells. *Biochemical Journal* **360**, 645-649 (2001).

257 Feilmeier, B. J., Iseminger, G., Schroeder, D., Webber, H. & Phillips, G. J. Green fluorescent protein functions as a reporter for protein localization in Escherichia coli. *Journal of bacteriology* **182**, 4068-4076 (2000).

258 Reifenrath, M. & Boles, E. A superfolder variant of pH-sensitive pHluorin for in vivo pH measurements in the endoplasmic reticulum. *Scientific Reports* **8**, 11985, doi:10.1038/s41598-018-30367-z (2018).

259 Agrawal, R., Pandey, A., Rajankar, M. P., Dixit, N. M. & Saini, D. K. The two-component signalling networks of Mycobacterium tuberculosis display extensive cross-talk in vitro. *Biochemical Journal* **469**, 121-134 (2015).